Synthesis and Processing of Amorphous Si(Al)OC Bulk Ceramics: High Temperature Properties and Applications

A dissertation submitted to the

Department of Materials Science
Darmstadt University of Technology
in partial fulfillment of the requirements for the degree of

Doktor−Ingenieur

by

Rahul Ramesh Harshe
Master of Technology (M. Tech)
from
Kirloskarwadi, India

Referee:	Prof. Dr. R. Riedel
Co-referee:	Prof. Dr. H. Ortner
Date of submission:	19 August 2004
Date of oral examination:	07 September 2004

Darmstadt 2004
D 17

Acknowledgments

Hardly-if-ever PhD is the sole achievement of one person. It rather is a journey where the traveller is dependent on many aid on the path, has to ask for directions, and often needs a helping hand. It is only just to name my debts and thank the people who helped me on my way −here is the right place for it as I sincerely think that seldom is anything accomplished without the assistance or encouragement of others.

First I would like to pay my sincere thanks to Prof. Dr. R. Riedel. He has always been extremely generous with his time, knowledge and ideas and allowed me great freedom in this research.

Likewise, I owe much to the advice and intellectual support of Prof. Dr. C. Balan. His deep understanding in research helped me in understanding basic concepts. I want to thank Prof. R. Raj for giving me the opportunity to work together with his group in Boulder, USA.

My special thanks goes to Prof. Dr. H. M. Ortner, Chemical Analytic group in TU-Darmstadt for his acceptance as a co-referee.

Further thanks to:

Dr. C. Konetschny for introduction to this project and kind help
C. Fasel for TGMS and discussion
Dr. I. Kinski for MAS-NMR characterization
Dr. Sandeep Shah for compression creep experiments and useful discussion
Dr. Stephan Flege for SIMS characterization

I appreciate the help from collogues and all those who have provided kind support, without which a great deal of this work would have been impossible.

I express my gratitude for the chance and financial support provided by the State of Hessen, Germany to realize this research.

Much appreciation goes to my mother and father, and the rest of my family for their support and belief in me which have always inspired me in my endeavors.

This list is far from exhaustive; I pray for forgiveness from those I did not mention by name and include them in my heart-felt gratitude.

Contents

List of Figures

List of Tables

1 Abstract

The research work presented in this thesis is concerned with the bulk Si-Al-O-C ceramics produced by pyrolysis of commercial poly(methylsilsesquioxane) precursors. Prior to the pyrolysis the precursors were cross-linked with a cross-linking-agent, or modified by the sol-gel-technique with an Al-containing alkoxide compound, namely alumatrane. This particular procedure yields amorphous ceramics with various compositions ($Si_{1.00}O_{1.60}C_{0.80}$, $Si_{1.00}Al_{0.035}O_{1.63}C_{0.46}$, $Si_{1.00}Al_{0.070}O_{1.69}C_{0.47}$, $Si_{1.00}Al_{0.107}O_{1.86}C_{0.47}$) after thermal decomposition at 1100-°C in Ar depending on the amount of Al-alkoxide used in the polymer reaction synthesis.

The ceramics obtained are amorphous and remain unchanged up to 1300°C. Up to this temperature the ceramics undergo softening between 1100-1300°C and at high temperature >1300°C the system crystallizes forming mullite and SiC. The deformation continues at all higher temperatures (>1300°C) and is accompanied by mass loss. An activation energy of 503 ± 60 [kJ/mole] equivalent to mullite crystallization is calculated and it is believed to occur by nucleation rate control, which is similar to monophasic gels. Bulk transformation in SiAlOC ceramics are characterized in terms of microstructure and crystallization in the temperature regime ranging from 1100 to 1700°C. Aluminum-free SiOC forms SiC along with cracking of the bulk compacts. In contrast, the presence of Al in the SiOC matrix forms mullite and SiC and prevents micro-cracking at elevated temperatures due to transient viscous sintering at high temperature. The nano-crystals formed are embedded in an amorphous Si(Al)OC matrix in both cases.

The oxidation resistance of SiOC ceramic also differs to that of SiAlOC ceramic. Weight loss is observed for SiOC ceramic at all temperatures and times whereas aluminum modification indicates mass gain. SiOC ceramics have large cracking in the oxide layer and is discussed by the formation of cristobalite formation and its volume change during cooling. A minimum oxidation rate constant

of 6.142 x 10^{-2} [mg^2/cm^4 x h] is calculated for the oxidation of pyrolyzed aluminum modified ceramic at 1400°C and is one power higher than reported for CVD SiC. The rate constant can be improved by post-treatment of the ceramic bulks and it is severely altered for the ceramic compositions which already passes through softening phase by post-treatment. An average activation energy of 197 kJ/mole is quantified for the SiOC ceramic with low aluminum content. A lower activation energy is quantified for high aluminum SiAlOC ceramic indicating the reduction of oxidation resistance with excess aluminum.

The change in the viscosity and activation energy with aluminum content is discussed in the thermal deformation or creep behavior of the SiAlOC ceramics. The viscosity value is lowered from 3.47 x 10^{12} to 1.71 x 10^{11} [Pa.s] at 1250°C with increasing amount of aluminum content. A transition temperature of 1220-1300°C similar to SiOC ceramic is mentioned and decreases with increasing content of aluminum in the material. The activation energy of shear viscosity calculated from creep is similar to that observed for softening of ceramics, indicating similar molecular motions are involved.

Potential application of polysiloxane derived SiOC ceramics in the field of ceramic **M**icro **E**lectro **M**echanical **S**ystems (MEMS) and CMC's is reported.

2 Introduction & Motivation

In the modern world where things are changing at a incredible rate a good support from the development of new materials with easy processing to replace existing materials is of prime importance. For example in the automobile industry (for high temperature engine component applications) more emphasis in the present time is on searching new materials, mainly advanced ceramics to replace the metals. In the last decades ceramics did replace metals in some high temperature application areas but its high processing costs made the industry difficult to accept them. Indeed, it opens an area of research and development of these ceramic materials from cheap raw materials and making them suitable for mass production and reduce the processing costs by near-net-shape formation.

In recent years, material scientists have made significant efforts to develop alternative techniques for the fabrication of ceramics. Of these techniques, the use of preceramic polymer is one of the most promising methods in terms of net-shape forming of high temperature ceramics and ceramic composites. Generally, preceramic polymers can be defined as organometallic polymers which pyrolyze to ceramics upon thermal treatment. Suitable precursor polymers for high performance ceramics are based on cross-linked poly(silanes), -(carbosilanes), -(silazanes), -(siloxanes) and molecular mixtures thereof. Some components from the automobile engine or thermal-elements from furnaces or thermocouples can be prepared from polymer derived ceramic route and required properties can be obtained/optimized from proper filler mixtures. The filler material can modify the composite properties like: electrical conductivity, oxidation resistance, high-temperature deformation resistance. The polymeric material in this case initially acts as a binder material (but in large volume fraction) to fillers and generate a stable shape, which can withstand handling. After thermal treatment due to decomposition process the polymeric material is converted to the inorganic ceramics with the final composition dependent on the initial chemistry of the

polymer. Although techniques for polymer preparation can be complex, through careful control of synthesis parameters, polymer compositions and structures can be tailored to yield the desired ceramic upon pyrolysis.

In the last decade many polymers are available commercially but many polymers mentioned above have problem in handling as they are very sensitive to atmosphere. Among all the above mentioned polymers poly(siloxanes) are available easily and are cheap in cost and can be converted to silicon oxycarbide **(SiOC)** ceramic by thermal pyrolysis treatment. Poly(siloxane) polymer can be handled in air and are available in both liquid, semi-solid (viscous) as well as solid (powder) form. Among all available polymers a proper selection should be done which satisfies the require processing properties. For example, if the polymer is in the liquid state at room temperature it can be easily injected in the mold cavity to form a component but as soon as it reaches the cavity it should possess property to cross-link and retain the mold shape. This cross linking can be done thermally (vinyl, phenyl end groups containing polymers) or with hydrolysis and condensation reaction in presence of cross-linking-agent. But if the polymer itself is in the powder or solid state it must be initially meltable and should have cross-linking behavior.

Synthesis and characterization of SiOC ceramic material from polymer pyrolysis route is a main focus in the past decade. Researchers modified these materials by aluminum, boron, zirconium to yield Si-Al-O-C, Si-B-O-C, Si-Zr-O-C ceramics and much of the research was aimed for the synthesis, structural characterization and crystallization behavior for these materials. As such, no paper directly reports further properties at high temperature namely, oxidation resistance, time dependent thermal deformation or creep, crystallization kinetics etc. The present research is hence focused on the following points:

1. Search for different available poly(siloxane) polymer in market and initial characterization of these polymers for process feasibility. This characterization was done by keeping in mind that the polymer or polymer-filler mixture will be used in an injection molding device for component preparation. Accordingly, rheology was the best tool to investigate the physical changes in the material with temperature and will be reported.

2. Modify the polymer with aluminum using cheap commercial chemicals to

form Si-Al-O-C ceramic system. Aluminum can be incorporated in two different ways: First, in metal form to obtain a composite material; here aluminum reacts with the polymer decomposition product or its components to form stable inorganic compound or remain unreacted in molten metal form after thermal treatment. The second is in molecular level using a chemical reaction route.

3. Optimize the green and ceramic body formation without generating cracks during any stage of processing. In this the parameters like temperature, pressure, heating rates, holding times, identifying mass loss regions plays key role.

4. Investigating the polymer-to-ceramic transformation process.

5. Characterization of transformed ceramic: chemical, physical or dimensional changes during transformation, phase development of the material after pyrolysis, effect of high temperature on the phase generation.

6. Investigate the bulk material properties by softening/crystallization kinetics, oxidation kinetics and by creep test at high temperature.

7. Examine the material for new applications namely MEMS, CMC's. More emphasis will be given on formation of very small scale components. Formation of various CMC's are not investigated by the author himself but will be briefed from the reports investigated by other members involved on the above system as a part of the whole project.

Researchers report that modification of SiOC ceramic system with elements like Al, B etc., upgrades the properties. The present research hence look into this system in more depth and only concern with the modification by aluminum and investigate its positive or negative effects on certain high temperature properties. The main advantage of this research is to provide materials for all those industries who produce/develop components for high temperature applications, against corrosive/oxidative environments as well as where electrical properties is also a concern (contuctivity/resistance) at temperatures as high as 1300°C.

It is a well known fact that not all modifications produce positive results and their controlled used are sometimes beneficial for optimize material properties.

Improving one property may or may not damage the other. Inspite, researchers should always look forward to use the advantages and reduce the drawbacks by proper optimization.

3 Literature Review

3.1 Ceramics from Pyrolysis of Preceramic Polymers

The importance of high performance, oxide and non-oxide ceramic material such as SiC, Si_3N_4, B_4C, BN, AlN, TiC and TiN, coupled with limitations associated with conventional processing techniques have focused increased attention on manufacturing ceramics and ceramic matrix composites (CMC's) via the pyrolysis of preceramic polymers.[(1),(2)] Additional investigations show that a variety of other compounds such as AlB_{12}, CaB_6, TiC, BP, TiB_2, SiB_6, TiN, and $TiSi_{12}$ can be produced from polymers.[(3)] The typical processing scheme involves adjustment of the molecular weight of the polymer (synthesis and purification), shaping of the product (e.g., fiber spinning, warm pressing), cross linking of the product (annealing in oxidative atmosphere; chemical catalyst, chlorosilane cross linking; micro-wave, electron, or γ-ray radiation curing; etc.), and finally, pyrolysis in an inert- or reactive - (e.g., NH_3) gas atmosphere at temperatures typically between 1000°C and 1400°C.

The pyrolysis mechanism generally involves several distinct steps:

1. An organometallic-to-inorganic transition between 500°C and 800°C, leading to an amorphous hydrogenated solid built on tetrahedral structures of the type $Si(C_aO_bN_cB_d)$, depending on the polymer composition.

2. Nucleation of crystalline precipitations - such as SiC, Si_3N_4, or SiO_2 - and an additional carbon phase at temperatures between 1200°C and 1600°C.

3. Grain coarsening that results in consumption of the residual amorphous phase and reduction of oxygen content due to the probable evaporation of SiO and CO.

Active research in preceramic polymer technology was promoted by the pressing need for new materials that could serve as replacements for metals and metallic alloys in demanding structural applications, particularly in the defence and aerospace industry, where metals and metallic alloys were no longer suitable. Advanced ceramic and ceramic matrix composite materials have potential in applications such as advanced heat engines, high efficiency turbine and diesel engines, and high-specific impulse engines, where the need exists for lightweight structural materials with high temperature performance and environmental stability better than metals. A variety of other applications for ceramics prepared by polymer pyrolysis also exists. Precisely, foams as heater-heat exchangers, insulation, and filters should be of interest. Use of polymer pyrolysis to produce coatings may also have a variety of applications for wear oxidizing and corrosive chemical environments. Polymer pyrolysis may also provide a method of ceramic-ceramic or ceramic-metal joining, provided shrinkage problems can be overcome.[1]

To replace existing materials, the new generation of materials need to possess exceptional properties which include: thermal stability at elevated temperature (>1200°C), higher fracture strength, higher fracture toughness, better oxidation resistance, and better thermal shock resistance, to name the few. Initially, the outstanding properties of carbon-carbon composites, such as superior strength and thermal stability, made them a viable substitute for metals and metallic alloys; however, their poor oxidation resistance limited their use at higher temperature. Improvement in oxidation resistance was achieved by infiltrating carbon preforms with preceramic polymer and subsequent transformation to ceramic yielding improvement in properties particularly, oxidation resistance. Simultaneously, work was launched for producing inorganic fibers by new processing techniques from the preceramic polymers which possess high temperature stability, oxidation resistance and strength retention. As a result, researchers focused their efforts on the synthesis and pyrolysis of inorganic polymers to produce ceramic materials which exhibits superior high temperature properties relative to carbon-carbon composite materials. Due to their potential for excellent high temperature properties, silicon based materials namely, silicon carbide and silicon nitride and combination of phases from Si, C, N, B, O were of immediate interest and as a result, the initial focus was on the synthesis and pyrolysis of

organosilicon and inorganic silicon polymers.

The formation of ceramics from polymer pyrolysis can be traced back to the early work of Ainger and Herbert in 1960 and Chantrell and Popper[4] in 1967. They were the first to suggest that inorganic polymers might serve as precursors to ceramics; however, the first practical conversion of organo-silicon compounds to non-oxide materials was developed by Verbeek, Winter, and Mausmann[5],[6] in the early 1970's. In the laboratories of Bayer AG, Verbeek manufactured β-SiC fibers containing minor amounts of α-SiC and β-Si_3N_4 by pyrolysis of a carbosilazane polymer at 1800°C in an inert atmosphere. The carbosilazane resin was produced from condensation of $CH_3Si(NHCH_3)$ in the presence of H_2SO_4. The resin was melt spun at 220°C and heated in air at 100°C for 20 h to produce infusible fibers which would be pyrolyzed. In a variation of their process, Verbeek and co-workers synthesized poly(methylsilsesquiazanes), which were dry-spun (with poly(ethylene) oxide as a spinning aid) to produce poly(silazane) fibers. These fibers were subsequently pyrolyzed in nitrogen at 1200°C to produce silicon carbonitride fibers.

Although Verbeek and Winter also developed a preceramic polymer process for production of SiC fibers, much of the credit for development of the production of SiC fiber is attributed to Yajima *et al.*[7],[8],[9] in the late 1970's. Yajima *et al.* intensively investigated the pyrolysis of poly(carbosilanes) to form SiC fibers. The subsequent production of SiC fibers by Nippon Carbon Co. was a major factor in generating interest in the field.

Since the early work of Verbeek and Yajima, significant improvements in preceramic polymer synthesis techniques have resulted in the development of a great variety of organosilicon polymers that have been used to produce ceramic products in the Si-C-N-B-O system. Polymer pyrolysis synthesis was successfully implemented for production of SiC, Si_3N_4, BN, B_4C. More recently, mixtures of Si-C-N, Si-B-C, Si-B-C-N suggest wide possibility of forming mixed products for various combined properties.[10], [11], [12], [13]

One of the early application of polymer pyrolysis to noncarbon ceramics was the formation of SiO_2-based materials using silicone polymers. However, the diverse array of other methods of processing SiO_2 materials has restricted the use of SiO_2 preceramic polymers. Other emerging processes for making SiO_2-based materials include sol-gel technique, which are related to polymer pyrolysis

and are also of increasing interest for other *oxide* ceramics. Another particular *oxide* based ceramic of technological interest is mullite which comes under *aluminosilicate* group. Sol-gel methods have been employed widely in the synthesis of mullite either through boehmite (AlOOH) and TEOS (tetraethylorthosilicate) or through $Al(NO_3)_3$ and TEOS mixtures.[14] Researchers also tried to synthesize aluminosiloxanes by polymerization reaction between silicon and aluminum monomers.[15] Polymer pyrolysis route used provide atomic scale mixing of different species which favor mullitization at lower temperatures. Small-scale mullitization is driven by diffusion of the aluminum moiety into a siliceous matrix until the critical concentration required for mullite nucleation is achieved. The discussion focused above indicate the usefulness of polymer pyrolysis in synthesizing *oxide* and *nonoxide* ceramic materials with higher homogeneity.

The usefulness of preceramic polymers as precursors to low dimensional products such as fibers and thin films, has been well recognized.[1] However, the applications of preceramic polymers to fabricate dense ceramic matrices and monolithic bodies are still limited. Loss of volatiles during polymer pyrolysis leads either to high amounts of residual porosity or to large shrinkages due to substantial differences in density between the starting polymer precursor and the final ceramic product. Typical polymer densities are $\sim$1 g/cm^3, while densities of the pyrolyzed product can range from $\sim$2 to $\sim$6 g/cm^3.[16] This density difference often results in linear shrinkages in excess of 30% during pyrolysis. Furthermore, if structural changes in the polymer derived phase cannot be relaxed by either viscous flow or diffusional processes, extensive cracking and pore formation generally destroy the integrity of the component.

3.2 Advantages over Conventional Fabrication Methods

The preceramic polymer route numerous advantages over conventional processing methods. These include the following:

- processing versatility, e.g., plastic forming ability
- lower temperature processing

- high purity
- preparation of metastable phases typically un-achievable by conventional methods
- Near-Net shape processing capability

3.3 Synthesis and Chemistry of Preceramic Polymers

Since the focus of this thesis is not on the synthesis of the preceramic polymers, but rather on utilizing preceramic polymer technology to develop new ceramic system, only a brief and basic review of synthesis techniques will be presented. Furthermore, the focus of the literature review will be on synthesis of silicon based preceramic polymers with further emphasis on poly(siloxanes).

The actual chemical structure, molecular size, and molecular size distribution of an organosilicon polymer are determined by the nature of the starting reagents and their processing parameters; however, in general, chloro-organosilicon compounds, e.g., dichlorodimethylsilanes and trichloromethylsilanes, are employed as precursors to manufacture silicon containing preceramic polymer. Chlorosilanes are commonly formed as by-products in the silicone industry; hence, they are relatively inexpensive and readily available. Most silicones are produced from a process utilizing the Rochow reaction which allows for the direct reaction of organic halides with silicon metal in the presence of an electron-transfer catalyst (usually copper). Although dimethyldichlorosilane is the predominant reaction product, methyltrishlorosilane and trimethylchlorosilane are also produced in smaller quantities.

The basic reaction employed to produce preceramic polymers is similar to the Wurtz synthesis reaction which essentially involves dechlorination of mixtures of various chlorinated silane monomers in the presence of catalyst.[17] A variety of preceramic polymers can be synthesized utilizing the reaction [1, 3] which include poly-(silanes), -(carbosilanes), -(silazanes), -(borosilazanes), -(silsesquioxanes)

and -(carbosiloxanes).

$$xMe_2SiCl_2 + 2xNa \longrightarrow (Me_2Si)_x + 2xNaCl \tag{3.1}$$

$$(Me_2Si)_x + heat\ (350°C) \longrightarrow (MeHSiCH_2)_x \tag{3.2}$$

$$(MeHSiCH_2)_x + air \longrightarrow (MeO_{1/2}SiCH_2)_x \tag{3.3}$$

$$(MeO_{1/2}SiCH_2)_x + heat\ (1200°C) \longrightarrow SiC \tag{3.4}$$

Metallorganic compounds in monomeric, oligomeric, or polymeric forms have been employed for production of non-oxide ceramic materials since 1960; however, it was only after the work of Yajima *et al.* that the preceramic polymer field was extensively studied and further developed. Yajima *et al.*[8] in 1975 was the first to prepare SiC containing ceramic fibers from a polymeric precursor. Their process, shown as Eq. (3.1-3.4), is based on permethylpoly(silanes), produced from dimethyldichlorosilanes by a Wurtz coupling reaction with sodium [reaction (3.1)]. Thermal decomposition of the permethylpoly(silanes) at 350°C, catalyzed by 3 to 5% poly(borodiphenylsiloxane), yield a poly(carbosilane) [reaction (3.2)]. The poly(carbosilane) is fabricated to remove both higher and lower molecular weight fractions. The mid-range fraction, with a number average molecular weight of 1000 to 2000, is considered to possess properties suitable for melt spinning into 10 to 20 μm diameter fibers. The fibers are cross-linked by oxidation of Si-H bonds by heating in air at ∼110 to 190°C [reaction (3.3)] and finally pyrolyzed at ∼1200°C in an inert atmosphere to produce SiC fibers [reaction (3.4)].

According to Whitmarsh and Interrante, Yajima's original polymer contained twice the stoiciometric amount of carbon and was treated with various cross-linking agents that introduce contaminants. This resulted in a final pyrolysis product that contained significant amount of excess carbon and silica which greatly degraded the high temperature performance of the fibers. Consequently, since the early work of Yajima, a variety of polymers have been synthesized and pyrolyzed with the intend of obtaining high yield precursors to pure SiC fibers.

Examples of such includehe following: poly(silanes),[1, 3, 18, 19] poly(carbosilanes),[1, 3, 18, 19, 20] poly(silastyrenes)[1, 3] and copolymers derived from disilaryls, vinylsilanes, allylsilanes. A description of the synthesis processes for these precursors will not be given; however, it is important to recognize that the bulk of the starting reagents for a majority of the precursors mentioned above were chlorosilanes or derivatives thereof.

Most polymeric precursors for SiC, possess either a Si-Si poly(silane) or Si-C poly(carbosilane) backbone. Basic differences in the precursors arises from differences in chemical structure, e.g., linear, branched, or cyclic, and the nature of functional side groups attached to the polymeric backbone, e.g., phenyl, vinyl, methyl, or hydrogen. The structure and the nature of the functional side groups have been shown to significantly affect the polymer's ceramic yield as well as the free carbon content in resulting pyrolysis product. For example, Carlsson *et al.*[18] discovered that by substituting methyl groups for phenyl groups on a poly(silane), the ceramic yield of the polymer decreased from ∼75 wt.% to 30 wt.%, while the SiC yield (percent of ceramic yield constituted by SiC) increased from ∼0.8% to ∼13.7% (extremely low yields).

Simple variation in synthesis parameters are often employed to manufacture precursors to other important ceramic material which includes silicon nitride and boron nitride; however, the starting reactants are again almost always organochlorosilanes. For example, reacting dichlorosilanes or organotrichlorosilanes with ammonia, shown as reactions (Eqs.3.5−3.6) below, result in silazane or organosilsesquiazanes (Si-N-Si backbone) polymers, which after pyrolysis at 1200°C led to form silicon nitride or a mixture of silicon carbide and silicon nitride.[21]

$$H_2SiCl_2 + xNH_3 \longrightarrow (H_2SiNH)_x + NH_4Cl \tag{3.5}$$

$$RSiCl_3 + xNH_3 \longrightarrow [RSi(NH)_{3/2}]_x + NH_4Cl \tag{3.6}$$

Examples of precursors to ceramic products other than SiC, which have achieved significance, include the following: vinlylitic poly(silane),[22] poly(silazanes) from $[H_2SiNCH_3]$,[23] poly(silazanes) from $[SiHCl_3]$,[24] and hydridopoly(silazanes),[25] for Si_3N_4; poly(silazanes) from $[CH_3SiHCl_2]$ for Si_3N_4/SiC, poly(iminoalanes) for

AlN, and borosilazanes for BN.[26]

Employing chlorosilane with variable molar functionalities (f), such as triethylchlorosilane where f = 1 or dimethyldichlorosilane where f = 2, allows for modification of polymer structures to form linear to highly branched polymers. Such synthesis versatility can be used to tailor certain important precursor properties, such as viscosity and solubility. Furthermore, through careful control of synthesis parameters, ceramic yields of the polymer can be improved, where polymers with yields in excess of 70 wt.% are considered to be of particular interest for the manufacture of monolithic ceramics. Most polymers that possess an inorganic backbone contain substituents on some or all of the backbone atoms. The substituents are usually hydrogen or organic groups, but can be of other types. During pyrolysis, these substituents are either incorporated into the ceramic product or evolved as volatiles. Obviously, the higher the ceramic yield, the smaller the quantity of evolved volatiles during pyrolysis. If a large quantity of volatiles are evolved over a narrow temperature range during pyrolysis, cracking or rupture of the ceramic product may occur. Thus high ceramic yields are important not only economically, but also in compensating for significant density changes in going from polymer to ceramic. Table: 3.1 lists the ceramic yields of several important organosilicon polymers currently being employed to manufacture silicon-containing ceramics.

Little is known of the chemical processes by which polymers are converted to ceramics. IR, thermal gravimetric analysis (TGA), and x-ray data have been used to study the gross features of the conversion process. Considering the complex polymer structures that serve as precursors, and the even more complex, amorphous, intractable structures that are intermediates in the pyrolysis process, it is clear that mechanistic studies pose a formidable challenge. Despite a lack of detailed chemical knowledge, some trends with respect to structure/yield relationship on *unconfined* pyrolysis are summarized by Wynne and Rice.[1]

1. Linear polymers give negligible ceramic yield because of reversion reactions, i.e. the generation of large, volatile molecules and cyclics. This feature is particular clear for polymers with Si-Si, Si-C, and Si-C-N backbone structures.

2. Polymer structures containing rings (or cages) give good ceramic yields.

Ring or cage structures slow the kinetic of reversion reactions, as the liberation of relatively large, volatile molecular fragments (e.g. cyclics), which are responsible for rapid weight loss, is sterically hindered and requires multiple chemical bonds rupture. However, solid state cross-linking necessary for preceramic structure buildup, which involves localized reactions and the evolution of smaller molecules H_2, HCl, CH_4), proceeds continuously. Carborane siloxane polymer give high ceramic yields (Table: 3.1) because of the presence of the 12-atoms C_2B_{10} cage in the polymer microstructure.

3. Branched-ring polymer structures give high ceramic yields. The combination of branched and ring structures markedly slows the kinetics of reversion reactions, and most successful preceramic polymers developed thus fall into this category.

Apart from *nonoxide* ceramics, *oxide* ceramics represents a separate class in engineering ceramics. A brief overview will be given of the past utilization of metal-organics in producing fine-powder derived monolithic ceramics and sol-gel derived ceramics.

Several classes of metal-organic compounds can be converted into oxide ceramic materials: metal alkoxides, $M(OR)_n$, $M(HCOO)_n$, $M(CH_3COCHCOCH_3)_n$, $M(C_xH_{2x+1})_n$, $M(OCOC_xH_{2x+1})_n$. Of these metal-organic compounds, the metal alkoxides and the metal acetates are more frequently utilized in forming ceramic materials.

Roy *et al.* recognized the usefulness and flexibility provided by the hydrothermal decomposition of metal-organic precursors for forming ceramics. Mazdiyasni *et al.* utilized several metal alkoxides for synthesizing various types of submicron particle size ceramic powders and monolithic ceramics. Most metal-organic compounds are very sensitive to moisture, heat, and light. These conditions necessitate the need for controlled atmospheres and very clean reaction equipment for the synthesis of metal alkoxides. Exposure of most alkoxides to moisture and/or heat causes a decomposition of the alkoxide, and thus provides a method for forming fine ceramic materials. A few examples for decomposing the metal-organic compounds are thermal decomposition, hydrolytic decomposition, and flame spray decomposition.

The direct pyrolysis of the metal alkoxides, which form very fine ceramic pow-

Polymer Precursor	**Atm.**	**Pyrolysis Product**	**Ceramic Yield**	**Ref.**
Poly(methylsilane)	Ar	SiC	0.85	(27)
Poly(methylvinylsilane)	Ar	SiC	0.83	(28)
Tetraphenylsilane	Ar	SiC	0.06	(29)
Diphenyldipropenylsilane	Ar	SiC	0.03	(29)
Poly(carbosilane) + Ti-butoxide	N_2	SiC/TiC	0.72	(30)
Poly(titanocarbosilane)	N_2	$SiC_xO_yTi_z$	0.75	(31)
Poly(silaethylene)	N_2	SiC	0.87	(29)
Poly(hydridosilazane)	N_2	Si_3N_4	0.74	(25)
Poly(methylsilazane)	NH_3	Si_3N_4	0.85	(29),(32)
Poly(vinylsilazane)	N_2	SiC_xN_y/C	0.85	(33)
Poly(vinylphenylsilazane)	N_2	Si_3N_4	0.85	(34)
Poly(cyclomethylsilazane)	Ar	Si_3N_4/SiC	0.88	(35)
Poly(borosilazane)	Ar	BN/Si_3N_4	0.90	(36)
Carborane-siloxane	Ar	SiC/B_4C	0.70	(28)
Ammonioborane	N_2	BN	0.65	(28)
Poly(boronsiliconimide)	NH_3	SiB_xN_y	0.72	(37)
Poly(methylsiloxane)	He	SiO_xC_y	0.85	(29)
Poly(phenylsilsesquioxane)	Ar	SiO_xC_y	0.78	(38)

Table 3.1: Ceramic yields of silicon containing preceramic polymers.

ders, was reported by Mazdiyasni. The overall thermal decomposition of a liquid zirconium tertiary butoxide [Eq. (3.7)] to ZrO_2 is as follows:

$$Zr(OR)_4 \xrightarrow{\triangle} ZrO_2 + 2ROH + Olefin \tag{3.7}$$

The thermal decomposition method is very rapid and the products formed are volatile olefins, alcohols, and fine ceramic powders.

The hydrolytic decomposition of metal alkoxides, with subsequent dehydration, has been used to form many types of fine ceramic powders. The decompo-

sition of the metal-organic is initiated via the hydrolytic reaction of the water with subsequent thermal dehydration of the resulting precipitates. The general decomposition is described as a two-step process:

Hydrolysis

$$M(OR)_{\mathrm{n}} + nH_2O \quad \longrightarrow M(OH)_{\mathrm{n}} + nR(OH) \tag{3.8}$$

Dehydration

$$M(OH)_{\mathrm{n}} \quad \longrightarrow MO_{\mathrm{n}/2} + \frac{n}{2}\ H_2O \tag{3.9}$$

These reactions usually occur below 600°C and results in the formation of very fine ceramic particulates, i.e., 2−5 nm. This method has been used to make high-purity submicron sized oxides from several metal alkoxides. Flame hydrolysis of metal-organic precursors, used for the formation of many oxides from metal halides, involves the direct oxidation of a metal-organic compound in gas oxygen flame. For example:

$$Si(CH_3)_4 + 8O_2 \quad \longrightarrow SiO_2 + CO_2 + H_2O \tag{3.10}$$

Metal-organics are also used in the field of sol-gel processing of ceramics. There are two general ceramic processing methods.

Method one: The colloidal process method is based on the use of surface chemistry for suspending ultrafine particles in a solution to form a colloidal sol. The subsequent formation of a cross-linked particulate network induces the gellation of the sol suspension. The gel material can then be dried to form a porous ceramic body which may then be densified by sintering.

Method two: The metal-organic polymerization method utilizes the reactivity of metal-organic precursors. The metal-organic precursors are polymerized by controlled hydrolysis which results in the formation of a cross-linked amorphous gel. These gelled materials can also be dried and sintered into ceramic bodies.

3.4 Silicon Oxycarbide: General

Silicon oxycarbide is a term used to denote the chemical structure in which silicon is simultaneously bonded with carbon and oxygen. These tetrahedral network species can be generally described as $[SiC_xO_{4-x}]$ where x = 1, 2, or 3. The incorporation of carbon in silicate glasses presents the possibility of replacing some oxygen, which is only two-coordinated, with carbon which can be four-coordinated. This increased bonding per anion is expected to strengthen the molecular structure of the glass network, and thereby, to improve the thermal and mechanical properties.

Attempts to manufacture silicon oxycarbide glasses can be traced back to the 1950's when Ellis was one of the first to attempt incorporation of carbon into glass.[39] Ellis infiltrated porous Vycor^{TM} glass with aqueous solutions of carbohydrates and subsequently heated the body in an inert atmosphere at 1200°C to decompose the carbohydrate to carbon. The presence of carbon in the interconnected porosity of the glass made the body electrically conductive. The low-temperature resistivity of the glass was found to depend on the amount, size and shape of the carbon particles. Smith and Crandall,[40] hot-pressed a mixture of fine colloidal silica and carbowax at 1000-1150°C and 2000 psi to obtain a dense mass of glass containing 1.2 wt.% carbon. This glass, wherein the carbon was "physically inseparable and microscopically indistinguishable from silica", was found to exhibit a greater resistance to devitrification and a higher viscosity than pure vitreous silica. This result was significant because the usefulness of fused silica is limited at temperatures over 1000°C due to the formation of cristobalite. Elmer and Meissner[41] incorporated carbon into porous (high-silica) glasses by impregnation with furfuryl alcohol and heat treatment in nitrogen at 1250°C. A marked increase in the annealing point was observed as a result of carbon incorporation. This increase was attributed to the removal of hydroxyl group from the porous glass by carbon.

Homeny *et al.*[42] used SiC as the carbon source and synthesized glasses containing up to 2.5% carbon in the Mg-Al-Si-O-C system by melting at 1750-1800°C under nitrogen. Due to the high temperature melting and consequent loss of CO, CO_2, and SiO gases, the final compositions were difficult to control. The synthesized glasses were shown to be homogeneous (except for a few metallic inclusions)

and free of crystallites by X-ray diffraction and electron microscopy examination. The Mg-Al-Si-O-C glasses showed an increase in density, Young's modulus, Shear modulus, Vicker's hardness and fracture toughness with increasing carbon content. Coon[43] studied the effect of silicon carbide additions on the crystallization behavior of a Mg-Li-Al-Si-O glass. SiC was mixed into a Mg-Li-Al-Si-O glass melt and then the black glass was heat treated to study its crystallization behavior. The carbon containing glass was found to be much more refractory than the parent glass.

In all these studies of carbon-containing glasses, separate sources for silica and carbon were mixed and pyrolyzed at high temperature to allow them to react to yield *intimate* mixture of the two phases. There was no verification of carbon substitution in the glass network in any of these studies. In fact, the early products can be best described as "black glasses", which contains second phase dispersions of elemental carbon. In these studies, the property changes supported the idea of a silicon oxycarbide structure, but it is also possible that reduction or dehydroxylation of the glass (by the carbon additions) caused the property variations. By comparison, according to Zhang and Pantano,[44] true silicon oxycarbide glasses should be homogeneous glasses where carbon and oxygen atoms share bonds with silicon in an amorphous, continuous network structure.

It is also important to point out that there are no known thermodynamically stable phases of silicon oxycarbide. This is in contrast to the situation with silicon oxynitride glasses where there exists the equilibrium crystalline phase Si_2N_2O. This probably accounts for the greater ease of melt synthesis of silicon oxynitride glasses. Nevertheless, the existence of amorphous, metastable silicon oxycarbide phases has been confirmed in a number of studies.

In a study of the oxidation product of SiC, Pampuch *et al.*[45] obtained evidence for the existence of a ternary SiOC phase situated between the silica layer and the SiC. The SiC powder was cleaned with HF solution, and was then subjected to varying degrees of oxidation conditions in the temperature range of 675 to 1775 K. The solid oxidation products were analyzed using SEM, X-ray photoelectron spectroscopy (XPS), infrared spectroscopy and X-ray microanalysis. The presence of a considerable amount of SiOC phase was indicated by all the analytical methods. An extra Si-2p peak, with binding energy higher than that of the Si-2p peak of SiC but lower than that of the Si-2p peak in SiO_2, was found

in samples heat treated below 1575 K. The additional peak was claimed to be due to the formation of SiOC phase. The infrared spectra showed some unique peaks, and suggested that this ternary phase was present at intermediate stages of oxidation of SiC, and was not stable above oxidation temperatures of 1400- 1500 K. More recently Yurkov and Polyak [46] re-examined the oxide/silicon-carbide interface and confirmed the formation of silicon oxycarbide phase.

Lipowitz *et al.*[47],[48] studied the synthesis, composition, structure and properties of polymer-derived ceramic fibers (NICALON). They performed extensive structural characterization by X-ray diffraction, ^{29}Si NMR, IR, Raman, XPS, and Auger depth-profile analysis. They found that the microstructure contained a continuous, amorphous SiOC phase with nano-crystalline β-SiC. TEM micrograph revealed that the β-SiC crystals, in the size range of 4.0−2.6 nm, were embedded in this amorphous matrix. ^{29}Si NMR proved to be the most useful method for characterizing the oxycarbide phase. It showed a broad peak covering the range of SiC (-15 to -25 ppm), $CSiO_3$ (-70 ppm), $C_2Si_2O_2$ (-30 ppm), and C_3SiO (10 ppm). XPS analysis showed a Si-2p peak which did not correspond to SiO_2 or SiC. The binding energy value was between that of SiO_2 and SiC and was considered to be the binding energy of Si-2p photoelectron in the oxycarbide amorphous phase.

The formation of SiOC intermediate phase has also been found by White *et al.*[49],[50] in the synthesis of high surface area SiC powder. Gels were synthesized from organosilicon precursors having various organic groups using sol-gel processing. A black "glassy, carbon containing silica phase" was observed upon pyrolysis of the gels at temperatures close to 1000°C under inert atmospheres. Pyrolysis at 1500°C typically yielded large, shiny black particles containing a partially crystalline and partially amorphous mixture of SiC, carbon and silica. Since the focus of their work was to synthesize SiC, the nature of the black glassy was not studied in any detail.

It is now widely recognized that the chemical/polymer-processing of silicon carbide and especially fibers such as Nicalon, can create a silicon oxycarbide phase. The thermal stability of this phase is fundamental to the high temperature behavior of these important engineering materials. Thus the widespread interest in chemical/polymer-processing of silicon carbide ceramics has provided an additional driving force for synthesis and study of the phase−pure silicon

oxycarbide.

3.4.1 Processing of Silicon Oxycarbide Glasses

Currently two methods are in use for synthesis of SiOC glasses namely, sol gel processing of organosilicon compounds and direct pyrolysis of silicone resins. The following parts covers an brief review, which will focus mainly on the preceramic polymer processing, polymer to ceramic transformation characterization.

3.4.1.1 Processing of Silicon Oxycarbide Glasses: Sol-Gel Method

The sol-gel process has enabled the low-temperature synthesis of silicon oxycarbide glasses without the problem of decomposition and oxidation during melting. This is achieved through the use of polymeric precursors containing Si-C bonds; viz, organically-modified alkoxysilanes of the general formula$-[R_xSi(OR´)_{4-x}]$. These precursors provide a direct Si-C bonds in the starting solution which is preserved in the gel and glass structures. In this way, carbon could be retained, and most importantly, some of the carbon is covalently bonded to the central silicon cation. This is in contrast to the alkoxysilanes $[Si(OR)_4]$ which was commonly used for sol/gel synthesis of silica glass. In the case of these modified alkoxysilanes, one or more of the alkoxy groups are replaced by saturated (e.g., CH_3, C_2H_5, C_3H_7) or unsaturated (e.g., C_2H_3, C_6H_5) 'R' group(s). The carbon chain length, and the number and nature of 'R' group modifications, allow a control of the amount of carbon introduced. An additional degree of compositional control is afforded by mixing the organically-modified alkoxysilanes, in desired molar ratios, with other alkoxysilanes. The gels, obtained after hydrolysis and condensation of the precursors, contains Si atoms bonded simultaneously to oxygen and carbon atoms.

Chi[49] reported on the sol/gel processing of monolithic glasses from mixtures of tetraethylorthosilicate (TEOS) $[Si(OC_2H_5)_4]$ and methyltrimethoxysilane (MTMS) $[CH_3Si(OCH_3)_3]$, cohydrolyzed and mixed with colloidal alumina monohydrate and colloidal silica fillers. Upon pyrolysis in argon at 1200°C, the gels turned black. The maximum carbon content was 12.5%. Only limited structural characterization was reported on these gels and glasses, but the black glass showed very high thermal stability and resistance to crystallization.

A systematic series of silane precursors were used to prepare oxycarbide glasses by Zhang and Pantano.[44),(51)] Methyl-, ethyl-, propyl- and phenyl-trimethoxysilanes with chemical formulae $CH_3Si(OCH_3)_3$, $C_2H_5Si(OCH_3)_3$, $C_3H_7Si(OCH_3)_3$, C_6H_5-$Si(OCH_3)_3$, respectively, were hydrolyzed in H_2O (1:6 molar) and ethanol (1:1 volume) using HCl as the catalyst. ^{1}H NMR indicated that the majority of Si-OR groups had been hydrolyzed to Si-OH, while the methyl, ethyl, propyl and phenyl groups bonded directly to Si, were retained. Ammoniated solutions were added to initiate the gelation which occurred within a few days to several weeks. ^{13}C and ^{29}Si MAS NMR of these gels showed that the alkyl groups were still present in the gels, while the Si-OH terminal bonds had been largely replaced by Si-O-Si through condensation. The dried gels were translucent, but turned black upon heat treatment in argon at 800-1000°C. X-ray and electron diffraction confirmed the amorphous state of these materials. Detailed investigation of the structural evolution during all stages of transformation is reported. ^{29}Si NMR of liquid precursor [methyltriethoxysilane (MTES)] exhibit one type of Si-species. Sharp signal is observed due to the rotational degrees of freedom provided in the liquid state. The amorphous, solid-state of the gel and glass causes the broadening of the lines. The dried gel shows two types of Si-species. One is a Si tetrahedra with two non-bridging sites (Si-CH_3 and Si-OH) and two bridging oxygen sites. The other is a Si tetrahedra with one non-bridging site (Si-CH_3) and three bridging oxygen sites.[51)] Obviously, these species confirm to the chemical structure that defines a silicon oxycarbide. The final black glass has a wider distribution of Si-species, and clearly, two of these have been created during the pyrolysis step. One of the new line is due to a silicon-oxygen tertahedra$-[SiO_4]$. This is the usual building block of silicate glasses, and its presence here indicates that some decomposition of the oxycarbide species occurred in the gel during pyrolysis. The other new species that forms during the pyrolysis is a Si tetrahedra with two bridging oxygens and two carbon bonds, i.e., $[C_2SiO_2]$. Clearly, these species were created through condensation and/or exchange reaction during pyrolysis of the gel. It has to be emphasized that these ^{29}Si NMR spectra cannot characterize the functionality of the carbon bonded to silicon; i.e., they can be non-bridging methyl groups ($\equiv$Si-CH_3), or bridging groups such as $\equiv$Si-CH_2-Si or even $[CSi_4]$.

A number of studies have focused on the effects of precursor chemistry on the

carbon-content of the gels and glasses. Zhang and Pantano also studied the effect of increasing carbon chain length on the amount of carbon retained in gels and glasses. Precursors having *saturated* hydrocarbon groups modifications, e.g., methyl, ethyl, propyl groups attached directly to the Si atom were subjected to hydrolysis and condensation. The carbon content of the gels was found to increase proportionally with increasing carbon chain length of the alkyl group. Yet the carbon content of the oxycarbide glasses obtained after pyrolysis at 900°C did not show a proportional increase with carbon content of the precursor/gel. Oxycarbide glasses obtained from metyltrimethoxysilane (MTMS) and propyltrimethoxysilane (PTMS) precursor displayed nearly equal carbon contents. A clear trend towards increasing oxycarbide fraction with a decreasing content of carbon in the alkyl group is observed in ^{29}Si NMR. But in general, about 45% of the silicon is bonded with one carbon and 3 oxygens [$CSiO_3$], about 45% of the silicon is bonded with 4 oxygens [SiO_4], and about 10% of the silicon atoms are bonded with 2 carbons and 2 oxygens [C_2SiO_2]. Thus it is proposed that only the carbon atom bonded directly to Si atom can be retained in the glass structure. The cleavage of the Si-C bonds in the PTMS gels before the high temperature thermal decomposition is attributed to the kinetics of β-elimination reactions, which are known to occur at temperatures <450°C in silicon compounds.

Gels and glasses synthesized from precursors having *unsaturated* hydrocarbon modifications (e.g., vinyl, allyl and phenyl groups) behave differently. Comparisons were made between the carbon contents of glasses obtained at 900°C from gels modified by saturated and unsaturated organic groups containing the same number of carbon atoms. Comparison of the results of the ethyl (C_2H_5) gels vs. vinyl ($H_2C{=}CH$) gels, and propyl (C_3H_7) gels vs. allyl ($H_2C{=}CHCH_2$) gels showed much higher carbon-contents in the glasses made from gels containing unsaturated organic groups.

One of the key issues in synthesis is the ability to maximize retention of Si-C bonds (and thereby to minimize formation of free carbon). This problem has been successfully addressed through the introduction of reactive Si-H groups in the precursors; i.e., one or more of the Si-O bonds of the precursor are replaced by Si-H bonds. The Si-H bonds initiate early cross-linking of the network through reactions with the Si-C_xH_y bonds, and therefore polymerize the network through

Si-C-Si bridges. This is represented by the following reaction:

$$\equiv Si - H + CH_3 - Si \equiv \longrightarrow \equiv Si - CH_2 - Si \equiv + H_2 \qquad (3.11)$$

Singh and Pantano compared oxycarbide gels and glasses made from methyltrimethoxysilane {(MTMS) -[$CH_3Si(OCH_3)_3$]} with those made from methyldimethoxysilane {(MDMS) -[$CH_3HSi(OCH_3)_2$]}. The MDMS precursor possesses a Si-H functionality in addition to the Si-CH_3 ligand. MDMS and MTMS were mixed in various ratios with TEOS on order to vary the carbon content of the gels. The effect of the Si-H functionally upon the condensation of the oxycarbide network were investigated. It was found that the Si-H bonds survived the acidic hydrolysis and remained intact in the gel structures. Clear appearance of Si-CH_2-Si linkages (FTIR spectra: wave number 1360 cm^{-1}) through the reaction of the Si-H bonds with the methyl groups at temperatures below 500°C. A significantly higher oxycarbide fraction in the MDMS glasses is obtained after pyrolysis.

Further enhancement in the network cross-linking, and hence enhancement in oxycarbide content, were achieved by using Si-H bonds in both precursors: i.e., by mixing MDMS with triethoxysilane {(TES)-[$HSi(OCH_3)_3$]}.

Similar results on the effect of Si-H bonds have been obtained by Babonneau *et al.* and Soraru *et al.*[50],[52],[53] ^{29}Si NMR spectra of the gels were obtained to characterize the presence of Si-H in the gels, and also to measure the relative intensity of the oxycarbide phases in the various systems. The systems with the greatest amount of Si-H in the precursor gel exhibited the highest concentration of Si-C bonds, and at 1000°C, [SiC_4] species had already formed. Thus, it seems certain that the use of reactive groups such as Si-H can enhance the formation of stable oxycarbide species, and thereby, limit the creation of free carbon species. A different approach was proposed by Belot *et al.*[54],[55] The idea, in this case, was to use methyl-substituted silica gel having Si-Si bonds in order to reduce the total oxygen content of the system and favor the incorporation of tetravalent carbon in the oxide structure.

In order to compare the effectiveness of the different synthetic methods in the formation of oxycarbide phases, the amount of carbidic and free carbon should be estimated. This was done on the basis of chemical analysis (Si, O, C) considering the ideal stoichiometry, $SiO_{2-x}C_{x/2}$, and neglecting, as a first approximation, the

Precursor[a]	**Gel Precursors**			**Black Glasses**		
	Si [(b)] *units*	*O/Si* [(c)]	*C/Si* [(d)]	*Chemical Formula*	*C/Si* [(d)]	C_{free} % [(e)]
MTMS [(44)]	T	1.5	1	$SiO_{1.26}C_{1.26}$	(0.37)	34
MTMS[(44)]	T	1.5 [1.7]	1 [1]		[0.18]	80
TREOS/ MDMS1/1[(50),b]	T^H D^H	1.25 (1.4) [1.28]	0.5(0.51) [0.50]	$SiO_{1.45}C_{0.47}$	(0.28) [0.31]	40
TREOS/ MDMS2/1	T^H D^H	1.33 (1.4) [1.35]	0.33(0.35) [0.32]	$SiO_{1.39}C_{0.32}$	(0.31) [0.34]	3
TREOS/ MDMS 1/1[(50),b]	T^H T^H	1.5 (1.78) [1.67]		$SiO_{1.65}C_{0.54}$	(0.17) [0.16]	68
TEOS/ MDMS 1/1[(50),b]	Q D^H	1.5 (1.67) 1.64	0.5 (0.64)	$SiO_{1.67}C_{0.53}$	(0.16) [0.15]	70
TEOS/ MDMS 1/1[(50),b]	Q D^H	1.5 [1.6]	1	$SiO_{1.79}C_{0.50}$	(0.11)	78
$Me_2Si_2O_2$[(54),b]		1 (1.14)	1 (1)	$SiO_{1.30}C_{0.77}$	(0.35)	54
Ethoxy-subst. PCS[(54)]	T D	1 (1.75)	1 (1.46)	$SiO_{1.44}C_{0.88}$	(0.28) [0.36]	68
TEOS/ + MDMS 1/1[(50),b]	Q D^H	1.5 (1.67) [1.56]	1 (0.97)	$SiO_{1.55}C_{0.56}$	(0.22) [0.23]	60

[a]Nomenclature: MTMS: Methyl-trimethoxysilane, $MeSi(OMe)_3$; TREOS: Triethoxysilane, $HSi(OEt)_3$; MDMS: Methyl-diethoxysilane, $MeHSi(OEt)_2$; DMDES: Dimethyldiethoxysilane, $MeSi(OEt)_2$.

[b]Silicon units are designed according to the conventional silicon chemistry: $(Si)O_4$:Q; $C(Si)O_3$:T; $C_2(Si)O_2$:D; $C_3(Si)O$:M; $C_4(Si)$: X; $H(Si)O_3$: T^H, $CH(Si)O_2$:D^H

[c]Theoretical values; measured values from chemical analysis ( ); estimated values from ^{29}Si MAS NMR data [ ].

[d]C/Si ratio of the $SiO_{2-x}C_{x/2}$ phase: derived from chemical analysis ( ), derived from ^{29}Si MAS NMR study [ ].

[e]Calculated as $100(C_{total}\text{-}C_{oxy})/C_{total}$, C_{oxy} value derived from chemical analysis data.

Table 3.2: Various equivalence measured by chemical analysis and MAS-NMR for precursor gels and corresponding black glasses.

presence of residual hydrogen; indeed less than 1 wt.% of H is usually measured on materials fired at temperature ≥1000°C. Thus, from the experimental O/Si ratio, it is possible to estimated the C/Si ratio in the stoichiometric oxycarbide phase, as well as the amount of C_{free}.

A different approach to the quantitative evaluation of the oxycarbide phase is based on ^{29}Si MAS NMR analysis. This technique allows a quantitative evaluation of the various silicon units, $SiO_{2-x}C_{x/2}$ in the oxycarbide network. By assuming that each carbon atom, in the mixed oxycarbide units, is shared between four silicon atoms, it is possible to derived the $(C/Si)_{oxy}$ ratio. The comparison of this value with the chemical analysis leads to the estimation of the amount of free carbon.

Table: 3.2 shows literature data on various oxycarbide glasses obtained from different precursors. The amount of carbidic and free carbon have been extracted from the reported chemical composition and from NMR results. The main silicon units in the starting gels as well as the theoretical and experimental values of $(O/Si)_{gel}$ and $(C/Si)_{gel}$ have also been reported. All the oxycarbide phases synthesized so far have a $(C/Si)_{oxy}$ ratio in the range $0.10-0.38$ and a C_{free} content between 24 and 90%. The amount of $(C/Si)_{oxy}$ seems closely related to the $(O/Si)_{gel}$ ratio in the precursor gels. The general trend of an increase of $(C/Si)_{oxy}$ when $(O/Si)_{gel}$ decreases is evident. This fact implies that the nature of Si-O bonds in the system does not change during the pyrolysis process. In fact the pyrolytic transformation from the gel to the black body is a very complicated process far from being fully understood. It has been shown for many alkyl substituted silica gels that the redistribution reactions between Si-O, Si-C and Si-H groups can occur in the early stage of the pyrolysis with the evolution of various silane compounds and thus, can lead to a variation of O/Si and C/Si ratio. Moreover, as seen in Table: 3.2, for the systems, namely MTMS-derived gels and the ethoxy-substituted PCS, chemical processes leading to a decrease of the O/Si ratio must be active at some stage of the pyrolysis process. Actually, the later system shows quite different behavior compared to the others, inspite of a high $(O/Si)_{gel}$ ratio (1.75), the corresponding oxycarbide phase is rich in carbide carbon, $(C/Si)_{oxy} = 0.28$.

To obtain a black glass with no or low C_{free} content, all the carbon atoms which are not incorporated in the silicon oxycarbide network should be removed from

the system as volatile species. As already pointed out, the maximum amount of carbon that can be incorporated into the black glass can be estimated from the oxygen content of the gel $(O/Si)_{gel}$ through the stoichiometric relationship, i.e., $(C/Si)_{stoich.} = [2 - (O/Si)_{gel}]/2$. Thus by comparing the experimental value $(C/Si)_{gel}$ with the stoichiometric one, it is possible to estimate the amount of carbon that has to be removed from the system if a C_{free} oxycarbide phase is desired. The data indicated in Table: 3.2 show that generally $(C/Si)_{gel}$ is much larger than $(C/Si)_{stoich.}$ and this partially explains the high amount of C_{free} in the corresponding black glasses.

3.4.1.2 Processing of Silicon Oxycarbide Glasses: Silicone Resins

Although the sol-gel process can be versatile because of the advantage of low-temperature processing, drawbacks such as shrinkage and cracking, caused by solvent or byproducts evolution during drying and pyrolysis steps have motivated research to search for new synthetic methods for this class of materials. For example, the volume changes associated with the sol-gel processes and with the pyrolytic conversion of the precursor to the ceramic materials, must be minimized, to maximized the ceramic yield and the densification during the ceramic conversion step. Consequently the selection of suitable polymers which have low shrinkage, larger ceramic yield as well as easy processing properties, is fundamental to the development of useful ceramic composites. It would therefore be desirable to select a precursor with the ability to effectively cross-link before pyrolysis.

Recently, poly(siloxanes) have been used as precursors for ceramics and glasses such as silicon oxycarbide.[56],[57],[58] These polymers are generally known as silicones and can generate a broad range of products because there is a large number of different building blocks commercially available. Poly(siloxanes) or poly(organosiloxanes) are polymeric compounds comprise of Si-O-Si units as the polymeric backbone. The general formulae for poly(siloxanes) are $[R_2SiO]_n$ for linear or cyclic poly(siloxanes) and $[RSiO_{1.5}]_n$ for poly(silsesquioxanes). In general, polymers are synthesized via the hydrolysis and condensation of difunctional silanes and/or trifunctional silanes, $RSiX_3$, where the R can be a variety of alkyl or aryl groups and X is a hydrolyzable functional attachment such as an

alkoxy group or a chlorine atom. A majority of poly(siloxanes) contains units of general structure [$R_3SiO_{0.5}$], [R_2SiO], [$RSiO_{1.5}$], [SiO_2] where each R independently stands for hydrogen atoms, alkyl radicals containing 1 to 20 carbon atoms, phenyl radicals, and vinyl radicals. In general, poly(siloxane) containing phenyl groups posses lower ceramic yield and higher free carbon contents relative to poly(siloxanes) where R is exclusively methyl groups. Poly(siloxanes) which contain vinyl groups and hydrogen are often preferred since these groups attached to silicon provide a mechanism for curing by hydrosilyation reaction prior to pyrolysis, which lead to higher ceramic yields.

In 1989, Renlund *et al.*[56] reported on the production of a silicon oxycarbide glass by pyrolysis of a methylsilsesquioxane polymer. This silicone resin was from General Electric Silicon Products Div., Waterford, NY under trade name SR350. The resin was synthesized by a hydrolysis-condensation polymerization reaction of dimethyldichlorosilane (2-8%) and methyltrichlorosilane (92-98%). The structure of the resulting polymer was described as a partially branched silicon-oxygen chain with methyl and hydroxyl substituents, terminated by methyl groups. Ensuring pyrolysis of the resin in He at 1100°C resulted in a silicon oxycarbide glass. Rendlund proposed that it was the intimate mixture and bonding arrangement of Si, O, and C on the atomic scale in the polymeric precursor that allowed the formation of a metastable SiO_xC_y glass.

Siloxane polymers differ in the number of oxygen atoms per silicon and in the chemical composition of the ligands. Initially, it was not obvious how the stoichiometry and properties of the pyrolysis products should be related to that of the initial polymer. Therefore, chemical analysis was used to determine the stoichiometries of the ceramic products and other techniques to determine their properties. Wilson *et al* and co-author[58] showed that the stoichiometry of pyrolyzed siloxanes is easily estimated based on the initial polymer composition and the char yield, provided that the initial polymer is highly cross-linked or branched such that the parent backbone does not *unzip* and evaporate during heating. Assumption was made that the entire weight loss is due to carbon and hydrogen and that all the hydrogen leaves the materials. Chars of the same final stoichiometry can be prepared from polymers of different initial composition. For example, phenyl-containing polymers might be expected to give chars of different properties than those of vinyl or methyl-containing polymers, even if the final

Precursor	**Gel Precursors**			**Black Glasses**		
	Si [a] *units*	*O/Si* [b]	*C/Si* [c]	*Chemical Formula*	*C/Si* [d]	C_{free} % [d]
PMS [56]	T	1.5[e]	1	$SiO_{1.24}C_{1.50}$	(0.38)	24
Polysiloxane	T	1.25	3.75	$SiO_{1.33}C_{2.75}$	(0.33)	90
	M	1.29	[3.63]		[0.30]	
		(1.1)	(1.79)			
P1(50:50)	D + D^H	-	-	$(SiO_{1.01}C_{1.59}H_{0.37})$	[0.49]	69
[59][f]	M+T+Q	-	-	$[SiO_{1.02}C_{0.49}]$		
P3(80:20)		-	-	$(SiO_{1.30}C_{1.32}H_{0.39})$	[0.36]	73
		-	-	$[SiO_{1.28}C_{0.36}]$		
P6(97:3)		-	-	$(SiO_{1.55}C_{0.98}H_{0.30})$	[0.26]	73
		-	-	$[SiO_{1.47}C_{0.26}]$		
LM130 [60]	D+T[g]	[1.43]	[0.28]		[0][h]	
					[0.28][i]	
L901[60]	D+T[j]	[1.47]	[0.26]		[0][k]	
					[0.19][l]	

[a]Silicon units are designed according to the conventional silicon chemistry: $(Si)O_4$:Q; $C(Si)O_3$:T; $C_2(Si)O_2$:D; $C_3(Si)O$:M; $C_4(Si)$: X; $H(Si)O_3$: T^H, $CH(Si)O_2$:D^H

[b]Theoretical values; measured values from chemical analysis ( ); estimated values from ^{29}Si MAS NMR data [ ].

[c]C/Si ratio of the $SiO_{2-x}C_{x/2}$ phase: derived from chemical analysis ( ), derived from ^{29}Si MAS NMR study [ ].

[d]Calculated as $100(C_{total}\text{-}C_{oxy})/C_{total}$, C_{oxy} value derived from chemical analysis data.

[e]^{29}Si MAS NMR shows only 1 peak of fully condensed T units, however, no quantitative data of NMR or chemical analysis are presented

[f]Mixtures of PHMS:D^4Vi. The carbon atoms not taken into account in these NMR results were considered not bounded to silicon. The difference in carbon between elemental analysis and ^{29}Si NMR corresponds to free carbon.

[g]$0.13(D^2) + 0.09(T^2) + 0.78(T^3)$units

[h]Pyrolysis in air with $0.04(Q^3) + 0.96(Q^4)$ units.

[i]Pyrolysis in nitrogen, forming SiOC glass with $0.10C_4(Si) + 0.17C_2(Si)O_2 + 0.37C(Si)O_3 + 0.36(Si)O_4$ units.

[j]$0.06(D^2) + 0.15(T^2) + 0.66(T^3) + 0.13(T^2$ - Ar) units

[k]Pyrolysis in air with $0.04(Q^3) + 0.96(Q^4)$ units.

[l]Pyrolysis in nitrogen, forming SiOC glass with $0.08\ C_4(Si) + 0.10\ C_2(Si)O_2 + 0.25\ C(Si)O_3 + 0.57\ (Si)O_4$ units.

Table 3.3: Various equivalence measured by chemical analysis and MAS-NMR for commercial siloxanes and corresponding black glasses.

stoichiometries of the chars are identical. These authors address this question by examining three highly cross-linked poly(siloxane), so that they would produce roughly the same stoichiometry after pyrolysis to a sufficiently high temperature. Other resent work has shown that the initial chemical environment around silicon in a siloxane polymer is only maintained up to about 500°C. These authors state: "Further heating results in a scrambling of the silicon environment". On the basis of this, one expects these three materials pyrolyzed at 1000°C to show similar properties. The behavior of these materials upon electrochemical insertion of lithium was studied using lithium cell was reported. The electrochemical behavior upon the insertion and deinsertion of lithium into these materials is the same. Thus, authors concluded that it is the final char stoichiometry, not the precise nature of the starting polymer, which controls the bulk properties of the Si-O-C glasses. In resent work Soraru et al.[53] had indicated that the local environment of the Si is determined by the Si-O ratio in the char, which is related to the initial precursor. Wilson *et al.* argued that this, however does not mean that the overall structure of the char only depends on the Si-O ratio. Series of materials with the same Si-O ratio but with different amounts of carbon have been reported. These materials have different diffraction patterns and have different electrochemical behavior, which is controlled by the overall stoichiometry of the char and not by the local environment around Si, which is probably the same.

Synthesis of silicon oxycarbide is reported by Radovanovic *et al.*[59] from commercially available siloxanes. Polymer resulting from the hydrosilylation reaction between poly(methylsiloxane)(PMHS)[from Hüls], and 1,3,5,7-tetravinylcycletetrasiloxane (D_4Vi) [from Dow Corning] in the presence of platinum divinylcomplex as a catalyst, have been pyrolyzed to silicon oxycarbide ceramics, with ceramic yield varying as a function of the mixture composition. PMHS, as the majority of linear poly(organosiloxanes) gives negligible pyrolysis yields, due to the abundant extrusion of volatile cyclic oligomers during the firing process. However, when combined with compounds containing vinyl groups, this polymer can be cross-linked leading to elastomeric materials. The gelation time, which occurs between PMHS:D_4Vi mixture, after the catalyst addition, was directly proportional to the D_4Vi amount added. Also the amount of oxycarbide phase formed is related to on the amount of D_4Vi, i.e., decrease in the amount of D_4Vi as

indicated by (P6 precursor 97:3); refer in Table: 3.3, reduced the amount of oxycarbide phase along with increase in the C_{free} content. PMHS contains an excess of reactive Si-H groups, in relation to vinyl groups of the D_4Vi cyclic siloxane. These excess Si-H groups provide cross-linking sites. The exothermic peak reported between 100-200°C, associated with the decrease in the relative intensity of the υ (Si-H) absorption were indicated as evidences of these additional cross-linking reactions. The authors observed no detectable structural and density change between 200-400°C. ^{13}C MAS NMR investigation between 400-600°C reveal no variation, which may indicate that carbon atoms present in the material continues to occupy practically the same sites. Above 600°C the beginning of reorganization reactions of Si-O and Si-C bonds were reported according to following reactions:[59],[54],[55]

$$2D \longrightarrow M + T \tag{3.12}$$

$$D + T \longrightarrow M + Q \tag{3.13}$$

$$D + M \longrightarrow C + T \tag{3.14}$$

$$D + Q \longrightarrow 2T \tag{3.15}$$

where:
M = C_3SiO; D = C_2SiO_2; T = $CSiO_3$; Q = SiO_4 and C = SiC_4.

The formation of M, T, Q and C units from starting precursors containing D and D^H units has to be considered according to the redistribution reactions. Above 600°C the methyl groups are active, with the formation of a large distribution of aliphatic C sites and graphite carbon. The evolution of methane and hydrogen, concurrent with the formation of graphite carbon have been described in the pyrolysis of methyl derived siloxane precursors, by the following reactions:

$$\equiv Si - CH_3 \longrightarrow \equiv Si\bullet + \bullet CH_3 \tag{3.16}$$

$$\equiv C - H \longrightarrow \equiv C\bullet + \bullet H \tag{3.17}$$

$$\equiv C - H + \bullet CH_3 \longrightarrow \equiv C\bullet + CH_4 \tag{3.18}$$

$$\equiv C - H + H\bullet \longrightarrow \equiv C\bullet + H_2 \tag{3.19}$$

Combination of different ≡ Si• and ≡ C• radicals in the formation of the Si-C-Si bridges and free carbon in the ceramic products was discussed.

Brus *et al.*[60] in his contribution, used commercially available poly(siloxane) resins namely; poly(methylsiloxane) with a trade name Lukosil M130 and poly[methyl(phenyl)siloxane] containing reactive groups with the trade name Lukosil 901* to produce silicon oxycarbide glasses and study the chemical changes during heat-treatments in oxidative and nitrogen atmosphere. In air atmosphere, predominantly oxidation processes occur, due to the absence of linear bifunctional D^2 [-O-Si(C_6H_5)$_2$-O-] structural units and the presence of siloxane units with aromatic substituents, the resistance of the precursor to oxidation reactions increases strongly. Also small amount of redistribution reactions leading to the formation of silicon oxycarbide glasses were reported.

In contrast to the oxidation atmosphere the authors reported, formation of a large extent of the silicon oxycarbide glasses during the pyrolysis of both precursors in N_2. He reported a different behavior under pyrolysis in N_2 for both precursors. Accordingly, for LM130 precursor, the siloxane network structure have very slight modification up to 600°C, But, more dramatic changes in the siloxane networks structure for L901 precursor was detected. The condensation reactions and the redistribution reactions are more intensive. The $C_2(Si)O_2$ and $C_3(Si)O$ units formed up to 800°C decreases and the extent of condensation reactions leading to the mineralization of product increases. He concluded that, due to this mineralization, the C/Si ratio significantly decreases at high pyrolysis temperatures. Also as the weight loss of these polymer is relatively small (ca. 5 wt.%), lower molecular weight and volatile products do not form, rather forming free highly condensed aromatic phase.

*These are commercial products of Lučební závody Kolín, Czech Republic.

More recently Mutin et al.[61] reported the role of redistribution reactions in the formation of SiOC ceramics by polymer route. He discussed many redistribution reactions namely; Si-O/Si-O, Si-O/Si-H, Si-O/Si-Si and Si-O/Si-C. He first observed the unambiguous occurrence of Si-C/Si-O redistribution during the pyrolysis, under argon, of polymethylsilsesquioxane. The continuous evolution of the ^{29}Si MAS NMR spectra of the residue with the pyrolysis temperature indicates that Si-C/Si-O redistributions takes place in the 500°C to 1400°C range, involving not only Si-Me bonds, but also any Si-C bonds in the residue. Apart from cross-linked polymethylsiloxane which was first reported by above author, this reaction was identified in the pyrolysis of all organosilicon polymer precursors containing Si-C and Si-O bonds, regardless of their structure:

1. in polysiloxanes containing methyl, phenyl, or vinyl substituents in mono-, di-, tri-, or tetrafunctional building units,

2. in polysiloxanes cross-linked Si-Si or $SiCH_2CH_2Si$ bridges,

3. in polycarbosilanes cross-linked by Si-O-Si bridges.

He added that, the occurrence of Si-O/Si-C redistributions accounts for the distribution of $[SiC_xO_{4-x}]$ sites found in all the SiOC glasses at $\sim$ 1000°C. Moreover, SiOC glasses with similar O/Si ratios display similar ^{29}Si MAS NMR spectra, regardless of the structure of the precursor. Thus, at the end of the mineralization stage, the environment of the Si atoms in an oxycarbide glass is dependent only on the amount of Si-O and Si-C bonds in the glass (O/Si ratio) and is not dependent on the environment of Si atoms in the precursor. This finding suggested that the redistribution of Si-O and Si-C bonds attained an equilibrium state.

Some conclusions can be tentatively drawn from the above analysis. For the synthesis of free-carbon free oxycarbide glasses with high carbidic carbon concentrations, the following points should be considered:

1. The $(O/Si)_{gel}$ should be kept as low as possible and thus the number of terminal groups in the gel should be minimized by forcing the condensation process as far as possible.

2. The $(C/Si)_{gel}$ should be kept as close as possible to the stoichiometric value.

3.4.2 SiOC Ceramic and Post Treatment Characterization: MAS-NMR, TEM, EELS, Mechanical.

After discussing the processing of oxycarbide glass by different routes, it is important to investigate further these glass with different techniques for structural evolution and some physical and mechanical properties.

Soraru *et al.*[62] and co-authors in their post-pyrolysis study on sol-gel derived silicon oxycarbide glasses used thermal annealing to further investigate the effect of high temperature on thermal stability and structural evolution. He suggested that, by increasing the firing temperature, a structural evolution occurs, leading to the crystallization of very fine β-SiC crystals. Indeed, starting from 1200°C, the typical diffraction peaks of the cubic silicon carbide crystals are clearly seen. Along with XRD study the structural evolution is even more evident from the ^{29}Si MAS-NMR analysis. By increasing the temperature from 1000-1200°C, the oxycarbide network becomes richer in SiC_4 and $(Si)O_4$ units with a concurrent decrease of the amount of $C(Si)O_3$ and $C_2(Si)O_2$ units. It should be noted that this structural evolution occurs without any variation in the chemical composition of the oxycarbide phase as well as without any appreciable weight loss. From 1200 to 1400°C, the relative amount of various silicon units in the oxycarbide network is stable. Conversely from 1400 to 1500°C, NMR analysis show a dramatic decrease of a mixed species and simultaneously strong increase of the SiC_4 units. The NMR analysis clearly indicates that the starting homogeneous oxycarbide network undergoes structural rearrangements that lead to a phase separation. The formation of $[SiC_4]$ species is significant. Pantano *et al.*[51] reported that, in the case of oxycarbide glasses made with MTMS only, the $[SiC_4]$ does not appear until $\sim$ 1200°C, whereas the glasses synthesized with MDMS or TES precursors containing Si-H show $[SiC_4]$ formation at lower temperatures. The formation of SiC through carbothermal reduction of SiO_2 (by C) occurs only at much higher temperature ($\geq$1500°C). Thus, it is likely that these $[SiC_4]$ species are created through exchange reactions and decomposition of $[SiO_xC_y]$ species. This is analogous to the formation of SiC through pyrolysis of carbosilanes which starts at 1000°C. Since all of these glasses are X-ray amorphous, the $[SiC_4]$ species must be quite dispersed. Nevertheless, they can be considered nuclei for subsequent crystallization at higher temperatures.

Additionally, Soraru[62] observed that, the number of Si-C bonds is constant from 1000 to 1400°C, $\approx 1.2 \pm 0.1$, confirming the compositional stability of the oxycarbide phase. At 1500°C, the increase of the number of Si-C bonds indicate that some free carbon has reacted with the oxycarbide network to form new Si-C bonds. Indeed, the chemical analysis and the ^{29}Si MAS NMR results in this study explicitly suggested the presence, in the pyrolyzed product, of an extra C_{free} phase. The paper reports the structure of the free carbon phase using Raman spectroscopy, which is the most suitable tool to characterize various forms of crystalline as well as disordered graphitic carbon. Soraru explained two main distinct features: (i) The pair of Raman bands are superimposed upon the luminescence background whose spectral intensity is strongly dependent on the processing temperature. For temperatures below 1300°C, the luminescence background whose maximum is around 2750 cm^{-1} is particularly broad and intense. In contrast, a nearly flat and relatively weak luminescence background is reported after annealing at 1500°C, (ii) The Raman band itself, observed in the $1300-1600$ cm^{-1} region are the diagnostic features of all known disordered graphitic forms of carbon, which are referred to as the D and G bands, respectively.

Authors observed the presence of both D and G bands in the Raman spectrum for glasses prepared after pyrolysis at 1000°C, which clearly indicates the presence of disordered graphitic-like component even at this temperature. They also reported that, the band position and broadening change with the firing temperature. At high temperature i.e., 1500°C, the Raman spectra indicated formation of turbostratic microcrystalline graphite and glassy carbon in which typical domain sizes are around 2 to 3 nm.

More recently, researchers used HRTEM and EELS (particularly ELNES) to investigate phase separation in silicon oxycarbide glasses.[63],[64] Kleebe *et al.* report the effect of firing temperature on phase separation in his study on sol-gel derived glasses from TREOS/MDMS 2:1 mixture, (refer in Table:3.2). This particular composition was used because, according to literature,[53] it leads to the formation of a pure silicon oxycarbide glass on pyrolysis. At 1000°C, author observed in some refined regions, the local arrangement of silicon and carbon atoms is close to that found in crystalline SiC. Also the C_K peak reveal a small π^* prepeak at 283 eV, characteristic of the $s \longrightarrow p$ transition and representing the sp^2 hybridization of carbon in EELS spectrum of glasses treated at 1000°C.

At 1200°C significant reduction in porosity and decrease of the C_{free} content was reported. The small lamellar features observed were thought to represent the so-called basic structural units (BSU) of carbon. In addition, HRTEM images show, in some regions, weak fringes, with spacings close to those of SiC. Along with diffused halos of SiC, the separation of the (220) and (311) β-SiC reflections in the EDP at this temperature imply an evolution towards the formation of better ordered SiC crystallites. The authors argued that, compared with material pyrolyzed at 1000°C, the supplementary peak at $\sim$ 125 eV, characteristic of an Si-O environment in the $Si_{L2,3}$ edge of EELS spectra indicate local formation of SiO_2, which is seen as a clear evidence for the phase separation process in stoichiometric SiOC, starting at a temperature slightly $<$ 1200°C. At still higher temperature (1400°C) spherical crystallites of β-SiC are formed, with an average size of 5$-$10 nm. Similar somewhat pronounced supplementary peak, representing Si-O bonding, enabled Kleebe to conclude that, at 1400°C, the nanosized SiC crystallites are embedded in amorphous SiO_2 and the phase separation process is close to complete.

Kaneko *et al.*[64] used oxygen-controlled polycarbosilane (PCS) for his post study of Si-O-C bulk ceramics by HRTEM and ELNES. Oxygen controlling was performed by the thermal oxidation treatment at elevated temperature (180°C) in air and with different heating schedules. Subsequent pyrolysis to 1200°C under Ar atmosphere produces SiOC ceramics with different chemical compositions. Kaneko observed that, the β-SiC grain size, namely the total crystallinity of the material, substantially depend on the oxygen content controlled by the thermal oxidation treatment before the pyrolysis step. Introduction of oxygen constituent delays structural rearrangement of amorphous-to-crystalline transition in the overall microstructure. The fine structures of the Si-$L_{2,3}$, C-K and O-K edges ELNES were influenced by each chemical environment of the SiOC ceramics. There are some minor changes among the ELNES spectra, e.g., the chemical shift of major peak of the Si-L edge, the height of the π^* peak of C-K edge and the chemical shift of the major peak of the O-K edge. Changes in the shapes of the peaks were also observed. In particular with a increase of the oxygen content in the ceramic, a shift of the edge onset to the higher energy and the energy onset of the major peak becomes sharper and the shape becomes similar to the O-K edge of SiO_2.

Property	**Silicon Oxycarbide**	**Vitreous Silica**
Density g/cm^3	2.35	2.20
Coefficient of Thermal Expansion x 10^{-6}/K	3.14	0.5
Vickers Hardness[a] (kg/mm^2)	855	600 to 700
Critical Stress Intensity[b] Factor (MPa $*$ $\sqrt{\text{m}}$)	1.8	3
Fracture Strength[c] (MPa)	153 $\pm$ 25	wide range but typical values are $\sim$ 375 for fibers
Young's Modulus (GPa)	97.9	70
Glass Transition	1350	1190
Electrical Conductivity (/ohm-cm)	4(10)$^{-13}$	$\sim$(10)$^{-22}$

[a] 200 g load
[b] Indentation technique using 1 Kg load
[c] 3-pt. bending of 0.74 mm diameter fiber

Table 3.4: Properties of silicone derived silicon oxycarbide glasses and vitreous silica.[66]

Soraru *et al.*[65] went ahead with a more comprehensive mechanical study on sol-gel derived oxycarbide glasses, especially prepared from various mixtures of TREOS/MDMS, including a hardness and the elastic modulus characterization and, more importantly, an investigation of the relationship between the mechanical properties and the carbon content in the oxycarbide phase. He observed that, the elastic modulus (E), flexural strength, (MOR), and Vickers hardness (H_v), increases markedly with the amount of carbon in the oxycarbide glasses pyrolyzed at 1000°C reaching the maximum values ($E \approx 115$ GPa, MOR ≈ 550 GPa, and $H_\text{v} \approx 9$ GPa) for the samples with highest carbon load: E and H_v values were 50% higher than those typical for fused silica.

Among the various mechanical properties measured in his study, Soraru focused on the discussion about Young's modulus, which being an intrinsic material property, as a function of the composition of the dense silicon oxycarbide glasses obtained at 1200°C, and then related the amount of substituted carbon in the amorphous oxycarbide network, i.e., the x value in $SiO_{2(1-x)}C_x$. He observed that, $D^HT^H0.5$ gel lead to a pure oxycarbide glass, with the elastic modulus (102± 8 GPa). For the glasses with excess carbon, i.e, D^HT^Hy with y = 0.75 and y = 1, elastic modulus of C_{free} phase, assumed to be isolated basic structural units, can be neglected. Moreover, he argued that, when the volumetric percentage of C_{free} is very low, $\leq \approx 3\%$ (observed for these compositions), than its contribution to the elastic modulus of the pyrolyzed ceramics should not be important. Accordingly he found the E values of 102 ± 6 GPa for $D^HT^H0.75$ and 113 ± 6 GPa for D^HT^H1, respectively, and can be assumed to be a direct measure of the elastic constant of the oxycarbide glasses. He compared these experimental elastic modulus values with the calculated values on these glasses, which were obtained from Voigt (E_v) and Reuss (E_R) models (using chemical composition, elastic modulus and volume fraction of different phases), and found them in good comparison. His work suggest that, the elastic modulus of the amorphous silicon oxycarbide materials can be estimated from the chemical composition. Accordingly, the paper report (E_v) and (E_R) values calculated for all compositions together with the experimental results. All the measured data, except for the E values from glasses prepared from gels with $0 \leq y \leq 0.3$ after pyrolysis at 1000°C, fell well between the theoretical limits and approaching the Voigt model. This deviation from the theoretical values was tentatively explained due to the presence of fine residual porosity. He concluded, the Voigt model shows a strong dependence on the composition for D^HT^Hy with $0 \leq y \leq 0.5$ and exhibits a plateau for D^HT^Hy with $0.5 \leq y \leq 1$, and exactly the same trend was experimentally observed for the investigated temperatures.

Renlund compared the properties of a silicone derived silicon oxycarbide glass, to those of a typical vitreous silica.[66] He observed that the increased average coordination state of silicon in the oxycarbide glass lead to improved values as mentioned in Table:3.4.

3.5 Formation of Si(M)OC Ceramics; M = Modifiers (Elements or Compounds)

Inspite of enhancement in the properties, explained in the previous section, two distinct drawbacks are observed in the processing and properties of silicon oxycarbide ceramics. The combination of volatile loss during polymer pyrolysis and large density difference between the starting polymer and the final ceramic resulting in large shrinkages, produce difficulty for the monolithic ceramic preparations. Along with the difficulties in the processing, silicon oxycarbide ceramics are only stable up to $\sim$ 1200°C. Hence, researchers worked on different ways and conditions for facilitating the crack-free processing and improve the high temperature performance of these class of ceramics. Accordingly, modification of the ceramics by different elements and compounds to produce Si(M)OC ceramics is reported by many researchers. Modifications can be achieved on different scales namely, macro (fillers) and molecular (sol-gel method), and will be explained in the following sections.

3.5.1 Modifications with Fillers

If during pyrolysis, there is unconstraint microstructural relaxation, transient porosity created by evolving volatiles can be completely eliminated by material transport and a fully dense body which exhibits maximum shrinkage was observed. However, if microstructural relaxation is completely constrained, a body which exhibits no shrinkage but possesses a significant porosity is reported. Usually, a volume reduction as well as residual porosity are observed in real systems. As a consequence, it is impossible to produce near net-shape, high density monolithic ceramic components from the pyrolysis of preceramic polymers alone. This made researchers to investigate further the effect of active and passive fillers on the bulk body processing of ceramics by pyrolysis of preceramic polymers.

3.5.1.1 Inactive Filler Controlled Pyrolysis of Preceramic Polymers

The intrinsic problems of low density and extensive shrinkage associated with pyrolysis of preceramic polymers can be partially overcome by incorporating

chemically passive fillers, such as SiC, or Si_3N_4, into the preceramic polymer. Schwartz and Roweliffe,[67] derived a model to describe the effect of mixing ceramic powders with preceramic polymers on the pyrolyzed density. Accordingly, he evaluated a relation for the pyrolyzed density, (ρ') of the final body as:

$$\rho' = \rho_{\mathrm{p}}(Vf_{\mathrm{p}})\alpha + \rho_{\mathrm{F}}(Vf_{\mathrm{F}}) \tag{3.20}$$

Where ρ_{p}, ρ_{F}, $\mathrm{Vf_p}$, $\mathrm{Vf_F}$ and α, are density of polymer, density of filler, volume fraction of polymer, volume fraction of filler and polymer's ceramic yield, respectively.

In general, Eq. (3.20) holds true for all cases where $\mathrm{Vf_P} + \mathrm{Vf_F} < 1$ ($\mathrm{V_v} > 0$), where $\mathrm{V_v}$ is volume of pores or voids between the filler particles unoccupied by the polymer. However for the specific case $\mathrm{V_v} = 0$, the sum of $\mathrm{Vf_p} + \mathrm{Vf_F}$ is equal to unity and increasing the volume fraction of one component comes at the expense of the other. As a consequence, when ($\mathrm{V_v} = 0$), Eq. (3.20) reduces to:

$$\rho'_{(\mathrm{V_v}\,=\,0)} = \alpha\rho_{\mathrm{p}}(Vf_{\mathrm{p}}) + \rho_{\mathrm{F}}(1 - Vf_{\mathrm{p}}) \tag{3.21}$$

$$= \rho_{\mathrm{F}} - Vf_{\mathrm{p}}(\rho_{\mathrm{F}} - \rho_{\mathrm{p}}\alpha) \tag{3.22}$$

Together with Eq. (3.20) and Eq. (3.22), the authors described the effect of filler addition on the pyrolyzed density for any polymer-filler system which exhibits no volume change during pyrolysis. Eq. (3.20) is valid at low polymer concentration when the volume of polymer is insufficient to completely fill all void space between the filler particles ($\mathrm{V_v} > 0$). Eq. (3.22) describes the behavior at higher polymer concentration where sufficient polymer is present to completely fill the voids ($\mathrm{V_v} = 0$).

For a given polymer-filler system, the physical properties of the two components fix many of the variables in Eq. (3.20) and Eq. (3.22). For example, the densities of the filler and polymer are fixed and the polymer-to-ceramic yield is a constant if pyrolysis progresses to completion (fixed T and atmosphere). Hence, fixing the volume fraction of the filler phase Eq. (3.20) and Eq. (3.22) reduces to first order linear equations with $\rho' = f(\mathrm{Vf_p})$ only. This model was explained by plotting the variation in pyrolyzed density (ρ') as a function of

initial polymer volume fraction for a variety of poly(silazanes) filled with Si_3N_4 powder. A maximum in (ρ') represents the intersection of the curves for $Vf_p + Vf_F < 1$ [Eq. (3.20)] were $V_v > 0$, and $Vf_p + Vf_F = 1$ [Eq. (3.22)] were $V_v = 0$. The corresponding Vf_p is the critical volume fraction, Vf_c, which represents the instance when all the voids between the filler particles are filled with the polymer. The authors observed that when $Vf_p < Vf_c$, increasing the polymer volume fraction actually increases the overall product density. When $Vf_p < Vf_c$, the volume fraction of the filler is essentially a constant and any increase in Vf_p comes at the expense of V_v. As a consequence, the pyrolyzed density increases linearly as a function of Vf_p and V_v decreases proportionally until a maximum ρ' is reached where $V_v = 0$. In contrast, when $Vf_p > Vf_c$, where $V_v = 0$, increasing the Vf_p must come at the expense of Vf_F since the sum $Vf_p + Vf_F$ is now equal to unity. In addition, since the employed model is restricted to no change in volume, the reduction in mass of the pyrolyzing polymer must be accommodated by the creation of porosity. Hence, when $Vf_p > Vf_c$, increasing the polymer content proportionally reduces the filler content which act to reduce product density.

Schwartz and Roweliffe model demonstrated the benefits of adding ceramic fillers to improve the final density of preceramic polymers; however the model neglects to address the issue of shrinkage during polymer pyrolysis. Shrinkage often causes micro-cracking of the resulting product which further reduces product density and results in reduced properties. In 1989, Greil *et al.*[16] developed models which addressed the effects of inactive fillers on the shrinkage and density of preceramic polymers. Accordingly, the reduction in total linear shrinkage, ε^{pf}, and residual porosity, V_v^{pf}, of inert filler-polymer systems during pyrolysis, can be expressed as:

$$\varepsilon^{pf} = \left\{ \frac{V_F^{max} - V^F}{V_F^{max}} \right\} \varepsilon^p \tag{3.23}$$

and

$$V_V^{pf} = (1 - V^F) V_V^p \tag{3.24}$$

for $V^F < V_V^*$ and

$$V_V^{pf} = (1 - V^{\mathrm{F}})V_V^p + (V^{\mathrm{F}} - V_F^*) \tag{3.25}$$

for $\mathrm{V^F} > \mathrm{V}_V^*$

Where V_V^p, V_F^*, V_F^{max}, $\mathrm{V^F}$, and ε^{p} are the residual porosity of the unfilled polymer after pyrolysis, the critical filler loading , the maximum packing fraction of the filler powder, volume fraction filler, and linear shrinkage of the unfilled polymer during pyrolysis, respectively. The critical filler loading was defined as the filler content at which the filler particles form a rigid network on shrinkage of the polymer matrix phase. Greil reported that, the critical filler loading will always be smaller than the maximum packing fraction and is related to V_F^{max} by

$$V_F^* = V_F^{max} - (1 - \alpha\beta)(1 - V_F^{max}) \tag{3.26}$$

Where, β is density ratio i.e., $\rho_{\mathrm{p}}/\rho_{\mathrm{c}}$

Greil predicted influence of filler addition on the expected linear shrinkage and residual porosity of polymer-inactive filler systems based on Eq. (3.23) and Eq. (3.25) during pyrolysis. According to the authors, three major regions can be distinguishes: (1) filler fractions below the critical filler fraction, (2) filler fractions intermediate between the critical filler fraction and the maximum packing fraction, and (3) filler fractions above the maximum packing fraction.

When $\mathrm{V^F}$ is less than V_V^*, the mass loss associated with polymer pyrolysis can be completely compensated for by shrinkage without creating porosity and a fully dense body which exhibits maximum shrinkage can result. In contrast, when $\mathrm{V^F}$ is greater than V_F^{max}, shrinkage is not possible since the filler particles are already packed to their densest configuration and the mass loss associated with polymer pyrolysis is fully accommodated by the creation of porosity. In an intermediate region, the mass loss of the pyrolyzing polymer can be accommodated by both shrinkage and porosity. The weight loss associated with the pyrolyzing polymer can be initially accommodated by shrinkage without creating porosity; however, when the body shrinks to the point where the particles start to form a rigid structure, the remaining weight loss of the polymer is accommodated by the creation of porosity.

Greil demonstrate the usefulness of adding inactive fillers in increasing density and reducing shrinkage; however, he concluded from his model predictions, a

high density material which exhibits no shrinkage cannot be manufactured from pyrolysis of inactive filler-polymer systems. Accordingly, processing and pyrolysis conditions can be tailored to produce either a zero shrinkage body which has a low density or a fully dense body which exhibits significant shrinkage, but cannot be tailored to produce a fully dense body which exhibits no shrinkage. The authors claim that in most inactive filler-polymer systems, both shrinkages and porosity will always result. In fact, research to date by a number of researchers serve as experimental support for their conclusions.

3.5.1.2 Active Filler Controlled Pyrolysis of Preceramic Polymers

The limitations cited for inactive filler controlled pyrolysis of preceramic polymers in forming zero shrinkage, high density materials can be overcome by employing chemically active fillers instead of, or in addition to, inactive fillers. The concept of active filler controlled pyrolysis (AFCOP) of preceramic polymers was originally proposed by Greil [17] as a potential solution to the inherent problems of shrinkage and low density associated with pyrolysis of preceramic polymers. According to the AFCOP concept, in the presence of an active filler, the polymer pyrolysis reactions can be significantly changed due to the chemical and physical interactions of the incorporated filler with constituents of the pyrolyzing polymer. The concept itself is relatively simple in that a chemically active filler, which can react with pyrolysis products of the polymer or with a reactive atmosphere to form carbides or nitrides, is incorporated into the preceramic polymer prior to pyrolysis. For example, an active transition metal filler can react with solid carbon pyrolysis product or gaseous hydrocarbon pyrolysis product of the polymer to form a carbide.

With active filler controlled pyrolysis of the polymers, it is also possible to use a reactive pyrolysis atmosphere to transform the active filler to a carbide or a nitride. For example, for carburizing of active fillers, CH_4 can be employed, while for nitridation of active fillers, N_2 or NH_3 can be employed.

If the specific volume of the resulting filler reaction product is higher than the sum of the corresponding volumes of the starting active filler phase and the solid carbon pyrolysis product, a volume expansion is observed during the transformation. The volume expansion which occurs during active filler transformation

may then be used to compensate for the shrinkage which occurs during pyrolysis of the preceramic polymers. Furthermore, in contrast to the shape invariant behavior of inactive filler particles which do not change their morphology but only their inter-particle distances during polymer pyrolysis, active fillers may change their morphology during reactive transformation. As a result, porosity created by the pyrolyzing polymer may be occupied by the active filler reaction product, thereby increasing the final product density. These are the fundamental bases for the AFCOP concept which allows for the manufacture of zero shrinkage, high-density composite materials.

Thus dispersion of Ti, Cr, V, Mo, Si, B, $CrSi_2$, $MoSi_2$, etc., in polymers results in shape-invariant precursor-ceramic conversions in argon or nitrogen atmospheres, making formation of components with complex geometries possible. Typical particle sizes of the active filler powders are 1 to 10 µm, which partly can be replaced by additional inert filler powders, such as SiC, Si_3N_4, Al_2O_3. The inert filler particles are used to stabilize a homogeneous distribution of the active filler phase particles by reducing sedimentation effects during processing. Based on the AFCOP concept, a variety of novel ceramic composite materials − such as Si-O-C/TiC, Si-O-C-N/TiN, Si-O-C-N/BN, and Si-O-C-N/($Cr_3C_2 + Si_3N_4$) − have been fabricated as bulk components. Greil focused on poly(silsesquioxane) preceramic polymer, and the resulting composite materials are characterized by three-dimensional interconnected network of the carbide (pyrolysis in argon) or nitride (pyrolysis in nitrogen) filler reaction products embedded in the nano-structured polymer-derived Si-O-C matrix.[17],[68] More recently, authors investigated the development of mullite-SiC nano-composite using the concept of AFCOP, from commercial polysiloxanes filled with Al_2O_3, aluminum and Al/Al_2O_3.[69],[70] Additionally, poly(silazanes) and poly(carbosilazanes) have been demonstrated to be suitable reactants for the AFCOP process.[71]

Inspite of the claims from the model explained by Greil, the composite materials produced by the active-filler-controlled reaction pyrolysis process still contain various amounts of residual porosity. The open porosity can be reduced by well dispersion of very fine filler particles. The temperature at which the open pores form and close can be shifted to higher temperatures with increasing external gas pressure. Improvement in the modulus of rupture, with controlled porosity (which need improved processing), is demonstrated by many researchers. Along

with the room temperature properties, the authors demonstrate enhancement in the secondary creep property. Because of the high hardness and chemical stability of the carbidic or nitridic filler reactant phases, the composite materials offer a high potential for good wear resistance.

3.5.2 Modification of Preceramic Polymers without Fillers

As mentioned before, the most attractive and challenging features of polymer pyrolysis process is the possibility of controlling the microstructure and the properties of the final ceramic material by chemically modifying the polymer composition and/or its structure. This modification differ from filler-modified system by the scale of modification, i.e., filler-modified system is on macro/micro scale, whereas chemical modification is at the atomic scale.

By reacting, in solution, a polycarbosilane (PCS) with a titanium alkoxide, Yajima *et al.*[30] demonstrated a new polymer called polytitanocarbosilane (PTC) that gives, after pyrolysis, ceramic material of the Si-Ti-O-C system. He indicate that, fibers produced from this precursor display superior tensile strength compared with SiC (Nicalon) fibers.

The same reaction motivated Babonneau *et al.* to modify the polycarbosilane with different elements just by changing the nature of metal alkoxide. Therefore, by using this strategy, it was possible to prepare a large variety of new metal−organic polymers, precursors for Si-M-O-C systems. Babonneau's attention was first focused on Si-Ti-O-C system, and then on two new systems, Si-Al-O-C and Si-Zr-O-C[72],[73] and more recently along with Soraru *et al.* on Si-B-O-C[74],[75] and Si-Al-O-N[76] system. The main goals for these studies were the following:

1. A structural characterization of the polycarbosilane-modified precursor to understand how the metallic alkoxide react with the polycarbosilane, and

2. A study of the structural evolution of the material during the pyrolysis to see the influence of the extra metallic atoms on crystallization process

3.5.2.1 Structural Characterization of Si-Al-O-C Polymers

From the above mentioned systems, we will only focus our interest on Si-Al-O-C and Si-Al-O-N systems, as they provide basic background for present work. Accordingly, polyaluminocarbosilane (PALC) was synthesized from (PCS)* and aluminum sec-butoxide with xylene as a solvent. This polymer, after distillation of solvent, is cross-linked by heating to around 300°C. ^{29}Si, ^{13}C and ^{27}Al MAS-NMR was used for structural investigation of PALC. The author observed that the structure of the (PCS) is not greatly modified during the reaction with the aluminum alkoxide, from ^{29}Si NMR data.[73] Also, for the aluminum environment, both ^{13}C and ^{27}Al show an extensive hydrolysis of the butoxy groups, certainly due to a high reactivity of the aluminum alkoxide towards moisture. She concludes saying, this precursor could be described as a mixture of (PCS) chains and $Al(OH)_3$-based particles. Chemical bonding between the two components could exist via Si-O-Al bonds that should give rise to a ^{29}Si NMR peak around 10 ppm [C_3(Si)O] sites. Authors did not observe any such component in the ^{29}Si spectra,[77],[73] however, the presence of these bonds cannot be rejected but should involve only a small number. Additionally, Wootton *et al.*[77] with ^{27}Al spectra reported, tetrahedral [Al(4)] and octahedral [Al(6)] coordination, where [Al(6)] being the preferred coordination.

3.5.2.2 Pyrolysis Process to Si(Al)OC Ceramics and Post Treatment Characterization

Babonneau *et al.*[73] compared the pyrolysis process, and subsequent heat-treatment up to 1700°C, for PALC to that with PCS, the summary for this research is presented in the following paragraphs. As already mentioned, a pure PCS starts to crystallize around 1200°C, and, up to 1700°C, show the presence of SiC-3C polytype. Also, ^{29}Si MAS-NMR indicated the presence of 3C polytype (main peak centered at -16 ppm) and α polytypes (with two minor peaks at -20 ppm and -25 ppm).

In contrast, PALC system, reveal presence of SiC-3C polytype at 1100°C. Above 1300°C, the evolution of the system differs from the pure PCS system. At and above this temperature, a noticeable amount of SiC-2H which increases with

*Dow Corning Corp., Midland, MI

temperature was reported. At the same time, the ^{29}Si NMR spectrum presents an increase of the -16 ppm peak to -19.9 ppm (3C polytype is known to give a main peak around -16 to -18 ppm). This difference seems to be related to some disorder inside the polytype. As for the 2H polytype, only one type of silicon sites are present. No NMR spectrum has been reported yet, but the corresponding chemical shift has been predicted to be at -31 ppm. Author, tentatively assigned this peak at -19.9 ppm to silicon sites in the 2H polytype and indicated that the difference in chemical shifts from the calculated value could be due to the presence of aluminum atoms in the silicon environment.

Babonneau concluded that, the formation of 2H polytype seems the be related with the presence of aluminum atoms. This is because the aluminum oxycarbide Al_2OC with the wurstite structure is isostructural to the SiC-2H and can favor the formation of this polytype. It assume the formation of an aluminum oxycarbide phase inspite to explain the SiC-2H phase found by XRD in the pyrolyzed sample. However, unavailability of the ^{27}Al NMR data on the crystalline phase Al_2OC unable author for precise description of the aluminum environment.

Babonneau *et al.*[73] and Wotton *et al.*[77] in their ^{27}Al MAS NMR investigation, observed disordering of the material up to 850−900°C with only a broad peak centered around 30 ppm. This peak covers the chemical shift range of Al−O bonds. The peak position of $\sim$ 28 ppm indicate penta-coordinated aluminum Al(5). Also, the transformation of Al(5) to Al(4) [55 ppm] and mainly Al(6) [1 ppm] with temperature, indicate a unique phase formation; namely mullite. However, the possibility of Al-C bond (in very small amount) cannot be ignore, and a extra peak at 140 ppm at high temperature was referred to be the signature of these bonds.

3.6 Kinetics of the Process

The dependence of high temperature on the crystallization, oxidation and flow (deformation) with time; i.e. *kinetics*, is investigated in this research. The thermodynamics of the various structural states of materials governs the transformation from one state to another, as well as the reaction. However, although a negative free energy change is a necessary prerequisite for a material transfor-

mation to occur, it is not guarantee that it will do so at any measurable rate. The rate depends on the mechanism of the reactions involved and may bear no relation to the magnitude of the free energy reduction which drives the transformation. This is illustrated by the effect of catalyst on chemical reactions − they do not change the free energy of the phases but do provide a faster mechanism.

If kinetics are determined by factors other than ΔG, it is necessary to consider the states through which a system passes during the transformation. Equilibrium thermodynamics does not describe these states and so need some additional concepts to be able to deal with the transformation rates. In this section some basic ideas of kinetic theory, and methods for extracting information from laboratory experiments with transformation rates will be explained.

At equilibrium, when $\Delta G = 0$, no transformation can take place. Some overstepping is always required to provide the free energy reduction. Laboratory experiments are carried out at higher temperatures, far from equilibrium, where reactions proceed at a measurable rate, and the data are extrapolated to lower temperature, near equilibrium, where reaction rates are much slower.

3.6.1 Basic Theories

The problem of the pathways through which a material system passes during a transformation from the initial to final state is done by defining an *activated state* which has some intermediate configuration. This is a 'quasi-equilibrium' approach an unique values of the thermodynamic functions to this activated state is assigned. The shape of the free energy curve is a consequence of the fact that if the initial and the final stages are in equilibrium (either stable or metastable), their free energies must be at minima, and any pathway from one to another must pass through a maximum.

The free energy of activation ΔG_a depends on the reaction pathway, and in heterogeneous reactions is independent of the thermodynamics of the initial and the final states. The pathway with the lowest ΔG_a will be the one taken. A necessary condition for a transformation to takes place at a measurable rate is that sufficient atoms have enough energy to achieve the transition state. This energy is supplied by thermal fluctuations. At all temperatures above 0 K atoms are in motion, collisions between them producing wide variations in the energy

of individual atoms, with some having energies greatly in excess of the mean.

This concept of an activation energy barrier qualitatively explains a number of following features of material reactions:

1. the persistence of metastable states, due to ΔG_a being very large compared to the mean free energy,

2. the effect of catalysts which change ΔG_a, i.e., provide a reaction path with lower free energy of activation, and

3. the slow rate of many transformations, due to the fact that, at any one time, only a small number of the available atoms have sufficient energy to overcome the activation energy barrier.

3.6.2 Rate of a Single Thermally Activated Process

For a process which involves only one basic atomic step, characterized by the unique activation energy ΔH_a, the rate equation can be formulated as follow:

$$Rate \quad \propto \quad p \cdot \quad \nu \cdot \quad exp\left\{\frac{-\Delta H_a}{RT}\right\} \quad = \quad \frac{dy}{dt} \tag{3.27}$$

1. the frequency with which atoms attempt to jump from one site to the next, i.e. the vibrational frequency ν.

2. the fraction of atoms with enough energy to surmount the activation energy barrier, i.e,

$$f = exp\left\{\frac{-\Delta H_a}{RT}\right\}$$

3. the probability p that the atom which has required energy satisfies some geometrical conditions i.e jumping in the right way.

Here it is necessary to discuss little between the free energy G_a and H_a. The assignment of the thermodynamic functions to the activated state includes values

of internal energy U_{a}, volume V_{a}, enthalpy H_{a} and entropy S_{a}. The Gibbs free energy G_{a} for the activated state is:

$$G_{\mathrm{a}} = H_{\mathrm{a}} - TS_{\mathrm{a}} \tag{3.28}$$

where the subscript refer to the activated state.

For most solid state reactions at low pressures, the volume changes is small and hence the changes in enthalpy ΔH_{a} is approximated to the internal energy of the activated state. The term activation energy is commonly used, although it is very important to note that this is not the same as the free energy of activation.

The activation energy is the difference between the internal energy (or enthalpy) of the transition state and the initial state. The curve is similar to the one for free energy except that the overall enthalpy change ΔH for the transformation may be positive or negative. If ΔH is positive the reaction is endothermic, while if ΔH is negative the reaction is exothermic.

Form Eq. (3.27) with the dependence on the free energy of activation $\Delta \mathrm{G}_{\mathrm{a}}$ the probability p is related to the entropy of activation ΔS_{a} in the following way:

$$p = \frac{\omega_{\mathrm{a}}}{\omega_{\mathrm{I}}} \tag{3.29}$$

i.e the number of complexions associated with the transition state to that associated with the initial state. The probability of a correct atomic jump is related to the number of possible pathways for the transformation.

Since

$$\begin{aligned} \Delta S_{\mathrm{a}} &= Rln\frac{\omega_{\mathrm{a}}}{\omega_{\mathrm{I}}} \\ p &= exp\left\{\frac{\Delta S_{\mathrm{a}}}{R}\right\} \\ Therefore; \qquad \frac{dy}{dt} &= \nu \cdot exp\left\{\frac{\Delta S_{\mathrm{a}}}{R}\right\} exp\left\{\frac{-\Delta H_{\mathrm{a}}}{RT}\right\} \\ Since; \qquad G_{\mathrm{a}} &= H_{\mathrm{a}} - TS_{\mathrm{a}} \\ \frac{dy}{dt} &= \nu exp\left\{\frac{-\Delta G_{\mathrm{a}}}{RT}\right\} \end{aligned} \tag{3.30}$$

More commonly we write

$$\frac{dy}{dt} = A \cdot exp\left\{\frac{-\Delta H_{\mathrm{a}}}{RT}\right\} \tag{3.31}$$

where the pre-exponential factor A is known as the *frequency factor*. Eq. (3.31) is known as the *Arrhenius equation*.

A plot of $\ln\frac{dy}{dt}$ against 1/T is termed as *Arrhenius plot*:

$$ln\frac{dy}{dt} = lnA - \frac{-\Delta H_{\mathrm{a}}}{RT} \tag{3.32}$$

and if both A and ΔH_{a} are independent of temperature, this is linear with a gradient -$\Delta H_a/R$ and an intercept on the rate axis of $\ln A$. The magnitude of ΔH_a describes the temperature dependence of the reaction rate while the pre-exponential A, which contains the entropy of activation term, determine the absolute reaction rate.

3.6.3 Rate Equations for Heterogeneous Reactions

Reactions which involve nucleation and growth of the product phase(s) within the parent phase are termed heterogeneous. Empirically it is found that the isothermal kinetics of a wide range of materials can be described by an equation of the general form

$$\frac{dy}{dt} = k^{\mathrm{n}} \cdot t^{\mathrm{n\text{-}1}}(1-y) \tag{3.33}$$

where k is a rate constant, t is the time, y is the fraction transformed and n is a constant which depends on the mechanism.

Separating the variables and integrating gives

$$\int \frac{dy}{1-y} = \int k^{\mathrm{n}} \cdot t^{\mathrm{n\text{-}1}} dt$$

$$ln\frac{dy}{1-y} = (kt)^{\mathrm{n}}$$

where the term 1/n has been incorporated into the constant. This can also be

written

$$y = 1 - exp(-kt)^{\mathrm{n}} \tag{3.34}$$

Where rate constant k has dimension time^{-1} and is defined as the effective overall reaction rate, which is usually assigned an Arrhenian temperature dependence like that in Eq. (3.31).

Eqs. (3.34) and (3.31) have served as the basis of nearly all treatments of crystallization in DTA or DSC experiments. It should be noted, however, that Eq. (3.34) strictly applies only to isothermal experiments. Nevertheless, Eq. (3.34) has been extensively used to derive expressions describing non-isothermal crystallization.

Various authors summarized different treatments of non-isothermal crystallization based on Eq. (3.34) and Eq. (3.31) and assuming a constant heating rate in the DTA and DSC experiments and is reviewed by Yinnon and Uhlmann *et al.*[78]. The goal of all the methods is to identify two parameters, which, when plotted one against the other, will result in a straight line. From the slope of such line, the overall effective activation energy, E, or the order of reaction can be calculated. It is shown by Moynihan *et al.*[79] that under certain conditions the dependence of the transition on the heating or cooling rate β is given by:

$$\frac{d(ln\beta)}{d(1/T_{\mathrm{s}})} = \frac{-E_{\mathrm{s}}}{R} \tag{3.35}$$

where β, E_s, T_{s} are the heating rate, activation enthalpy and the softening temperature respectively. His theory is used to calculate the softening/relaxation kinetics of many glasses.

The activation energy for crystallization and the Avrami constant or a shape factor is estimated from non-isothermal analysis using Kissinger theory:

$$ln\frac{\beta}{(T_{\mathrm{p}})^2} = \frac{-E_{\mathrm{cry}}}{RT_{\mathrm{p}}} + C \tag{3.36}$$

where β is the heating rate, T_{p} is the peak temperature, E_{cry} is the activation energy for crystallization, R is the gas constant and C is a constant. The crystallization mechanism can be determined from the factor (n), which is determined

as:

$$n = \frac{2.5R(T_{\mathrm{p}})^2}{\Delta T E_{\mathrm{cry}}} \tag{3.37}$$

Where, ΔT is full-width-half-maximum (FWHM). Accordingly, various phenomenon can be quantified by estimating the rate of the reaction and the activation energies, namely, glass structural relaxation and crystallization. In the present work this kinetic data will be compared with viscous flow of SiAlOC ceramics.

3.7 Thermo-Mechanical Behavior

3.7.1 Developments in Thermo-Mechanical Behavior for Si(C)O Systems

All the research for incorporating carbon in the silica network was aimed to improve the room temperature mechanical properties. Indeed, in doing so the high temperature properties can also show improvement in the thermo-mechanical properties and inspite of early development of SiOC glasses it took last decade for creep investigation of this class.

The creep viscosity and its temperature dependence is recently reported by Rouxel *et al.*[80] The viscosity coefficient (η), hereafter referred as viscosity, was reported and calculated from the strain-rate ($\dot{\varepsilon}$) versus stress (σ) data, recorded during a three-point bending creep test (span length = 15 mm) in nitrogen atmosphere (tight chamber), on the rod-shaped specimens, using silicon carbide pistons and device. The specimen deflection (u) was measured in situ by means of a differential device using a linear variable displacement transducer. The composition used for this method was denoted as $D^{H}T^{H}0.5$ or TREOS/MDMD2/1 and $D^{H}T^{H}1$ or TREOS/MDMD1/1 the details are given in Table: 3.2. The creep deformation is studied for two different temperature ranges: 1000−1200°C and 1200−1400°C and the obtained flow properties are discussed below.

Although between 1000−1200°C contains the transition region for vitreous silica, the oxycarbide viscosity is very high, above 10^{14} Pa.s, up to 1200°C. Furthermore, the difference between the data of the SiOC glass and of fused silica increases with rising temperature, and the apparent activation energy for flow is

much smaller for the oxycarbide glass (ΔG_a 296 kJ/mol) than for silica ($\Delta G_a \approx 500-700$ kJ/mol). A transition temperature of 1350°C, identical to that reported by Renlund *et al.*,[66] is reported by extrapolation of the viscosity curve of the oxycarbide glass to the conventional viscosity range of $10^{12}-10^{12.6}$. This transition temperature of 1200 to 1300°C has already been reported for the grain boundary glassy phase of a Si_3N_4/SiC nano-composite, suggesting that some carbon was present in the glass network. This difference in viscosity values are coming from the introduction of covalently bonded carbon to silicon. Also in this temperature range the authors observed 3% rise in the elastic modulus though there is no crystallization detected by XRD. This increase is due to a structural relaxation phenomenon and to the concurrent densification.

In the higher temperature range (1300-1400°C) the flow kinetics are influenced by crystallization. Before this region between 1150°C to 1215°C, the SiOC system follow a creep-hardening. At and above this temperature crystallization process starts and leads to the formation of β-SiC nano-crystals. The average size of crystallites, as estimated from the XRD spectra, was 2.5 nm. The crystallization process resulted in a composite microstructure where β-SiC crystals were dispersed almost homogeneously, although some relatively large crystals (5−8 nm in diameter) are also formed. It is reported that the hardening behavior is dependent on the composition (or free carbon) and is pronounced in the case of D^HT^H1 grade. Rouxel suggested that because of the strain hardening mentioned above in the intermediate temperature range, the values of viscosity increases sharply. This viscosity value is dependent on the volume fraction of SiC, size of the particles and are fitted on model derived from analogy between pure Hookean elasticity and Newtonian flow. However, no time hardening effect was observed by the authors for the $D^HT^H0.5$ glass on the strain rate vs. time curve. This is probably because the SiC volume fraction is not large enough to affect noticeably the viscous flow. Therefore, the only incidence of the presence of SiC would lie in the tendency for the activation energy for flow to be higher above 1200°C, getting closer to the value for a pure silica glass, as is expected from the decrease of the carbon content in the residual glass that follows crystallization.

Here we report the effect of aluminum modification on the thermo-mechanical property development in SiOC ceramic system and compare it with the above research.

3.8 Oxidation Resistance

Silicon based ceramics and composites are prime candidate for heat engines and heat exchanger structural components. In such applications these materials are exposed to combustion gases at high temperature. The following discussion is aimed to review the current state of knowledge of the interacting oxidizing atmospheres, mainly air or oxygen on Si-based ceramics, for e.g. SiC and Si_3N_4.

3.8.1 Oxidation Review on Silicon Based Ceramics

The focus of this section is on the fundamental studies of SiC and Si_3N_4 oxidation. These studies provide an atomistic understanding of the mechanism of SiO_2 scale growth. These include determining the slow reaction step (or steps) and understanding the diffusion mechanism.

SiO_2 has some unique properties that influence its performance as a protective oxide. In most oxidation experiments SiO_2 forms as an amorphous film and then crystallizes to either cristobalite or tridymite. It is generally accepted that the mobile species is oxygen, not silicon. For this reason the chemical reaction occurs at the SiO_2/Si or SiO_2/ceramic interface.[81] Transport through SiO_2 can occur by diffusion of molecular oxygen as interstitials or by network exchange of ionic oxygen. The latter is referred to as either "network exchange diffusion" or "ionic diffusion". It is noteworthy to say that the molecular oxygen diffusion coefficient is roughly 10^6 times greater than the ionic oxygen diffusion coefficient.

3.8.1.1 Oxidation of Silicon

Before discussing the oxidation of ceramics, namely SiC and Si_3N_4, it is appropriate to discuss the oxidation of pure silicon. The classic paper in this area is by Deal and Grove.[82] They view oxidation as consisting of three distinct steps. The three steps are: transfer of the gaseous oxidant to the outer surface of the oxide film, diffusion through the oxide film, and reaction of the oxide/silicon interface. From this steps they derived the following linear-parabolic relationship:

$$x^2 + Ax = B(t + \tau) \tag{3.38}$$

where
x = scale thickness
B = Parabolic constant
t = time
τ = time shift corresponding to the presence of initial oxide layer
The quantity B/A is the linear rate constant and the parabolic rate constant is given by

$$B = \frac{2D_{\text{eff}}C^{*}(O_2)}{N_{\text{o}}} \tag{3.39}$$

where
D_{eff} = Diffusion coefficient through the film
$C^{*}(O_2)$ = Equilibrium concentration of oxidant in the scale
N_{o} = Number of oxygen molecules incorporated in the SiO_2 scale per unit volume.

For short oxidation times, oxidation follows a linear rate law. The physical interpretation of the linear region is still controversial; it has been attributed to interface control or to diffusion control which is non-parabolic due to strain effects in the oxide. For longer times, oxidation follows parabolic law, and diffusion through the thicker oxide is rate controlling.

An activation energy can be determined from a plot of lnB vs 1/T. The magnitude of the activation energy can reveal useful information about the diffusion process. Calculation of the parabolic rate constant that are based on the molecular oxygen diffusion coefficient show good agreement with the measured values, and the activation energy for parabolic oxidation is close to that for molecular oxygen diffusion through SiO_2. Thus it is generally accepted that molecular oxygen diffusion through the SiO_2 layer is rate controlling.

3.8.1.2 Oxidation of Silicon Carbide (SiC)

The oxidation of SiC is more complex. Here, we have a countercurrent of gas. Note that, N_{o} from Eq:3.39 must be modified for SiC oxidation due to the formation of CO. The following reaction is generally accepted:

$$SiC_{(\text{s})} + 1.5O_{2(\text{g})} = SiO_{2(\text{s})} + CO_{(\text{g})} \tag{3.40}$$

However the actual process may involve other reactions. The production of CO in the oxidation of SiC has been reported in the literature, although the possibility of further oxidation to CO_2 must be considered. There has been no clear observation of the production of elemental carbon. Note that, even though the reaction leads to a net weight gain, there is also some weight loss due to gas evolution. These reactions may be monitored by following net weight gain, scale thickness as a function of time, or even gas evolution. Mainly the first method, i.e., change in weight with time during oxidation is used and the parabolic growth law of type indicated in Eq. (3.41) is used.

$$\left(\frac{\Delta m}{A}\right)^2 = K_{\mathrm{p}}(T) * t + constant \tag{3.41}$$

where, Δm being the mass gain, A the sample surface, t the oxidation time, T the temperature, and $K_{\mathrm{p}}(T)$ is the parabolic constant.

The oxidation process of SiC involves five steps:

1. Transport of molecular oxygen gas to the oxide surface.
2. Diffusion of oxygen through the oxide film.
3. Reaction at the oxide/ceramic interface.
4. Transport of product gases through the oxide film.
5. Transport of product gases away from the surface.

The key question concerns the rate-controlling steps. Another question deals with the transport mechanism through the SiO_2 scale. Is it permeation through the network by oxygen molecule or a network exchange mechanism of O^{2-}? Even less is known about the transport mechanism of the product gasses outward through the SiO_2 scale.

The key observations for the oxidation of SiC ceramics have been summarized by several investigators.[83), (84)] Many investigators have observed a brief ($<<$ 1h) linear region followed by a parabolic region. The focus of most investigators has been on the parabolic region. We now discuss three rate-controlling steps:

Investigator	Temp. Range (K)	Activation Energy. E(kJ/mole)
Deal and Grove (Si)	1073−1473	119.3
Costello and Tressler (CNTD SiC)	1473−1673	142
Zheng *et al.* (single crystal SiC)	1673−1773	293
C face	1473−1623	120
C face	1623−1773	260
Si face	1473−1773	223−298
Schiroky *et al.*	1640−1820	125.5
Narushima *et al.*	1823−1948	345

Table 3.5: Reported activation energy for silicon and SiC oxidation.

- **Oxygen Diffusion Inward**

In general, most of the data imply oxygen diffusion inward as rate limiting. Rates are parabolic and dependent on the partial pressure of Po_2. Motzfeld *et al.*[85] after correcting for the stoichiometry difference (i.e the additional oxygen necessary to oxidize carbon), he finds that silicon and SiC have essentially the same rates and same activation energies. Therefore he concludes that the same process that controls the silicon oxidation also controls SiC oxidation (i.e., oxygen diffusion inwards). Resent measurements on single crystal SiC give rates somewhat slower than those for silicon.

Table: 3.5 summarizes the activation energies for the oxidation of high-purity SiC. There is generally a low-temperature (T < 1623 K) and a high-temperature (T > 1623 K) regime. In the low-temperature regime the activation energy is low, about 120 to 140 kJ/mole, and is similar to that for oxidation of pure silicon and molecular oxygen diffusion through amorphous SiO_2. This supports molecular oxygen diffusion inwards as a rate-controlling step for SiC oxidation below 1623 K. Zheng *et al.*[86],[87] explained this by forming a scale in ^{16}O and then reoxidizing in ^{18}O. An accumulation of ^{18}O at the SiO_2/SiC and SiO_2/gas interface, as determined by SIMS, supports this.

- **CO Diffusion Outward**

Some investigators have attributed the higher activation energies at higher temperatures to a transition to CO-diffusion-outwards rate control. Two factors tend to discount this. Zheng *et al.* have oxidized SiC and examined the resultant scale by using SIMS. They found no carbon gradient, as one would expect if CO diffuses outwards slowly. Thermodynamic arguments also support the rapid transport of CO outward. Suppose the reverse is true and CO diffuses outwards slowly. Then Po_2, at the SiC/SiO_2 interface must be close to 1, and, as required by diffusion control, Eq. (3.40) equilibrium is maintained; the P_{co} has a value of about 10^{27} bar at 1600 K. Extremely high pressure would be expected to blow the scale off, but this is not observed.

- **Interfacial Reaction**

The other possibility for rate control is interfacial reaction. Some investigators have reported linear reaction rates for the silicon face of the single crystal SiC, which is attributed to interfacial reaction control.[88] However most of the data for pure SiC indicate parabolic kinetics for the majority of the reaction period. However, most of the data for pure SiC indicate parabolic kinetics for the majority of the reaction period.

However, the situation is not so clear. The most resent data indicate that single crystal SiC has rates slower than that of pure silicon, even with the stoichiometry correction. Furthermore, the assumption of oxygen diffusion inward and CO diffusion outward assumes that one is fast and the other is slow. Although CO is polar and molecular oxygen is not, it is difficulty to imagine that they would have dramatically different permeation properties. These three facts make it difficult to accept that oxygen diffusion inwards as completely rate controlling. Physical phenomenon do not always fall into distinct categories. As Luthra reports,[83] it may be that a mixed control mechanism is operative and both diffusion and the interface reaction are rate controlling. Because of the different rates of single-crystal SiC and silicon, Luthra advocates mixed interface and CO diffusion outward control. However, the limited evidence for high CO pressure at the SiO_2/SiC interface and lack of a carbon gradient tend to oppose CO diffusion outwards.

3.8.1.3 Additive Containing Materials

The discussion thus far has centered on highly pure materials oxidizing in pure oxygen for short times and forming amorphous SiO_2. The situation in actual is more complex. First, consider isothermal oxidation of less pure materials. In the actual situation the amorphous scale may often crystallize because of impurities in the substrate or water in the environment. Generally it crystalizes to cristobalite. In general, transport in cristobalite is slower than transport in amorphous SiO_2. Costello and Tressler[84] have correlated a slowing of reaction rates with crystallization of the oxide scale. The exact nature of crystallization is highly dependent on impurities in the specimen and/or the atmosphere. However, for sintered α-SiC with boron and carbon additives, crystallization begins at the SiO_2/SiC interface and spreads to the surface.[81],[89]

Densification aids in SiC have an even more complex effect. The refractory oxide additives, such as magnesium oxide (MgO), alumina (Al_2O_3) and yttria (Y_2O_3), tend to migrate out to the SiO_2 scale and form the corresponding silicate.[90],[91],[92] The additives are initially present as a grain-boundary silicate glasses. The initially pure SiO_2 layer creates a gradient and a driving force for the cations to diffuse into this glass. The free energy of silicate formation in the surface SiO_2 is a second driving force. Enough aluminum diffuses into the scale to form an aluminosilicate. Generally this phase appears to accelerate rates. In the case of SiC sintered with boron and carbon sintering aids, boron diffuses into the scale. It creates a lower viscosity scale, which leads to somewhat higher oxidation rates over pure SiC.[91],[93]

More recently, the oxidation behavior of SiC ceramics with aluminum nitride (AlN) and rare-earth oxides (Y_2O_3, Er_2O_3, Yb_2O_3) as sintering additives has been characterized.[94] It is postulated that the amount of aluminum in the sintering additives, the cationic radius of rare-earth oxides, densification, and annealed atmosphere, and the formation of compatible oxidation product to SiO_2 contributes to the superior oxidation resistance of the SiC ceramics.

Luthra *et al.*[88], reported oxidation studies on Al_2O_3−SiC and mullite−SiC composites at 1375°C to 1575°C in O_2. The reaction product contained alumina, mullite, an aluminosilicate liquid, and gas bubble. The parabolic rate constant were about 3 orders of magnitude higher than those expected for the oxidation

of SiC. Higher rates are caused by higher oxygen permeabilities through the reaction product than through pure silica.

3.8.2 Oxidation of SiOC Ceramics (Fibers and Powder)

Till date, oxidation of silicon oxycarbide phase is explained with the help of Nicalon fibers. Polycarbosilane−(PCS) derived SiC fibers (Nicalon and Hi−Nicalon, Nippon Carbon Co., Tokyo, Japan) used for these investigation have a microstructure composed of β-SiC crystallites, free carbon, and an amorphous silicon oxycarbide phase SiC_xO_y phase.[95] In particular, Nicalon fibers have large amount of SiC_xO_y phase, which generates both SiO and CO gases to crystallize into β-SiC at 1500°C. Although both oxidation of free carbon and thermal decomposition of the SiC_xO_y phase yield mass loss, passive oxidation of β-SiC crystallites causes mass gain. Finally, passive oxidation of the Nicalon fibers is thought to yield mass gain and will be explained below.

Recently Chollon[96] investigate various fibers in Si-C-N-O system. In this study he discussed oxidation of Si-C-O, Si-C-(O), Si-C fibers. These fibers are processed by spinning polycarbosilane and is referred by famous name, namely Nicalon. Changing the processing condition changes the oxygen and free carbon level of the final ceramic fiber. For example, curing the fiber in air increases the oxygen content and is referred as Si-C-O fiber, whereas curing the fiber with electron beam result in lower oxygen level but contain excess free carbon. It has been proven that the first two systems, i.e., Si-C-O and Si-C-(O) contain amorphous silicon oxycarbide phase on the surface but is absent for the third system, namely Si-C.

As mentioned earlier, the oxidation of pure SiC is controlled by Eq. (3.40). The rate controlling step imposing the oxidation rate for SiC below 1400°C, is generally admitted to be the permeation of O_2 through the silica scale inward. The Si (0001) face of a SiC single crystal exhibits significant lower parabolic oxidation rates and a higher activation energy than the C (000-1) face.[84] More recently, the same conclusion were reported and extended to highly textured CVD-SiC.[97],[98] This behavior was suggested to arise from the presence of a Si-C-O sublayer appearing only for the slow oxidation rate faces of the SiC single crystal and the CVD-SiC film. This sublayer, more resistant to oxygen diffusion,

Material	E_{oxi}	x	C_{free} [at.%]
Si-C-O	70 ± 7	0.85	15.0
Si-C-(O)	95 ± 1	0.96	18.5
Si-C	107 ± 3	0.99	17.5
SiC	90/140 ± 7	1.00	0

Table 3.6: Reported activation energy (E_{oxi}), stoichiometric constants for bonded and free carbon (x, C_{free}) in $SiC_xO_{2(1-x)}$ composition, during Si-C-O fibers oxidation in pure oxygen.

would result in much lower parabolic constants than on the opposed faces.

All the materials described by Chollon have an isotropic microstructure (either amorphous or nano-crystallized). Their oxidation behavior is therefore expected to be dominated by the highest oxidation rate of SiC monocrystals (that of the C-face), consistently with the large majority of the data obtained from similar materials. The magnitude of the oxidation parabolic rates obtained for the Si-C-O fibers are generally close to those reported for crystalline SiC and the corresponding activation energies fall all within the range 70−110 [kJ/mole], close to the value of SiC. The oxidation activation energies for various fibers investigated by Chollon are listed in Table: 3.6. This feature suggests that, similar to pure SiC, the oxidation kinetics of the Si-C-O fibers is controlled by the same mechanism as that of the oxidation of silicon, i.e. the permeation of molecular oxygen inward through the growing silica layer. The general oxidation reactions for the Si-C-O fibers is written by Chollon as follow:

$$SiC_xO_{2(1-x)(s)} + 3/2_xO_{2(g)} \longrightarrow SiO_{2(s)} + xCO_{(g)} \tag{3.42}$$

with $0 \leq x \leq 1$ for the $SiC_xO_{2(1-x)}$ continuum and

$$C_{(s)} + 0.5O_{2(g)} \longrightarrow CO_g \tag{3.43}$$

for the free carbon phase.

More insight into the oxidation chemistry of SiOC ceramics from passive oxidation is reported recently by Brewer *et al.*.[99] The oxidation chemistry of SiOC ceramics is explained with the help of two similar simple reactions, namely Eqs. (3.42) and (3.43). Reaction (3.42) involves a net weight gain from the ceramic

however, reaction (3.43) produce a net weight loss. Inspite of these simple reactions, discerning between the two of them or the extent to which each takes place is not a trivial matter.

Brewer *et al.* approached the oxidation insight with four different materials derived form silsesquioxane-based precursors over the temperature range of 600 to 1200°C. The four different materials have following compositions: $SiO_{1.24}C_{4.08}$, $SiO_{1.30}C_{2.41}$, $SiO_{1.28}C_{1.39}$, $SiO_{1.35}C_{1.14}$. These compositions produce Si-C ratios of 0.38, 0.35, 0.36, 0.325 and free carbon (C_{free}) of 90.6, 85.4, 74.1 and 71.5%, respectively. The authors found that, a combination of techniques both qualitative: visual experience and optical microscopy and quantitative: weight and the compositional change combine to yield a reasonable picture of the changes that takes place upon oxidation of SiOC's.

For all compositions, Brewer reported weight loss at all oxidation temperatures studied. The weight loss is highest for the ceramic whose composition contains the maximum excess carbon. Even those most oxidatively stable compositions, with the lowest amount of excess carbon, show continued weight change at all the temperatures. Interestingly he observed that, the highest weight loss and appearance of the powder after oxidation (changing it to white) are not associated with the highest oxidation temperatures. There is an retention of the black color even after long times (100 h) at 1200°C while at 800 the same material appears gray in less than 30 min of exposure. He argued that, these differences at different temperatures likely lies in the relatively rates of the two reactions shown in Eqs. (3.42) and (3.43). At lower temperatures (600 to 800°C) Eq. (3.43) dominates the initial oxidation chemistry causing porosity. This increase in the porosity gives oxygen access to essentially all the samples allowing the higher oxidation of the Si−C bonds Eq. (3.42) to proceed through the entire material. Additionally, at higher temperatures (1000 and especially 1200°C) the rates of two reactions are more comparable. The reaction product of Eq. (3.42) form an expanded silica barrier at the surface of the material, which slow the diffusion of oxygen and, therefore, inhibits oxidation from proceeding rapidly throughout the entire material.

Brewer et al. extracted more information about the chemistry that takes place in oxidation, by analyzing the changes in equivalents of Si−C bonds, Si−O bonds and equivalents of excess carbon after oxidation. He observed that, there is a

very rapid initial chemistry that takes place, loss of excess carbon and oxidation of Si−C bonds to form Si−O bonds in the first hours of oxidation. In general, this research illustrate how dramatic the composition change is for the high carbon material upon oxidation and the relative 'stability' of the low carbon material. He elaborate the oxidation chemical change of two composition: one with high free carbon and the other with low.

For high free carbon containing material, a quantitative analysis show that the excess carbon disappear quickly and the silicon species is completely converted to SiO_2 within 5 hours of exposure at 600 and 800°C. But at higher temperature this material behave differently i.e., between the time domain of 100 and 200 h of oxidation, all of the Si−C bonding is oxidized but excess carbon persists even after 500 h of oxidation. In contrast, the low free carbon containing material undergoes a very rapid initial oxidation (within the first 15 min) followed by a rather slow continuous change even after 500 h regardless of the temperature examined. The free carbon and Si−C bond equivalents are still presents even after this long oxidation time. This indicate that the free carbon content controls the oxidation process.

Brewer attempt to quantify these differences in oxidation by calculating the slope of both excess carbon and the Si−C bonds equivalence for low and high excess carbon containing material. This analysis demonstrated that those materials with significant amounts of carbon continue changing at a faster rate than those with small amount of excess carbon after this initial oxidation. These high carbon materials will continue to change until they are completely oxidized to SiO_2. This oxidation of the high carbon material is significantly faster at 600 or 800°C compared to 1000 or 1200°C. The low carbon materials continue to change after this initial oxidation but at the slow rate.

No real oxidation investigation of bulk SiOC ceramics is reported. This research hence focus on the oxidation resistance study of SiOC bulks and ahead look into the effect of modifying the ceramic chemistry by aluminum on oxidation and change in surface morphology.

3.9 Applications

Although a large variety of silicon containing polymers with high ceramic yields have been developed, only low-dimension products, such as fibers and thin films, have found wide application. To date, most preceramic polymers have been employed as precursors to ceramic fibers, matrices, and as binders for ceramic powders. The applications will be briefly reviewed in the following section.

3.9.1 Polymer Derived Ceramic Fibers

The most notable application of preceramic polymer technology to date is in the manufacture of non-oxide ceramic fibers. Preceramic polymer technology has been utilized almost exclusively to prepare silicon carbide, silicon nitride, or amorphous silicon carbonitride fibers. Synthesis of hybrid continuous silicon carbide-titanium carbide fibers through sol-gel processing is reported.[100] These gels were prepared from novolac-type phenolic resins, TEOS and titanium tetrakis(2,4-pentanedionate)at 65°C. Just before gelation the viscosity of the solution increases with time and at some particular range $\sim$ 30 cm long fibers are drawn. These gelled fibers are transformed into ceramic to form SiO_2-TiO_2 inorganic fibers which via heat-treatment in argon at high temperature transforms to SiC-TiC hybrid fibers. Such fibers provide many desirable properties for application in continuous fiber-ceramic composites intended for high temperature use in oxidative and non-oxidative atmospheres. For example, SiC fibers have advantages over carbon fibers in certain applications where greater resistance to oxidation, superior compressive strength, and greater electrical resistance, are desired. Along with SiC fibers other ceramic fibers like Si-Ti-C-O, SiC-C fibers exhibit better strength retention at high temperature than the carbon fiber.[101] The tensile strength of the ceramic fibers do not show a marked decrease until $\sim$ 1000°C. In contrast, the strength of the carbon fiber starts to decrease at a significantly lower temperature ($\sim$ 400°C).

In line with the present thesis i.e development of Si-Al-O-C ceramic, Ishikawa *et al.*[102] developed new sintered SiC fibers by sintering of an amorphous Si-Al-O-C fiber precursor at high temperature. Si-Al-O-C fiber was synthesized by the use of polyaluminocarbosilane prepared by the reaction of polycarbosilane with

aluminum acetylacetonate. The transformed fibers possess high strength (>2.9 GPa) and high modulus (>300 GPa), high heat resistance (up to 2000°C). The other counterparts namely Nicalon[NL201], Tyranno[LoxM] (Si-Ti-C-O fiber), Hi-Nicalon and Tyranno[ZM] (Si-Zr-C-O fiber) looses strength at around 1600°C and at very high rate. The fiber showed better high-temperature creep resistance even at 1300°C and 1 GPa, in air, compared with other commercial counterparts.

Advantages of the polymeric route in the formation of ceramic fibers include: the ability to control fiber purity, the ability to control fiber crystallinity and crystallite size, and the ability to produce continuous, fine diameter (<30 μm) suitable for weaving and knitting of the fiber preforms for resin transfer molding. One of the most unique advantages is the ability to prepare fibers with new and metastable compositions unobtainable by other methods.

3.9.2 Other Applications

Preceramic polymers are frequently employed as precursors to matrices in ceramic matrix composites (CMCs).[103],[104],[105],[106],[107] The development of low viscosity preceramic polymers offers the use of well developed tools and techniques, that are commonly employed for polymer composite fabrication, to the manufacturing of ceramic composites. One of the most promising technique for manufacturing high temperature, ceramic composite structures is impregnation/resin transfer molding (I/RTM). In (I/TRM), preceramic polymers are infiltrated into 2-D and 3-D fiber preforms and pyrolyzed to convert the polymer to a ceramic matrix phase. For example, *Allied Signal, Inc.* currently manufactures ceramic fiber reinforced composite materials employing a poly(siloxane) preceramic polymer. Using resin transfer molding, 2-dimensional or 3-dimensional high density ceramic fiber reinforced composites are manufactured by infiltration and pyrolysis of a poly(siloxane) to an amorphous silicon oxycarbide matrix phase. For the formation of a 2-D composite, fiber tows or woven fabric are impregnated with the poly(siloxane) resin to produce a prepreg that can be handled like an epoxy material. After a lay-up and autoclaving step to form, consolidate, and cure the polymer infiltrated composite, the body is pyrolyzed in an inert atmosphere at temperatures less than 1100°C to convert the polymer to the silicon oxycarbide. For the formation of a 3-D composite, a 3-D fiber preform is infiltrated with

the poly(siloxane) and subsequently cured to produce a rigid specimen. The cured specimen is then pyrolyzed in an inert atmosphere at T < 1100°C to convert the polymer to the silicon oxycarbide. Due to the loss of volatiles during pyrolysis of the preceramic polymer, the porous bodies are re-infiltrated with polymer and pyrolyzed to increase the final density of the composite. According to some literature, 5 to 7 reinfiltration/pyrolysis cycles are often necessary to achieve porosities less than 12%. Employing this process, complex shaped components, such as gas mixing tubes, turbine engine blades, engine tail cones, and vanes have been successfully manufactured by companies such as Auto-Air, Rohr, Northrop-Grumman, and Loral-Vought.

Polymeric precursors are actively being investigated as precursors to interface coatings in ceramic matrix composites. Using polymeric precursors for interface coatings offers the potential for reduced cost compared with conventional chemical vapor deposition techniques. The coatings could be applied to fibers by dip coating from a polymer solution and cured to serve as sizing to protect the fibers during further handling and/or weaving and pyrolyze to form ceramic interfaces between the fiber and the matrix. Furthermore, by tailoring the composition of the starting precursor, the chemistry and properties of the interface between the fiber and the matrix could be engineered, to improve overall composite properties. Heimann[108] dip coated SiC fibers with poly(silsequioxane), poly(borosilazanes), and poly(carbosilanes) and pyrolyzed them in an inert atmosphere to produce Si-O-C, Si-B-N, and Si-C coatings, respectively. SiC fibers coated with Si-C-O were then incorporated into a reaction-bonded silicon nitride matrix. The author claimed that the coated fibers provided a weaker interface than the uncoated fibers. The author suggest that the weaker interface promoted fiber debonding which ultimately improved toughness of their composite material. Ueno *et al.*[109] studied the effects of poly(carbosilane) coatings on SiC whiskers, on the toughness of Si_3N_4 matrix composites. Twenty percent by weight SiC whiskers were dip coated with poly(carbosilane) and blended with Si_3N_4 powder. The mixture was compacted to form a green body and hot-pressed at 1850°C under pressure of 30 MPa. During sintering, pyrolysis of the poly(carbosilane) resulted in a SiC/graphite interface between the SiC whisker and the Si_3N_4 matrix. According to the fracture toughness measurements author claim that the composite containing the coated whisker had a higher fracture toughness, 7.9 MPa.$\sqrt{m}$.

It was proposed that the slight increase in fracture toughness resulted from a weaker whisker-matrix interface due to the presence of graphite at the interface.

Preceramic polymers have found significant use as binders for ceramic powders for the fabrication of parts by compression or injection molding. A preceramic polymer can play the role of traditional organic binders during the consolidation steps; however, preceramic binders pyrolyze into ceramic materials which remains in the void spaces that would normally be left by removal of traditional organic binders.

Another area of polymer derived ceramics exist in the formation of coated layer on high strength but low oxidation property materials. Bill *et al.*[110] used commercial polysilazane NCP 200 to form an amorphous SiCN ceramic dip-coating on C/C−SiC composites. This composite material possess carbon fibers as a reinforced material and is one of the most promising materials with which to realize light weight structures at high temperatures, and find application in areas such as the aircraft and space industry as well as in automotive and energy technologies. The crucial drawback for C fibers is their low stability in an oxygen-containing atmosphere at elevated temperature. Similar work is perform by us on carbon fiber reinforced composite also using commercial polysilazane namely Ceraset.[111] All polymer-to-ceramic transformations involve volume shrinkage, added with different coefficient of thermal expansion, which lead to crack formation in the coated layer. To compensate this shrinkage it is suggested in this research to use fillers which also posses inherent high oxidation resistance. It has been shown that coating quality can be improved by optimizing polymer concentration, speed of drawing, filler particle size, multiple coating and pyrolysis cycle.

Present promising are of polymer derived ceramic in applied research is the development of ceramic matrix composites. Active research is in development and reported by Greil *et al.*.[17] Manufacturing of bulk ceramic components from materials in the system Si-Me-C-N-O (Me = Ti, Cr, V, Mo, Si, B, $CrSi_2$, $MoSi_2$, etc.) from preceramic organosilicon polymers such as poly(carbosilane), poly(silazanes), or poly(siloxanes) has become possible by incorporating filler into the liquid or solid precursors. During pyrolytic decomposition of the polymer matrix, the filler particles react with carbon from the polymer precursor or nitrogen from the reaction gas atmosphere to form new (oxy)carbide or (oxy)nitride phases

embedded in the nanocrystalline Si-O-C-(-N) matrix. With this development the Near-Net-Shape forming of bulk ceramic components, even with complex geometry is possible and are of particular interest for wear-resistance machinery components, fiber-reinforced, light weight components for aircraft structures; surface sealing of porous structures; and biomedical dental restorations.

Most recent application of small scale ceramics is seen in the development of Micro Elecro Mechanical Systems (MEMS). This is reported in the present papers on SiCN ceramics using the techniques like microforging and photolithography and will be discussed in the final section of the thesis in more detail. We used the commercial polysiloxane to demonstrate the feasibility of MEMS processing and also its use as a ideal material for injection molding of components in complex shapes with fillers.

4 Experimental Procedure

This research work is divided into two parts: (1) formation of silicon oxycarbide glasses from commercially available preceramic polymer, and (2) modification of commercial polymer by aluminum, forming Si-Al-O-C ceramics after pyrolysis. The processing of both types will be discussed in the following sections.

4.1 Unmodified Preceramic Polymer

4.1.1 Basic Materials

The polymer used for this research is a product from Wacker Chemie GmbH, Burghausen, with a trade name Wacker-Bensil PMS MK (MK polymer). MK polymer is a solid solvent free poly(methylsilsesquioxane) polymer with $(CH_3\text{-}SiO_{3/2})_x$ basic structure and fall under silicone resin group.

The odorless, colorless flakes of MK-polymer has a softening range between 45-60°C and a good solubility in organic solvent; namely, aromatic solvents and ketones. The polymer possess approximately 2 Mol.% hydroxy and ethoxy groups, as functional units. Accordingly, the possible structure of the used resin along with its functional groups is illustrated in Fig. 4.1 and Fig. 4.2.

With evolution of water and ethanol by polycondensation reaction, a three dimensional network with Si-O-Si backbone takes place. In order to achieve an acceptable process regime, a suitable *CLA* in sufficient amount and a thermal treatment are necessary. As a cross-linking-agent, Zirconium acetylacetonate (henceforth referred as *CLA*), with an amount of 1 wt.% related to the polymer mass is used. The *CLA* is an zirconium complex with a chemical formula; $C_{20}H_{28}O_8Zr$.

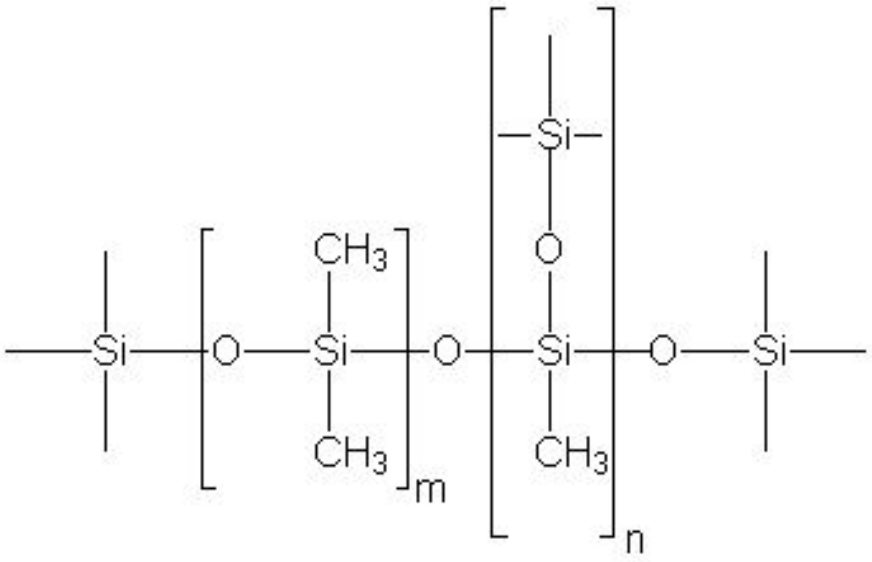

Figure 4.1: Possible structure of MK-polymer with linear and branched components.

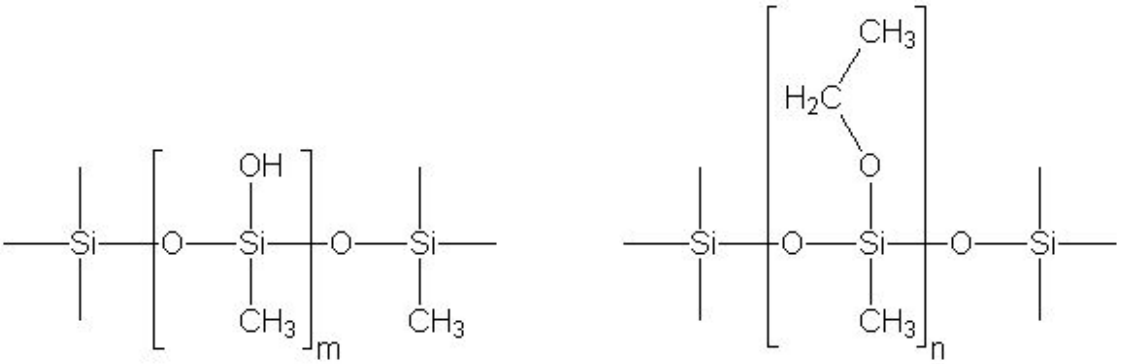

Figure 4.2: The oligomers and functional groups present in MK-polymer

4.1.2 Mixing Procedure, Cross-linking and Shaping

Keen attention must be paid on the mixing procedure to attain a good distribution and homogeneity between all components. This defines the necessary and sufficient precondition(s) for the later processing; namely, complete cross-linking, shaping and pyrolysis.

The investigation of properties are measured on polymer and *CLA* mixture prepared by two different ways; namely, *Dry route* and *solution route*. The *CLA* amount is varied to 0.5, 1, 1.5 and 2 wt.% and an optimized value of 1

wt.% (explained later in results) is used for further study. In *dry route* method mixture, polymer and *CLA* powders are milled in a planetary mill for long time. Whereas, in the *solution route* the polymer was dissolved in isopropanol along with 1 wt.% *CLA* and the solution is stirred by a magnetic stirrer for 30 min. The *CLA* added polymer solution was dried under vacuum at moderate temperature (40−50°C). The resulting powder is in a semi-dried condition, containing some big particles with entrapped solvent. Therefore, the mixture is milled using a ball mill followed by redrying in vacuum for long time (3−5 h), and subsequently sieved from 100 μm mesh producing free flowing powder. This method results in homogeneous distribution of the *CLA* in the polymer as compared to the mechanical mixing.

The shaping of the powder mixture together with cross-linking of the poly(methyl-silsesquioxane) to an un-meltable polymer mass with a three dimensional network of polymer chains is achieved by warm pressing under pressure and high temperature in an metallic form. For warm pressing, a cylindrical steel die with 10 mm internal diameter is used. Around this die, a heating element is attached, which can operate between ambient temperature to 500°C. The temperature control is made by a thermocouple, which by an appropriate drilling on half the height of the cylinder is directly positioned beside the pressed powder. Pressure is applied with an oil hydraulic press (Model from Fa. Paul-Otto-Weber GmbH) with a maximum load of 100 kN. Before every pressing process, the inner side of the warm press form and the used side of the stamps is coated with silicone oil as a lubricant. This treatment is necessary, to reduce friction between the green body and the press form, which if not done could cause demolding difficulty and may result in cracking of the green body. The initial weight of the polymer powder mixture filled in the mold cavity varies from 0.5 and 1 g. The filled press form is inserted in the press and heated up with constant load (4.8 kN for 10 mm diameter form, ≈ 50 MPa) to the selected warm pressing temperature (150−170°C) in this case. In addition, for all attempts a constant heating rate of 10°C/min is selected. During the heating cycle, continuous sinking of the applied load is observed between 60-110°C and the load rises with further heating, but is constantly corrected by manual readjustment to the desired value. The compression pressure is maintained for 10−15 min after reaching the final temperature. The pressure is gradually reduced to zero during the cooling cycle and when the

temperature is reached to 100°C the green body is ejected. This gradual reduction in the applied pressure in the cooling cycle and the ejection of the sample at relatively high temperature than room temperature avoid damage of the sample. Ejecting sample at room temperature could lead to crack formation, because of the brittle nature of the cross-linked green body. The thick green body is sliced by diamond wire saw for maximum thickness of 0.6−0.8 mm, before pyrolysis.

4.1.3 Pyrolysis

In all attempts pyrolysis is accomplished in quartz tube (h = 50 cm, d_i = 3 cm). Here, simultaneous pyrolysis of up to five green bodies is possible without any practical problems. No sticking together or deformation is observed because of neighboring or stacked green bodies. For pyrolysis, the green bodies are heated to 1100°C at a rate of 25 °C/h, held at this temperature for 2 h, and then cooled to room temperature at a rate of 100°C/h. Due to such long duration of pyrolysis cycle, and in order to avoid the oxygen contamination, the top lid of the quartz tube is closed using a high temperature grease (Apiezon H, Fa. Roth). The quartz tube is inserted perpendicular in an electrically heated vertical Al_2O_3 tube furnace. It is made certain that the samples are positioned always in the correct height of the furnace where planned temperature could be reached. This position is frequently calibrated by an external temperature controller. Lower end of the furnace is closed, in order to prevent variations in temperature by radiation. Pyrolysis takes place under a constant argon stream via plastic/rubber tubing, which are connected to a flow controller. Argon stream succeeds easy and continuous exhaust of the decomposition gases from the quartz tube. The decomposition products along with used argon leaves the system through two exhaust bottles partially filled with Glycerin. This prevents any entrance of air in the reverse direction inside the quartz tube. All samples are removed from the quartz after ensuring complete cooling of the tube down to room temperature. At most care is taken during removal of samples, to prevent any contamination of the applied grease, which was applied initially to the opening of the tube.

4.2 Modified Preceramic Polymer

4.2.1 Basic Materials for Aluminum Modification

As mentioned earlier, modification of the polymer or a system on atomic scale can be easily achieved by sol-gel method. The modification work is continued on the commercially available poly(methylsilsesquioxane) (MK-polymer), and its availability and properties are already explained in the previous section. Out of various possible modifications; namely Ti, Zr, Al, and B reported in the literature part of this thesis, this work will be concentrated on aluminum modification, producing polymer and resulting ceramic therefrom after pyrolysis in Si-Al-O-C system.

Accordingly, Alumatrane (commercial Al-alkoxide from ABCR, with general formula: $C_6H_{12}NO_3Al$) was used as an aluminum modifier. This yellowish colored powder with a density of 1.05 g/cm^3 is sensitive to moisture and must be stored in dry place.

4.2.2 Modification Procedure: Sol-Gel Method

Alumatrane was dissolved in isopropanol in different mass ratios, namely 2.5, 9.1, 16.6, and 23.6 wt.% followed by dissolution of the polymer in isopropanol. Dissolution of both components are done in an ultrasonic mixture at room temperature. A polymer:isopropanol ratio of 4g:25mL was kept constant for all the mixtures. A sol-gel transition takes place at room temperature forming a yellowish milky white residue. Very low amount of alumatrane, namely 2.5 wt.% do not transform to a gel state at room temperature and instead requires temperature of 50°C for 5h. All gels were dried at 85°C in air for 24 h, ball milled and finally sieved to particle size < 63 µm.

4.2.3 Shaping and Pyrolysis

Same warm pressing die, with internal diameter of 10 mm (as mentioned in Section 4.1.2), is used for green body formation. Unlike unmodified system, a different procedure is used. Indeed, before filling the mold cavity with modified polymer powder weighing between 0.2 to 0.8 g (input material quantity is

related to the sample size required for post-pyrolysis characterization with different thicknesses), the inner parts of the mold along with pressing stamps are lubricated with a silicone spray. The filled press form is inserted in the press, and cold pressing at a constant load (8 kN for 10 mm diameter form, ≈ 80 MPa) for 5 min. is applied. Load is reduced to 4.8 kN (for 10 mm diameter form), which is equivalent to 50 MPa. Simultaneously, temperature is raised between 80−100°C with a heating rate of 10°C/min. Unlike sinking of the applied load with temperature; which is observed for unmodified system, a slight rise in load is observed for modified system, and this fluctuation is manually controlled to acheive constant pressure for the complete warm pressing heatng cycle. Samples are held at this temperature for 10−15 min. before cooling them to 50−60°C followed by ejection and subsequent pyrolysis. The ejection temperature is not as sensitive as that observed for unmodified system, but ejection at high temperature or at warm pressing temperature revealed surface cracking for some samples.

Pyrolysis was performed in the same system using quartz tube and under inert flowing argon stream; as explained earlier for unmodified system, with some variation in the pyrolysis cycle. The pyrolysis cycle offers flexibility for this system and the heating rate can be increased to reduce the processing time. All samples are heated to 1100°C with a heating rate of 30°C/h, held at this temperature for 2 h, and then cooled to room temperature at a rate of 10°C/min.

4.3 Sample Designation

The designation for the different samples in this study is also distinguished into two categories, namely unmodified and aluminum-modified. Accordingly, the unmodified silicon oxycarbide material, derived from MK polymer is designated as **SiOC** ceramic. Various compositions for aluminum modified silicon oxycarbide ceramics are designated as **SiAlOC2.5**, **SiAlOC1**, **SiAlOC2** and **SiAlOC3**, for gels prepared from MK polymer with 2.5, 9.1, 16.6 and 23.1 wt.% alumatrane; related to the polymer mass, respectively.

4.4 Post Pyrolysis Heat-treatments: Procedures

Further information about the properties of bulk Si(Al)OC ceramics from commercial polysiloxanes, are extracted by heat treating the samples in two different atmospheres, namely inert and air, and subsequently characterizing the material for its high temperature resistance and oxidation resistance. The procedures involved for these heat treatments will be explained in the following subsections.

4.4.1 Inert Atmosphere (Crystallization Behavior): Powder and Bulks

Thermal treatments were performed on bulks and powders in closed *h*-BN crucible to analyze the crystallization behavior. Before heat treatment the crucibles were boiled for 1 h in methanol and dried using vacuum and heat. The complete heating cycle is performed in two steps. Initial the samples were heated in vacuum up to 500°C in an ASTRO Oven. Later the temperature is raised between 1300−1600°C with a heating rate of 10°C/min in flowing argon atmosphere at a constant flow rate. The furnace is held at the maximum temperature for 5 h followed by cooling by 10°C/min to room temperature. The dimensions and masses for the samples were measured before and after heat treatment.

4.4.2 Air Atmosphere (Oxidation): Bulks

Oxidation of Si(Al)OC ceramics was performed by two different methods and on samples which had undergone different conditions, namely pyrolysis at 1100°C and heat treatment in argon at 1300°C.

Oxidation of pyrolyzed samples:

The as pyrolyzed cylindrical samples were sliced in the shape of bars and oxidation was performed using thermal gravimetry. The initial dimensions and masses of the bars were accurately measured before placing them in an Al_2O_3 sample holder. The samples were heated at 10°C/min to various temperatures, namely 1200, 1300 and 1400°C, under flowing argon with a flow rate of 100 L/h. After reaching the desired temperature, the weight change is recorded,

while temperature remaining constant, i.e., (isothermal treatment). The major drawback of using TGA for oxidation study is the sample size, which is very small. Here, errors could be generated in measurements of such sample dimensions.

As-pyrolyzed cylindrical samples were used in order to investigate the oxidation resistance for large samples. Samples were cleaned with acetone for 10 min and dried in drying oven between 80−100°C for 15−30 min. before measuring the weight and dimensions (diameter and height). Samples are placed on alumina plate and slowly inserted in oven, which is pre-heated to the desired temperature. The samples are withdrawn from oxidizing furnace after holding the samples for pre-decided time at constant temperature and reweighed. Repeating this procedure for different times on different samples is used to generates the kinetics of oxidation.

Oxidation of heat treated samples:

The pyrolyzed cylindrical samples are placed in closed *h*-BN crucible and inserted in ASTRO oven. The samples are heated at 10°C/min from room temperature to 500°C under vacuum and above this temperature to 1300°C under flowing argon followed by cooling. Treated samples are polished using different grade SiC polishing papers (similar to metallographic technique). Final polishing with 4000 grade paper approximately generate roughness of about 5 µm. Polishing is performed until a glassy mirror like appearance is achieved. Polished samples are washed by alcohol and carefully dried. Measuring the sample dimensions and weighing it completes the prerequisite conditions for oxidation.

Porous alumina boats specially designed to reduce the contact between the samples are used. These boats are prepared by carving soft porous alumina plates such that, only side edges of the samples (when inserted vertically) are in contact and the top and bottom surfaces of the cylindrical sample are exposed to air. The oxidizing furnace is heated to the predefined temperature and the boats along with samples are slowly drawn in the hot zone of the furnace. After holding the samples for a defined period (10, 15, 24, 36, 50, 75 and 100 h for this study) at isothermal temperatures (1200, 1300 and 1400°C) are withdrawn from the furnace and reweighed. All furnaces are cross-checked for the temperature accuracy and correct heating region with sintering rings and found to be in ±

20°C of the programmed temperature.

4.5 Mechanical Characterization of SiOC ceramic

The bulk processing of SiOC ceramic is demonstrated and in further discussion it will be shown that it results in dense ceramic. Mechanical properties like hardness and elastic modulus can be easily evaluated by indentation method. The elastic modulus can also be evaluated non-destructively by an acoustic method and both procedures will be explained in the following section.

4.5.1 Acoustic Method

The linear elasticity theory allows to give analytical expressions for the propagation velocity of acoustic waves in infinite media (continuum). For instance, the elastic modulus (E) and Poisson's ratio (ν) are expressed as follows:

$$E = \rho \, \frac{3V_l^2 - 4V_t^2}{(V_\mathrm{l}/V_\mathrm{t})^2 - 1} \tag{4.1}$$

$$\nu = \rho \, \frac{3V_l^2 - 4V_t^2}{2(V_l^2 - V_t^2)} - 1 \tag{4.2}$$

where ρ is the density of the material, V_l^2 and V_t^2 are the longitudinal and transversal wave velocities respectively.

When the specimen thickness is small, as in this case for SiOC ceramic (0.5 mm) the piezoelectric transverse transducers are often unable to efficiently promote the propagation of shear waves through the specimen. In this latter case, surface-type waves, also called Rayleigh waves, can be used. These waves are characterized by a velocity, $\mathrm{V_R}$, proportional to $\mathrm{V_t}$: $\mathrm{V_R} = \zeta \mathrm{V_t}$, where ζ is a function of Poisson's ratio, or of the $\mathrm{V_l}/\mathrm{V_t}$ ratio. $\mathrm{V_R}$ and $\mathrm{V_l}$ were measured in (LAIN, Montpellier)* and $\mathrm{V_t}$ was optimized to satisfy the following equation:

$$V_\mathrm{R} = \frac{V_\mathrm{t} \, \{0.715 - (V_\mathrm{t}/V_\mathrm{l})^2\}}{0.750 - (V_\mathrm{t}/V_\mathrm{l})^2} \tag{4.3}$$

*Experiments performed by Prof. T. Rouxel, University of Rennes, France

The elastic modulus and the poisson ratio for thin SiOC ceramics are investigated by acoustic measurement. The poisson ratio investigated from this measurement is used for investigating elastic modulus by indentation method, which are discussed ahead.

4.5.2 Indentation Method

The indentation behavior was investigated using a Vickers diamond indenter with the load ranging between 0.098 and 9.81 N and a loading time of 20 s. Most experiments were conducted with a load of 0.098 N to avoid any micro-cracking with the aim to get rheological parameters from the analysis of the indentation profiles by atomic force microscopy (AFM Nanoscope III, Digital Instruments). All the characteristics were averaged over measurements on 3 indentations per load value. Error bars on the experimental points mainly derived from the scattering of the AFM measurements. Specimen surfaces were mirror-polished with diamond suspension down to 0.25 μm particle size prior to indentation. Note also that all measurements were performed in a thermally regulated room, at 20°C. Meyer's hardness (H) is defined by:

$$H = 2\frac{P}{(d)^2} \tag{4.4}$$

Where P [N] is the load applied on the Vickers indenter and d [m] is the mean size of the two diagonals. When the elastic recovery is assumed to have little effects on the projected dimension of the indent, Meyer's hardness can be identified to the true hardness, defined as the mean normal stress over the contact region, and is thus a more fundamental measure of hardness than the Vickers one.

The permanent displacement is directly measured on the AFM (or confocal microscope) profile, whereas the total displacement is evaluated by extrapolation, by considering the ideal indentation shape at maximum load from the Vickers diamond shape. Then the reversible component, u_e, is deduced: $u_e = u - u_p$.

It is in principle possible to evaluate Young's modulus, E, from the indentation topometry analysis and is proposed by Lawn *et al.*[112] In this approach, a permanent Vickers indentation being loaded elastically from its actual state so

that the total penetration depth (u) comes into play in the equation for E to account for the pre-stress acting along the elastic recovery path:

$$E_{(\mathrm{L.H})} = \gamma^2 \frac{(1-\nu^2)\ P}{tan\psi\ (2u - u_\mathrm{e})u_\mathrm{e}} \tag{4.5}$$

where, subscript (L.H) refers to the authors of reference,[112] and ψ is half the value of the apical angle of the indenter which is assumed to be perfectly rigid. This value for Vickers indenter is 74.05°. A major difficulty with the use of Eq. (4.5) raises from the determination of parameter γ, the relative penetration depth, which is introduced to account for the fact that the penetration depth (u) may greatly differ from the contact depth (u_c). This parameter is evaluated by a ratio γ=u/u_c. In the case of a perfectly linear elastic material γ should be close to $\pi/2$. Nevertheless this may be regarded as an overestimation in the real cases where the behavior is obviously not purely elastic. It is noteworthy that to the knowledge of the present author, all previous studies assumed a constant value for γ although it depends much on the mechanical behavior of the material, being as high as 1.3 when elasticity predominates and as low as 0.8 when the material behaves essentially "plastic". For instance a value of 0.91 was proposed by Lawn *et al.* to get a good correlation between experiments and theory in the case of indentation experiments conducted with different materials, including a standard soda-lime-silica glass.

4.6 Thermo-Mechanical Behavior: Creep Test

The thermo-mechanical investigation (creep) was carried out in simple uniaxial compression using silicon carbide plates and graphite push rods. The schematic of this setup is shown in Fig. 4.3 and the actual setup is pictured in Fig. 4.4. The furnace element is made from tungsten mesh and tests were done in pure flowing argon. A constant load was applied to the specimen by means of hydraulic actuator, which was capable of maintaining the applied load within 1% of the set point over the duration of the test. The specimen is in the shape of a solid cylinder having height of 7 mm and diameter of 7 ±0.3 mm. The compressive displacement was measured with an LVTD (linear variable displacement

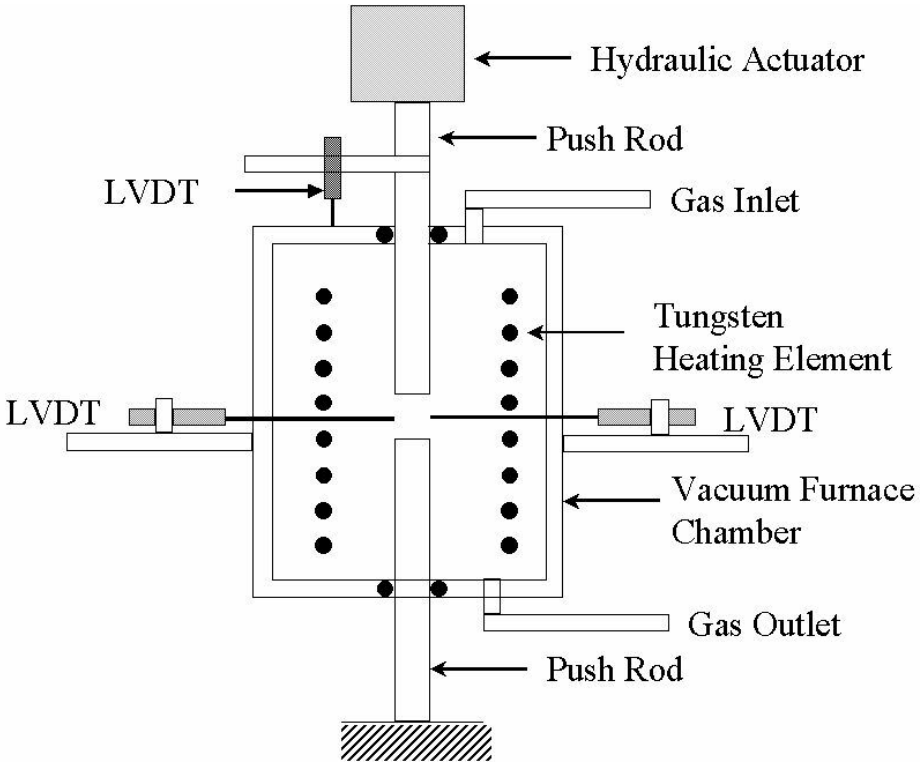

Figure 4.3: Schematic of the creep test setup.

transducer) which gave a signal of 1 mV for every 1.5 μm of displacement. The temperature of the specimen was measured with the independent thermocouple; this temperature varied less than 2°C from the set point. Under the operating conditions of the apparatus the minimum strain rate that could be measured was 3 x 10^{-9} s^{-1}. It is possible that friction at the plate-specimen interface may have caused some error in the measurement of the true uniaxial strain rate. In order to reduce the friction the SiC plate surfaces are coated with $h-$BN spray.

4.7 Methods for Material Characterization

4.7.1 Rheology

In the present work the evolution of viscosity and elasticity of the MK polymer, as function of the *CLA* concentration and temperature gradients were investigated

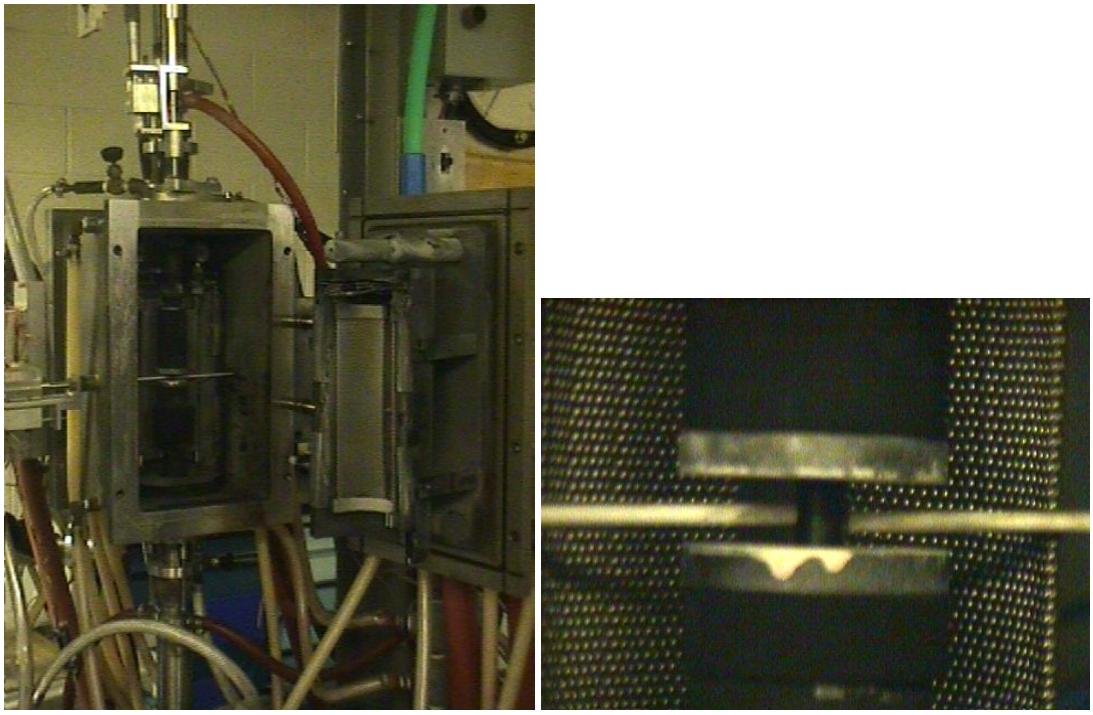

Figure 4.4: View of the creep furnace and sample: (Left) actual furnace (Right) SiAlOC ceramic bulk held between two SiC plates along with two LVDT for radial displacement measurement. Experiments were performed in the lab at Boulder, USA from Prof. Rishi Raj.

using dynamic rheological tests.* The evolution of viscous and elastic dynamic moduli of the samples are measured at constant frequency and constant torque (shear stress amplitude) in a plate and plate configuration, at a constant temperature gradient with Rheometrics RDS 200 controlled stress rheometer. The established test conditions are the following: frequency = 1 rad/s; shear stress amplitude = 10 Pa; temperature gradient = 5 °C/min; plates diameter = 25 mm, gap between plates = 0.6 mm. Qualitatively similar results have been obtained for different temperature gradients in the range (1 °C/min - 10°C/min).

4.7.2 Fourier Transform Infrared Spectroscopy (FTIR)

Transmittance infrared spectroscopy (Perkin-Elmer, Type FT-IR 1750 with a resolution of 4 cm^{-1}) was employed to characterize the bonding and evolution of

*W. Fimdley, J. Lai, and K. Omaran, *Creep and relaxation of nonlinear viscoelastic materials*, North Holland, Amsterdam, 1976.

these bonds with temperature during pyrolysis. Transmittance infrared spectra were collected using KBr pellets with small amount of grounded samples, from 400 to 4000 cm^{-1} at a resolution of 4 cm^{-1}. KBr powder was dried at 150°C and stored in glove box to prevent contamination from humidity. The polymer materials namely, MK + *CLA* and aluminum modified polymer at different temperatures are prepared according to the pyrolysis process explained earlier, i.e., with a heating rate of 25°C/h in flowing argon atmosphere.

4.7.3 Thermal Gravimetry and Mass Spectroscopy (TG/MS)

The decomposition reactions, generating during pyrolysis of the green bodies, continuously changes the chemical composition of the samples as a function of temperature. For optimization of the pyrolysis cycle from green stage to the ceramic stage without damaging the molded article, it is important to know the information about the temperature range and the quantity of decomposition products escaping the system. This information was extracted from simultaneous thermoanalyser (STA 429, Netzsch) technique. The thermo-gravimetric analysis (TGA) was performed in argon flow (5 l/h) with a heating rate of 10°C/min up to the maximum temperature of 1100°C. About 150 mg of the investigated material in Al_2O_3-crucible was used for this analysis. Also, standard Al_2O_3 powder was used as a reference material.

Sensing the type of decomposition gas, which are realized during pyrolysis help in identifying various possible decomposition reactions, namely polycondensation and radical reaction(s). Analysis of the pyrolysis gases was obtained in situ using a quadrapole mass spectrometer (QMA 400, Balzers). Thermo-gravimetry and mass spectroscopy together provide good physical and chemical information of the pyrolysis process.

4.7.4 Thermo Mechanical Analysis (TMA)

The contraction behavior of the green bodies during pyrolysis was performed with a vertical dilatometer (TMA 402, Netzsch). The displacement gauge is separated from the sample by quartz glass plate in order to prevent deformation of molded article or sinking of the gauge rods into the sample material. Contractions during

pyrolysis cycle was measured in only one direction, indeed in the direction parallel to the applied force during the green body preparation. The investigation was performed in flowing argon atmosphere with a heating rate of 5°C/min in a temperature range between 25 to 1000°C.

4.7.5 Dimensional Changes (Dilatometry)

The kinetic study of the dense and crack-free samples for structural relaxation or crystallization could be investigated by thermal dilatometry. Thermal dilatometry of the pyrolyzed ceramic cylindrical bulks was recorded with a horizontal dilatometric system (Model Netzsch 420 S). Alumina plate was used as reference. An argon atmosphere and different heating rate like 5, 10, 20 and 30°C/min were used and the corresponding change in dimension with respect to temperature is recorded.

4.7.6 Elemental Analysis

The chemical analysis for the investigated ceramic for the elements like silicon and aluminum is performed at a standard laboratory (Pascher, Germany). The determination of carbon in the pyrolyzed mass was done in an carbon analyzer (CS 800, Eltra GmbH, Neuss). The powdered material is weighed in Al_2O_3 crucible together with a mixture from tungsten and iron. The crucible with mixture is placed in high frequency electric field, and burned up in oxygen stream, which serves at the same time as a reference gas. Whereby, carbon contained in the sample is completely oxidized to carbon dioxide and possible remainders of carbon monoxide at CuO catalyst before passing it through an infrared measuring cell. Quantification of the carbon content is done according to Lambert Beer's law, where the absorption of the CO_2 is proportional to the carbon content.

The oxygen content, likewise on powdered ceramic sample, is analyzed with N/O analyzer (Leco, Type TC-436), by burning the sample in a graphite crucible at around 2700°C under helium atmosphere. The powdered sample is packed in an tin capsule before placing it in a heating zone, where the oxygen reacts completely to carbon monoxide and during downstream through CuO catalyst is oxidized to carbon dioxide and subsequently measured quantitatively.

Calibration was performed with certified standard substances like silicon carbide (NIST) for carbon and WO_3 (Leco) for oxygen. Measurements was repeated on same sample in order to get a reproducible results with good statistics.

4.7.7 MAS-NMR Spectroscopy

The SiALOC gels derived ceramic product is insoluble in any solvents used for NMR studies. Hence, solid state NMR is used for SiAlOC ceramics pyrolyzed at 1100°C in argon atmosphere. The mass thus formed is milled to powder state and used directly for the structural study. ^{29}Si, ^{27}Al magic angle spinning nuclear magnetic resonance (MAS-NMR) experiments were carried out on a spectrometer (Bruker ASX 400) operating at 9.40 T. Qualitative ^{29}Si and ^{27}Al MAS-NMR spectra were obtained employing following experimental conditions:

1. Nuclear probe: ^{29}Si; Frequency: 79.49 MHz; Pulse length: 2 µs; Repetations: 60 s; MAS rotation: 8 kHz; Chemical shift reference: $TMS_{(aq)}$.

2. Nuclear probe: ^{27}Al; Frequency: 104.26 MHz; Pulse length: 0.6 µs; Repetations: 0.5 s; MAS rotation: 6 kHz; Chemical shift reference: $AlCl_{3(aq)}$.

Line broadening of 120 Hz for the ceramic was applied for ^{29}Si spectra and 400Hz line broadening was applied to the ^{27}Al spectra to obtain adequate signal to noise ratio. The number of scans are 1000 and 6000-9000 for ^{29}Si and ^{27}Al MAS-NMR; respectively. The spectra thus observed are deconvoluted/fitted with a Gaussian fit using (dmfit) software.

4.7.8 X-ray Diffraction

X-ray diffraction (Model D500, Siemens AG), using a Ni-filtered Cu-K_α radiation source was employed to characterize crystalline pyrolysis product in heat treated and oxidized bulk samples. This instrument work in reflection mode and scans were taken between 2θ values of 10^o and 90^o with a step width of 0.02^o and a measuring time of 0.1 sec/step. Different phases are identified using a database, which is based on JFPD cards.

4.7.9 Scanning Electron Microscopy

Microstructural investigation on the heat treated samples was performed with an scanning electron microscope (SEM) (Philips, Modell XL 30 FEG). Because of very low electrical conductivity of the produced samples, sputtering of the samples with a gold-palladium nano-layer is necessary. Samples is mounted on aluminum sample holder with the help of carbon tape and placed under vacuum of about 10^{-4} mbar and sputtered with Au-Pd by applying high voltage in argon atmosphere. The thickness of the sputtered layer is controlled between 5 to 20 nm.

The oxidized samples are sectioned and mounted in warm setting resin before measuring them for oxidation layer thickness by SEM. To study the surface morphology the same procedure as mentioned above is used. The samples are pre-etched, using a dilute solution of hydro fluoric acid in order to create a phase contrast between the amorphous phase and crystalline phase, for investigation of crystalline morphology. All samples are investigated with the accelerating voltage of 10 to 20 kV.

Investigation of the elements present in the material is confirmed with energy dispersive x-ray analysis (EDX).

4.7.10 Secondary Ion Mass Spectroscopy (SIMS)

Secondary Ion Mass Spectrometry (SIMS) is based upon the sputtering of a surface of a sample, induced by a "primary ion" bombardment. A primary ion triggers a cascade of atomic collisions. Atoms and atomic clusters are ejected. During the ejection process, some of them are spontaneously ionized. These "secondary ions" are the characteristic of the composition of the analyzed area. They are separated according to their mass. Continuous etching if the sample surface by the primary ion beam gives progressive access to deeper areas in the specimen and thus chemical depth profiles can be estimated.

The Si(Al)OC ceramic materials in pyrolyzed and oxidized condition are investigated for chemical depth profiles using secondary ion mass spectrometry (Cameca, France: ims5f type). The secondary ion masses is analyzed by a double focussing sector field mass spectrometer. All samples were covered with a thin gold layer for better charge compensation. The crater size was 150 x 150

µm and the beam diameter was about 20 µm. The measurements were done with O^- primary ions, detecting positive secondary ions. The mass resolution was low (m/dm=300), so interferences of molecules and atoms are possible (e.g. H_2O, 18O). However, a considerably higher mass resolution usually means a lower transmission (by 2 or 3 orders of magnitude). Interferences were circumvented with the suppression of molecular ions, i.e. an offset voltage of several ten volts and an energy filter with a width of several eV. This works because there are a lot more atomic ions with higher energy than molecular ions. The energy was 12.5 kV (ion source - ground) plus 4.5 kV (sample - ground), effectively 17 kV. This value is somewhat high but results from the addition of the voltages given above, which cannot be avoided when choosing the polarities like it was done in this case. The depth resolution with a 17 kV beam and a relatively steep angle of incidence will not be smaller than, say 20 nm - but the limitation here is given by the roughness of the surface.

Being a sector field instrument only one ion can be detected at a certain time (more accurate: an ion with a certain m/q ratio). So when doing a depth profile mass1 is detected for a second, then the magnetic field is switched to mass2, detection of mass2, switching to mass3, etc., and after the last mass in the list switching to mass1 again and so on.

The total depth of the sputtered carter is measured by profilometer and the sputtering time is converted to the depth value in micro meter, assuming that the sputtering rate and the secondary ion yield is same for all samples.

5 Results and Discussion

5.1 Material Selection: Identifying Ideal Polymer

One of the first stage of any research in the material science is to identify appropriate material which can fulfill the requirements. Thus, it is also necessary to know the initial requirements. It was pre-decided that air handleable precursor polymers should be used which shortens the area to siloxane system. If at all this precursors should be further used the processing requirements by injection molding for high production rate need to be defined and are listed below:

1. The polymer should not adhere to the mold at any stage of processing.

2. Viscosity of the polymer in the cylinder should be between 200−5000 Pa.s. Hardening should be accomplished in the mold cavity. Polymer should not soften with time at the maximum temperature.

3. Maximum hardening temperature should be less than 190°C with the hardening time <45 s. The green body formed should not possess cracks or micro-cracks.

Various types of polysiloxanes are available commercially and the next task is to identify a suitable polymer satisfying to above mentioned requirements. Table :5.1 lists presently available polysiloxane polymers and gives some remarks on their properties or physical state. At the first glance the polymers are available in solid, liquid and semi-solid state. The useability of these polymers for injection molding fulfilling all the above mentioned requirements can be investigated by rheology.

The effect of temperature on viscosity change for the above mentioned polysiloxane polymers are presented in following discussion. Fig. 5.1 show such a effect

Manufacturer	Trade Name	Remarks
Allied Signal	OS-2100	Vinlyorgano(ketoximino)silane
Dow Corning	DC6-2230	OH-Functionality Phenylmethyl-silicone Resin
Hüls	NH-2100	Silicone Resin
Wacker	LR-3003	Liquid Silicone Rubber
Wacker	MK	Powdered Silicone Polymer

Table 5.1: Available commercial polysiloxane which can be used as precursor for SiOC ceramic.

on DC6-2230 polymer and indicate that the viscosity rises with temperature. The viscosity values in the temperature range specified for injection molding processing is not high enough to form a stable green body. Probably still high temperature is needed for reaching higher viscosity. Nevertheless, maintaining the temperature for long time does not change the viscosity greatly and appears constant. In contrast the viscosity for NH 2100 decreases to a very low value with temperature even after heating it up to 200°C and is shown in Fig. 5.2. This make the use of above two polymers practically inadequate for injection molding of components.

LR-3003 polysiloxane a rubber like thick polymer is available in two parts which need to be mixed before further use. Unlike last two polysiloxane polymers, LR-3003 show a significant rise in viscosity with temperature. Between 100−120°C a sharp rise in viscosity with three order of magnitude is seen in Fig. 5.3. Further rise in temperature does not affect the viscosity in that order. Holding the material at higher temperature say 150°C maintain the viscosity value almost constant. It is interesting to see if the material develops strength by network forming (cross-linking) with time and is easily investigated by measuring the dynamic elastic moduli change for different temperature below 100°C, as in this regime the effect of temperature is the highest. The effect on elasticity at different temperatures with long holding time is shown in Fig. 5.4. It is seen that, at low temperature for example 50°C cross-linking initiation starts after long time and to achieve strength in the body needs longer time. Increasing the temperature further reduces the time needed for cross-linking initiation. At these

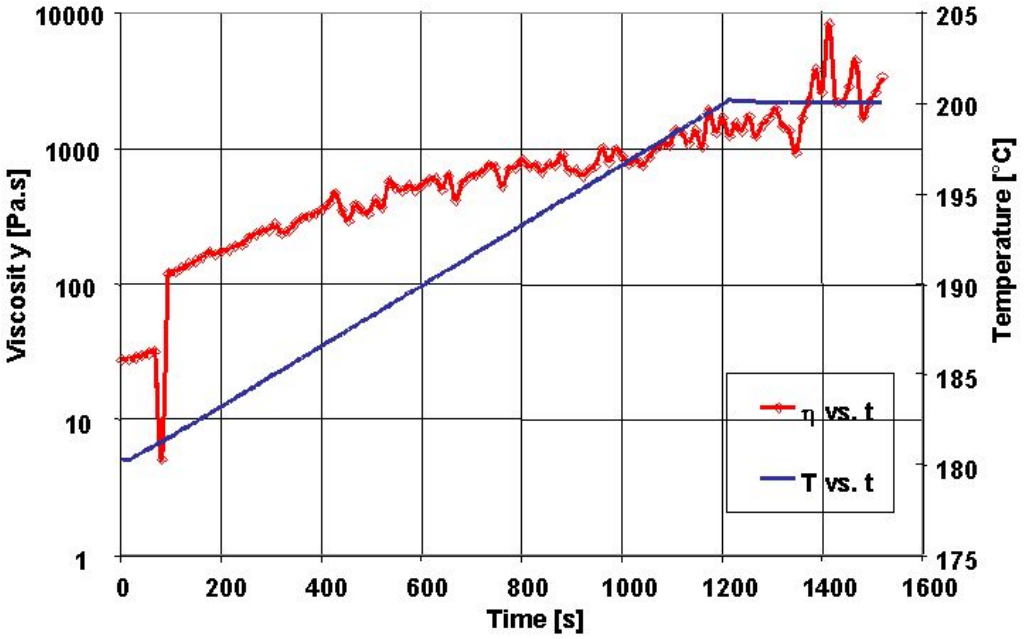

Figure 5.1: Development of viscosity for DC6-2230 polymer with temperature when heated at 10°C/min.

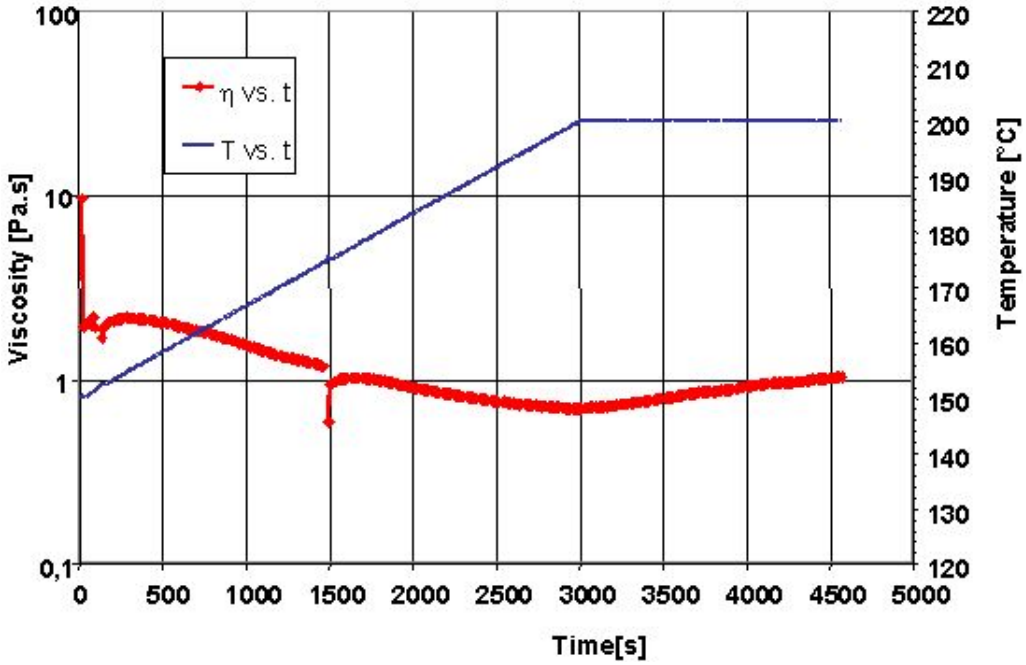

Figure 5.2: Development of viscosity for NH-2100 polymer with temperature when heated at 10°C/min.

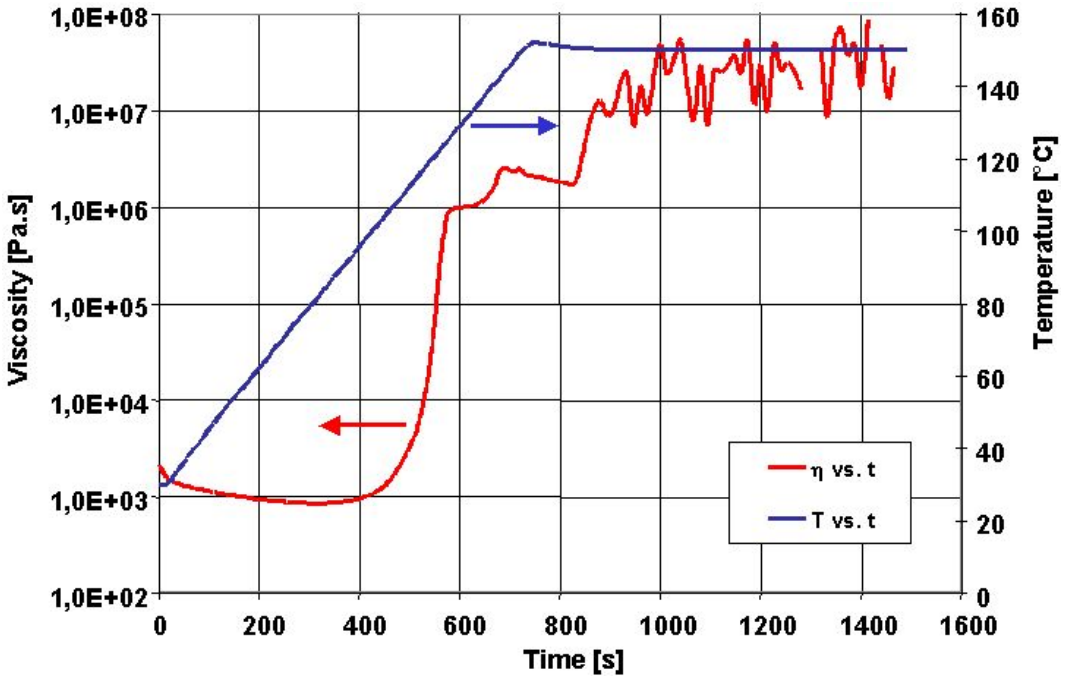

Figure 5.3: Development of viscosity for LR-3003 polymer with temperature when heated at 10°C/min.

temperatures the elasticity rises suddenly to a higher value. The cross-linking seems to proceed by single mechanism independent of temperature as the slopes of all the curves remains unaffected for all the tested temperatures. Thus, from above two figures it is seen that, the viscosity and strength values for LR3003 are fulfilling the requirements of its use in injection molding. Rather, the room temperature viscosity of this materials create difficulties in the processing. Fig. 5.3 show high initial viscosity value for LR-3003 polymer; nearly $>$ 1000 Pa.s. This makes its handling difficult because initially the polymer is available in two parts which must be mixed together and if filler material are added homogeneity is difficult to achieve between each components. Some pyrolysis experiments are also conducted using this polymer but micro cracking is seen in regions where no filler material is reached during mixing.

The final polymer in Table: 5.1 namely MK polymer will be discussed in the later part of the thesis as its rheological properties are suitable for the injection molding application. Some salient advantages of this polymer are: processing friendly powder state which make the mixing process clean and simple, good

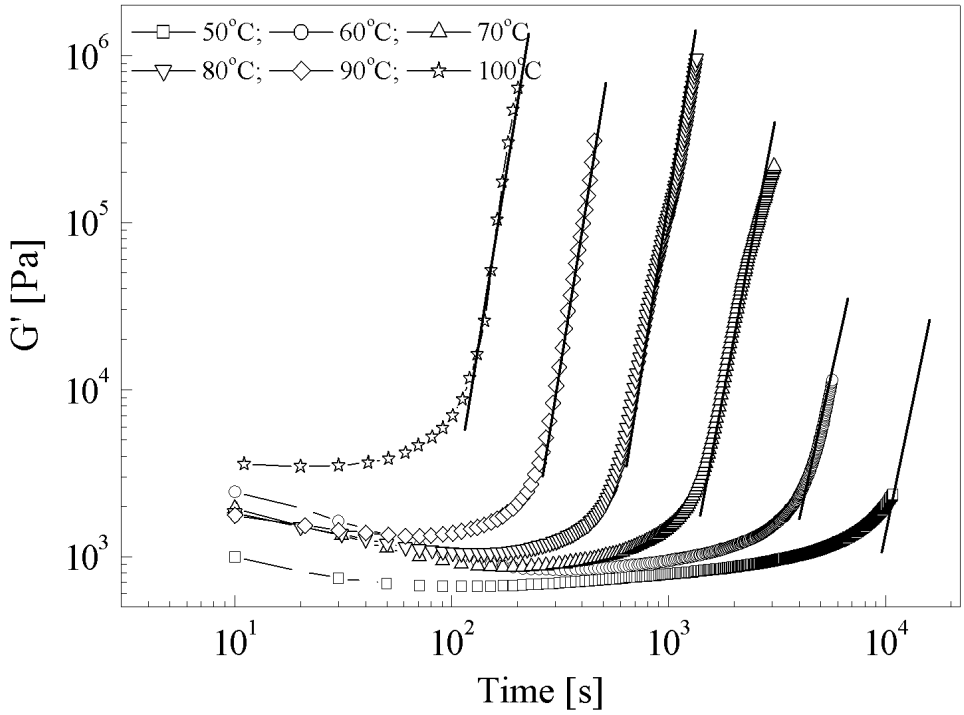

Figure 5.4: Isothermal development of G' for LR-3003 polymer with time at different temperatures.

rheological properties development with temperature and time.

The development of visco-elastic properties for all the polymers along with their initial physical state and final difficulties (in inorganic stage) discard the use of all top listed polymers from further use. MK polymer, which satisfy all requirements for processing will be used from this stage. Thus rheological investigation proved to be an ideal method for the polymeric material selection suitable for processing.

5.2 Unmodified Siloxane System

As discussed earlier, silicon oxycarbide ceramics could be produced from the siloxane polymer. Here, silicon atoms are covalently bonded to carbon and oxygen.

Presence of these bonds and polymer-to-ceramic transformation process is confirm by FTIR, TGMS, respectively. In addition, the supplier had indicated that the commercial product (MK polymer) possesses approximate 2 Mol% hydroxy, methoxy, and ethoxy groups, as functional units.

5.2.1 Investigating MK polymer: Chemical and Thermal Cross-linking Behavior

The first step to confirm the ability of MK polymer in producing silicon oxycarbide ceramic is to identify various types of vibration bands present at room temperature. Fig. 5.5 indicates the IR spectra of the polymer in as-received condition. Also the various bands indicated in figure are summarized in Table: 5.2. For siloxanes the characteristic vibration bands are clearly proven.[113] Additionally, the bands at 2860 cm^{-1} (2)* for C−H vibration and 625-480 cm^{-1} are recognized.

The bands from SiO−Si (4) and SiO−R (5) vibration are according to the literature i.e., in the range between 1100 to 1000 cm^{-1}. However, for siloxanes the band observed at higher wave number is assigned to SiO−Si and for lower wave number to SiO−R. Additionally, the presence peaks in infrared spectrum ar 1275 cm^{-1} (3) and 767 cm^{-1} (6) confirms the presence of Si−C bonds in the polymer.

The transformation of as received MK polymer to SiOC ceramic was studied with thermal gravimetry (TG). Pyrolysis of MK polymer from room temperature up to 1100°C result in total mass loss of about 22% as indicated in Fig. 5.6. MK polymer shows three regions of mass losses: 200−450°C (≈ 12%), 450−600°C (≈ 3%), and 600−800°C (≈ 8%). On the basis of the result from differential thermal gravimetry (DTG), as shown in Fig. 5.6, the exact temperatures for each stages can be determined. Accordingly, the strong peak at about 240°C reported in Fig. 5.6, is due to the degassing product of polycondensation reaction, namely water and ethanol. Mass spectra (not shown in figure) identify masses related to H_2O (m/z = 18), ethoxy ($-C_2H_5O$, m/z = 45) and methoxy ($-CH_3O$, m/z = 31) groups. From this it follows that the reactions for cross-linking from functional groups takes place at the same time. Together with all above mentioned masses,

*Number in bracket indicate the marked bands in Fig. 5.5

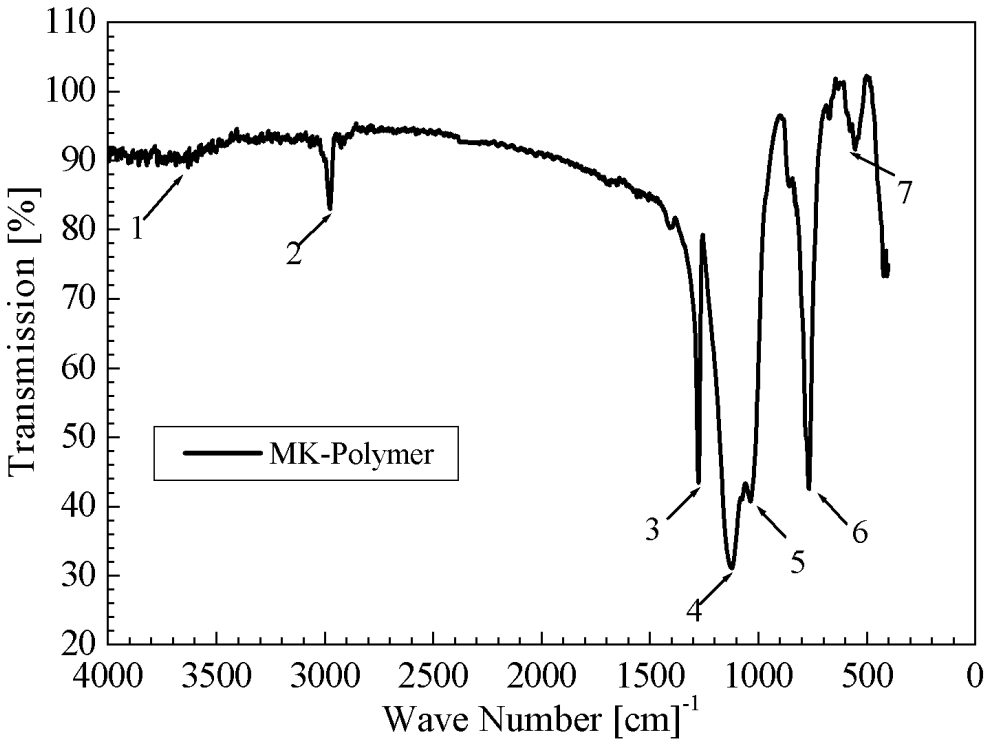

Figure 5.5: FTIR spectrum of MK polymer in as-received condition. Indication of the bands is given in Table: 5.2.

oligomer with high mass numbers are evolved in this temperature range.

The second peak in the DTG with a maximum at 550°C correlates with the release of remaining ethoxy groups, and also indicates the beginning of hydrogen and methane formation. The maximum for the release of these two species is observed at about 710°C. Over the entire temperature range, an almost constant intensity for water is measured, while at and above 700°C evolution of ethanol does not appear in the mass spectra.

The cross-linking by polycondensation reactions due to functional groups can be achieved at low temperature with a cross-linking-agent; *CLA*. The *CLA* should react with the polymer in a suitable range, which is helpful for realizing bulk components. The basic question arises that, how and in what amount the *CLA*

Wave Number $[cm]^{-1}$	Vibration Bands	Designation
3400	$SiO-H$	1
2860	$SiCH_2-H$	2
1275	$Si-CH_3$(asym. vib)	3
1125-1010	$Si-OSi$	4
1000-1100	$Si-OR$	5
767	$-Si(CH_3)$	6
625-480	$Si-O-CH_3$	7

Table 5.2: Characteristic FTIR-vibration bands in as-received MK polymer (SiOC system).

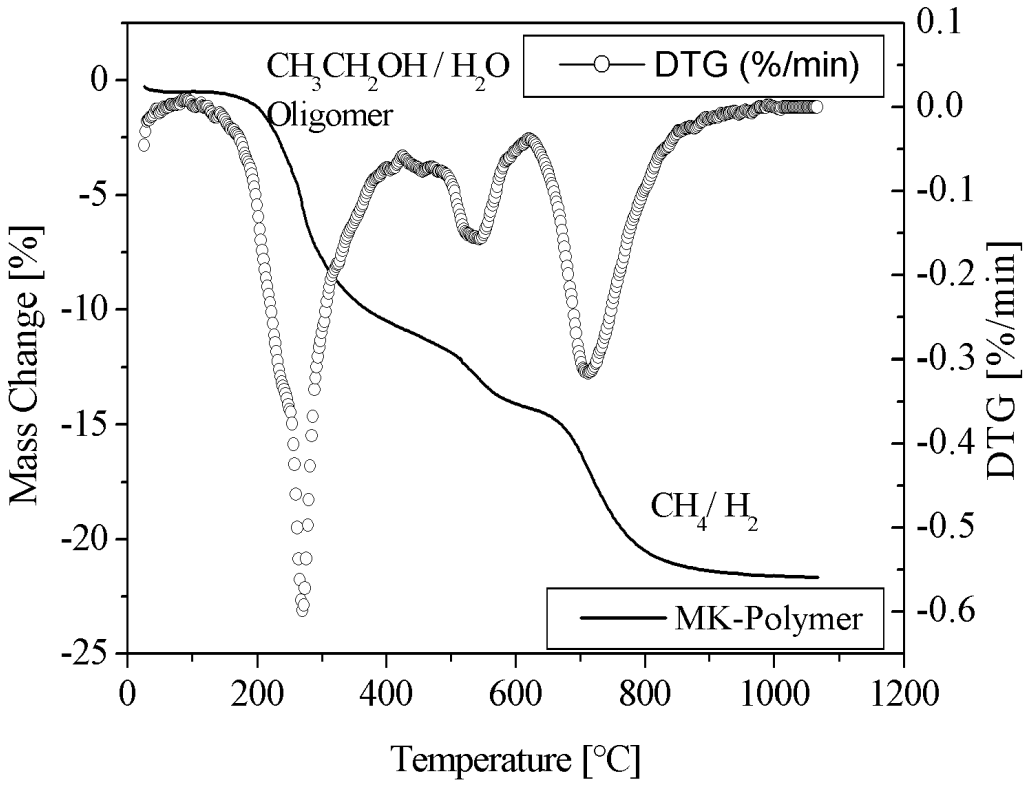

Figure 5.6: Thermo gravimetric and differential thermo gravimetric analysis of commercial MK polymer (5°C/min, Argon)

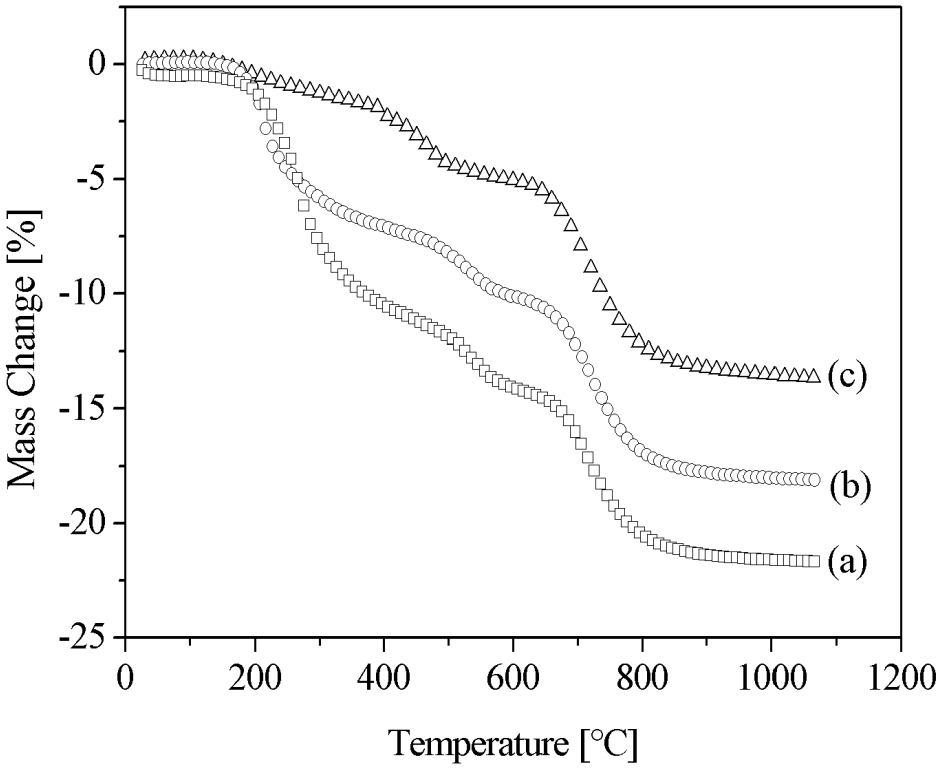

Figure 5.7: Thermal decomposition comparison of MK polymer (5°C/min, Argon), after mixing the CLA with different methods (a) polymer without CLA (as received condition), (b) mixing 1 wt.% CLA by dry route and (c) mixing 1 wt.% CLA by solution route.

should be added to the MK polymer in order to achieve homogeneous properties for the bulks. For example, the *CLA* should not produce any agglomeration, creating locations where cross-linking is active but leaving some regions without any *CLA*. Also, the *CLA* should not be too less to delay the process of cross linking and should not be in excess that it becomes the modifying agent, which significantly changes the properties of the end product.

The first question is examined by employing two different methods for mixing. In the first, powdered *CLA* is added in different proportions to MK polymer powder and the mixture is mixed in an planarity mill *(Dry route)* for 5 h. The second method is already explained in the sample preparation, i.e. dissolving *CLA* and MK polymer in isopropanol *(Solution route)*, and drying the solution

mixture under vacuum. The effect of *CLA* reaction on the pyrolysis process can be easily evaluated by TG. Fig. 5.7, which clearly indicates the comparison of the thermal decomposition behavior on different pre-treated polymers, and mainly pointed out an influence of the *CLA* in the initial stage region, which is critical for bulk processing. It also indicates the importance of the processing method employed for incorporating the *CLA*. Mainly, the sharp mass loss ($\approx$ 12%) observed for as received MK polymer [curve (a)] at 200°C is reduced to about 5 mass% [curve (b)]. Above 400°C, both curves travel parallel to each other, up to the end of the pyrolysis process. This confirms that, the *CLA* is only influencing the cross-linking process and is not changing the final transformation process. A total mass loss of about 17.8% is measured, which is about 4% lower than *CLA*-free system.

Adding *CLA* to the polymer by solution route, significantly changes the pyrolysis process, [curve (c)]. Up to 400°C, mass loss of only 2−3% is observed; compared to 11% and 7% for as-received MK polymer [curve (a)] and dry route mixing [curve (b)], respectively. Curve (c) is almost horizontal and first significant mass loss is observed after 400°C, which could be assign to the second mass loss step in [curve (a)] and [curve (b)]. The major difference is the temperature shift in the second major weight loss step, by almost 100°C. Again it confirms that, for all the materials mentioned, the strong decomposition step above 700°C remains the same. Changes are also observed in the DTA curve (not shown in the figure), with broadening of the first peak along with reduced intensity, and shifting the second peak positions towards low temperature. The third peak remain unchange in its intensity and peak position, which may indicate similar types of decomposition and transformation mechanism for the polymer to ceramic conversion.

Indeed, it is clear that the method used to introduce the *CLA* in the polymer alter the degree of cross-linking. Mixing the *CLA* homogeneously as done by the solution route improves consistency in achieving reliable results. Efficient use of *CLA* creates possibilities for low temperature processing. It is difficult to form bulk bodies from MK polymer itself; as it shows great mass loss, starting from 200°C. Such a mass loss in the form of degassing species when happen in the warm pressing stage result in cracking of the green bodies. Adding *CLA* by solution route reduces this mass loss by promoting early cross-linking reactions,

and increases the processing temperature window, possibly up to 350°C.

Now, the second question comes into picture, to investigate the effect of *CLA* content on the cross-linking and optimizing the process. This problem was attacked with the help of rheology, and will be discussed in the following subsection.

5.2.2 Cross-linking Investigation by Rheology: Optimizing Cross-Linking-Agent Content

After optimizing the mixing procedure of the *CLA* in the polymer it becomes necessary to extract more details from different mixture prepared by solution route, i.e., optimizing the content of *CLA*, which are important for the processing. Generally, two different forms could be generated from processing, namely bulks (monoliths) and fibers. Before discussing rheology for investigated polymer it will be advantageous to look into some basic concepts of rheology.

5.2.2.1 Rheology: Introduction

Heraklit von Ephesos (540−480 BC) stated: "panta rei − everything flows" or in other words the whole universe is in constant motion. Flow means an irreversible deformation of a material under externally applied force. Actually every material flows. This behavior is not always sensed on the macroscopic scale as the observation time may be small in reference to the relaxation time of the material. For example, the motion of mountains is visible with respect to the history of the earth but it remains unchanged if seen in the time span of a human life.

Since seventeenth century, scientists are intensively studying the characteristics process for flow and its related phenomenons. Inspite the early basic rheological fundamentals reported by Robert Hooke in his book "Micrographia" in 1665 and by Isaac Newton in his work "Philosophiae Naturalis Principia Mathematica" in 1686 it took another 250 years till Eugene Bingham and Markus Reiner developed rheology as a science as its own. Today rheology itself not only serves the area of scientific research but also used in detecting and controlling the production processes and quality.

5.2.2.2 Theoretical Background and Definitions

Rheological properties can be investigated using various Rheometers, namely rotational rheometer, oscillatory rheometer, capillary viscosimeter and falling ball rheometer. In the course of this work mainly the first two rheometers found compatibility with the material state. For the measurements with rotational and oscillatory rheometer either the angular velocity or the torque is given. The geometrical arrangement differs depending on the initial viscosity of the tested material from coaxial system to plate-plate-system till cone-plate-system.

In contrast to rotational rheometer where constant shear force is applied to the substance, the oscillatory rheometer allows a vibratory motion of small amplitude to the measuring unit. The oscillatory rheometer method is suitable for analyzing the influence of internal structural forces in the material. Hence, distinct measurement of complex rheological properties of a material is possible only with oscillatory rheometer.

The Rheological Base:
Newton‘s liquid model and Hooks solid body model are defined as rheological base.

The Newton's liquid model is an ideal viscous material which deforms irreversibly and linearly with time and shows the proportionality between stress and the shear strain rate.

$$\dot{\gamma} = \frac{\tau}{\eta} \qquad and \qquad \dot{\varepsilon} = \frac{\sigma}{\eta_e} \tag{5.1}$$

where
η, η_e = shear and extensional viscosity [Pa.s],
$\dot{\gamma}$, $\dot{\varepsilon}$ = shear and tensile strain rate,
τ, σ = shear and tensile stress [Pa]

The Hook's solid body model is an ideal elastic material which undergoes reversible deformation with stress and shows the proportionality between stress and the strain.

$$\gamma = \frac{\tau}{G} \qquad and \qquad \varepsilon = \frac{\sigma}{E} \tag{5.2}$$

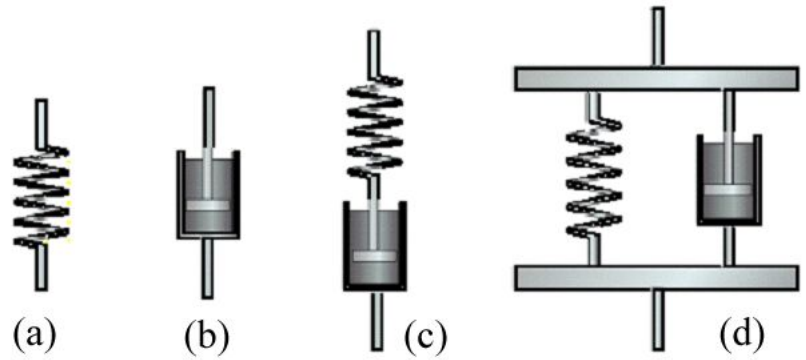

Figure 5.8: Mechanical analogs reflecting deformation processes in polymeric solids: (a) elastic; (b) pure viscous; (c) Maxwell model for viscoelastic fluid; (d) Voigt model for viscoelastic solid.

where
G, E = shear and tensile modulus [Pa]
γ, ε = shear and tensile strain.

Newton's liquid model and Hooks solid body model describes the ideal behavior. In reality, the material behaves as a combination of the above two. To illustrate the ideal elastic and viscous behavior models, spring and dashpot are used and the mechanical analogs are represented in Fig. 5.8 (a) and (b), respectively.

The Maxwell-Model:
When the spring and dashpot are in series, as in Fig. 5.8 (c) (called Maxwell model), we are able to describe the mechanical response of a material possessing both elastic and viscous components. In this case, the elastic strains is recovered, but the viscous strain arising from creep of the dashpot remains. Since the elements are in series, the stress on each is the same, and the total strain or strain rate is determined from the sum of the two components.

$$\frac{d\gamma}{dt} = \frac{\tau}{\eta} + \frac{1}{G}\frac{d\tau}{dt} \tag{5.3}$$

The Kelvin-Voigt-Model:
When the spring and dashpot elements are combined in parallel, as in Fig. 5.8

(d) (the Voigt model), this unit predicts a different time-dependent deformation response. First, the strains in the two elements are equal, and the total stress on the pair is given by the sum of the two components. The stress-strain behavior of this model show absence of any instantaneous strain and is related in a physical sense to the infinite stiffness of the dashpot at $t = 0$. The creep strain rise quickly thereafter, but reach a limiting value τ_0/G associated with full extension of the spring under that stress. Upon unloading, the spring remains extended, but now exerts a negative stress on the dashpot. In this manner, the viscous strain are reversed, and in the limit when both spring and dashpot are unstressed, all the strain have been reversed.

$$\begin{aligned} \gamma_{\mathrm{T}} &= \gamma_{\mathrm{S}} = \gamma_{\mathrm{D}} \\ \tau_{\mathrm{T}} &= \tau_{\mathrm{S}} = \tau_{\mathrm{D}} \end{aligned} \tag{5.4}$$

Therefore,

$$\tau_{\mathrm{T}}(t) = G\gamma + \eta \, \frac{d\gamma}{dt} \tag{5.5}$$

Consequently, the Maxwell and Voigt models describe different types of viscoelastic response. A somewhat more realistic description of polymer behavior as obtained with four-element model consisting of Maxwell and Voigt models in series which takes account of elastic, viscoelastic, and viscous strain components. Even this model is overly simplistic with many additional elements often required to adequately represent mechanical behavior of a polymer. For example, such a model might include a series of Voigt elements, each describing the relaxation response of a different structural unit in the molecule.

Even so, the four-element model is useful in characterizing the response of different types of polymers. For example, a stiff and rigid material, such as a polyester thermoset resin, can be simulated by choosing stiff springs and high-viscosity dashpots. These elements would predict high stiffness and little time-dependent deformation, characteristic of a thermoset material. On the other hand, a soft and flexible material such as low-density polyethylene could be simulated by choosing low stiffness springs and dashpot with low viscosity levels. Accordingly, considerable time-dependent deformation would be predicted. Finally, the temperature dependence of the mechanical response of a polymer can be modelled by appropriate adjustment in dashpot and spring values (i.e., lower spring stiffness and dashpot viscosity levels for higher temperatures and vice

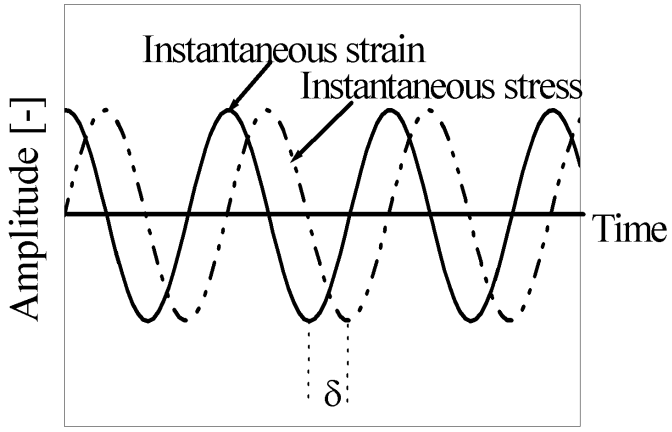

Figure 5.9: Definition for phase angle δ.

versa for lower temperature conditions).

The Phase Angle δ:

The time-dependent moduli and energy-dissipative mechanisms are examined through the use of dynamic test methods. In one such method, the instrument introduce to the sample a forced vibration at different frequencies. The amount of damping is found by noting the extent to which the cyclic strain lag behind the applied stress wave. The relation between the instantaneous stress and strain values is shown in Fig. ref{Fig:phase-angle-delta. Note that the strain vector γ_0 lags the stress vector τ_0 by the phase angle δ. It is instructive to resolve the stress vector into components both in phase and 90°C out of phase with γ_0. These are given by

$$\begin{aligned} \tau' &= \tau_0 cos\delta \qquad (in-phase-component) \\ \tau'' &= \tau_0 sin\delta \qquad (out-of-phase-component) \end{aligned} \tag{5.6}$$

The corresponding in-phase and out-of-phase moduli are determined directly

from Eq. (5.6) when the two stress components are divided by γ_0 Hence

$$\begin{aligned} G' &= \frac{\tau'}{\gamma_0} = \frac{\tau_0}{\gamma_0} cos\delta = G^* cos\delta \\ G'' &= \frac{\tau''}{\gamma_0} = \frac{\tau_0}{\gamma_0} sin\delta = G^* sin\delta \end{aligned} \tag{5.7}$$

where G^* = absolute modulus = $\sqrt{(G')^2 + (G'')^2}$.
As per the definition:
when
$\delta = 0°$(material is purely elastic)
$\delta = 90°$(material is purely viscous)
$0° < \delta < 90°$(material is viscoelastic)

The Complex Modulus:
G' reflects the elastic response of the material, since the stress and strain components are in phase. This part of the strain energy, introduced to the system by the application of stress τ_0, is stored but then completely released when τ_0 is removed. Consequently, G' is often referred to as the *storage* modulus. G'' on the other hand, describes the strain energy that is completely dissipated (mostly in the form of heat) and for this reason it is called the *loss* modulus. The relatively amount of damping or energy loss in the material is given by the loss tangent, tanδ.

$$\frac{G''}{G'} = \frac{G^* sin\delta}{G^* cos\delta} = tan\delta \tag{5.8}$$

Or

$$\frac{G''}{G'} = tan\delta \tag{5.9}$$

Processing of the ceramic precursors for particular applications requires the rheological characterization of the sample during the fluid-to-solid transition. The control and prediction of rheological properties at different stages of ceramics processing is of great importance in establishing the final quality of products. Each technological process has to be designed for an optimum interval of the magnitude and temperature - time evolution of rheological properties, respectively viscosity and elasticity. In the present work the evolution of viscosity and elasticity of the MK polymer, as function of the *CLA* concentration and

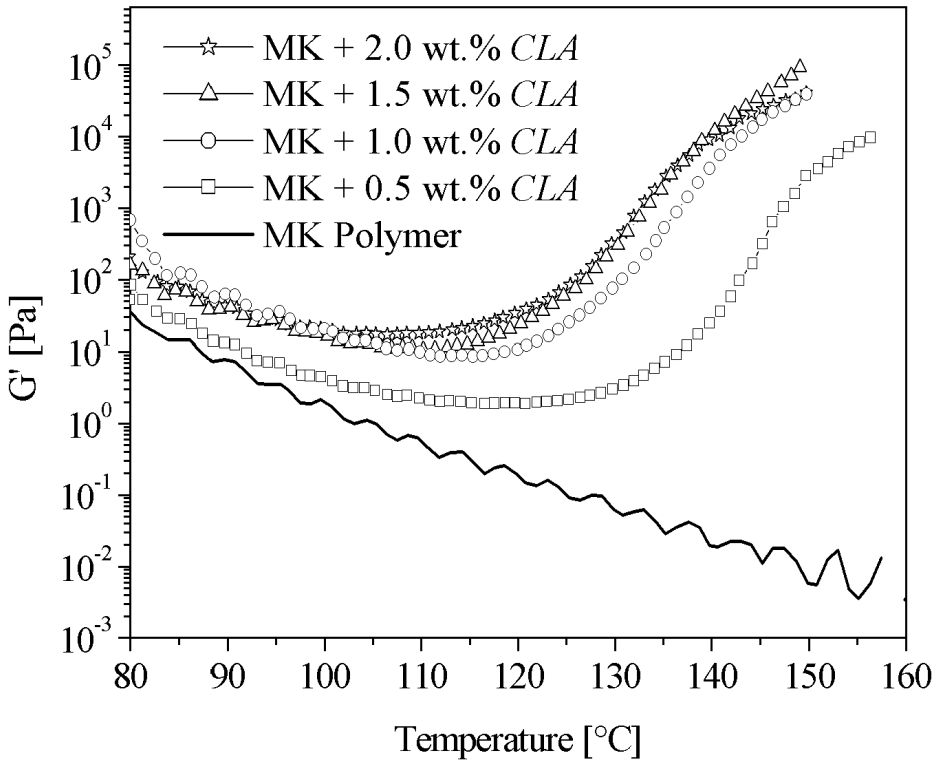

Figure 5.10: Evolution of elastic modulus with temperature, as function of CLA concentration within the MK based polymer.

temperature gradients were investigated. This also help to optimize the *CLA* concentration for network formation.

Network formation, which gives stability to the green compact, is one of the important steps in polymer pyrolysis processing. From rheological point of view the strength of network is characterized by the magnitude of dynamic elastic moduli. The rheology results prove incapability of the unmodified *CLA*-free MK to visco-elastic behavior necessary for cross-linking, i.e. G′ continuously decreases with temperature when heated at a constant heating rate, (5°C/min in this case), see Fig. :5.10. In contrast, Zr-acetylacetonate (*CLA*) containing polymer shows initial decrease of G′ with temperature indicating melting or liquid like behavior. Further heating results in a sharp increase of G′ due to network

formation by polymer cross-linking. Enhanced *CLA* concentration increases the level of elasticity (i.e. the value of G′) and the starting temperature of network formation decreases. Consequently, the minimum of G′ is reached at 105°C with 2 wt.% *CLA* while 120°C is required for the network formation in the presence of 0.5 wt.% *CLA*. It is observed that increasing the *CLA* concentration above 1 wt.% generate almost same elastic level in the cross-linking temperature region. Following this analysis of the rheological tests, the level of optimum *CLA* concentration could be fixed to 1 wt.%.

5.2.3 Rheology and its Advantage in Processing

5.2.3.1 Rheology for Fiber Formation

For fibers preparation, the ability of the polymer to get spined or spinability has to be tested. In both types of application, rheology plays an important role and investigating various variables like elastic modulus (G′), dynamic modulus (G″) and loss tangent generates basic feasibility data.

Initially, keeping the heating rate constant (5°C/min), the effect of changing the *CLA* concentration on the loss tangent is investigated. Spinning ability is discussed only for elasticity values above 100 Pa, which is the minimum requirement. As reported,[114] the polymer melt is well spinnable for $\tan\delta > 10$, partially or poorly spinnable for $5 \leq \tan\delta \geq 10$ and is un-spinnable for $\tan\delta \leq 5$.

According to this requirement, if we concentrate on the marked window between 85−100°C in Fig. 5.11, for all concentrations (with or without *CLA*) the loss tangent values almost constant and above 10. It means that if we heat the MK polymer and *CLA* mixture in this temperature regime, the polymer is well spinnable. This was experimented by heating the polymer mixture (MK + 1 wt.% *CLA* mixture in particular) on a plate which was maintained at 90°C and subsequently dipping a spatula in the melt and pulling the melt to form long fibers. Unfortunately, heating the spined fiber at 5°C/min for cross-linking, which happens above 120°C, caused remelting. This is because, at this heating rate the non-cross-linked polymer again follows the same path, as it follows for the material in its original mixed state.

Thus the material is further characterized by rheology such that with heating elastic modulus remains constant (i.e., without undergoing melting) and further

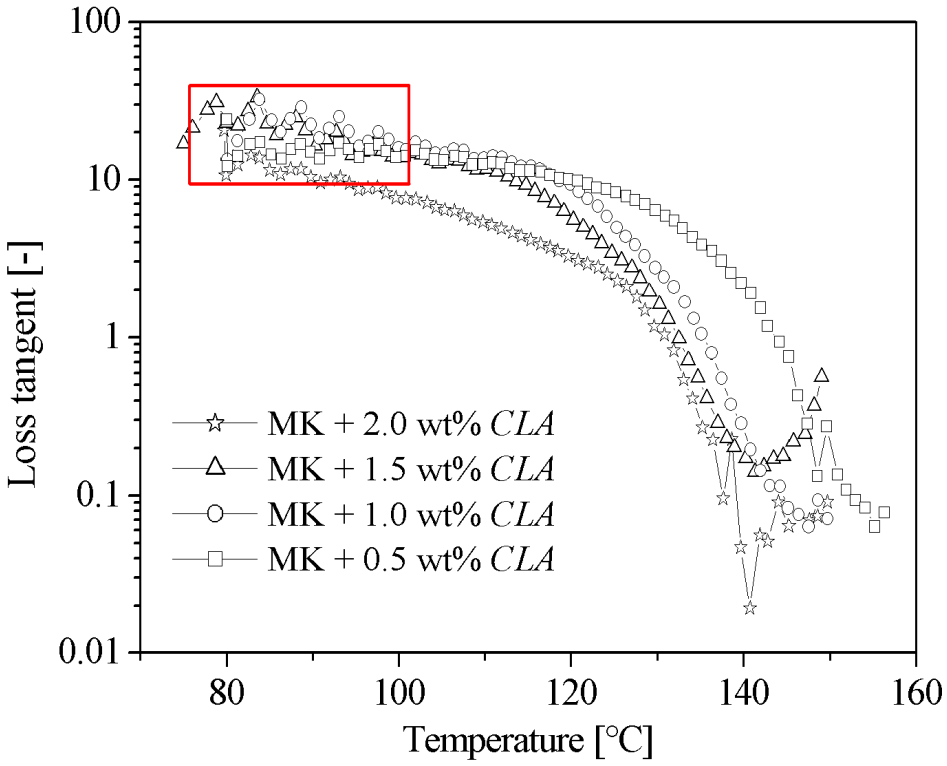

Figure 5.11: Evolution of loss tangent with temperature, at constant heating rate (5 °C/min) for various CLA concentrations.

heating cause cross-linking to achieve stable material.

At first the effect of heating rate on the elastic-viscous behavior and tanδ of MK polymer with 1 wt.% *CLA* mixture is investigated. With reference to Fig. 5.12, reducing the heating rate increases the elasticity minima (i.e. the value of G′) and decreases the starting temperature of network formation. For example, a minimum of G′ = 2 Pa is reached at 125°C with 10°C/min, whereas reducing the heating rate to 1°C/min; the level of elasticity (G′) increases approximately to 30 Pa and the starting temperature of network formation is lowered to 100°C. Heating rate also show a significant effect on the loss tangent (tanδ) value. With low heating rate (1°C/min), the spinning window is reduced and fall in a close range of ≈ 10°C, which for higher value (10°C/min) have a broader range. Thus,

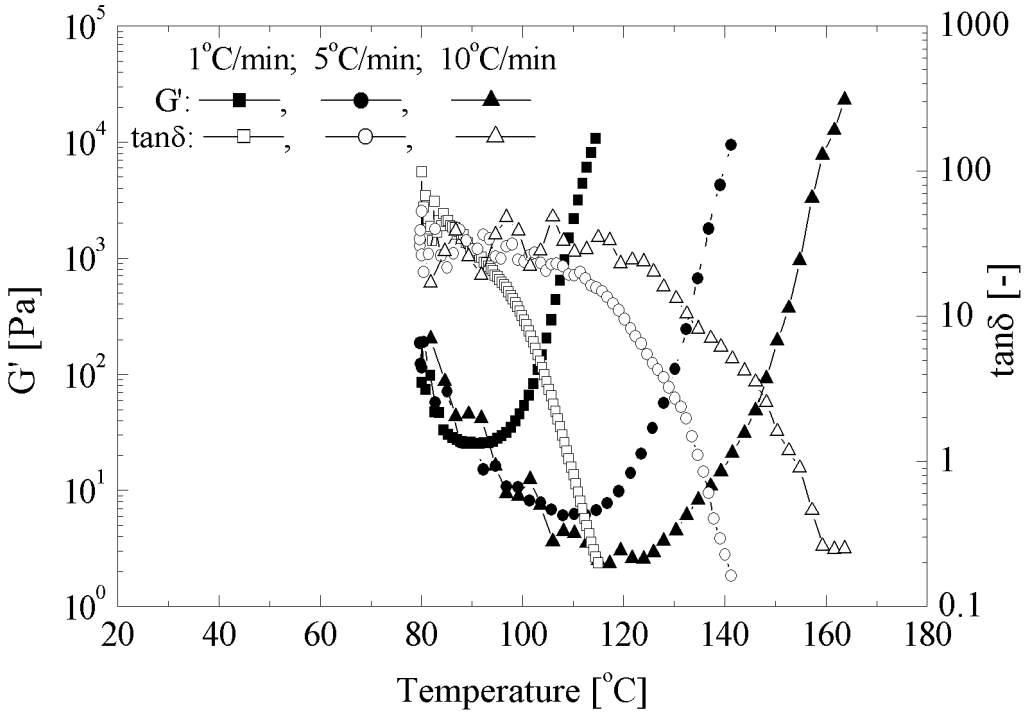

Figure 5.12: Evolution of elastic modulus and loss tangent with temperature, for constant CLA concentration (1 wt.%), as a function of heating rate.

the elastic modulus can possibly be maintain constant with temperature (to a value higher than say 100 Pa) by designing various heating rate stages in the elastic region, and further increasing the elasticity to very high value (fast cross-linking) with temperature.

Accordingly, different heating schemes are designed along with the normal constant heating rate and isothermal holding, with an ideal scheme mentioned in Fig. 5.13 and its effect on the evolution of G′ is shown in Fig. 5.14. Dotted lines from Fig. 5.14 represents minimum requirements for G′ i.e. 100 Pa. The effect of single step heating [scheme (a)] is already discussed, which shows a continuous decrease in the G′ with temperature up to a certain temperature and sharp increase in the G′ with further rise in the temperature. In contrast, the multiple heating rate scheme, namely scheme (b), which show different steps for the heating rate (between 85-87, 87-100 and 100-130°C), show a constant value

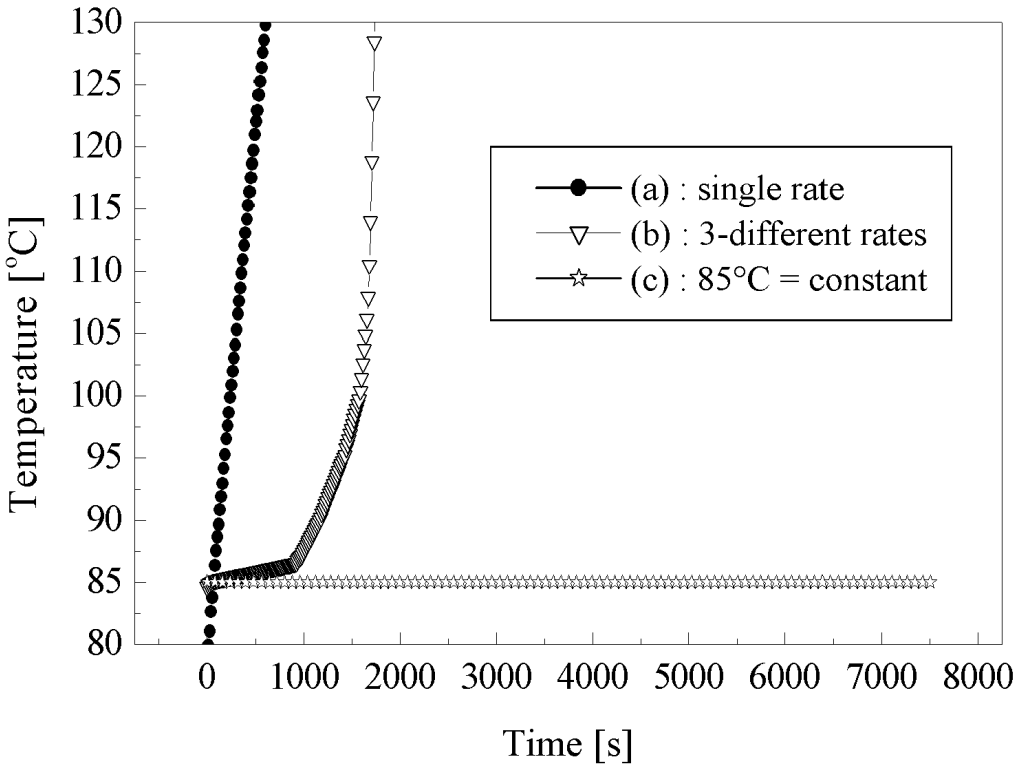

Figure 5.13: Different time-temperature schemes used to study the effect of heating rate on elastic modulus.

for G′ above 100 Pa (up to 100°C), and further cross-linking the polymer mixture during the final heating stage of the scheme. Similar observation is observed if the polymer is maintained at constant temperature, for e.g., 85°C, where the G′ remains constant for a long time and later increases with time, as found from Fig. 5.15. This investigation is performed by time dependent study of G′ at constant temperature i.e., 85°C.

This investigations gave hint for maintaining the spunned fibers in stable form. This could be done according to the following steps: (1) heating the polymer catalyst mixture to 85°C with a constant heating rate in order to melt the polymer, (2) spinning the fibers immediately when the temperature is between 85-87°C (as tanδ > 10 with the elasticity values exceeding 100 Pa), (3) transferring the

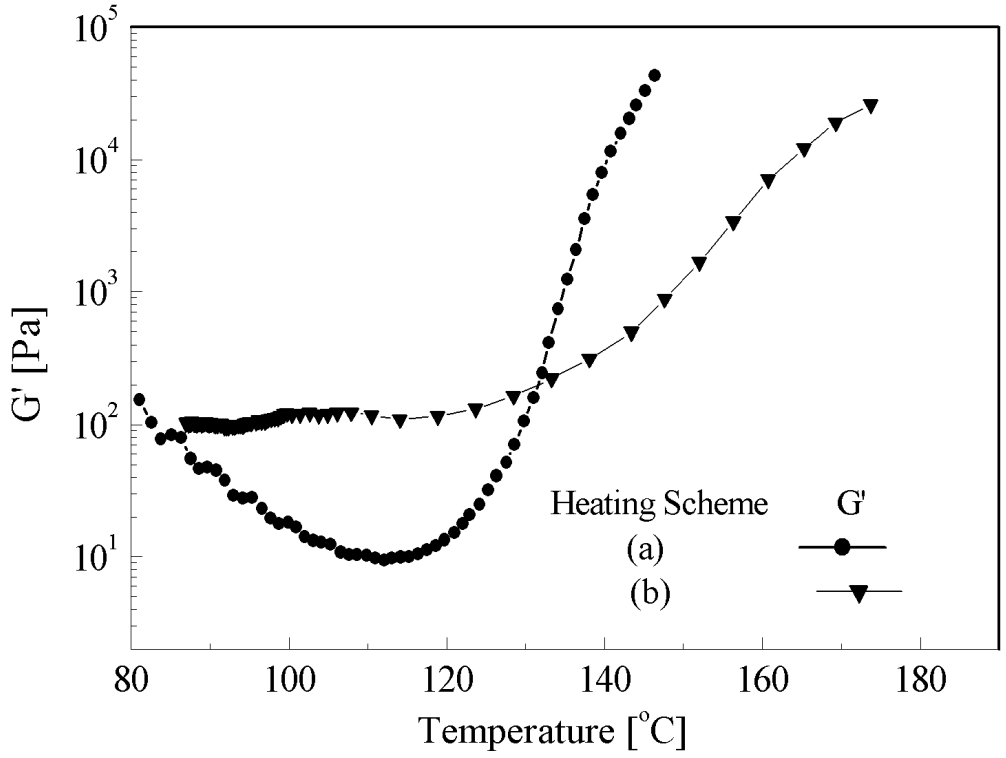

Figure 5.14: Effect of various heating cycles from Fig. 5.13 for maintaining constant elastic modulus with temperature.

spun fibers immediately in a isothermal oven kept at 85-87°C without allowing them to cool down to room temperature and/or heating the fibers by scheme (b) as mentioned in Fig. 5.13.

The possibility for stable fiber preparation is only characterized and not experimented due to the unavailability of a melt spun device attached with all post furnaces with precise temperature control. Inspite, the rheological investigation provides sufficient data to correlate different possible processing variable with the spinnability of the fibers.

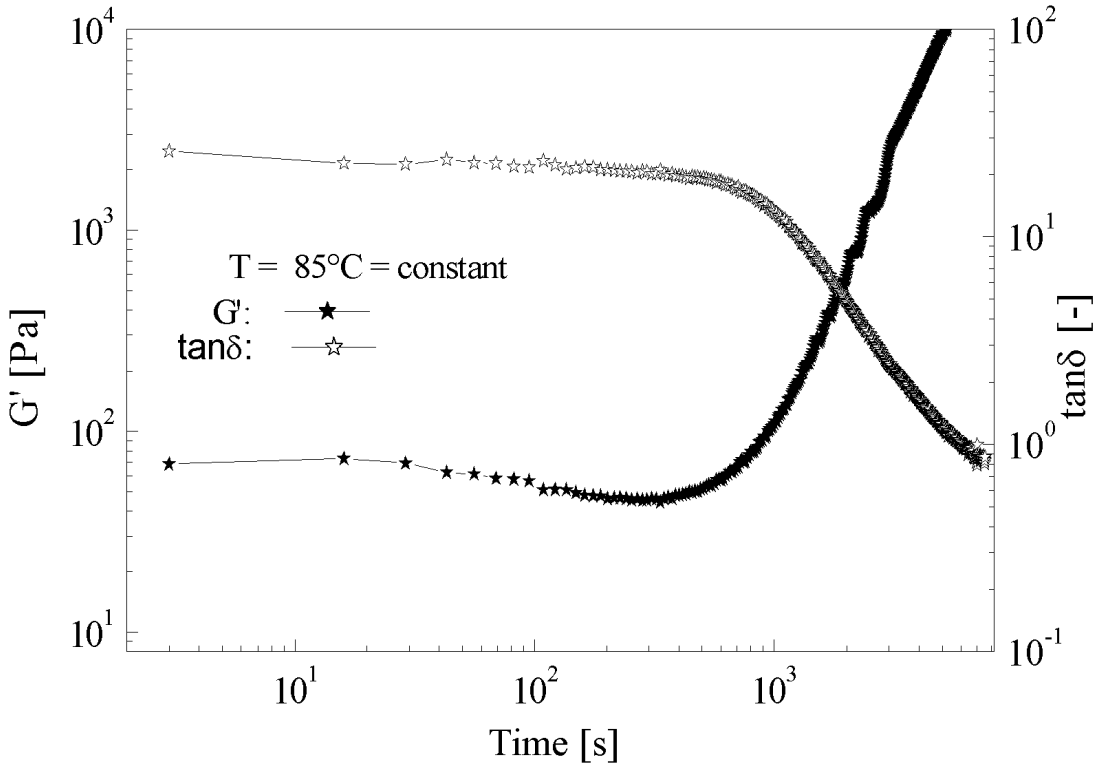

Figure 5.15: Effect of constant temperature on elastic modulus (G').

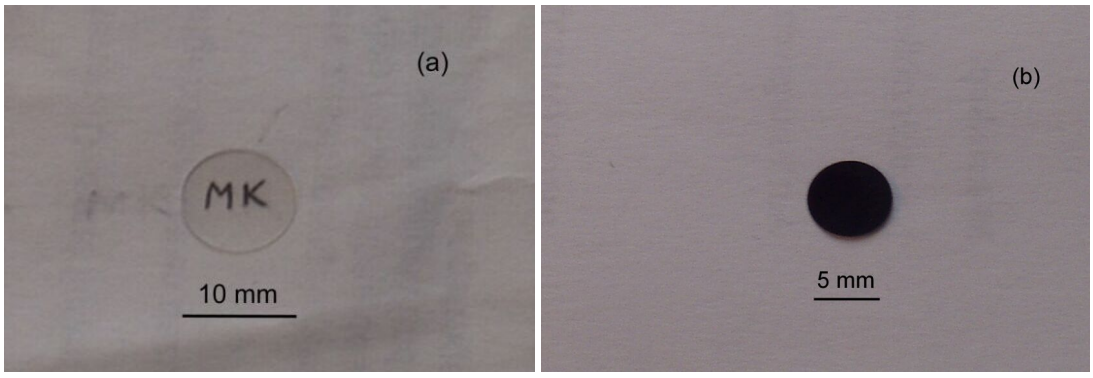

Figure 5.16: View of the specimens at various processing steps: (a) SiOC thin green body and (b) SiOC ceramic after pyrolysis at 1100°C.

5.2.3.2 Rheology for Green-Bulk Formation

In industry, monoliths (or production of direct complex forms) from preceramic polymer are generated with the help of injection molding technique. This technique, being a state of the art on its own, helps to produce components in huge volumes, if optimized properly. For injection molding, the injecting mass should develop low elastic modulus with temperature during the injection stage. This creates a possibility to inject the mass in the cavity in short time and fill the cavity completely. After injection, the injected mass should generate viscosity with temperature. With higher viscosity at high temperature, the formed shape retains its shape intact after ejection from the cavity.

Fig. 5.10 (page 105) clearly proves the capability of the MK polymer with *CLA* to undergo above mentioned requirements with temperature. This investigation will also be used for the later section for preparation of ceramic MEMS. At this stage, preparation of green bodies from MK polymer with 1 wt.% *CLA* and converting them to crack free SiOC ceramics will be mentioned. The polymer *CLA* mixture gets cross-linked in the warm pressing mold forming transparent green body. The sliced green body with a maximum thickness of 0.6 mm is shown in Fig. 5.16(a), and the crack-free SiOC ceramic after pyrolysis is shown in Fig. 5.16(b).

5.2.4 Pyrolysis of Unmodified Polymer: Polymer-SiOC Ceramic Conversion Process

As discussed earlier, addition of 1 wt.% of *CLA* shift the polycondensation reactions to the lower temperature and simultaneously increase the ceramic yield. This is reflected in very low mass loss between 100−400°C. Together there are three mass losses identified for the complete pyrolysis cycle, as shown in Fig. 5.17. The first weight loss between 100−400°C indicate enhanced cross-linking in this temperature regime. This results the release of water, ethanol and methanol identified by the masses related to water (H_2O; m/z = 18), ethoxy ($-C_2H_5O$; m/z = 45) and methoxy ($-CH_3O$; m/z = 31) groups. In this temperature regime mainly polycondensation reactions are active and the presence of *CLA* increases the extend of cross-linking of the polymer.

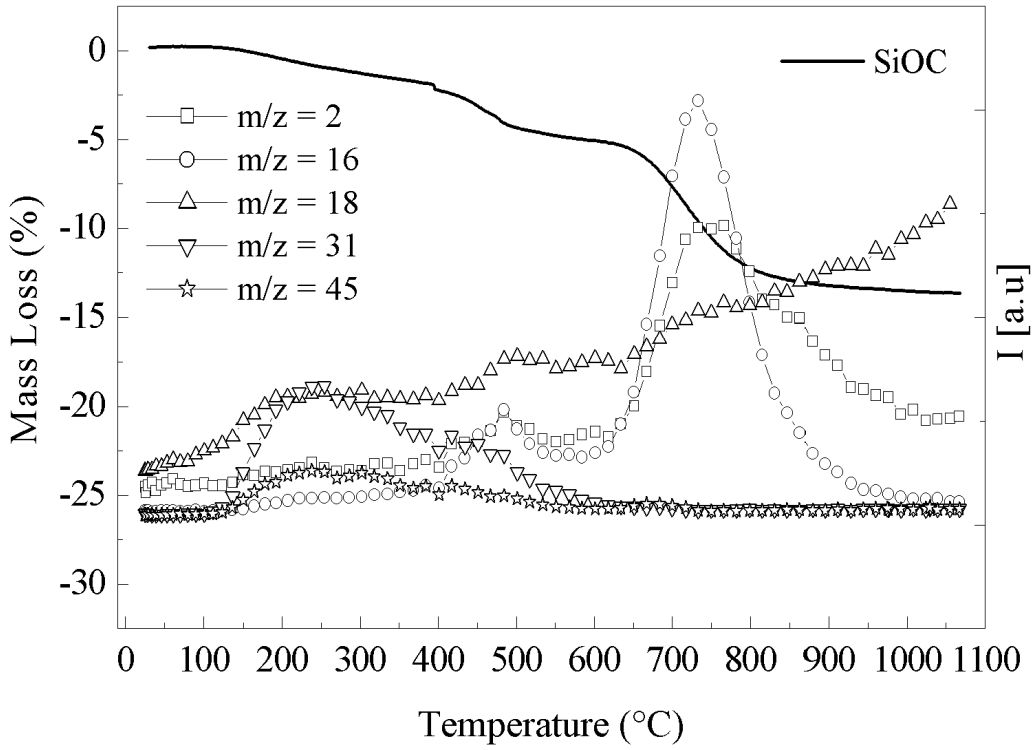

Figure 5.17: TG/MS of MK polymer + 1 wt.%CLA heated with 10°C/min in helium atmosphere.

In the second regime, particularly between 400−500°C, along with water (H_2O; m/z = 18) and methoxy ($-CH_3O$; m/z = 31) groups, hydrogen (H_2 m/z; = 2) and methane (CH_4; m/z = 16) are detected. The change in vibration band intensity with temperature is investigated and indicated in Fig. 5.18. It is evident that after annealing the sample above 400°C the C−H vibration band intensity reduces. This is explained by the radical reaction[115),(116)] between the remaining Si−OH bonds and the C−H bonds, which in consequence results by the evolution of water. The radical reactions for evolution of water and hydrogen are explained by Eqs. (5.10), (5.11) and (5.12). The evolution of methane in this temperature range may lead to formation of Si−O−Si bonds according to Eq. (5.13), releasing methane. The overall contribution of these reaction to weight

loss amounts about 2−3%.

$$\equiv Si - OH \quad \longrightarrow \quad \equiv Si\bullet \quad + \quad \bullet OH \tag{5.10}$$

$$\bullet OH \quad + \quad \equiv C - H \quad \longrightarrow \quad \equiv C \quad + \quad H_2O \uparrow \tag{5.11}$$

$$\bullet OH \quad + \quad H_2 \quad \longrightarrow \quad \bullet H \quad + \quad H_2O \uparrow \tag{5.12}$$

$$\equiv Si - OH \quad + \quad Si \equiv CH_3 \quad \longrightarrow \quad \equiv Si - O - Si \equiv \quad + \quad CH_4 \uparrow \tag{5.13}$$

The third mass loss, which is very significant begins at 630°C with a mass loss of 10%. In this temperature regime, evolution of methane, hydrogen and water are detected. As reported,[59] at 615°C the methyl groups are active, with the formation of a large distribution of aliphatic C sites and graphitic carbon. The evolution of methane and hydrogen, concurrent with the formation of graphite carbon have been described in the pyrolysis of methyl derived siloxane precursors, by the following reactions:

$$\equiv Si - CH_3 \quad \longrightarrow \quad \equiv Si\bullet \quad + \quad \bullet CH_3 \tag{5.14}$$

$$\equiv C - H \quad \longrightarrow \quad \equiv C\bullet \quad + \quad \bullet H \tag{5.15}$$

$$\equiv C - H \quad + \quad \bullet CH_3 \quad \longrightarrow \quad \equiv C\bullet \quad + \quad CH_4 \uparrow \tag{5.16}$$

$$\equiv C - H \quad + \quad H\bullet \quad \longrightarrow \quad \equiv C\bullet \quad + \quad H_2 \uparrow \tag{5.17}$$

The formation of the Si−C−Si bridges and free carbon in the ceramic products probably results from these combination of the different ≡ Si• and ≡ C• radicals.

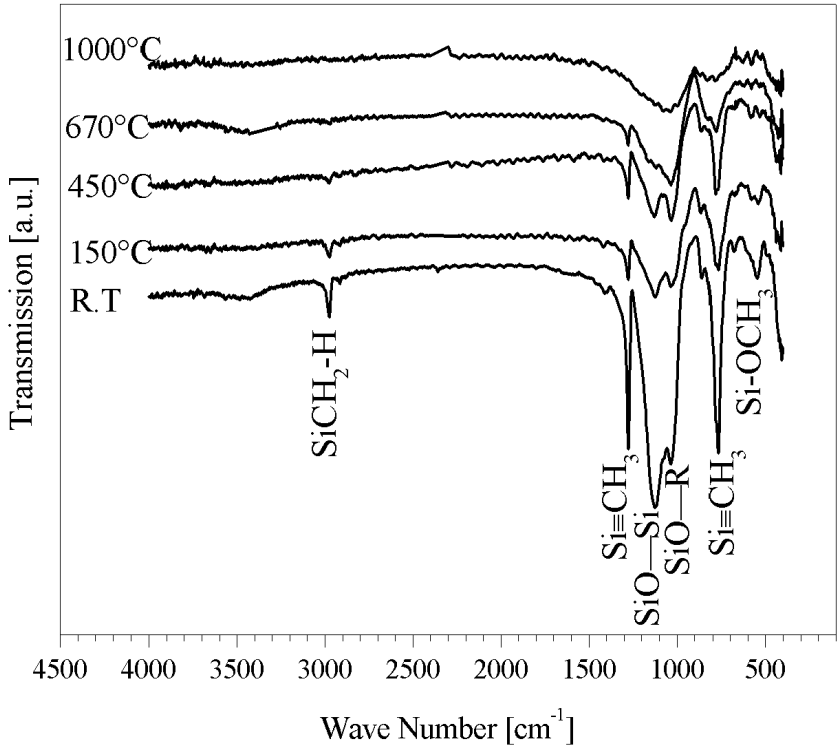

Figure 5.18: FTIR-spectra of catalyzed MK polymer heated to different temperatures.

5.3 Aluminum Modified Siloxane System

5.3.1 Gelation Process

Is it possible to modify (cross-link) commercial poly(methylsilsesquioxane), MK polymer by aluminum on the atomic scale, and if so, how? Modification can be performed by two methods, melting two chemical components together (*melt route*) and dissolving two components in a solution (*solution route*).

Melt route:

Alumatrane, an commercial aluminum alkoxide was added to MK polymer and the mixture is heated at various temperatures, (80, 100, 120, 140°C). This temperature was used as the polymer has a softening temperature at 60°C. It is

found that, at all temperatures, alumatrane swims on the top of the melt and do not possess any solubility with the melt. No marked changes in the viscosity is observed, even if the melts are isothermally held for long time at above mentioned temperatures. After solidification by cooling to room temperature and reheating the mass causes remelting. This indicates that, it is not possible to modify the MK polymer by aluminum alkoxide by melting, as the polymer is not cross-linked (normally cross-linked polymers are difficult to remelt).

Solution route:

MK polymer contains hydroxy, ethoxy and methoxy groups as functional groups, and these groups can react with alkoxide for cross-linking. Cross-linking reaction of MK polymer with aluminum alkoxide compounds like alumatrane used in this work proceeds via a sol-gel process at room temperature. The sol-gel transition is found here with isopropanol as the solvent. Sols prepared in acetone, methanol, ethanol, diethyl ether or n-hexane do not transform to gel at room temperature. Alumatrane reacts to a gel like state with MK polymer in the presence of non-dried isopropanol by alcoholysis or hydrolysis and subsequent polycondensation. Alumatrane is hydrolyzed by water which is present in non-dried isopropanol. This results in the formation of aluminum hydroxide as shown by first reaction in Fig. 5.19. Further aluminum hydroxide [$Al(OH)_3$] reacts with the polymer according to condensation reaction as shown by bottom reactions in Fig. 5.19. Increasing the alumatrane content changes the color of the polymeric gel from white to faint yellow. The gel time is dependent on the amount of alkoxide present. Gel time of 2, 5, and 11 h was observed for the 9.1 (SiAlOC1), 16.6 (SiAlOC2) and 23.6 wt.% (SiAlOC3) alumatrane mixture, respectively. Very low amount of alumatrane, namely 2.5 wt.% do not transform to a gel state at room temperature and instead requires temperature of 50°C for 5h. A physical view of one such sol like SiAlOC1 and corresponding gel, is represented in Fig. 5.20.

5.3.2 SiAlOC Polymer-Ceramic Transformation Process

The thermal gravimetric analysis between room temperature and 1100°C under argon flow show a total weight loss of 21−29%. As analyzed by in situ mass spectrometry (refer in Fig. 5.21), between 100 and 400°C water, methanol and

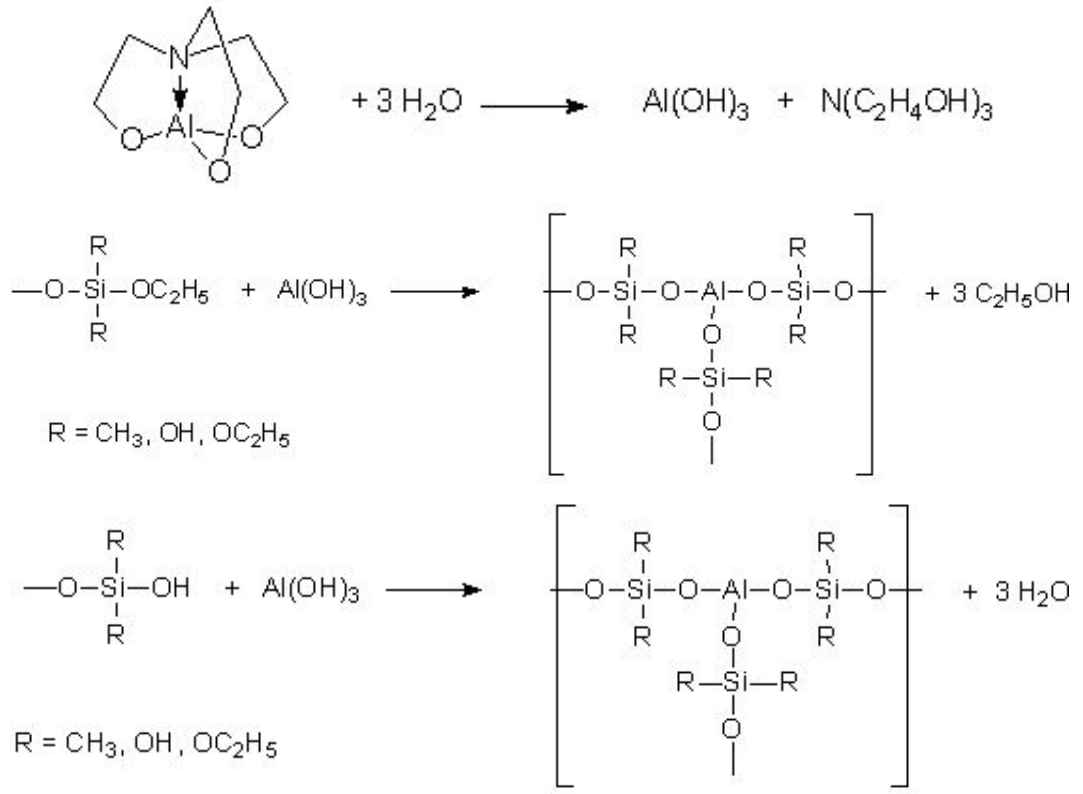

Figure 5.19: Possible hydrolysis and condensation reaction of alumatrane with MK polymer in isopropanol.

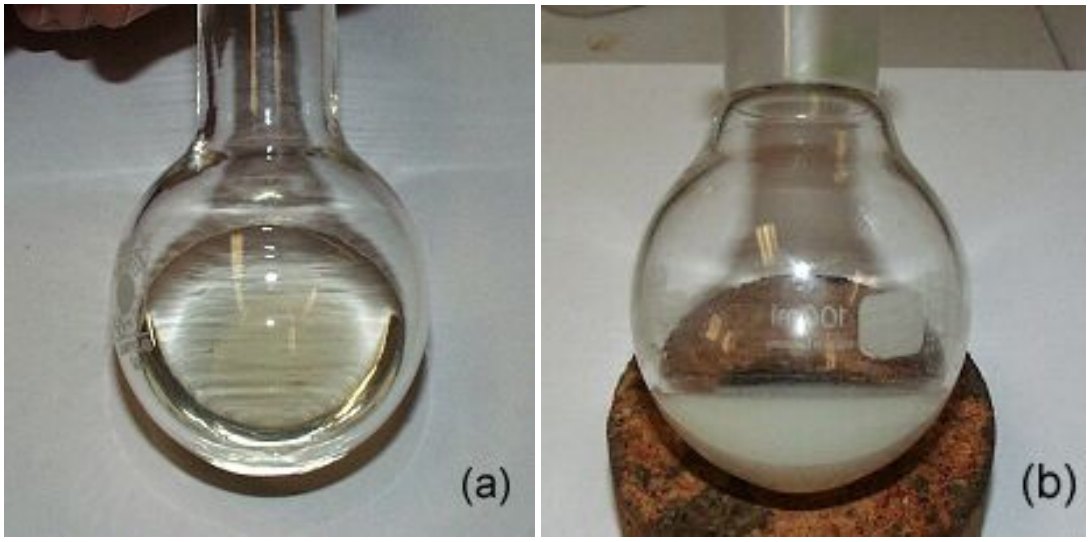

Figure 5.20: View of the reaction system at various processing steps: (a) SiAlOC1 sol and (b) SiAlOC1 gel after gelation at room temperature.

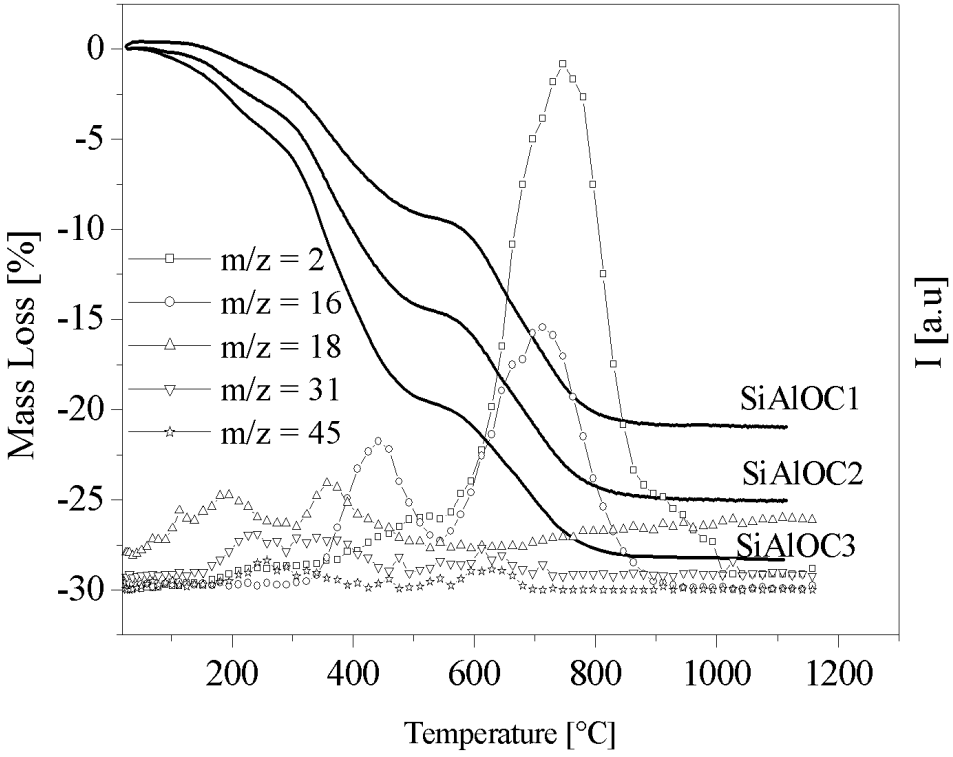

Figure 5.21: TG/MS of aluminum modified (SiAlOC) MK polymer heated with 10°C/min in helium atmosphere.

ethanol are evaporated indicating further polycondensation reaction. The masses are identified by m/z = 18 for H_2O, m/z = 31 for methoxy (CH_3O) and by m/z = 45 for ethoxy (C_2H_5O).

The significant differences in the weight loss between 350−500°C, is related to the amount of alumatrane in the system. For example, addition of high alumatrane, increase the amount of ($-CH_2$) groups, which are present in alumatrane. Thermal gravimetry of only alumatrane (figure not included), possesses major sharp mass loss step between 350−400°C. Mass spectroscopy confirms this to ($-CH_2$) for m/z = 14, which gets decomposed during the thermal treatment. Additionally, the fragments of (hydroyethyl)amine [$N(C_2H_4OH)_3$] with m/z = 149 and boiling point of 360°C is detected in this temperature regime.

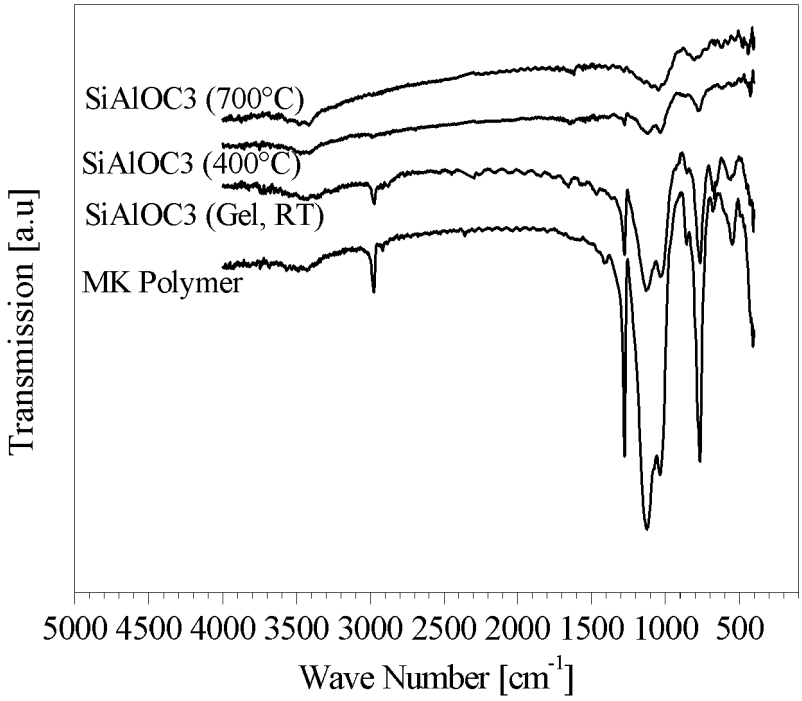

Figure 5.22: FTIR of aluminum modified (SiAlOC3) MK polymer heated to different temperatures.

At higher temperatures, between 550 and 850°C, methane and hydrogen are released exclusively. Also, the nature of mass loss is same for all three mixtures in this temperature range. Alumatrane influences the formation of CH_4 compared to the Al-free siloxane and results in increased mass loss. At 850°C the mineralization process is complete, as observed by plateau in weight change behavior above this temperature. This result coincides nicely with that of the IR spectroscopic investigation. No significant changes is observed in the IR-spectra obtained for unmodified MK polymer and alumatrane modified polymer at room temperature. As can be taken from Fig. 5.22, after annealing of the polymer between 400 and 700°C the relative intensities of the C−H absorption bands at 2960−2890 cm^{-1} and that at 1260 cm^{-1} are remarkably decreased. The mineralization process involves the cleavage of Si−C and C−H bonds, according to Eqs:{5.14−5.17} and leads to the evolution of methane and hydrogen.

5.4 Chemical Analysis

In order to quantify the elements present in the pyrolyzed mixture and to confirm the modification process, elemental analysis of the pyrolyzed ceramic polymer is investigated and listed in Table: 5.3. It is found that, aluminum modification in SiAlOC ceramic reduces the total carbon content compared to that observed in SiOC ceramic.

According to the scheme reported by Soraru *et al.*[53], the quantitative amount of Si-C equivalence and the C_{free} content in the oxycarbide glass is determined. The sample calculations for SiOC and SiAlOC ceramic are as follow:

SiOC Cermaic

This calculation is done on the basis of chemical analysis (Si, C, O) and neglecting, the presence of residual hydrogen as a first approximation. It is assumed that only Si−C, Si−O, C−C chemical bonds are present in the silicon oxycarbide glass.

From Table: 5.3, the experimental glass composition of $Si_{1.00}O_{1.60}C_{0.80}$ is equated to SiO_xC_y.

Then we argue that all the oxygen is bonded to Si and is forming (formally) SiO_2. So, in this case we will have (x/2) SiO_2.

Hence,

Si−O equivalence is x/2 = 1.60/2 = 0.8

The remaining silicon, which is not involved in forming silica will form (1-x/2) SiC.

Thus,

Si−C equivalence is (1-x/2) = (1-0.8) = 0.2

The free C is then equal to: y-(1-x/2)

C_{free} = y-(1-x/2) = 0.80 - (0.20) = 0.60, ≈75%

SiAlOC Ceramic

A different approach will be used to calculate the Si−O, Si−C equivalence and the C_{free} in aluminum modified ceramics. In SiAlOC ceramic network, ^{27}Al MAS NMR (discussed later) confirmed that, aluminum is mainly coordinated octahedrally Al(6) with oxygen and no Al-C bonds are present. If we calculate the oxygen content bonded to Al forming (formally) Al_2O_3, the remaining ce-

Material	Si	Al	O	C	Chem. Formula	Si−C	C_{free}
SiOC	45.5	0	39.30	14.80	$Si_{1.00}O_{1.60}C_{0.80}$	(0.20)	75 %
SiAlOC1	46.05	1.56	42.65	9.02	$Si_{1.00}Al_{0.035}O_{1.63}C_{0.46}$	(0.21)	54 %
SiAlOC2	44.35	2.86	42.69	9.01	$Si_{1.00}Al_{0.070}O_{1.69}C_{0.47}$	(0.20)	56 %
SiAlOC3	42.05	4.36	44.51	8.59	$Si_{1.00}Al_{0.107}O_{1.86}C_{0.47}$	(0.15)	68 %

Table 5.3: Chemical characterization of pyrolyzed Si(Al)OC ceramic.

ramic composition will be reduced to that of the oxycarbide glass. The sample calculation for SiAlOC1 ceramic is as follow:

From Table: 5.3, the ceramic composition is taken as $Si_{1.00}Al_{0.035}O_{1.63}C_{0.46}$
Oxygen shared with Al will be 0.035 x 3/2 = 0.052
This reduces the total oxygen to 1.63 - 0.052 = 1.57

The oxycarbide composition now can be re-written as
$Si_{1.00}O_{1.57}C_{0.46}$ and equated to SiO_xC_y.
Hence, similar to the SiOC calculation:

Si−O equivalence is x/2 = 1.57/2 = 0.788

Si−C equivalence is (1-x/2) = (1-0.788) = 0.21

The free C is then equal to: y-(1-x/2)

C_{free} = y-(1-x/2) = 0.46 - (0.21) = 0.25, ≈54.1%

Accordingly, all Si−C equivalence and the corresponding C_{free} are calculated and are listed in Table: 5.3. It is found that, increasing the aluminum content in the ceramic decreases the amount of bonded carbidic phase and increases the free carbon content.

5.5 Presence of Residual Carbon in Si(Al)OC Pyrolyzed Products

The chemical analysis confirm that the processed Si(Al)OC ceramic does not produce stoichiometric composition but have excess free carbon. The presence formation of this free carbon can ideally be investigated by Raman spectroscopy. The following section is focused on the spectroscopic evolution of Si(Al)OC ce-

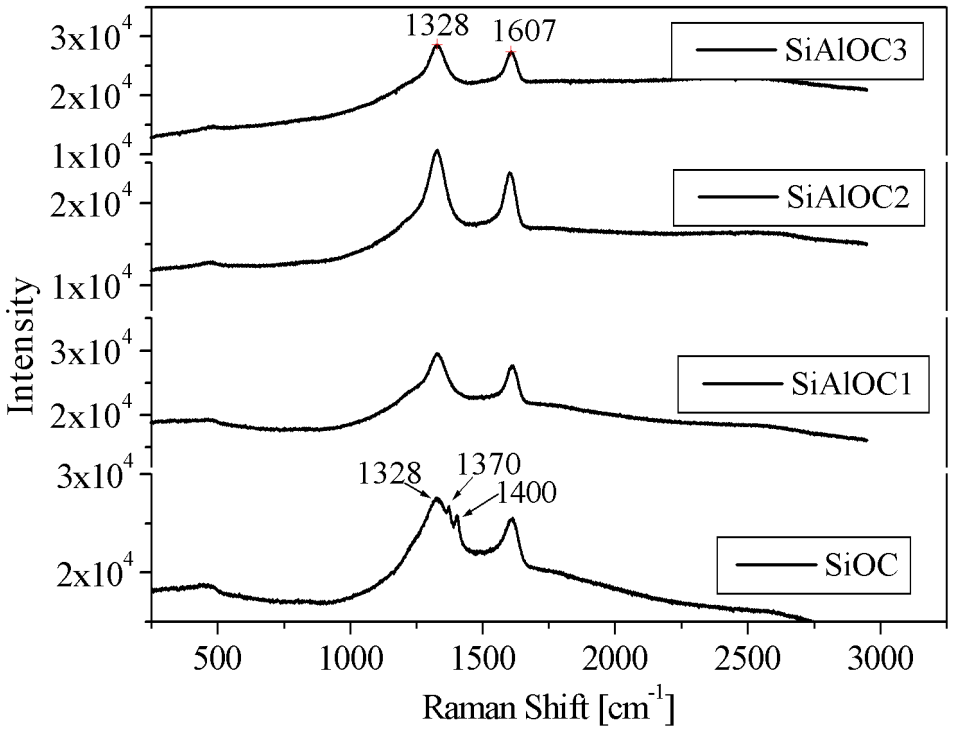

Figure 5.23: Raman spectra of the Si(Al)OC ceramics, pyrolyzed in Ar at 1300°C.

ramic.

These peaks are associated with graphitic carbon (G) with turbostratic stacking and diamond (D) like carbon. Graphite can be described as a sheet made up of six carbon atoms bonded in a ring with sp^2 types hybrid orbitals. Because the intra-layer bonding is stronger than the inter-layer bonding, there is a high tendency for ordering within the plane, but the c-axis direction has a tendency towards high disorder. A randomization of these ordered and disordered regions is described as turbostratic stacking.

It has been generally observed that the crystalline hexagonal graphite Raman spectrum is a single line at $\sim$ 1580 cm^{-1}, caused by in-plane C−C stretching vibrations. In disordered carbon structures, the G line becomes broadened and shifted to $\sim$ 1600 cm^{-1}, while an additional line (D) appears at 1360 cm^{-1}. This is exactly observed for SiOC ceramics. The (D) line, whose intensity increases

with decreasing domain size, results from structural imperfections in the carbon. Presence of this band suggest that the carbon domain size is relatively small for SiOC ceramic as compared to SiAlOC ceramics, which do not show this peaks at 1360 cm^{-1}. Such a small domain size may favor the crystallization of SiC at high temperature.

According to both Lespade *et al.*[117] and Knight *et al.*[118], there exists a coherent length, L_a, that must be exceeded to create a Raman signal. In the case of amorphous and crystalline carbons, this coherent length is estimated to be ∼2.5 nm. Here, it can be inferred that the turbostratic carbon species in the silicon oxycarbide and aluminum modified silicon oxycarbide ceramic network are dispersed at a scale >2.5 nm. Thus, the presence of free carbon in Si(Al)OC ceramics is demonstrated qualitatively by Raman spectra. Raman spectrum for the SiOC and SiAlOC ceramics pyrolyzed in Ar at 1300°C is shown in Fig. 5.23 . Both SiOC and SiAlOC ceramics show similar Raman spectra with two broad peaks at ∼ 1328 and ∼ 1607 cm^{-1}. The broad peak at lower wave number for SiOC ceramic show two additional peaks.

5.6 MAS-NMR Investigation of Si(Al)OC System

The presence of Si−O, Si−C bonds in the gel state or polymer state is well confirmed and their presence in the ceramic state need to be investigated before looking into the oxidation and creep behavior of these ceramic product. Also MK polymer has been modified by aluminum and its coordination with present elements need further investigation.

The ^{29}Si MAS-NMR spectrum as shown in Fig. 5.24 is for SiAlOC1 ceramic pyrolyzed at 1100°C in argon and indicates three peaks at -114, -78 and -44 ppm belonging to tetrahedral $(Si)O_4$, $C(Si)O_3$, $C_2(Si)O_2$ groups, respectively. This confirms that Si−C bonds have been retained during pyrolysis. As seen, the $(Si)O_4$ peak appears at more negative chemical shifts value.[119] This shift depends on the degree of polymerization and with the number of Al, C nearest neighbors in the polyhedra adjacent to the Si tetrahedron. Increasing the degree of polymerization from Q^0 to Q^4 increases the degree of shielding and leads to more negative chemical shifts. The presence of Al or carbon in the adjacent

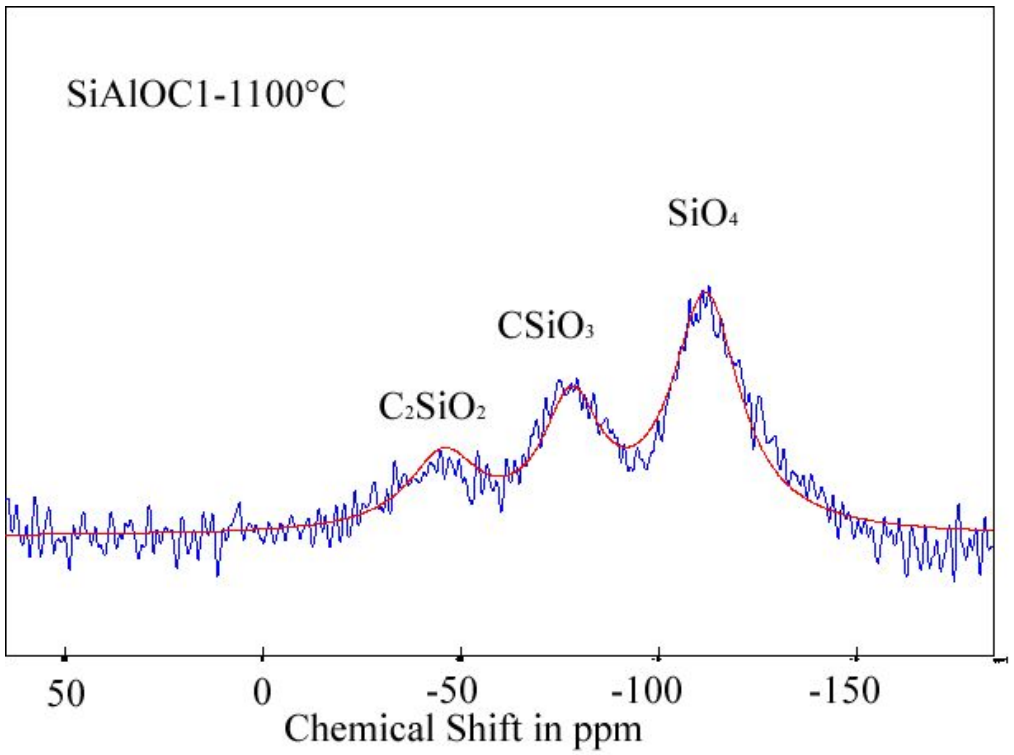

Figure 5.24: ^{29}Si MAS NMR spectrum for SiAlOC1 ceramic pyrolyzed at 1100°C in argon atmosphere.

sites has the opposite effect. Si-Al-O-C ceramic material is formed by a sol-gel method where the reaction between the aluminum containing species and the polymer occurs, chemical bonding between the two components could exists via Si−O−Al bonds. Such a peak can appear at less negative chemical shifts but such a component is not seen in the spectrum. However, the presence of these bonds cannot be rejected but should involve only a small number of silicon sites. Similar ^{29}Si spectrum is reported by Wootton *et al.*[77] for different Al_2O_3 containing Al-Si-O-C glasses with no peak coming from Si−O−Al bonds.

^{27}Al MAS-NMR is investigated for all three pyrolyzed compositions. It is seen that for SiAlOC1 and SiAlOC2 ceramic the spectra is unchanged and hence only one spectra is fitted namely for SiAlOC2 and compared with that of SiAlOC3 composition. Fitting the SiAlOC2 ceramic spectra to Gaussian-Lorentzian function indicate the peak positions at 13.5, 31 and 53.6 ppm, also listed in Table: 5.5. The first and the the third peak is coming from the octahedral Al(6) and

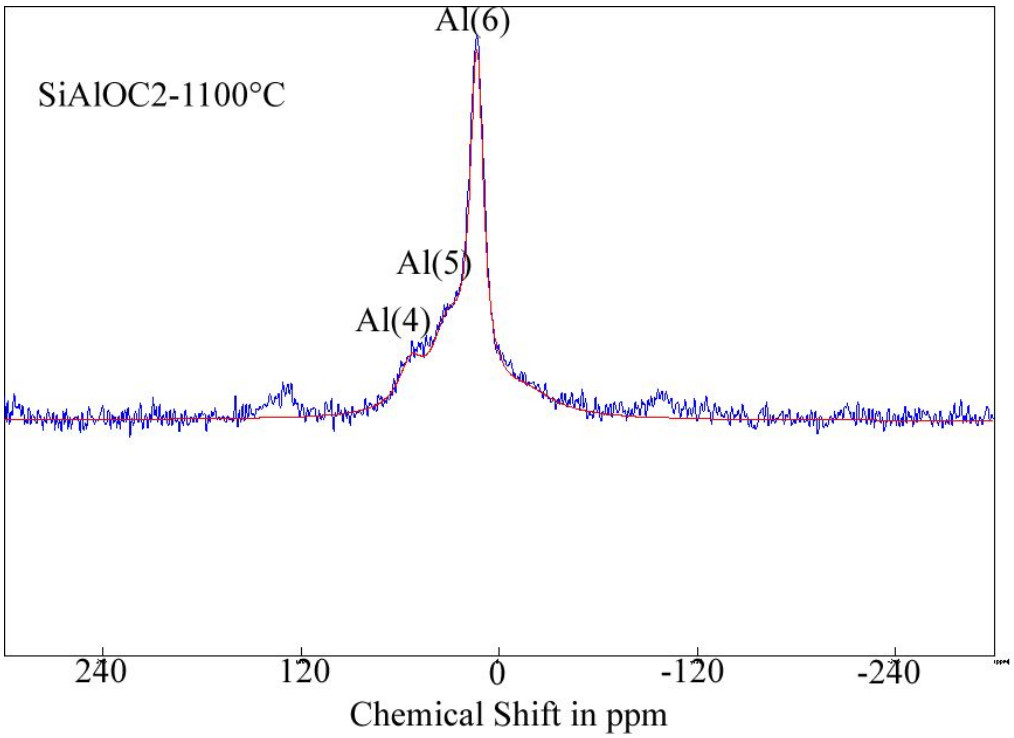

Figure 5.25: ^{27}Al MAS NMR spectrum for SiAlOC2 ceramic pyrolyzed at 1100°C in argon atmosphere.

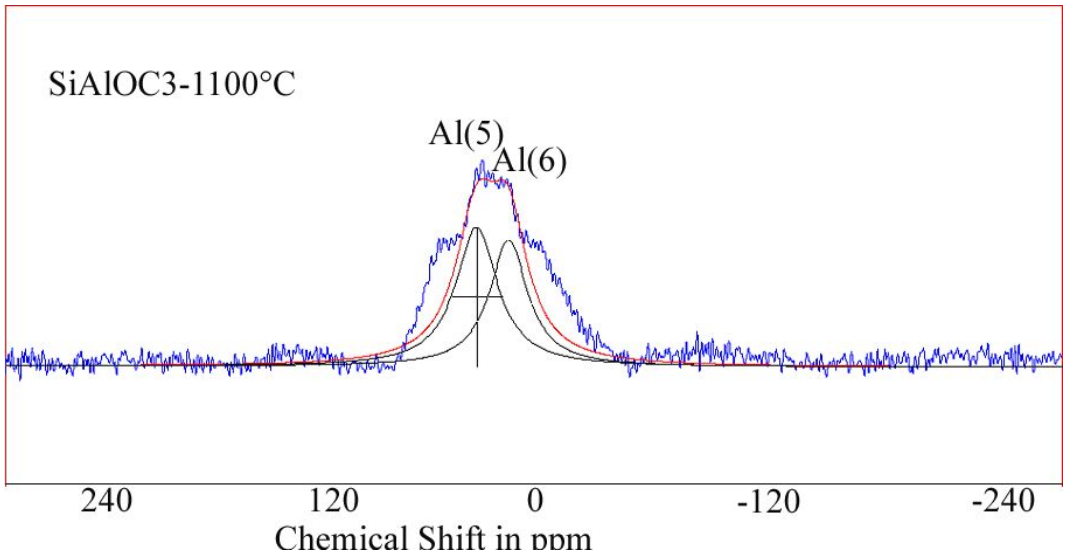

Figure 5.26: ^{27}Al MAS NMR spectrum for SiAlOC3 ceramic pyrolyzed at 1100°C in argon atmosphere.

Sample Preparation	Site[a]	δ (ppm)
Gibbsite and silica gel grounded for 1200 min$^{(120)}$	1	13
	2	39
	3	67
Kaolinite heated at 700°C for 30 min	1a	6
	1b	15
	2	37
	3	64
Sol-gel synthesis	1a	7
	1b	15
	2	37
	3	71
Spray pyrolysis	1	12
	2	43
	3	72
Quenched glass	1a	8
	2	37
	3	66
Mullite precursor gels	1	9.7
	2	42
	3	71
Crystalline mullite	1	7.5
	2	49
	3	69.4

[a]1: Al(6), 1a & 1b: two octahedral sites for some materials, 2: Al(5), and 3:Al(4)

Table 5.4: ^{27}Al MAS-NMR chemical shifts comparison for various amorphous mullite precursors from literature.

Sample	Site[a]	δ (ppm)
SiAlOC1	1	14.7
	2	32
	3	53
SiAlOC2	1	13.5
	2	31
	3	53.6
SiAlOC3	1	14.1
	2	32.3

[a]1: Al(6), 2: Al(5), and 3:Al(4)

Table 5.5: ^{27}Al MAS-NMR chemical shifts values for present SiAlOC ceramics.

tetrahedral Al(4) coordinated aluminum, respectively. Al(6) being the preferred coordination. In pyrolyzed state the spectra exhibit an additional coordination at the peak position of $\sim$ 32 ppm. This indicates penta-coordinated aluminum Al(5) and the peak positions are similar to the published values.[73], [77], [120], [121] The above mentioned peaks covers the chemical shifts range of Al−O bonds. It has been mentioned [73] for commercial Al_4C_3 indicate an peak at 150 ppm and was assigned to be for some Al−C bonds. Such kind of bonding seems to be absent in case of aluminum modified Si-Al-O-C ceramic.

The spectrum for SiAlOC3 ceramic shows broad peak, that can be deconvoluted into two namely at 14.1 and 32.3 ppm. The ceramic material is still disordered and needs high temperature for ordering to occur. It has been already shown[77] for the Si-Al-O-C system that, increasing the temperature transforms the pentahedral aluminum atoms Al(5) to tetrahedral Al(4) and mainly to octahedral Al(6) coordination. This Al-O aluminum coordination allows crystallization of the amorphous structure to mullite. Mullite is either formed directly or may form Al_2O_3 as an intermediate phase before transforming to mullite.

McManus *et al.*[120] reports aluminum coordination for various amorphous aluminosilicates which are listed in Table: 5.4 and are compared with SiAlOC results listed in Table: 5.5. It is seen that the octahedral and pentahedral sites are observed at almost similar positions for the first three materials listed in Table:

5.4. These values are far away from the last three materials. Additionally the tetrahedral site Al(4) for all SiAlOC ceramic appears at much lower side of the tetrahedral spectrum (+50 − +80 ppm), which indicates a higher shielding, as reported by Putnis[119]. He also explains that this shielding (more negative) depends on the mean Al−O−Si bond angle. The higher the bond angle the more pronounced is the shielding.

5.7 Bulk Formation: Physical Changes During Si(Al)OC Pyrolysis

5.7.1 Bulk SiOC Ceramics

The effect of rheology on formation of bulk green body has already been mentioned and shown in Fig. 5.16(a), (refer to page 111). During this discussion more emphasis was given on the chemical changes in the polymer to generate polycondensation reactions. Indeed, stable compacts are generated in the green state with this study, which form SiOC bulk crack free ceramic after pyrolysis. Measuring physical change, generated during the polymer-ceramic transformation, helps to know the insights during bulk processing.

Earlier, it is mentioned that very thin (<0.6 mm) bulk SiOC ceramics are prepared from the commercial MK polymer with *CLA*. Unfortunately, very thick samples show cracking on the surfaces of the cylindrical sample even if the pyrolysis is carried at very low heating rate. Pyrolyzing the thick green body at a heating rate of 5°C/h show cracks on the surface of the bulks. Investigating the cause for cracking is done by measuring the dimensional changes during the polymer-to-ceramic transformation. This was done manually i.e., by measuring the dimensions (diameter and height) of the cylinder before and after pyrolysis, and also by instantaneous measurement in the change in length parallel to the height of the cylinder using dilatometry (TMA). The manual measurements are listed in Table: 5.6 along with the densities in the green and pyrolyzed state of processing. SiOC bulks show almost isotropic shrinkage (average ≈ 18%) i.e., same shrinkage in axial as well as in radial direction. Along with isotropic shrinkage, out-gassing of organic matter is observed during polymer-to-ceramic

Material	Axial Shrinkage [%]	Radial Shrinkage [%]	Green Density [g/cm^3]	Pyrolyzed Density [g/cm^3]
SiOC	16.75	19.54	1.26	2.16
SiAlOC1	7.63	22.33	1.27	2.17
SiAlOC2	12.85	24.78	1.26	2.22
SiAlOC3	15.90	26.49	1.28	2.26

Table 5.6: Physical changes in Bulk Si(Al)OC ceramics during polymer-ceramic transformation.

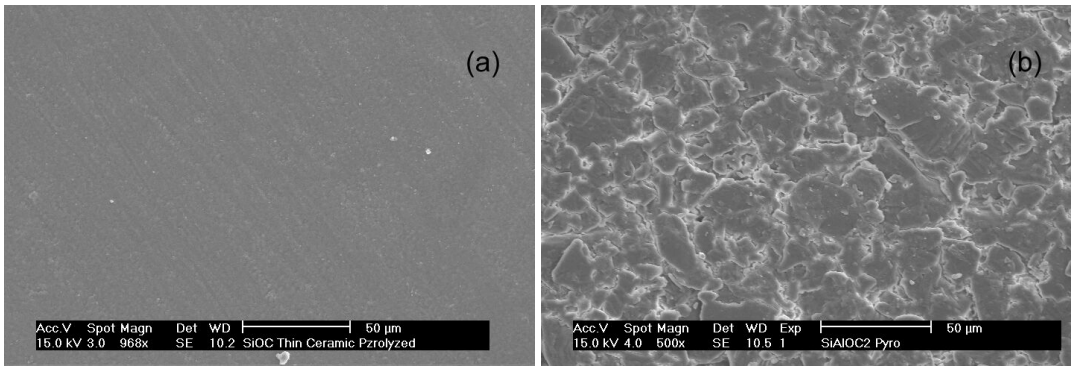

Figure 5.27: SEM micrograph of the surface of (a) SiOC and (b) SiAlOC2 ceramic after pyrolysis at 1100°C in argon.

transformation. Also SiOC green bodies are extremely dense and brittle in nature. Such a high density is due to the melting of the polymer *CLA* mixture during warm pressing and subsequent cooling. Eventually, evolution of gases from the dense bodies and shrinkage are responsible for cracking of the compacts during pyrolysis. However, for very thin bulks there is high constrain for shrinkage in the axial direction (because of less material). This makes the processing of dense, crack-free, thin SiOC ceramic feasible. The crack free, dense microstructure for the pyrolyzed sample shown in Fig. 5.16, is represented in Fig. 5.27 (a). The fractured surface shows a glassy finish on macro scale.

Thermal mechanical analysis (TMA) gives additional information for the dimensional changes in the bulk with increasing temperature. Accordingly, the TMA curve (refer Fig. 5.28) can be separated into two stages, namely stage [I] and stage [II]. In stage [I], expansion in the bulk is reported. Looking into more

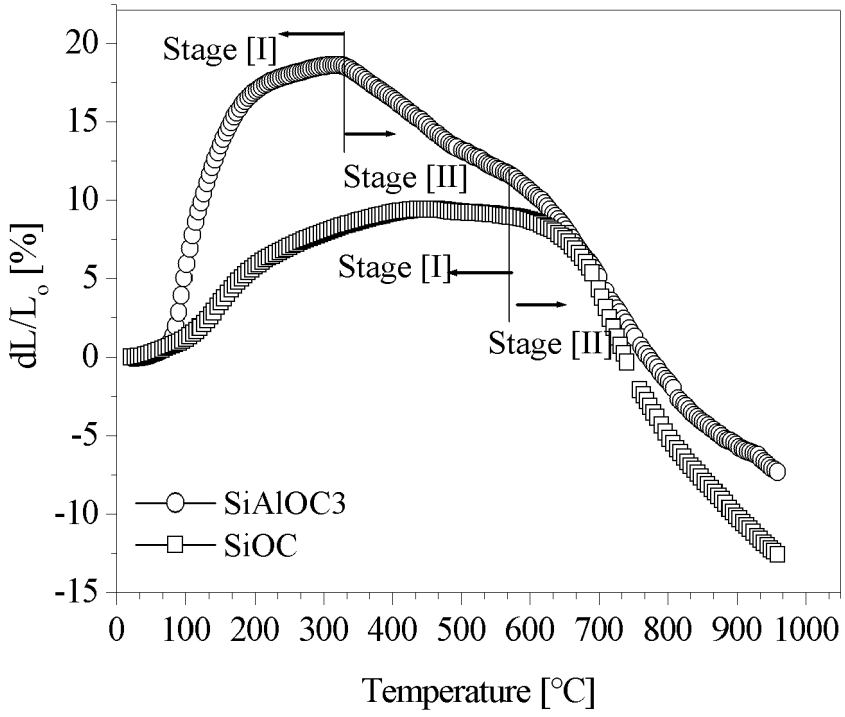

Figure 5.28: Thermal mechanical analysis (TMA) of non-modified SiOC and Al-modified SiAlOC ceramics measured with a heating rate of 5°C/min in argon atmosphere.

details with respect to thermal gravimetry of the polymer *CLA* mixture, which show no weight change up to 170°C, only thermal expansion is observed in the bulk. The mass loss (2−2.5%) stage found between 170−400°C, reduces the expansion in the bulks, i.e., the slope of the dl/L_o vs. temperature curve reduces. At T > 400°C, the shrinkage of the sample coincides with the decomposition process. The high temperature for shrinkage initiation and high shrinking rate found between 600 and 1000°C (stage II in Fig. 5.28) may be responsible for the cracking of the bulks.

5.7.2 Bulk SiAlOC Ceramics

Aluminum modified polymers produced from MK with alumatrane (SiAlOC), differs completely in bulk formation, from that of SiOC ceramic produced from

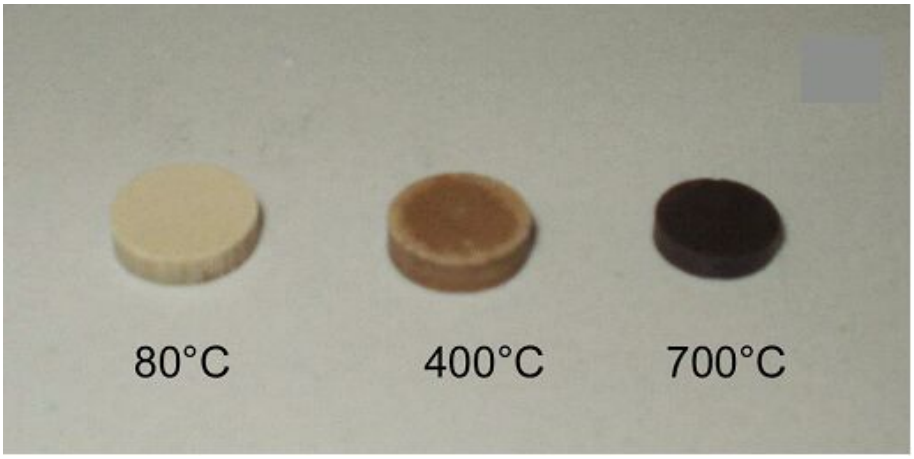

Figure 5.29: View of SiAlOC green and ceramic bodies obtained at different temperatures.

MK polymer with *CLA*. The SiAlOC polymers are formed by a sol-gel method, which completely cross-links the material, and prevents any further melting. In fact, some partial melting might be possible, otherwise it will be completely impossible to form bulk compacts, which require joining of particles with each other. Comparing the gelation process, here it is necessary to emphasize that the gelation time differ with the alumatrane content. It has been reported[59] that, material produced from fast gelation results in brittle monoliths, whereas when the gelation time is fairly long, the compacts possess more elasticity. These properties helped to produce stable bulk green compacts, by warm pressing the alumatrane modified polymer between 80−100°C. This temperature was chosen, because the thermal gravimetry confirm no decomposition up to this temperature for all gels. Indeed, mechanically stable cylindrical bulks are obtained after warm pressing the polymer, the physical view of which is shown in Fig. 5.29.

In contrast to SiOC ceramic, SiAlOC ceramic shrinks non-isotropically with higher shrinkage in radial direction than in the axial one as shown in Table: 5.6. Modification of the polysiloxane with alumatrane promotes cross-linking and prevents melting during warm pressing. Microstructural investigation of warm pressed bulks show interconnected transient porosity. As a consequence, non-isotropic compaction of the polymer powder occurs during green body formation resulting in an anisotropic shrinkage during polymer to ceramic transformation.

SiAlOC3 bulk is tested with TMA (Fig. 5.28) for the dimensional change with temperature. It is clear that, in the initial stage, up to 175°C only thermal expansion is seen. Between 175−300°C the extent of thermal expansion is reduced, which coincides with the first mass loss step due to polycondensation reactions. The material start to shrink at 300°C, which match with the mass loss due to mineralization process. Despite of this large dimensional change throughout the polymer-to-ceramic transformation process along with the degassing period the aluminum containing samples do not crack. The crack free ceramic bulk is shown in Fig. 5.29, and a crack free microstructure is indicated in Fig. 5.27(b). This behavior is explained by the enhanced expansion of the material and transient porous network formed in stage[I]. Mercury pressure porosimetry reveals the presence of 3−4 vol.% open porosity for the pyrolyzed SiAlCO ceramic. The shrinkage rate (Fig. 5.28) and rate of mass loss (Fig. 5.21) are lower and more gradual in stage[II] of the transformation process. Additionally, SiAlOC bulk start to shrink at lower temperatures compared to the SiOC bulks.

Thus, the combination of, gradual mass loss, transient porosity, low shrinkage rate, and wide shrinkage temperature range beginning from the lower temperature are necessary conditions for the synthesis of crack-free bulk ceramics.

5.8 Mechanical Characterization of SiOC Ceramics

5.8.1 Acoustic Method

Before measuring the longitudinal and Rayleigh wave velocities, which are necessary for the calculation of elastic modulus (E) and poisson ration ν, the density of the thin bulk SiOC ceramic is confirmed. The density was measured at 20°C by the Archimedean displacement technique using CCl_4. The measured density is $\rho = 2.23$ g/cm^3 with a relative error of $\pm 0.5\%$.

The elastic modulus and poisson ratio is then calculated from Eq. (4.1) and Eq. (4.2) (refer to page 79) with the longitudinal and Rayleigh wave velocity and density. The elastic modulus results are summarized in Fig. 5.30 at various position from the surface to the interior of the sample. A gradient was observed from the surface to the center of the SiOC disk, along a diameter, especially in a 2 mm thick ring including the surface. In a region showing a homogeneous color

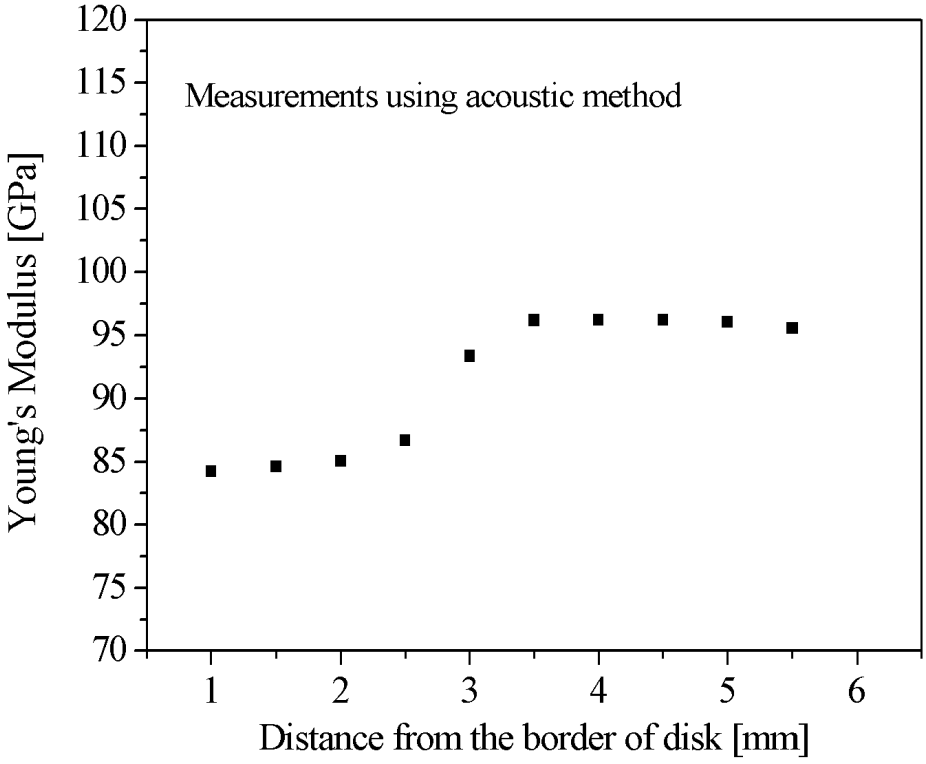

Figure 5.30: Elastic modulus of thin SiOC ceramic sample measured from the surface to the interior by acoustic method.

and located within 2 mm from the specimen center, E and ν values of 96.1 $\pm$0.5 GPa and 0.11 $\pm$0.02 were determined respectively.

The variation in the elastic modulus along the diameter indicates that the glass is inhomogeneous. There might exist a compositional variation, which is reflecting in the change in the elastic modulus of the sample across the section. The Young's modulus observed in this study is close to those of $D^HT^H0.5$ (104 GPa) and D^HT^H1 (110 GPa) reported by Soraru et al.[65] An most astonishing result is the low value for poisson ratio. It means that the material has a great tendency for volume change under mechanical loading (a value of 0.5 corresponds to a volume conservative process; most materials show values between 0.2 and 0.4; vitreous silica gives 0.148).

5.8.2 Indentation Method

The SiOC glass specimen exhibit a remarkable resistance against indentation cracking. Cracks usually do not appear at loads lower than 196.2 N (20 kg) as shown in Fig. 5.31. For comparison, a standard window glass exhibits radial cracks at load over 100 g and vitreous silica exhibits ring-type (intersection of cone cracks with the surface) cracks at a load higher than 50 g. When cracks tend to form, they show up as surface ring-type cracks, as visible on the bottom right side of the indentation in Fig. 5.31 (a). This behavior resembles that of vitreous silica or anomalous glasses.

The elastic modulus calculation, as described by Eq. (4.5) (refer to page 81), requires measurement of total (u) and reversible (u_e) displacement components. The displacement components or indentation profile can be measured either using a tilting procedure in a scanning electron microscopy[112] or as used in this studied by atomic force microscopy (AFM) as far as the indentation size remained smaller than 50 mm in diagonal length, i.e. as far as the load is smaller than 1 kg for SiOC ceramics. Accordingly the permanent (u_p), total (u) and reversible (u_e) displacement components were systematically estimated from the profiles following the procedure illustrated by the schematic drawing in Fig. 5.32.

The permanent displacement is directly measured on the AFM profile, whereas the total displacement is evaluated by extrapolation, by considering the ideal indentation shape at maximum load from the Vickers diamond shape. Then the reversible component, u_e, is deduced: $u_e = u\text{-}u_p$. Results are summarized in Table: 5.7. From the relationship $\gamma = 2.2\nu + 0.53$ for the relative penetration depth in Eq. (4.5), a value of $\gamma = 0.77$ is obtained if the Poisson's ratio ν of 0.11 evaluated by acoustic microscopy is used. Fig. 5.33 shows the indentation load dependence of Young's modulus calculation.

Young's modulus ranges between 90 (low load) and 180 GPa (high load). The load effect is possibly linked to the flow densification process, which occurs in the SiOC glass as well as in vitreous silica, and result in a harder and stiffer material beneath the indenter. Average hardness and Young's modulus of 6.4 $\pm$1 and 101 $\pm$15 GPa respectively were estimated from the experimental data obtained for indentation loads lower than 100 g.

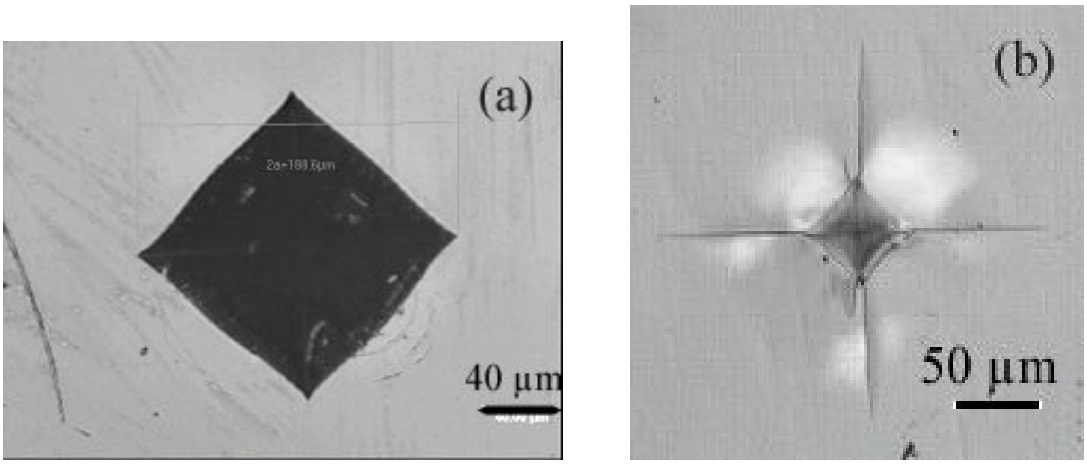

Figure 5.31: Vickers indentation: a) SiOC glass, 20 kg, 20 s; b) window glass, 1 kg, 20 s.

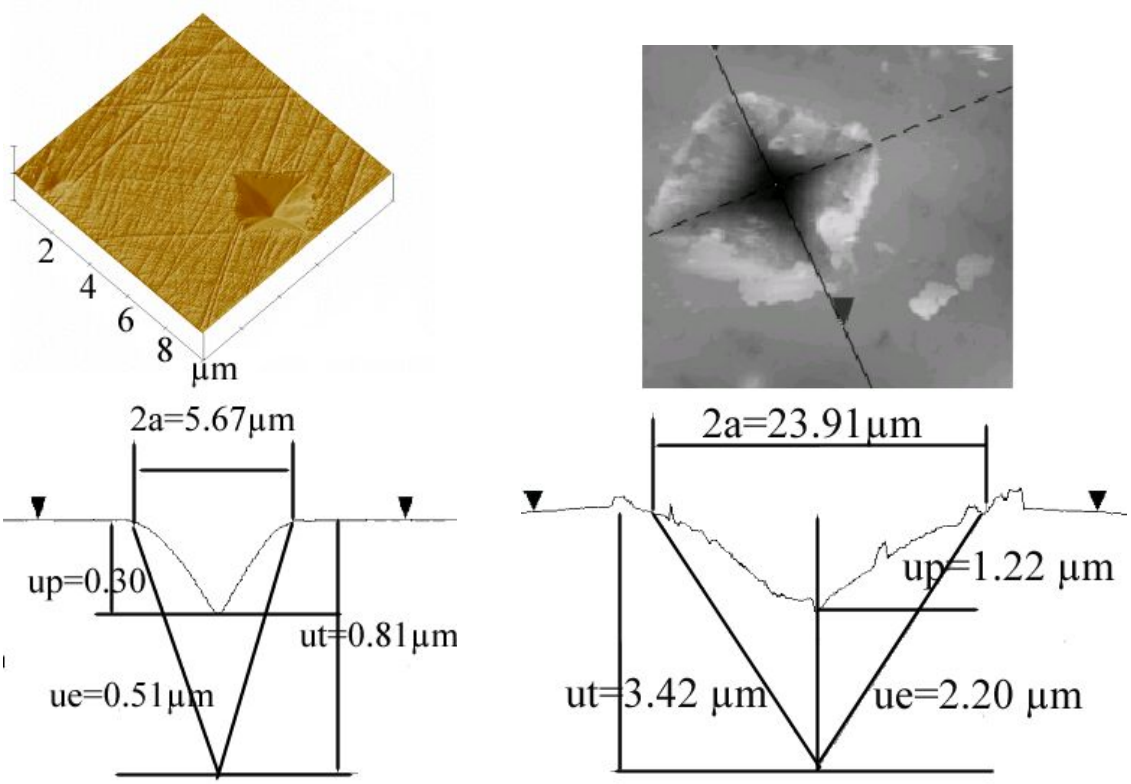

Figure 5.32: Indentation profiles with various displacement components from AFM: (a) 10 g; (b) 300 g.

Mass (g)	2a (µm)	u_t (µm)	u_p (µm)	u_e (µm)
1000	39.54	5.65	2.40	3.25
500	37.03	5.29	1.84	3.45
300	23.91	3.42	1.22	2.20
50	12.26	1.75	0.92	0.83
25	9.40	1.34	0.61	0.73
10	5.67	0.81	0.30	0.51

Table 5.7: AFM measurements from Vickers indentations performed at loads ranging from 10 to 1000 g.

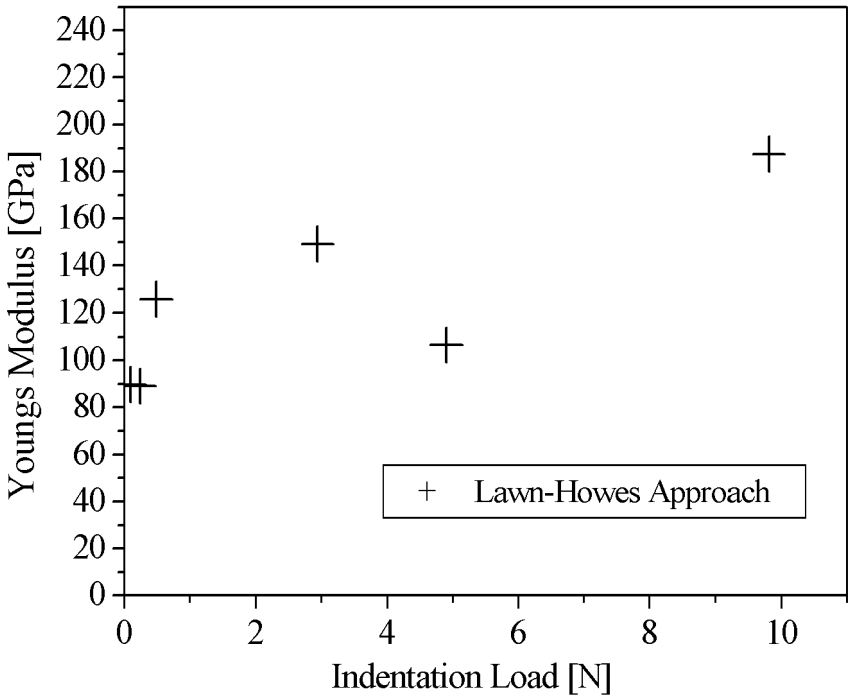

Figure 5.33: Young's modulus as calculated by means of Eq. (4.5) (page 81) as a function of the indentation load.

5.9 High Temperature Behavior

5.9.1 Crystallization, Phase Separation and High Temperature Stability in Si(Al)OC Ceramics

In the earlier discussion, Si(Al)OC ceramics are synthesized from commercial siloxane precursor. The products synthesized at 1100°C are covalent ceramics built up by a random array of silicon oxycarbide, $[SiC_xO_{4-x}]$ $(0 \leq x \leq 4)$ units. Additionally, the effect of increasing aluminum content on the decrease of $(C/Si)_{oxy}$ ratio and relative rise in free carbon C_{free} is discussed. The stability of this silicon oxycarbide phase at high temperature, and the effect of aluminum content in SiAlOC ceramic on the phase separation/transformation process along with dimensional changes in the bulks will be discussed in the following sections.

5.9.1.1 SiOC Ceramic

SiOC ceramics are X-ray amorphous up to the pyrolysis temperature. SiOC ceramic bulks (produced from MK-polymer + 1 wt.%CLA) crystallize to β-SiC and free carbon at temperatures beyond 1300°C, refer in Fig. 5.34. At 1400°C, the XRD results indicate the formation of β-SiC (3C and 2H polytypes), zirconia and graphitic carbon, along with amorphous phase. Cristobalite, which usually forms at temperature ≥1200°C, was not seen at high temperature in SiOC systems. This behavior is related to the presence of carbon (either as free C or residual carbon bonded in form of SiC) in the amorphous SiO_2 network. According to the calculation reported in the earlier section; as seen in Table: 5.3, the as pyrolyzed SiOC ceramic contain about 75% (of the total carbon content) of free carbon. Excess free C is assumed to prevent nucleation of cristobalite, because short-range diffusion is strongly impeded by the incorporation of carbon into the SiO_2 network. The density increases from 2.20 to 2.38 g/cm^3 for the pyrolyzed (1100°C) and heat-treated (1500°C) material, respectively. Weight loss of $\sim$ 2.15% is observed for the sample heated at 1500°C.

The crystallization behavior and the phase separation of SiOC ceramics are reported in the literature.[63; 122; 123] Researchers noticed that the distribution of silicon, oxygen, and carbon atoms might not be as random as commonly expected for such materials. Based on Rietveld refinement studies, those researchers pro-

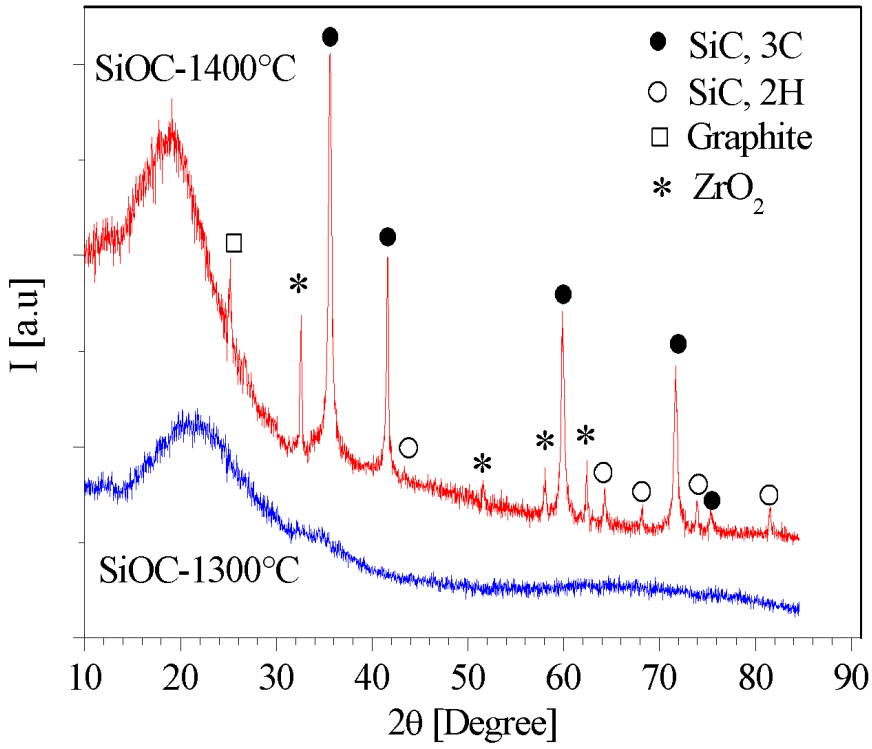

Figure 5.34: Evolution of the X-ray powder diffractogram recorded on the SiOC ceramic after annealing at various pyrolysis temperature in argon atmosphere.

posed the presence of local Si−C and Si−O environments in SiOC glass. From microstructural point of view, such SiOC glasses can be described as a mixture of amorphous SiO_2 and crystalline SiC at temperatures exceeding 1000°C thus implying that phase separation has occurred. Although a phase separation into SiC and SiO_2 occurs, a rather high amount of SiOC still seem to be present in the nano-dispersed material, as mentioned by Kleebe *et al.*.[63] Because nano-sized SiC crystallites are embedded in an amorphous SiO_2 matrix, assumed here, for the sake of simplicity, to be pure fused silica (with no incorporated carbon), the SiO_2/SiC interface should be somehow disordered as a result of chemical inter-diffusion at the interface and/or local structural relaxations to decrease surface energy. Therefore, this SiO_2/SiC interface is thought to represent an extended

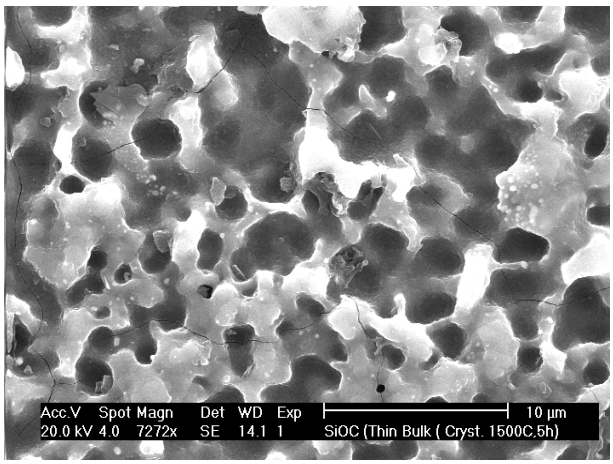

Figure 5.35: SEM micrograph of the surface morphology (surface without fracture) of SiOC ceramic after heat treatment in argon at 1500°C.

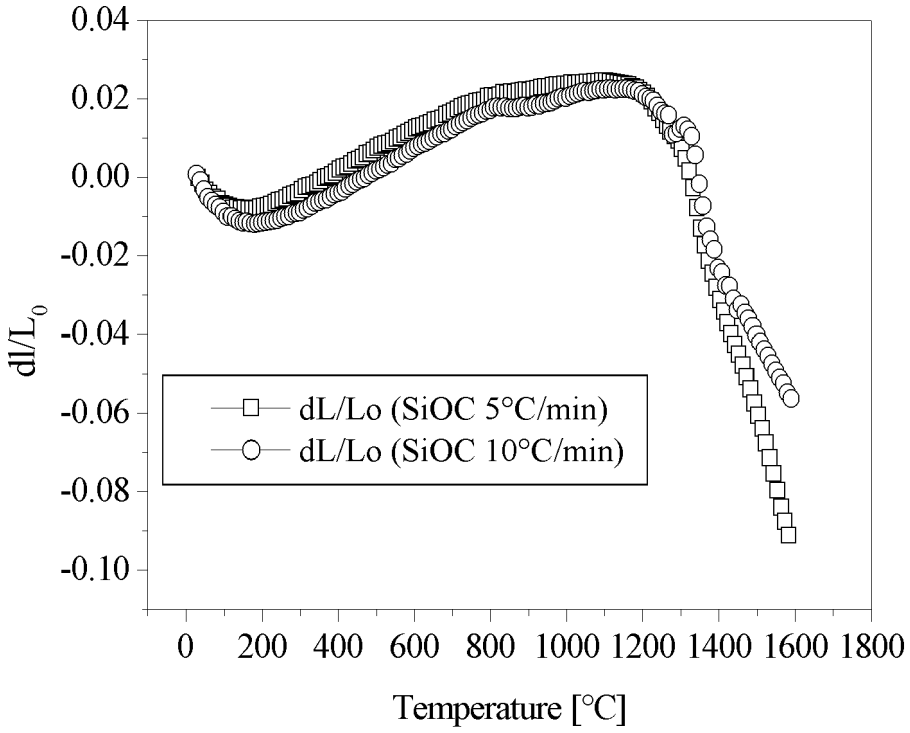

Figure 5.36: Dilatometrical evolution of dimensional changes with temperature in argon at 5 and 10°C/min for SiOC bulk samples.

SiOC interface.

Microstructural investigation of the bulks after heat-treatment at 1500°C show micro-cracking and surface roughening, as shown in Fig. 5.35. The rough surface can be explained by the degassing during the heat-treatment. The dimensional changes during the heat-treatment is investigated by thermal dilatometry and the results of are shown in Fig. 5.36. In the initial stage of heating up to 200°C, the bulk SiOC ceramic show contraction of 1%. From 200 to 1200°C, the sample expands and with further heating the densification starts. This densification is most likely due to a viscous sintering of the silicon oxycarbide matrix above its glass transition temperature. The linear CTE between 200−800°C is measured to be $4.69 * 10^{-5}$ (1/°C). This temperature range is chosen because a small deflection from linearity is observed above this temperature. This deviation is presumably related to the completion of the mineralization reactions leading to the late formation of $C_2(Si)O_2$, $C(Si)O_3$ units.

5.9.1.2 SiAlOC Ceramic

In contrast to SiOC ceramics, SiAlOC ceramics remain completely amorphous up to 1300°C and amorphous/nano-crystalline up to 1400−1500°C. Phase separation into cristobalite, β-SiC and mullite takes place for the aluminum lean glass composition, namely SiAlOC1. Here, the total carbon content together with the free carbon is reduced and the aluminum content is extremely low to prevent the cristobalite nucleation.

Increasing the amount of aluminum alters the phase separation process. Aluminum rich compositions SiAlOC2 and SiAlOC3 form nano-crystalline mullite and SiC along with an amorphous SiOC phase but no cristobalite up to 1500°C. Past studies on borosilicate glasses which undergo devitrification to cristobalite have shown that addition of alumina, aluminum nitride, cordierite and mullite can suppress the formation of cristobalite.[124],[125] This finding coincides with those in Fig. 5.37 supporting a strong influence of Al-cations on the crystallization of silica. Moreover, the literature data indicate that mullite most effectively suppresses the formation of cristobalite. Also, crystallization of cristobalite depends on the volume and the particle size of mullite. The lower the particle size the lower the amount of mullite required for complete suppression of cristobalite

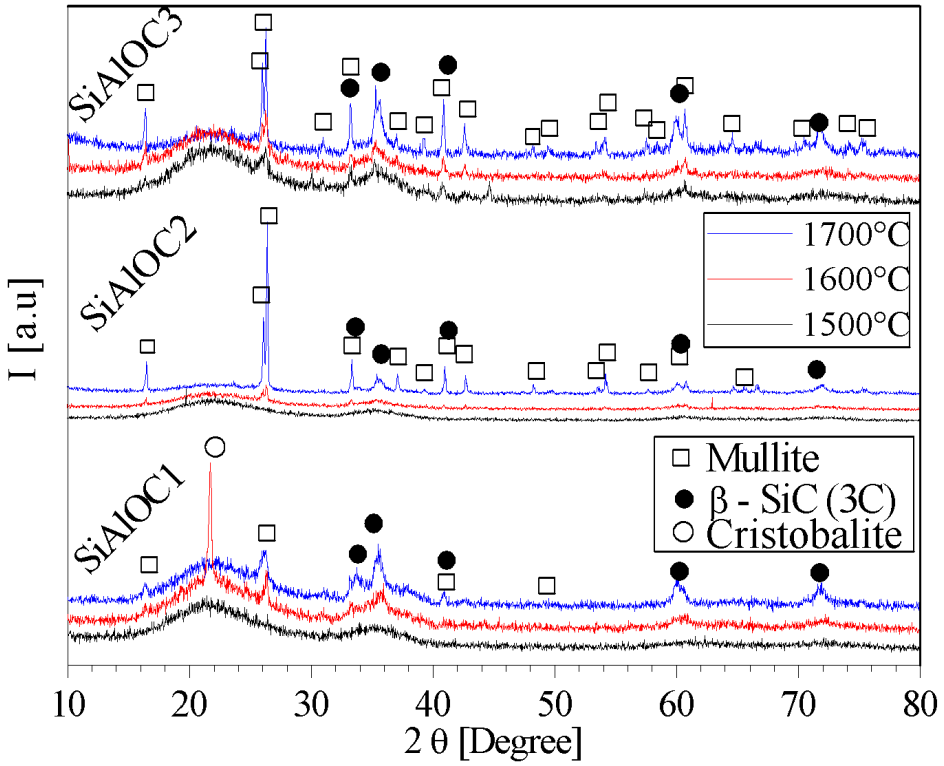

Figure 5.37: Evolution of the X-ray diffractogram recorded on the SiAlOC ceramics after annealing at various pyrolysis temperatures in argon atmosphere.

formation.

One distinct similarity for the phase formation behavior of all above mentioned compositions in Fig. 5.37 is the direct transformation of amorphous aluminosilicate phase to mullite without intermediate Al_2O_3. Such an intermediate phase is reported by Wootton[77] *et al.* on similar system. This transformation behavior helps in estimating kinetics and explained later in the crystallization kinetic study for these SiAlOC ceramics.

From XRD study, mullite is well detected between 1500−1600°C in SiAlOC2 and SiAlOC3 compositions but its presence or nucleation as nano-particles in the glass matrix could be at much lower temperature, i.e. ∼1300−1400°C, resisting any cristobalite formation. In general, aluminum in SiOC ceramics clearly

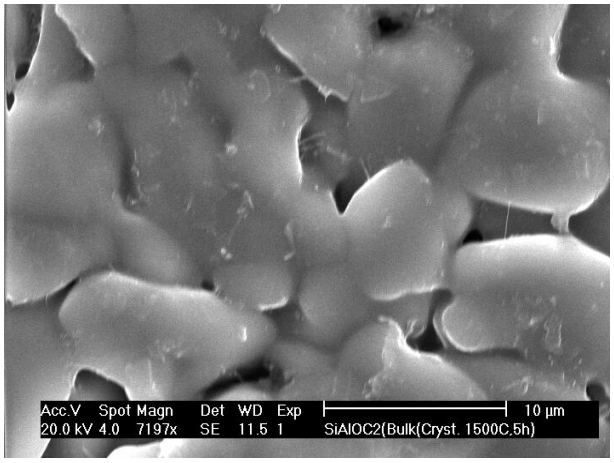

Figure 5.38: SEM micrograph of the surface morphology (direct surface) of SiAlOC2 after heat treatment in argon at 1500°C.

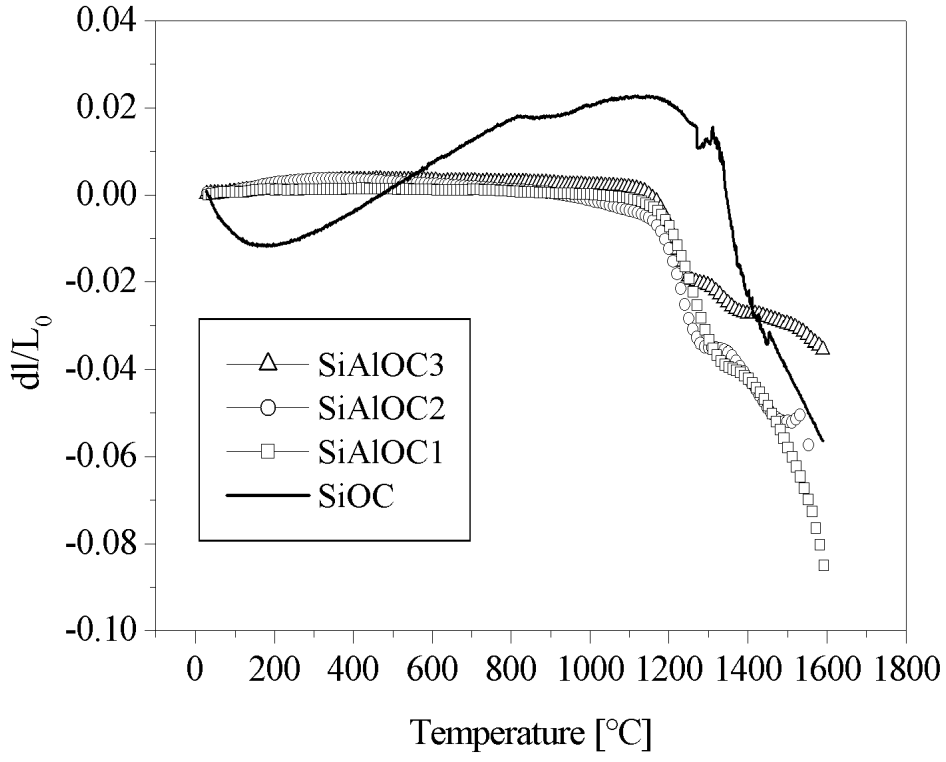

Figure 5.39: Dilatometrical evolution of dimensional changes with temperature in argon at 10°C/min for SiAlOC bulk samples.

Material	**Density** [g/cm^3]			**Mass Loss** [wt.%]			**Axial Shrinkage** [%]		
	1500	*1600*	*1700*	*1500*	*1600*	*1700*	*1500*	*1600*	*1700*
SiOC	2.389	–	–	2.15	–	–	–	–	–
SiAlOC1	2.312	2.260	1.795	1.90	2.41	10.13	4.43	5.82	-5.23
SiAlOC2	2.320	2.240	1.852	1.34	2.44	10.42	3.42	6.18	-7.93
SiAlOC3	2.306	2.265	1.888	1.11	1.80	6.82	2.88	4.77	-14.68

Table 5.8: Physical changes in bulk Si(Al)OC ceramics with temperature in argon at 10°C/min, (shrinkage measured geometrically without dilatometry).

inhibits cristobalite devitrification of the amorphous matrix at higher temperatures. The high temperature amorphous SiAlCO-phase is thermally stable at 1300 to 1500°C and supports densification.

The densification process between 1200 to 1600°C is well explained in literature for the low temperature production of high-density mullite ceramics.[126] In short, when Al_2O_3 and SiO_2 are used to form mullite, densification is promoted when the temperature is held where SiO_2 first becomes viscous and then, after initial densification via (transient) viscous sintering, the reaction between Al_2O_3 and SiO_2 to form mullite is initiated simply by raising the temperature (commonly above 1600°C). In Si(Al)OC system the densification is via viscous sintering from the silica phase. Accordingly, there is a rise in the density up to 1500°C, refer to Table: 5.8. This is also seen in Fig. 5.38 where the microstructure indicates neck formation between particles similar to sintering process. The loss in density at higher temperature (>1600°C) is from the higher mass loss ($\sim$6$-$10 wt.%) along with volume increase (negative axial shrinkage) for all SiAlOC ceramics.

Linear thermal expansion was observed from room temperature to 1100°C (Fig. 5.39). The linear CTE between room temperature and 1100°C is measured to be 1.556 x 10^{-6} (1/°C). Densification as indicated by shrinkage is initiated above 1100°C. The shrinkage behavior above 1100°C is strongly dependent on the aluminum content and more insight on this will be explained in the next section.

5.10 Softening/Crystallization Kinetics of SiAlOC Ceramics

Transformations in glasses is usually followed by thermometric (differential thermal analysis, DTA) and/or calorimetric (differential scanning calorimetry, DSC) measurements. DTA and DSC monitor the temperature increase or decrease and heat evolved or observed, respectively, by the material as a function of time, most commonly during a constant heating rate. The thermodilatometric (TD) technique, on the other hand, monitors changes in the length as a function of time. The objective of this section is to characterize the transformation processes involved in the SiAlOC material by TD plots and their derivative (TDD) thermograms and estimate the activation energy for these transformations.

Glasses when nonisothermally heated, passes through a sequence of individual thermal effects, namely, structural relaxation, softening and crystallization over a temperature range. The change in enthalpy due to these thermal effects are usually reflected as (i) characteristic points, such as onsets, inflections, and apexes, and (ii) areas under the individual effect peak. Changes in these characteristics in the thermograms with heating rate can be used to determine reaction kinetics and mechanism for the thermal effects.

Fig. 5.40 presents the effect of heating rate on the dimensional change of the bulk samples. As the heating rate increases, the general nature of the thermograms remained unchanged, but shifted towards higher temperatures. Some authors use the temperature of deflection point in the dilatometry curve as glass transition temperature. The deflection point is the temperature where the TD curve looses linearity. But this deflection point is changing with the heating rate as explained in literature.[79] The linear part also deviates slightly at much lower temperatures for all heating rates in SiAlOC2 and SiAlOC3 ceramic. This deflections could be from the change in the material property like residual stress. It has been shown that viscosity controls the rate of these changes. Thus it will be more accurate to evaluate the glass transition temperature by calculating the shear viscosities (using time dependent deformation), and is done in the later section using compression creep.

After the linear part, Δl increases gradually with temperature at a constant

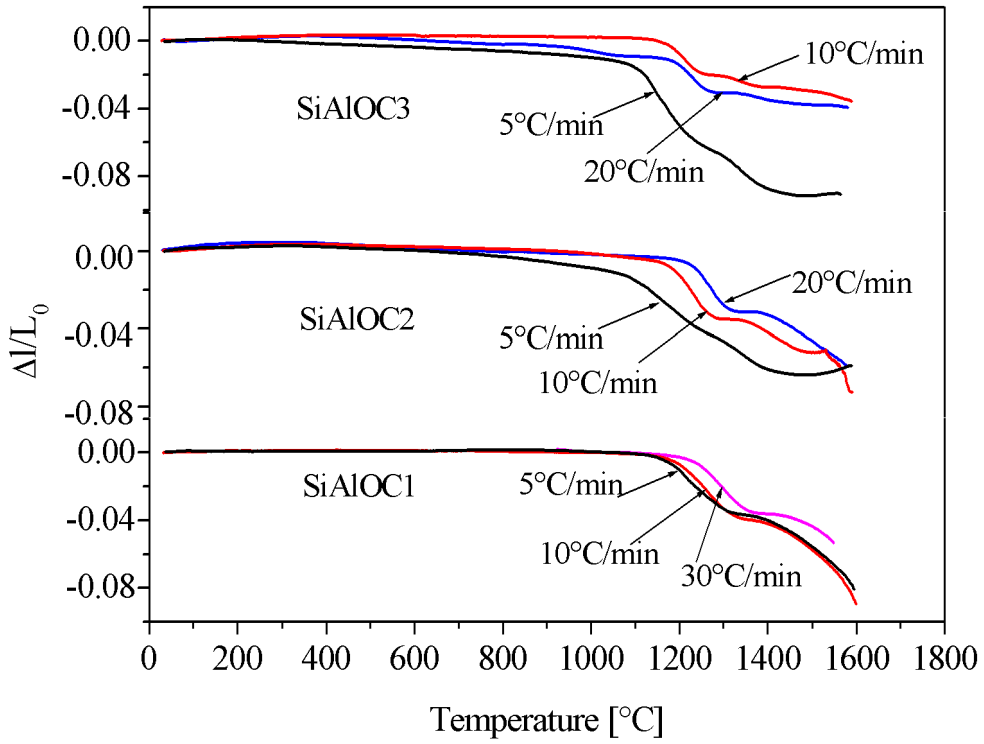

Figure 5.40: Thermal Dilatometry (TD) curves of as-pyrolyzed SiAlOC bulk ceramic at different heating rates.

rate with contraction. The nature of thermograms depends on the composition. For example, the low aluminum sample, namely, SiAlOC1 undergoes continuous contraction with temperature whereas increasing aluminum content, particularly the SiAlOC3 composition, halted the contraction between 1300°C and higher temperature.

The above phenomena i.e., initial contraction of sample between 1100−1300°C and resistance to this contraction at high temperatures changes the enthalpy of the system. This produces exothermic or endothermic peaks in the derivative curves and this change in energy is associated with the reaction/phenomena occurring in this temperature regime. Here, the phenomenons are softening in the first temperature regime and crystallization in the second. The deviations observed in the (TDD) curves with heating rate holds information about the above two phenomenons.

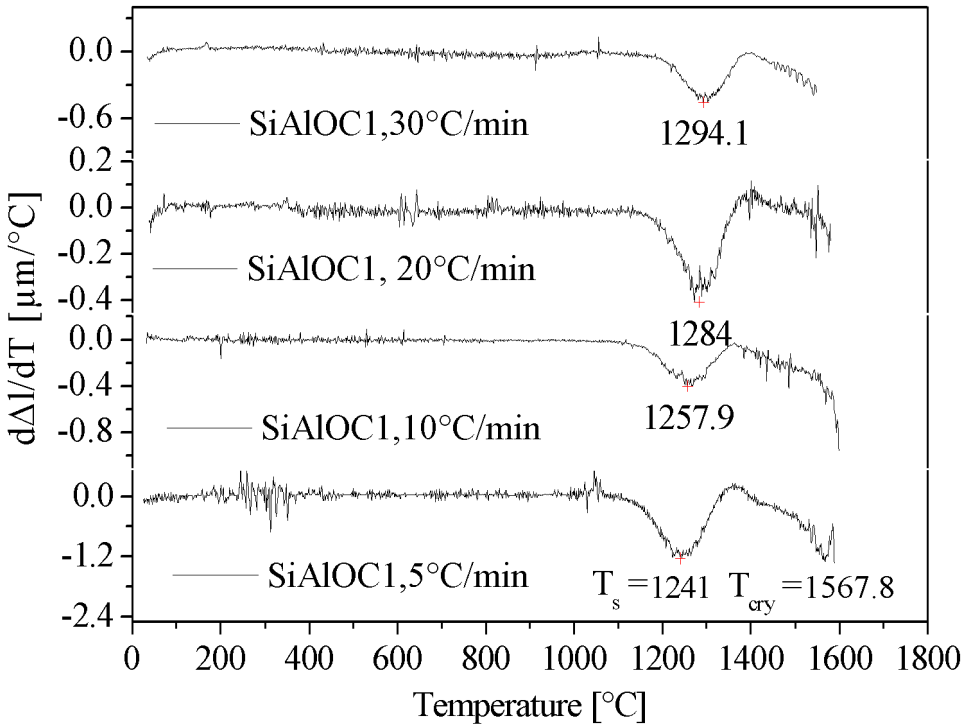

Figure 5.41: Thermal Dilatometry Derivative (TDD) curves of as-pyrolyzed SiAlOC bulk ceramic at different heating rates for SiAlOC1 composition.

It is found that with increase in heating rate the peak transformation temperature is shifted to higher values. This effect is shown in Fig. 5.41 and Fig. 5.42. Here in Fig. 5.41, the SiAlOC1 ceramic indicates only one peak in the softening regime whereas high aluminum containing material namely SiAlOC3 in Fig. 5.42 indicates two peaks in the derivative curve. As discussed in the crystallization behavior section (also refer Fig. 5.37) that, between the pyrolysis temperature and 1300°C the SiAlOC ceramics remain amorphous and could also lead to structural relaxation or softening. Also at higher temperature $\geq$1300°C formation of crystalline phases like mullite and SiC are indicated. Therefore from Fig. 5.41, the first peaks in the derivative curves can thus be assigned to the structural relaxation/softening (T_s), and the second causing resistance to deformation to crystallization of mullite and/or SiC, (T_{cry}). Below the effect of aluminum content on the relaxation kinetics of the material is discussed.

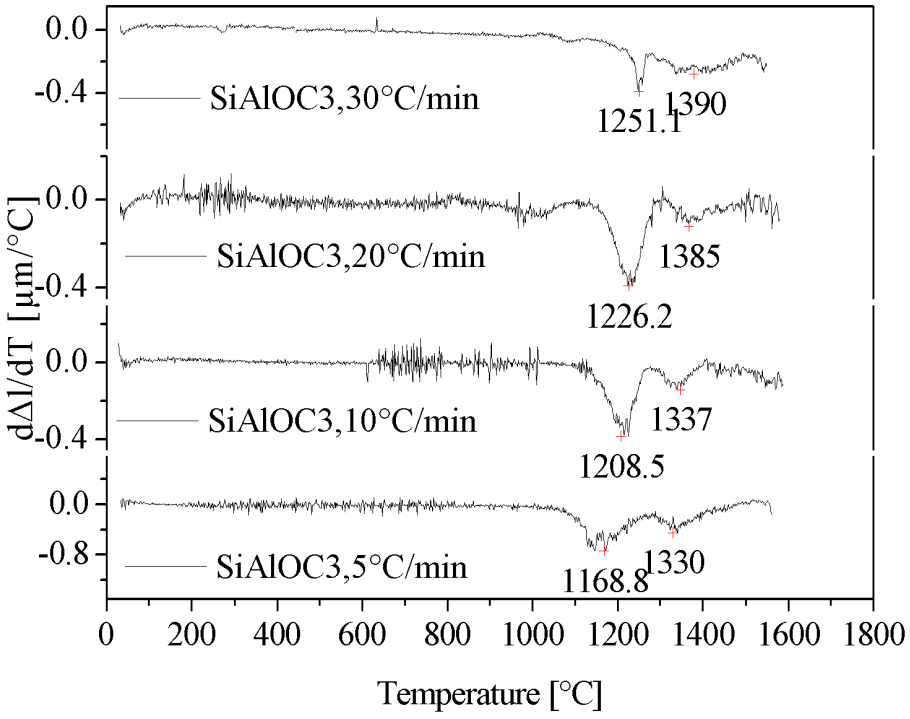

Figure 5.42: Thermal Dilatometry Derivative (TDD) curves of as-pyrolyzed SiAlOC bulk ceramic at different heating rates for SiAlOC3 composition.

The first maxima in Fig. 5.41 and Fig. 5.42 for SiAlOC ceramics changes with the heating rate as well as with the aluminum content. For example, the SiAlOC1 ceramic show maxima at 1241°C at 5°C/min, which increases to 1294.1°C with higher heating rate, i.e. 30°C/min. While the same peak temperatures is shifted to 1168.8°C at 5°C/min and 1251.1°C at 30°C/min for SiAlOC3 ceramics. This finding suggests that the SiAlOC1 ceramic which is aluminum lean as compared to the SiAlOC3 composition is more rigid and needs higher temperature for softening. The expansion or contraction of the silicate skeleton will be related to the ease with which the Si−O−Si(Al) deform. Substitution of aluminum; in tetrahedral and octahedral co-ordination, increases the bond lengths to a higher value. For example, the bond length of 1.74 and 1.91 Å for tetrahedral (Si, Al−O) and octahedral Al−O distance is reported.[127] In comparison the average bond length for Si−O bond is 1.61 Å. This increased Si−O−Si(Al) bond length due to

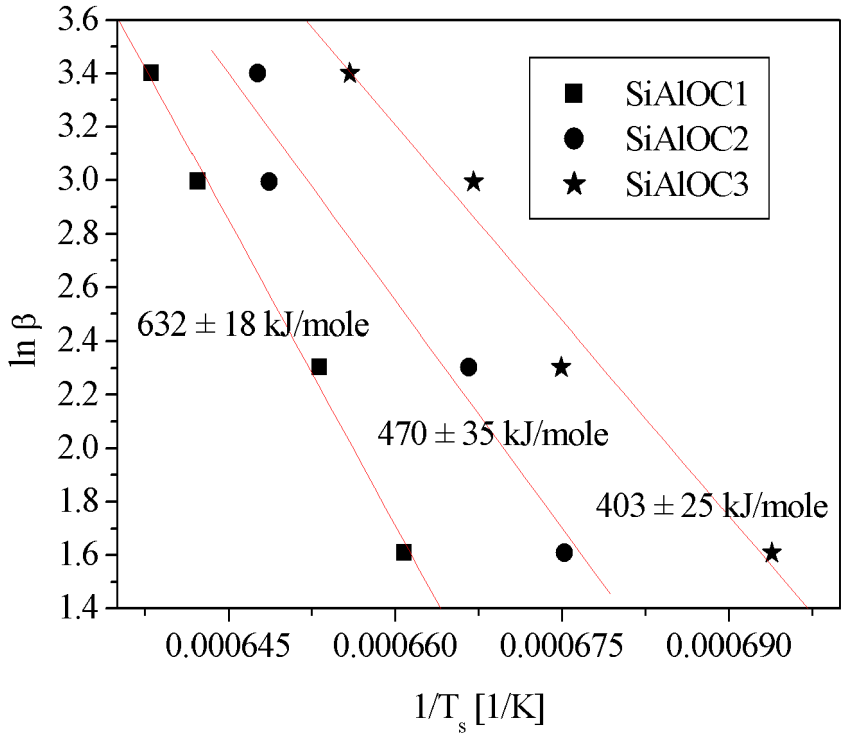

Figure 5.43: Plot of ln β vs $1/T_s$ with linear regression line for SiAlOC ceramics. The activation energies for softening are calculated from the slopes and using Moynihan theory discussed by Eq. (3.35) [from page 52].

aluminum addition shifts the softening of the glass to lower temperatures. The activation energy for the softening process is evaluated from Eq. (3.35) (refer to page 52) by plotting the heating rate against the reciprocal peak temperatures T_s. According to the above discussion the high aluminum material, namely the SiAlOC3 sample should show less activation energy for deformation. This is exactly observed in the present case and is shown in Fig. 5.43 and Table: 5.9. Thus, aluminum lean glasses could not soften or structurally relaxed easily and require higher energy compared to aluminum rich compositions.

Similar to the softening kinetics the peak temperature for crystallization at high temperature T_{cry} is dependent on the heating rate as well as the aluminum content. Increasing the heating rate shifts the peak temperature to higher temperatures. Thus as seen from Fig. 5.41 the crystallization peak is only observed

Material	Method for Kinetics Determination			
	Moynihan		Kissinger	
	Softening (E_s) [kJ/mole]	Crystallization (E_{cry}) [kJ/mole]	Crystallization (E_{cry}) [kJ/mole]	n[a]
SiAlOC1	632 ± 18	-	-	-
SiAlOC2	470 ± 35	-	-	-
SiAlOC3	403 ± 25	530 ± 60	503 ± 60	1.07

[a]average value given for all heating rate

Table 5.9: Calculated activation energies of various thermal processes (softening, crystallization) in SiAlOC ceramic bulks. The evolution of the data was performed according to Moynihan and Kissinger theory using Eqs. (3.35) and (3.36), (refer to page 52).

at 1567.8°C when heated at 5°C. The second peak for (T_{cry}) at higher heating rates is not visible for SiAlOC1 ceramic and needs higher temperature and could only be seen at temperature >1600°C. At these heating rate this peak temperature is out of the testing temperature limit. The limiting temperature for the thermal dilatometer instrument in the present case is 1600°C. Hence, the crystallization kinetics will be reported only for high aluminum composition SiAlOC3 ceramics.

Cassidy *et al.*[128] used dilatometry and density measurements on mullite gels prepared from different sol-gel routes to demonstrate the effect of composition on densification and phase development with temperature. The gels he investigated can be separated into two categories: *monophasic* and *diphasic* gels. Here, monophasic gels directly crystallizes to mullite whereas diphasic gels initially formed a mixture of γ-Al_2O_3 spinel and mullite, or simply γ-Al_2O_3 spinel, which subsequently transformed to mullite at high temperature. From the various phase developed mullite had an adverse effect on the densification and the differences are summarized below:

- Heating of materials produced from polymer-route, colloidal route and nitrate route results in the initial densification in the amorphous stage. However, heating them above 1200°C resulted in an additional densification at these temperatures, but the presence of the mullite phase ceases or reduces

the rate of densification.

- The presence of excess silica has a profound effect on densification at high temperature. The presence of silica promotes densification by viscous phase sintering.

Similar results are observed in the present research, i.e. densification at high temperature (>1000°C) and aluminum lean composition (SiAlOC1) have profound effect at still higher temperature by viscous phase sintering.

Li *et al.*[129] compared aforementioned results of mono phasic gel having stoichiometric composition with diphasic gels for the crystallization kinetics and the mechanism. They observed that the average crystallite particle size for mullite derived from monophasic gel is constant whereas with diphasic gels the crystallite particle size increased continuously with conversion. Many conclusive differences were drawn from this results. The rate of mullite formation from monophasic gels is apparently much faster than that in diphasic gels and is limited by nucleation mechanism. The observation of a constant particle size during mullite formation leads to a conclusion that single-crystal mullite is formed within each particle, and the ultimate mullite conversion is eventually limited by inter-particle diffusion phenomenon. Fitting the rate data to a constant nucleation rate Avrami-type model was not possible, but adequate fits were obtained using a model of two distinct nucleation rates. Deviation from linearity in the rate equation plots is observed. This deviation producing variable nucleation rates was argued to be originating from local inhomogeneities. From this, the activation energy of 293 ± 145 and 362 ± 145 for mullite crystallization with two different nucleation rates are reported. This activation energy is significantly lower than that measured for diphasic gels (800-1100 kJ/mole) indicating that the initial nucleation phenomenon of the latter is nearly completed prior to the first observation of mullite formation.

More recently, Takei *et al.*[130] tabulated quantified mullite kinetics data from past research with various raw materials, as listed in Table: 5.10. They also divided the various materials into two types: *monophasic* gel and *diphasic* gel. The tabulated values for monophasic gels[129] are about 300−500 [kJ/mole] while those from diphasic and hybrid gels are about 800−1300 [kJ/mole]. They also suggest that, there is no clear correlation between the mullitization temperature

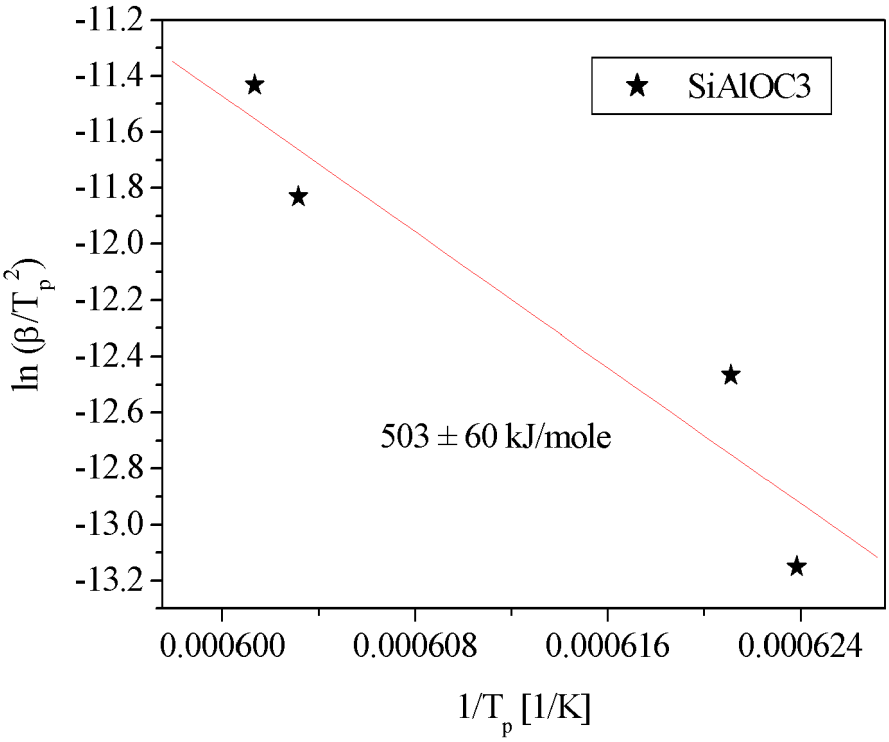

Figure 5.44: Plot of $\ln(\beta/T_p^2)$ vs $1/T_p$ with linear regression line for SiAlOC ceramics. Note that $T_p = T_{cry}$ as marked by second peak temperature in Fig. 5.41. The activation energies for crystallization are calculated from the slopes and using Kissinger theory discussed by Eq. (3.36) [from page 52].

regime and E_{cry} for mullite crystallization. SiAlOC ceramics clearly reveal the effect of aluminum modification on the deformation kinetics. The activation energy for crystallization of mullite calculated according to Kissinger theory from the slopes of Fig. 5.44 is 503 ±60 for SiAlOC3 composition and listed in Table: 5.9. The activation energy observed for crystallization is very low and well in the limit of monophasic gels. This result supports the crystallization investigation (refer to Fig. 5.37) that the amorphous ceramic directly forms mullite crystallization without intermediate γ-Al_2O_3 spinel phase. Moreever, these single phase SiAlOC ceramic materials produced via the sol-gel method, reducing the diffusion path length, consequently the process is not diffusion controlled which requires higher activation energy. Like monophasic gels, the crystallization of SiAlOC ce-

Starting Material	Composition (mol% Al_2O_3)	Activation Energy	Temp. (°C)	Expt. Condition
Diphasic gel[131]	60.0	1070±200	1200-1300	XRD
Hybrid gel[131]	61.4	984±71	1200-1275	XRD
Hybrid gel[132]	60.0	960±91	1200-1275	XRD
Diphasic gel[133]	33.3	1080±63	1300-1390	DTA
Diphasic gel[133]	60.0	1034±37	1300-1390	DTA
Single-phase[129]	66.6	293±145	940-1160	XRD
		362±145	940-1160	XRD
TEOS-coated Al_2O_3[126]	–	1042±32	–	–
Diphasic gel[134]	60.4	950±82	1200-1300	XRD
Kaolinite (KGA-1)[135]	33.3	523±34	1300-1400	–
Kaolinite (KGA-2)[135]	33.3	360±21	1300-1400	–
Diphasic gel[136]	60.0	880±30	1300-1400	DTA
Glass fiber[136]	36.1	1288±33	920-965	DTA
Glass fiber[137]	36.1	1195±31	1000-1200	XRD

Table 5.10: Reported activation energies for nucleation-growth of mullite from various starting materials.

ramic is supposed to occur by nucleation rate control. The low Avrami constant or shape factor n calculated from Eq. (3.37) (refer to page 53) supports that the crystallization dimensions are low.

Thus, a kinetic study reveals two processes occurring with temperature, namely softening or structural relaxation and crystallization. Deformation of the samples takes place during the structural relaxation phase which is hindered by fine mullite crystals originating at higher temperature. It has been reported[138] that densification proceeds through structural relaxation, a process by which excess free volume is removed allowing the structure to approach the configuration characteristic of the metastable liquid. Structural relaxation occurs irreversibly with no associated weight loss. The structural relaxation is confirmed by a rerun experiment on the same sample and the result is shown in Fig. 5.45. Here, after the first run up to high temperature the material is transformed to a glass-ceramic,

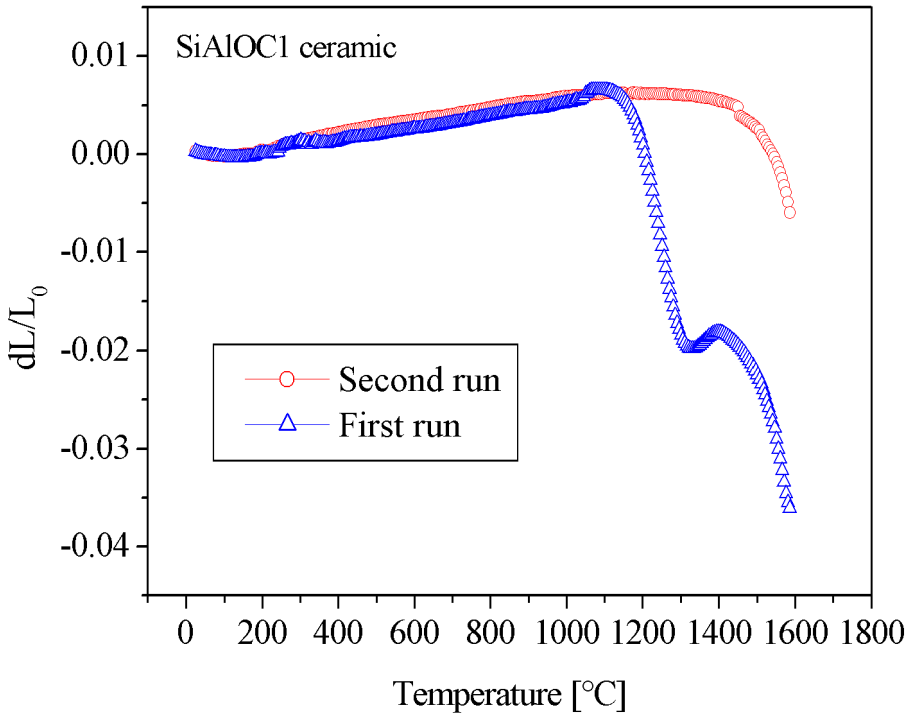

Figure 5.45: TD curves for SiAlOC1 ceramic for first and second heating at the heating rate of 10°C/min.

and therefore, the TD plot of such a material does not show the first large contraction due to softening and the associated weight loss in this regime is < 1 wt.%. At high temperature contraction again sets in because of the softening of the glass-ceramic matrix, which has changed composition due to crystallization during the first run.

In the later part of this study the effect of post heat-treatment on the oxidation resistance will be discussed. This is because if the samples are reheated in the softening regime at T < 1300°C the already transformed material shows no re-densification (dimensional change) in this temperature range. Therefore this treatment could change the properties of the material which may be reflected in the oxidation kinetics.

5.11 Creep in Bulk SiAlOC Ceramics

Substitution in traditional oxide glasses of some of the divalent oxygen atoms by different elements namely C and N results in the improvement of both mechanical properties and refractoriness.[139] The effect of addition of trivalent element like aluminum through sol-gel technique and polymer pyrolysis on high temperature deformation behavior is the focus of this section.

The experiments were performed at different temperatures (950, 1000, 1050, 1100, 1150 and 1250°C) and different stresses (25, 50, 75, 100 and 125 MPa) in order to cover the whole temperature-stress regime used to study the creep for glasses and ceramics. Creep and sintering or cavitation can occur at the same time during high-temperature deformation of ceramic materials. It is now recognized that the measured strain must be separated into densification or cavitation damage and true creep before analyzing the data further for shear viscosities and activation energies. True creep implies change in the shape of the specimen without any change in volume. On the other hand densification or cavitation changes the volume. This volume change will appear as time-dependent strain, and may be measured along with the creep strain.

The separation of creep and the densification or cavitation strain components are reported by different groups: Rahman, DeJonghe[140),(141)] and Raj.[142),(143)] The first two groups have attempted to measure shear and volume components of strain from the measurements of the axial strain, and the measurement of the change in density in the powder compacts obtained from series of interrupted tests. A comprehensive method developed by Raj *et al.*[143] will be used to separate the two components of the strain from measurements of the axial and the radial displacements in specimens of a cylindrical shape and his method is discussed below.

If a cylinder is compressed in axial direction, where σ_z is the axial applied stress, it generates strain in all the three directions. Thus, ε_z is the axial strain and ε_x and ε_y are the transverse strains in the other two direction of the Cartesian system. In the present condition ε_x and ε_y are same.

In the simple uniaxial test the loading axis and the two axes perpendicular to the loading axis will be the principal axes and hence $\varepsilon_z=\varepsilon_1$, $\varepsilon_x=\varepsilon_2$ and $\varepsilon_y=\varepsilon_3$ (since suffix (1,2,3) is used for principal stress or strains). For simplicity we

will use ε_z, ε_x, ε_y for the further discussion and derivation keeping in mind that they are the principal components. The three components of strain contain information about the volume change:

$$\varepsilon_a = \frac{\Delta V}{V} = -\frac{\Delta \rho}{\rho} = \varepsilon_z + \varepsilon_x + \varepsilon_y \tag{5.18}$$

where ε_a is the damage/densification strain which is equal to the fraction change in the volume $\Delta V/V$, or the fractional change in density $-\Delta\rho/\rho$.

The creep strain, that is the strain which occurs without any change in volume, can be written in terms of differentials between the principal components of the strain. Thus the creep strain, ε_e, is written as:

$$\varepsilon_e = \frac{2}{3}\sqrt{\frac{1}{2}\{(\varepsilon_z - \varepsilon_x)^2 + (\varepsilon_x - \varepsilon_y)^2 + (\varepsilon_y - \varepsilon_z)^2\}} \tag{5.19}$$

For uniaxial strain without any change in volume, $\varepsilon_x = \varepsilon_y = -\varepsilon_z/2$, and Eq. (5.19) reduces to $\varepsilon_e = \varepsilon_z$. In the case of uniaxial deformation Eq. (5.18) and Eq. (5.19) simplify considerably because there are only two independent components of strain: the axial component ε_z, and the transverse component ε_t. Making the substitutions in the previous equations the densification/cavitational strain and shear strain is obtained:

$$\varepsilon_a = -\frac{\Delta \rho}{\rho} = \varepsilon_z + 2\varepsilon_t \tag{5.20}$$

and

$$\varepsilon_e = \frac{2}{3}\left|\varepsilon_z - \varepsilon_t\right|$$

or (5.21)

$$\varepsilon_e = \frac{1}{3}\left|3\varepsilon_z + \tfrac{\Delta\rho}{\rho}\right|$$

Thus the creep strain ε_e, and the densification/cavitation strain ε_a, can be separated by measuring either ε_z and ε_t, or ε_z and $\Delta\rho/\rho$.

The sign conventions for the above parameters are as follow: ε_z and ε_t are negative if the specimen grows smaller. ε_a is negative if the volume of the specimen

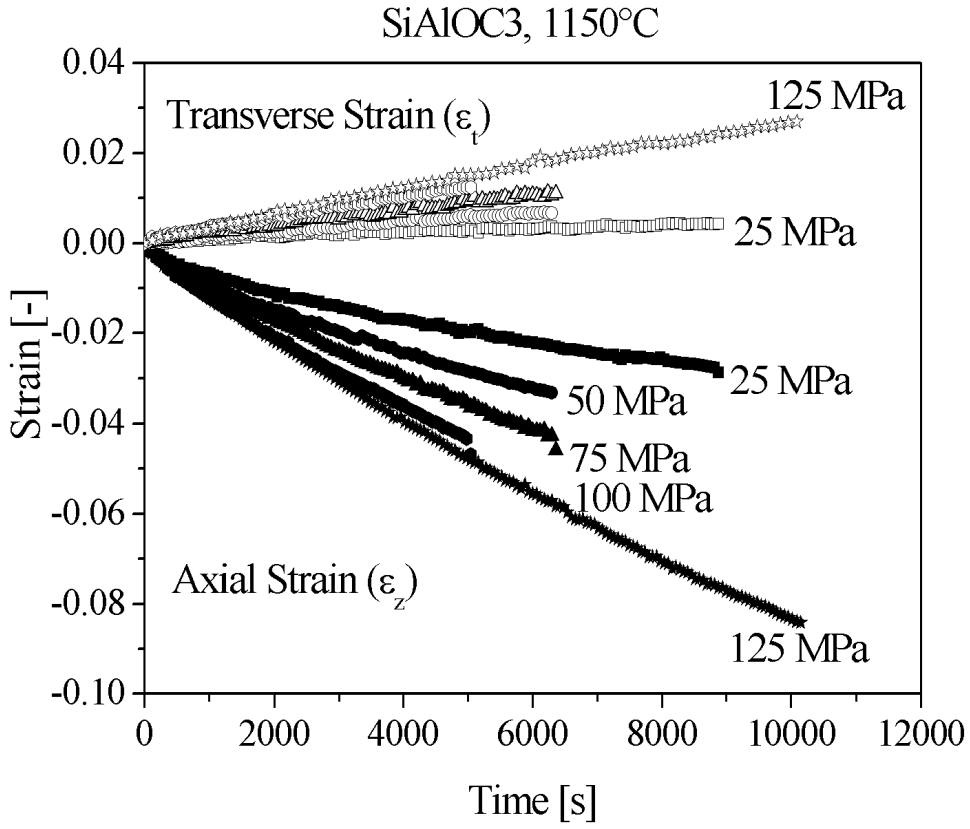

Figure 5.46: The axial and transverse strains, measured as a function of time at five different stress levels for SiAlOC3 bulk ceramic at 1150°C. The transverse strains were measured by two radial LVDT's.

decreases. Note that a negative value of ε_a leads to an increase in the density ρ, in Eq. (5.18). The shear strain ε_e does not have a sign since it represents a change in the shape, not a change in volume.

Measurement from the LVDTs provided data for the change in length and diameter of the specimen with time. These measurements were converted to strain by using the equation appropriate for large deformations. If the time-dependent length and the diameter of the specimen are given by $L(t)$ and $2R(t)$, then the equations for $\dot{\varepsilon}_z$ and $\dot{\varepsilon}_r$ may be written as:

$$\dot{\varepsilon}_z = \frac{d\ lnL}{dt} \tag{5.22}$$

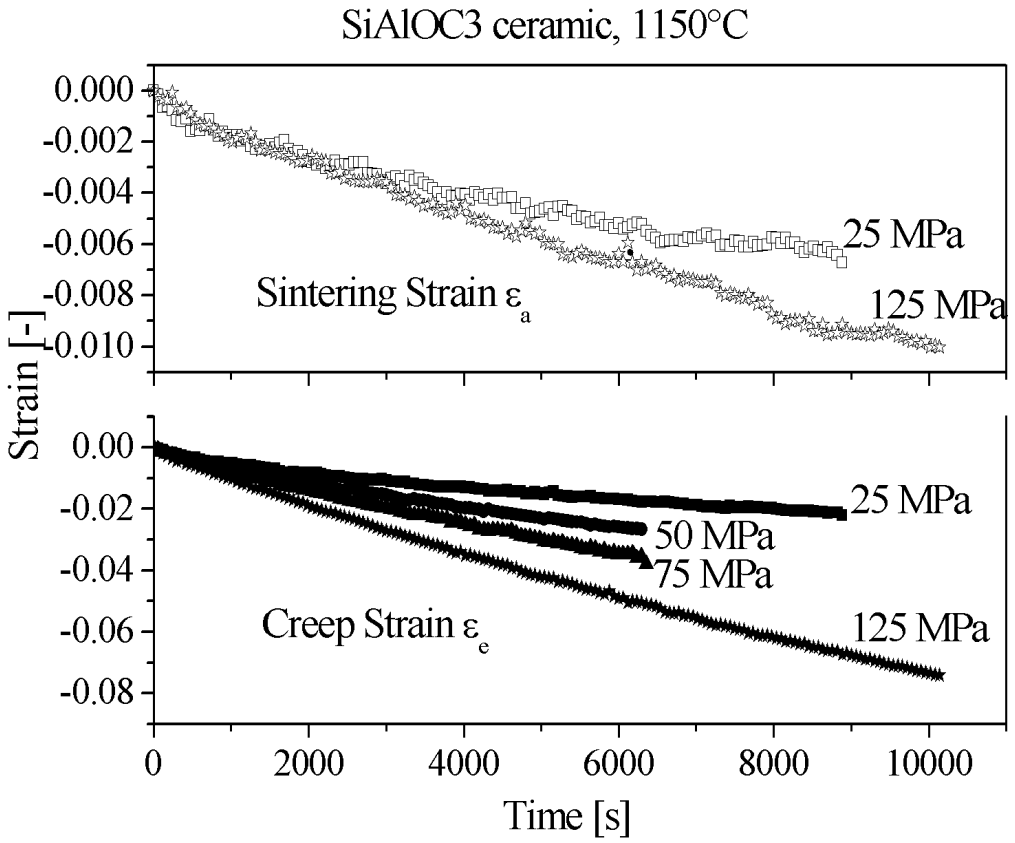

Figure 5.47: The sintering and creep strains, calculated as a function of time at five different stress levels for SiAlOC3 bulk ceramic at 1150°C. The transverse strains were measured by two radial LVDT's.

$$\dot{\varepsilon}_{\mathrm{r}} \quad = \quad \frac{d\ lnR}{dt} \tag{5.23}$$

In each experiment the applied axial load, P, was kept constant. Since the cross-sectional area of the specimen changed with time, the axial stress σ_{z} was also a function of time. The cross-sectional area of the specimen is given by $A = \pi R^2$. Integration of Eq. (5.23) leads to the result that $R = R_0 \exp(\varepsilon_{\mathrm{r}})$. Making this substitution in the equation for A gives the result that

$$A \quad = \quad A_0\ e^{2\varepsilon_{\mathrm{r}}} \tag{5.24}$$

where A_0, the initial cross-sectional area, is given by $A_0 = \pi R^2$.

Now using the equation that $\sigma_z = P/A$ and substituting from Eq. (5.24) we have the result that

$$\sigma_z = \frac{P}{A_0} e^{-2\varepsilon_r} \tag{5.25}$$

Looking at the deformation kinetics of SiAlOC ceramics, the time dependent measurements of the axial and transverse strains for SiAlOC3 ceramic (as an example) is given in Fig. 5.46. It can be seen that the axial strain is negative (compressive strain) and the transverse strain is positive (tensile strain). For creep deformation, when the volume is conserved, the transverse strain is half of the axial strain and in reverse direction. The transverse strain is in opposite direction but the magnitude of transverse strain is not exactly half that of axial strain i.e. ($\varepsilon_t/\varepsilon_a = 0.5$) and is $\approx$ 0.3-0.35. This result indicates that there must be a small change in volume which either leads to cavitation or densification. The substitution of strain data into Eqs. (5.20) and (5.21) separates densification and shear strains and are plotted in Fig. 5.47. Here ε_a is negative, indicating that the specimens are deforming by a sintering like process [from equation (5.20)] increasing the density but its overall effect is very small. In other words, it can be seen that almost all deformation of the specimen is due to creep strain and that the sintering strain is almost negligible. This separated creep strains can be used for further studies namely: calculation of steady state creep rate [SSCR] alternately used as strain rate $\dot{\varepsilon}$ (it is the slope of the linear part in strain-vs-time curve), stress exponent and the shear viscosity of the glass. To explain the viscosity and its temperature dependence it is worth at this moment to look into the insight of the concept of viscosity of silica and other silicate glasses, the mechanisms for viscous flow and factors affecting the viscosity and flow characteristics.

The shear viscosity η_s can be defined in terms of a engineering shear strain rate $\dot{\gamma}$ corresponding to the applied stress σ_s. For example, a cylindrical sample is compressed as it is done for this study by a stress σ_z, and it deforms at a rate $\dot{\gamma} = dL/dt$, where L is a length of the cylinder and t is the time, then

$$\eta_s = \frac{\sigma_s}{\dot{\gamma}} = \frac{1}{3}\left(\frac{\sigma_s}{\dot{\varepsilon}_e}\right) \tag{5.26}$$

where $\sigma_s = \sigma_z$, L_o is the initial length of the cylinder, and $\dot{\gamma}$ is the engineering

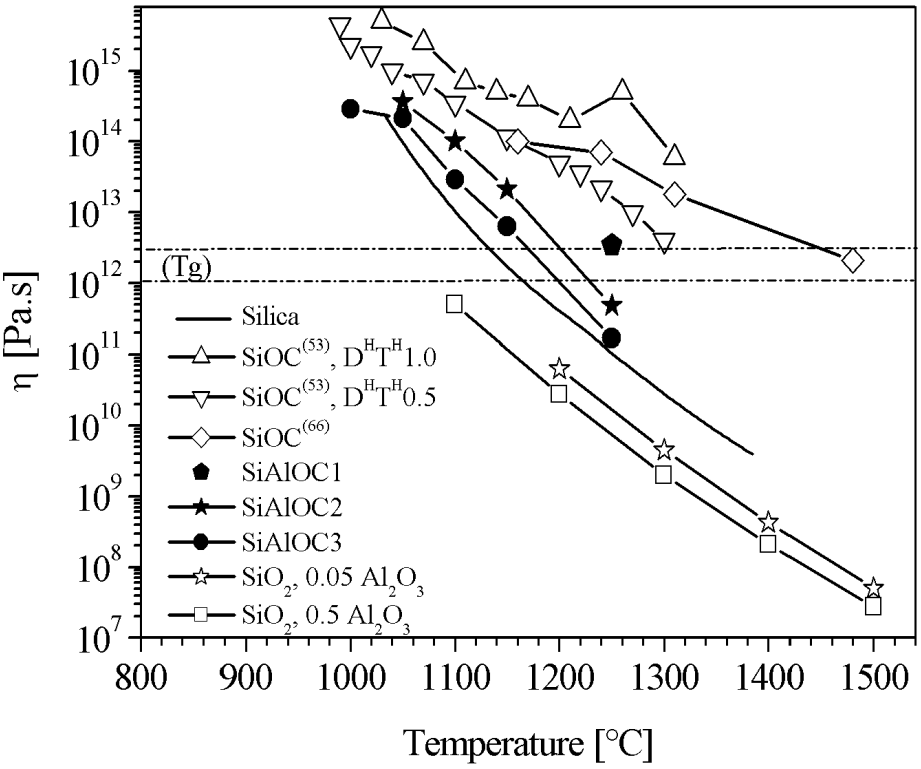

Figure 5.48: Temperature dependence of the viscosity η of SiAlOC glass. Data concerning vitreous silica, SiOC glasses from various authors are superimposed.

shear strain rate. Note that σ_z and σ_s are function of time. This strain rate in terms of the motion of a line defect is given by:

$$\dot{\varepsilon} = b\,\rho\,v \tag{5.27}$$

where b is distance of order of atomic dimensions, analogous to the Burgers vector of a dislocation, ρ is the density of line defects (the number of lines/unit area), and v is the velocity at which the line defects moves with the applied stress σ_z.

Then

$$\eta = \frac{\sigma_z}{b\rho v} \tag{5.28}$$

Upon application of stress the line defect rapidly accelerates to a steady-state velocity v. The velocity is a complicated function of the properties of the liquid, and can depend on the applied stress. The density ρ of line defects should be related to the volume density N of point defects that make up the line defect. An approximation is that ρ is proportional to N, or

$$\rho = fNa \tag{5.29}$$

where a is the distance between point defects along the line defect. It is probable that a is about the same as b in the above Eq. (5.27). The parameter f is the function of point defects that are incorporated into line defects. These line defects can nucleate by fluctuations in the bulk of the liquid or, more likely, with impurity particles in the liquid.

The following equation has enjoyed wide use for fitting the temperature dependence of viscosity data:

$$\eta = \eta_o exp\left\{\frac{B}{RT}\right\} \tag{5.30}$$

in which η_o, B, are temperature-independent constants, R is the gas constant and T the temperature. Doremus *et al.*[144] concluded that Eq. (5.30) does not fit accurate viscosity data at high and low temperatures, bringing into question theories that results in it. Eq. (5.30) may be useful for fitting experimental measurements over limited temperature ranges or that are rather scattered, but it cannot justify accurately theories of the temperature dependence of viscosities.

Many different ideas to explain the viscosity of glasses have been proposed. Douglas in his work on viscosity of silicate glasses assumed that the flow for silicate glasses was limited by breaking silicon−oxygen−silicon (Si−O−Si) bonds. He considered that the oxygen atom between two silicon atoms could occupy two different positions, separated by the energy barrier. The distribution of oxygen atoms between these two positions is then calculated from an entropy of mixing. Thus, Douglas anticipated the emphasis on configurational entropy and modified Eq. (5.30), which fits viscosities for wide range of liquids.

Mott suggested that the concentration of broken Si−O bonds in vitreous silica increases as the temperature increases, and provides easier flow. Mott showed

that motion of the broken bonds around an Si−O ring would lead to flow. Brawer has proposed a change in the coordination number of a glass constituent as the defect likely to result in flow. The distribution of coordination number is a function of temperature, pressure, and glass composition. The changes in the coordination number result in density fluctuation in the melt. Flow under the stress takes place by changing the distribution of low density region, although the total density is not changed. He claims that, the theory is in good quantitative agreement with structural relaxation in glasses. Additionally, Urbain[145] in his study on various silicate glasses indicated that the variation of viscosity with temperature for SiO_2 and $SiO_2-Al_2O_3$ is according to the Arrhenius relation. He reported that there is a substantial reduction in the viscosity in silica with addition of alumina. It has been assumed that a change in aluminum coordination from four to six fold, causes a decrease in viscosity as a result of an increase in the concentration of non-bridging oxygens in the melt.

More insights in the diffusion of silicon and oxygen in silicates of different melt compositions at different temperatures and pressures suggest that, the diffusion coefficients of oxygen and silicon were the same. The simplest explanation proposed for this result is that the silicon and oxygen atoms diffuse in the same molecules. The simplest molecule containing these two atoms is silicon monoxide, SiO. Silicon monoxide is the gaseous molecule that results from the vaporization of silica. The vaporization can be written:

$$SiO_2(l) = SiO(g) + 1/2O_2(g) \tag{5.31}$$

Doremus suggests that the diffusion of silicon and oxygen melts takes place by transport of SiO molecules formed in the melt. In this case Eq. (5.31) is modified to

$$SiO_2(l) = SiO(d) + O(d) \tag{5.32}$$

in which d is dissolved in melt.

The extra oxygen atom leads to five coordination of oxygen atoms around silicon. Breaking out a SiO molecule from the silica network leaves behind three oxygen ions and one silicon ion with unpaired electron. One of these oxygen ions can bond to the silicon ion. The two other dangling bonds result in two silicon

ions being five coordinated to oxygen ions. One of the five oxygen ions around the central silicon ion has an unpaired electron, and is not bonded strongly to the silicon ion. This electron "hole" should move between the other oxygen ions.

It is proposed that viscous flow in silica occurs by the transport of defects in the silica melts (silicon monoxide molecules). Mott and Brewer treated viscous flow in terms of the motions of point defects. However, flow from point defects, although possible, is much less efficient than flow resulting from the motion of line defects. In crystals it is well established that the plastic flow takes place by motion of line defects, called dislocations. Dislocations of this kind in glasses were proposed by Gilman.[146] Liquid defects can align themselves to form a line defect (not necessarily a straight line) and motion of this line defects leads to viscous flow. Line defects in liquids are of course not the same as dislocations in crystals. In silica the defects involved in flow are silicon monoxide molecules. In a sense these molecules result from broken silicon−oxygen bonds, as shown by Eq. (5.32). So the SiO molecules are five-coordinated silicon atoms involved in viscous flow derived from broken bonds.

The individual silicon monoxide molecules dissolve in interstices or silicon−oxygen "cages" in the silica structure, presumably with a five-coordinated silicon nearby. These structures reduce the silicon−oxygen bond strengths in their vicinity. To form a line they must have some sort of attractive interaction. This line can then move through the silica structure under stress because of the lower silicon−oxygen bond strength in its vicinity. Studies of the viscosity of other silicate melts report that the activation energy for flow is decreased by the lowered silicon−oxygen bond strengths near defects such as non bridging oxygen atoms and other ions in the structure, not by the broken silicon−oxygen bonds themselves.

The concentration of silicon monoxide formed in silica can be calculated in principle from Eq. (5.32). An equilibrium coefficient K can be defined for this equation:

$$K = \frac{[SiO][O]}{[SiO_2]} \tag{5.33}$$

The brackets represents thermodynamic activities, or concentrations if the system behaves ideally. Stebbins *et al.* suggested that the concentration of SiO can be estimated from measurements of the concentration of five-coordinated silicons.

Accordingly, for $K_2O.4SiO_2$ glass he reported the fraction of five-coordinated silicon at ambient temperature and pressure to be about 10% after rapid cooling and 6% after slow cooling from 1300°C.

The heat of reaction of Eq. (5.31) is 722 kJ/mole; that of Eq. (5.32) should be smaller, because the oxygen atom is bound in the melt. The temperature dependence of the concentration N_1 of SiO molecule dissolved in the silica should be given by an equation of the form:

$$N_1 = C_1 \quad exp\Big\{\frac{-H_1}{RT}\Big\} \tag{5.34}$$

where C_1 is a constant and H_1 is the heat of reaction to form the dissolved SiO molecules.

The diffusion coefficient D can be written:

$$D = D_0 \quad exp\Big\{\frac{-Q}{RT}\Big\} \tag{5.35}$$

Where D_0 and Q are constants independent of temperature. If diffusion results from motion of a defect, then the preexponent factor (D_0) should include the defect concentration, in the case of silicates, the concentration N_1 of SiO molecules. Then the activation energy Q is the sum of the enthalpy to form the SiO molecules (H_1) and the enthalpy of motion (H_m) of the defects. This shows that, there is a close relationship between viscosity and diffusion of silicon and oxygen in silica. These two transport properties are linked by the defects (SiO molecules) that control both. Nevertheless the detailed mechanism for the viscosity and diffusion are quite different. The viscosity is controlled by the motion of lines of SiO molecules, whereas the diffusion results from the motion of individual SiO molecules through the silica network.

At temperatures above 1400°C the fraction f, if SiO molecules form line defects, is not a function of temperature. However, below this temperature the viscous flow has a higher activation energy for silica than above this temperature. Nevertheless, the activation energy of diffusion of silicon in silica is the same above and below 1400°C. Thus the concentration of SiO molecules is still governed by Eq. (5.34) at all temperatures. The change in activation energy as explained by Doremus result from time and temperature dependencies of the

factor f in Eq. (5.29). Thus below 1400°C the fraction of SiO molecules in the line defects decreases as the temperature decreases, increasing the equilibrium viscosity from the values observed at higher temperature. This decrease of f depends on time, that is, the breakup of line defects is not instantaneous, but becomes slower as the temperature decreases. The reduction in the fraction f at a particular temperature leads to a smaller density ρ of line defects and thus to a higher viscosity.

We now come back to the viscosity and its temperature dependence for SiAlOC ceramics and its comparison with SiOC ceramic and silica glass. Shear viscosity curves are plotted in Fig. 5.48. This figure is superimposed with the data on vitreous silica, alumina containing silica and recent data on SiOC ceramics from various authors. It is seen that, for all tested temperatures the viscosities of all SiAlOC compositions are lower than that for SiOC ceramics (from literature) and higher than the silica glass with or without alumina. Additionally, if the SiAlOC ceramic viscosity values are compared among themselves, the viscosity values are lower for higher aluminum composition at all temperatures.

The higher viscosity observed as compared to the silica glass needs to be explained. As mentioned in the chemical analysis of Si(Al)OC ceramics, part of the silicon is covalently bonded to carbon atoms and the remaining silicon shares bonds with oxygen. It is also demonstrated that the amount of Si−C bonds decreases with the addition of aluminum. Introduction of carbon that is covalently bonded to silicon provides a significant increase in the viscosity η. Most viscosity data that have been reported so far on glasses that contain 10−20 at.% carbon are consistent with a ∼2-order-of-magnitude shift to higher values in comparison with vitreous silica. Such a high difference in viscosity is only observed in case of SiAlOC1 even at 1250°C and the difference reduces for SiAlOC2 and SiAlOC3 ceramic.

The reduction in the viscosity difference has different origins. The first origin lies in the presence of few Si−C bonds and the second in the amount of impurities (aluminum in the present case) and its coordinaiton. This is exactly seen for the SiAlOC2 and SiAlOC3 compositions, which show reduction in the Si−C bonds and corresponding increase in the impurity aluminum. Contradictory results to the assumption mentioned earlier is observed concerning the coordination number. It is seen that for SiAlOC1 and SiAlOC2 compositions the aluminum has

octahedral coordination and posses higher viscosity. Thus, the assumption that change in aluminum coordination from tetra to octahedral reduces the viscosity may not be correct. Moreover, the SiAlOC3 composition posses pentahedral and octahedral coordination with higher contribution from pentahedral. This may deform the sample easily and reduce the viscosity at high temperature. A glass transition temperature of these glasses can be estimated as the temperature where the viscosity reaches the value of $10^{12}-10^{12.6}$ [Pa.s] range, and this regime is marked as a bar along with a dotted line in Fig. 5.48. Accordingly, a glass transition temperature of 1220, 1250 and >1300°C (measured at 10^{12} Pa.s) is observed for SiAlOC3, SiAlOC2 and SiAlOC1 ceramics, respectively. The value for SiAlOC1 is estimated by extrapolation of the data above 1250°C.

The apparent activation energy for flow between 1000−1150 °C is estimated by plotting $\ln(\eta)$ against reciprocal temperature and found to be about 375 ± 20 kJ/mole 445 ± 20 for SiAlOC3 and SiAlCO2 ceramic, respectively. This indeed is lower than that of vitreous silica having value of 700 kJ/mole in the same temperature range. In comparison the reported activation energy for SiOC ceramic (296 kJ/mole).[80),(139)] Additionally, the activation energy for viscous flow values for SiAlOC ceramics are of the same magnitude as E_s mentioned in Table: 5.9 during softening kinetics study. It is a reasonable assumption that the molecular motions involved in structural relaxation are of the same type as those involved in viscous flow. Studies[147),(148)] for the structural relaxation in the glass transition region has shown that the activation energy for relaxation is of the same order as for shear viscosity. Unfortunately, we could only measure the creep data (shear viscosity) for SiAlOC2 and SiAlOC3 ceramics completely (i.e. for all predefined stresses and temperature) but could not complete it for SiAlOC1 ceramic. But assuming the above equivalence between the activation energies for softening and viscous flow to be true, the activation energy for flow could be assumed to be about 632 kJ/mole for the SiAlOC1 ceramic. This discussion rises the following questions: Why is the activation energy for SiAlOC1 ceramic smaller as compared to pure silica and higher than reported for SiOC ceramics? This is explained as follows.

As proposed the viscous flow in silica occurs by the transport of defects in the silica melt (silicon monoxide molecules) formed according to Eq. (5.32). The individual silicon monoxide molecules dissolve in interstices or silicon−oxygen "cages"

in the silica structure, presumably with the five-coordinated silicon nearby. These structures reduces the silicon−oxygen bond strengths in their vicinity. These defects form a line like dislocation form in crystals which move through the silica structure under stress because of the low silicon−oxygen bond strength in its vicinity. In the SiAlOC1 ceramic the regions where aluminum atoms are present either in tetrahedral coordination as Si−O−Al or octahedral coordination as Al−O−Al can act as origins for line defects and can reduce the bond strength in its vicinity. This argument supports the reduction in activation energy for flow mainly by the lowered silicon-oxygen bond strength. The activation energy is further reduced and lowest for higher aluminum content, which can be because of the excess pentahedral coordination which additionally act as defects and facilitates flow.

In case of the SiOC ceramic it has been reported that the activation energy for flow increases above 1200°C and approaches to that for pure silica. This was argued due to the crystallization of extremely small SiC nanocrystals at these temperatures and in large volume which decreases the carbon content in the residual glass. In other words crystallization increases the SiO_2 equivalence of the matrix. The SiO_2 equivalence for the mentioned SiOC ceramics is between 1.25 to 1.33 as compared to 1.57 for SiAlOC1 ceramic. In other words the silica equivalence is higher for the SiAlOC1 composition and this is reflected in the higher activation energy. Thus, the higher SiC and SiO_2 equivalence induce a dynamic increase in the viscosity and higher activation energy for the SiAlOC1 composition. Indeed, other aluminum modified compositions should also have similar Si−O equivalences which should show higher activation energy. The lower values observed for SiAlOC2 and SiAlOC3 compositions as compared to SiAlOC1 indicate that the amount of impurity atoms with different coordination sites has a pronounced effect on the flow of defects yielding a low activation energy.

5.12 Oxidation Behavior

This section will concentrate on the effect of oxidizing atmosphere i.e. air on the synthesized bulk Si(Al)OC ceramics at high temperature. The quantitative anal-

ysis of the oxidation reaction kinetic, effect of aluminum on the reaction kinetics and the activation energies of oxidation is investigated. Following discussion is based on two types of bulk samples; one which has been pyrolyzed at 1100°C and one after relaxation or softening by heat treatment at 1300°C. The differences in the oxidation kinetics is co-related with chemical depth profile measurements by SIMS and the oxide morphology by SEM.

5.12.1 Oxidation of As-Pyrolyzed Bulk Si(Al)OC Ceramics

5.12.1.1 As-Pyrolyzed SiOC Bulks

As mentioned earlier, the synthesized SiOC ceramic bulks are extremely dense in as-pyrolyzed condition (refer to Fig. 5.16(b). These thin polished samples are oxidized at different temperatures namely 1200, 1300, 1400°C and the corresponding mass change is noted. Mass loss is observed during oxidation of SiOC ceramics for all tested times and temperatures. Here, it is assumed that the mass change obeys a parabolic law. The square of mass loss per unit geometric area is calculated and plotted against isothermal time. The plot of $(\Delta W/ A)^2$ [mg^2/cm^4] against isothermal oxidation time t [h] is shown in Fig. 5.49. The parabolic law of type $(\Delta W/A)^2 = K_p(T) \cdot t$, with ΔW being the mass change, A the sample surface area, t the oxidation time, and $K_p(T)$ the parabolic rate constant at tested temperature is used in many oxidation studies. The linear relationship between $(\Delta W/A)^2$ vs. t in Fig. 5.49 confirms the parabolic nature of oxidation and the slope of which gives the parabolic rate constant. Fig. 5.50 is an Arrhenius plot of $ln(K_p)$ vs. $1/T$ for the parabolic oxidation regime. From the slope of this figure the activation energy of 190 ±5 [kJ/mole] is found to be associated with the SiOC oxidation. The parabolic rate constant and the activation energy are listed in Table: 5.11. The found activation energy is higher than that reported for silicon, silicon carbide[82),(84)], and nitride bonded SiC ceramics[149)]. Also the activation energy of 190 [kJ/mole] is higher than for oxygen diffusion in silica, which is 112 [kJ/mole].

If the oxidation is believed to be occurring by Eqs. (3.42) and (3.43) (refer to page 62), where oxygen is diffusing inside, the carbonaceous reaction product $CO_{(g)}$ or in some cases $CO_{2(g)}$ is removed through the silica scale. In order to investigate the chemical profile of the bulk after oxidation SIMS was performed on

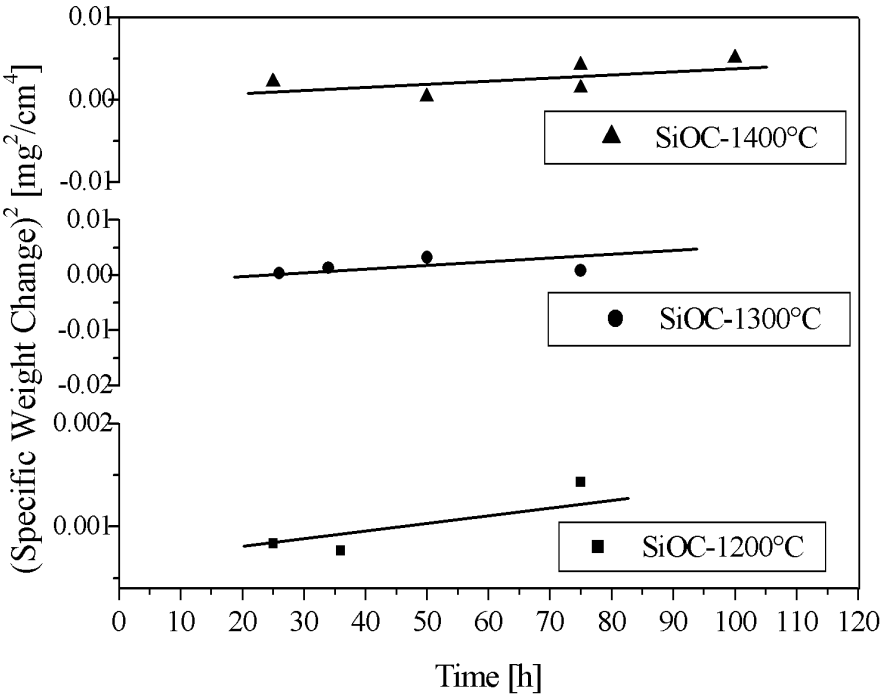

Figure 5.49: Oxidation weight change of SiOC bulk ceramic at various temperatures for long isothermal times.

Property	**Temperature (°C)**		
	1200	*1300*	*1400*
K_p(mg^2/cm^{4}h)	7.476 x 10^{-6}	2.187 x 10^{-5}	4.801 x 10^{-5}
E_{oxid} [kJ/mol]	190 ± 5		

Table 5.11: Parabolic rate constants at different temperatures, oxidation activation energy for oxidation of bulk SiOC bulk ceramics.

the samples after oxidation. A SIMS profile of the SiOC ceramic after oxidation at 1300°C for 26 h is shown in Fig. 5.51. This profile can be correlated with the cross-sectional view of the sample. Such a microstructure is shown in Fig. 5.52. The cross-section indicates that the oxide layer is about 0.5−0.6 µm thick after 26 h isothermal holding. The oxide depths on Si-C, Si-Ti-O-C (extremely low titanium content) reported by Chollon at 1300°C is 0.8 µm after 15 h holding time and 0.7 µm after 10 h, respectively. The oxide depths for the Si-C-(O)

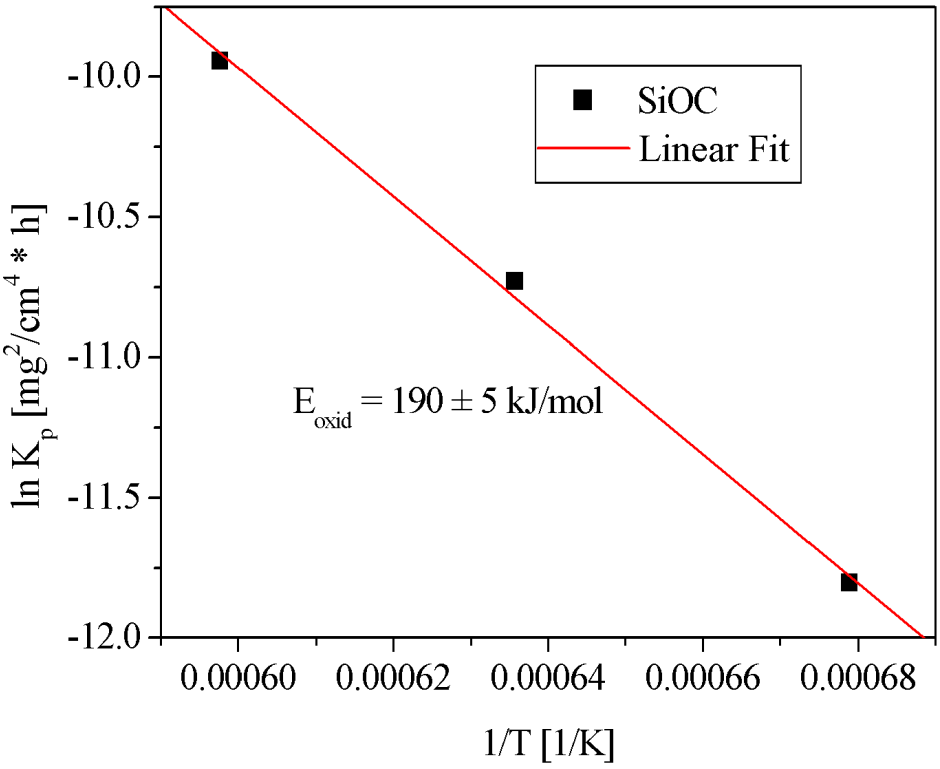

Figure 5.50: Temperature dependence of parabolic rate constant for oxidation of SiOC bulk ceramic.

system is not reported for 1300°C by the author but mentioned for 1400°C to be 0.65 µm after 7 h holding. This result indicates that the depths for the present investigated SiOC ceramic is lower in magnitude inspite of longer holding time. The intensities of various elements are normalized to the silicon intensity assuming no silicon diffusing inside or outside. The oxide layer is assigned up to the depth where the oxygen levels remain constant. The carbon level in this regime reaches its minimum. A gradient in intensity with increasing value of carbon towards the surface is observed in the SIMS profile in the oxide layer. Such a gradient in carbon profile could be due to retention of carbonaceous products in the viscous oxide.

The interface regime is indicated where the oxygen level deviates from remain-

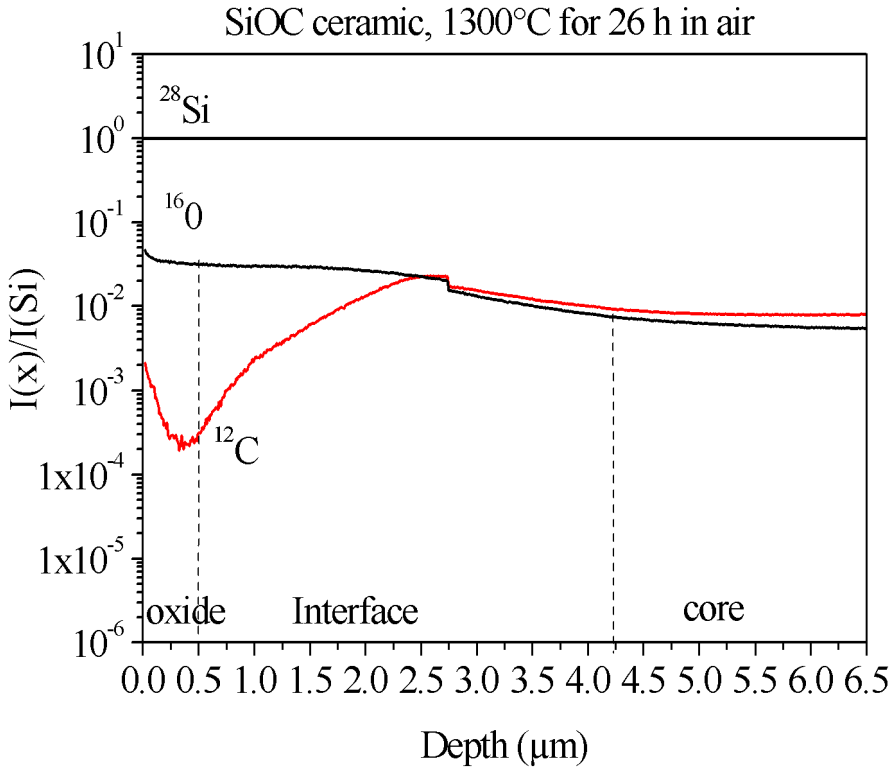

Figure 5.51: SIMS depth profile of SiOC bulk ceramic after oxidation in air at 1300°C for 26 h.

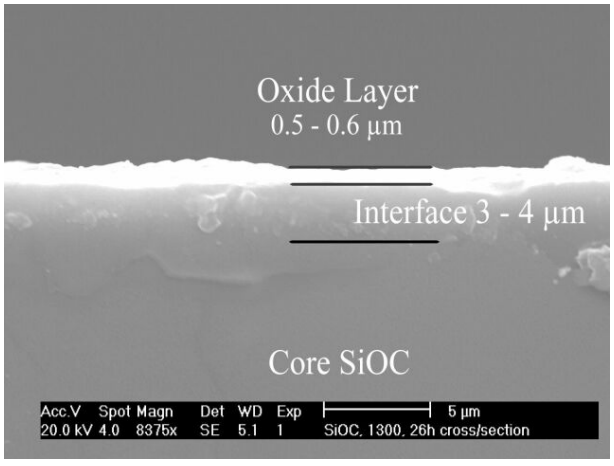

Figure 5.52: Cross-sectional view of SiOC bulk ceramic after oxidation in air at 1300°C for 26 h.

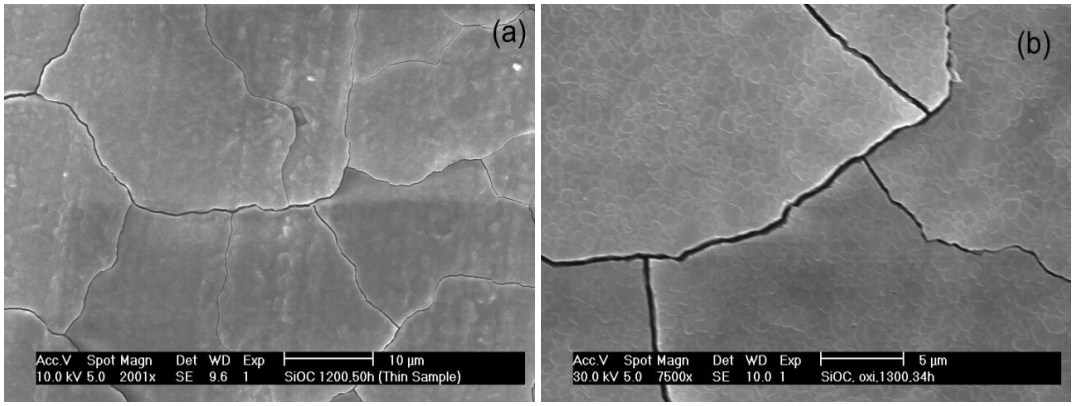

Figure 5.53: Silica scale formed after oxidation of SiOC bulk ceramic: (a) 1200°C with 50 h holding time and (b) 1300°C with 26 h holding time (etched sample).

ing constant until it again attains constant intensity in the core region. The interface is around 4 µm with a positive carbon gradient away from the oxide layer towards the core. The higher activation energy and the observed depth profiles for SiOC ceramic thus confirms that oxidation is controlled by mixed mechanism i.e. the inward diffusion of oxygen and outward diffusion of gaseous CO through the oxide layer.

The oxidation resistance is controlled by the vitreous silica and by the crystallization of the oxide layer to cristobalite having a lower diffusivity for the molecular oxygen than vitreous silica. The evidence of crystallization is investigated by X-ray diffraction and through SEM on an etched surface. Along with the advantage by reducing the diffusion rate crystallization of cristobalite in higher volume fraction further has negative influence on the appearance and stability of the oxide layer and is discussed below. Scanning electron microscopy of the sample oxidized at 1200°C for 50 h is shown in Fig. 5.53(a). The oxide surface morphology on the SiOC ceramic reveals excessive cracking at all temperatures. This surface morphology is the same as observed by Fergus *et al.*[93] in the comparative oxidation study of CVD β-SiC with sintered α-SiC. The authors concluded that material containing excess carbon as inclusions, e.g. CVD β-SiC, does not show any bubbling in the passive oxidation temperature regime. Absence of bubbles also clearly confirms that the decomposition products are removed rapidly from the oxide layer. The presence of bubbles are reported for sintered α-SiC and on sintered SiC (α and β), but not in the scale formed at

1300°C and 1400°C on single crystal SiC.[150] They attributed the bubbling to the oxidation of observed carbon inclusions in the sintered materials. The scanning electron micrograph presented in this SiOC research along with that by Fergus contradict the explanation that carbon is only responsible for the bubbling. However other inclusions namely boron and aluminum have to be considered to be responsible for bubble formation. The effect of boron is discussed by Fergus, and the same can be seen for high temperature oxidation study for aluminum rich ceramic SiAlOC composition, which will be explained below.

Cracking is believed to be generated during fast cooling of the ceramics. This is because of the thermal coefficient mismatch between the surface oxide and the core material. Additionally, cracking of these oxides can be attributed to the presence of cristobalite embedded in the amorphous glass matrix, which undergoes β to α transformation during cooling, accompanied by a 3−4% volume change. Fig. 5.53(b) shows the surface morphology of the oxidized sample after etching with cracks in the near vicinity of cristobalite and glass boundary.

5.12.1.2 Oxidation of As-Pyrolyzed SiAlOC Bulks

The focus of the present work is mainly on the study of the oxidation kinetics of the aluminum modified silicon oxycarbide glass. In order to confirm if the oxidation is having linear, parabolic or exponential dependence with time, thermo-gravimetry was performed on SiAlOC ceramic bars. SiAlOC ceramics when held in air at the oxidizing temperature indicate mass gain with time. A sample curve of SiAlOC1 ceramic at 1400°C is shown in Fig. 5.54(a). It is obvious from this figure that the data follow parabolic behavior. Hence, the data is replotted in Fig. 5.54(b) with the square of weight gain as a function of time. If the behavior is parabolic then the plot should be a straight line, which is exactly found in this case. The data is fitted to a linear function in order to calculate the rate constants. Slope of the straight line gives the parabolic rate constant value K_p, which for this particular case is 6.1 x 10^{-2} [mg^2/cm^4h]. This value is one order of magnitude higher than reported for CVD SiC (1.3 x 10^{-3} [mg^2/cm^4h]) analyzed in dry oxygen at 1400°C.[92] Thermal gravimetry has a limitation for sample size as only small samples could be tested. Hence direct oxidation of thick cylindrical samples are tested by inserting the samples in pre-heated furnace and

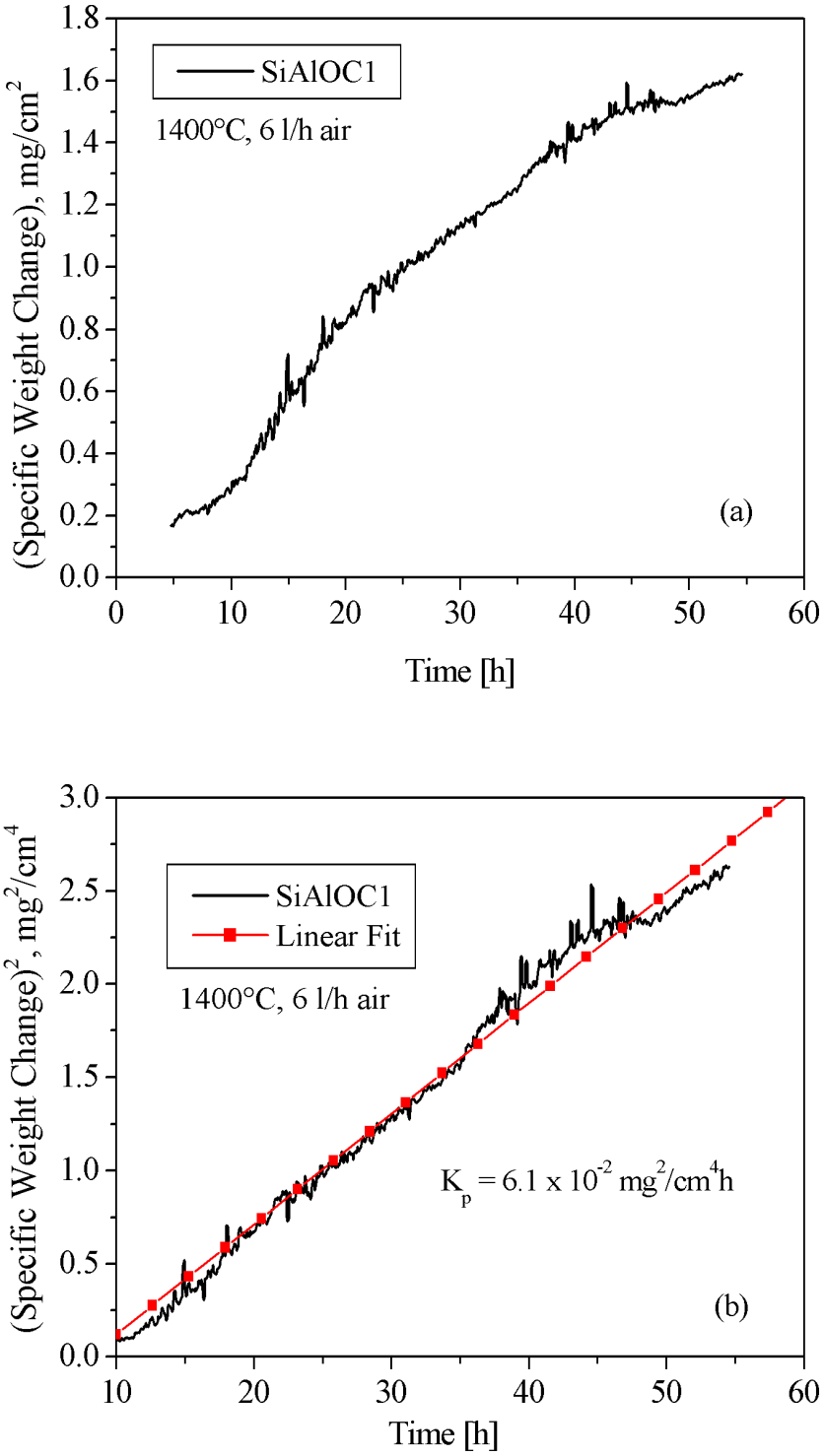

Figure 5.54: Thermo-gravimetric investigation of SiAlOC bulk ceramic in air at 1400°C: (a) weight gain versus time and (b) (weight gain)^2 versus time.

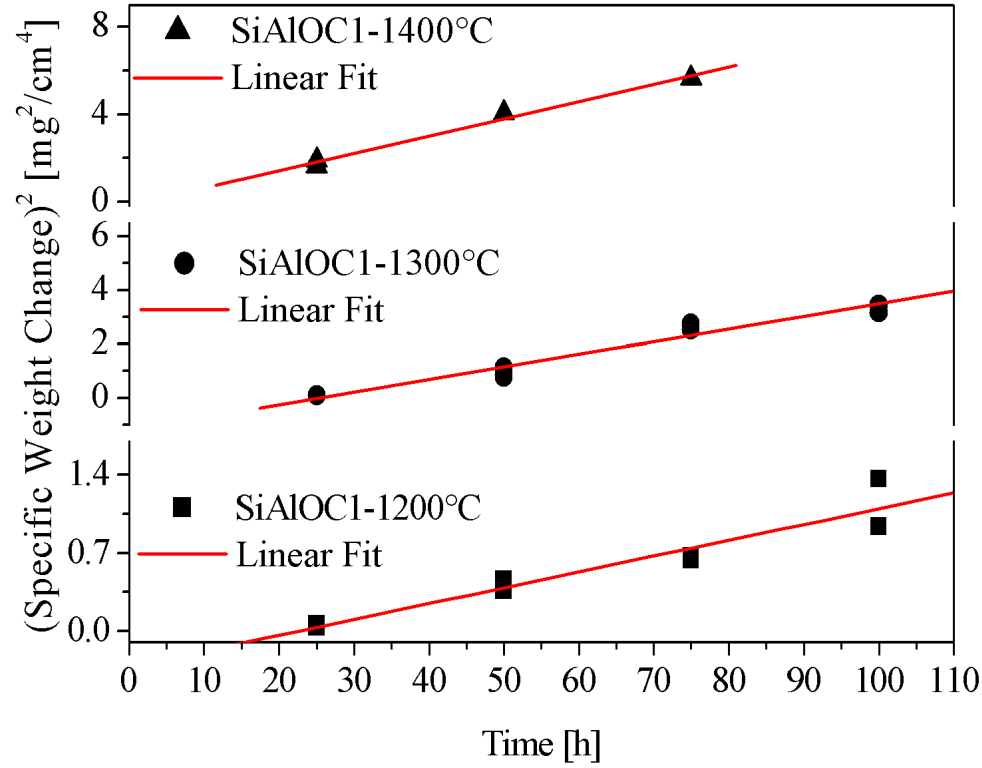
SiAlOC1-1400°C
Linear Fit
SiAlOC1-1300°C
Linear Fit
SiAlOC1-1200°C
Linear Fit
(Specific Weight Change)² [mg²/cm⁴]
Time [h]

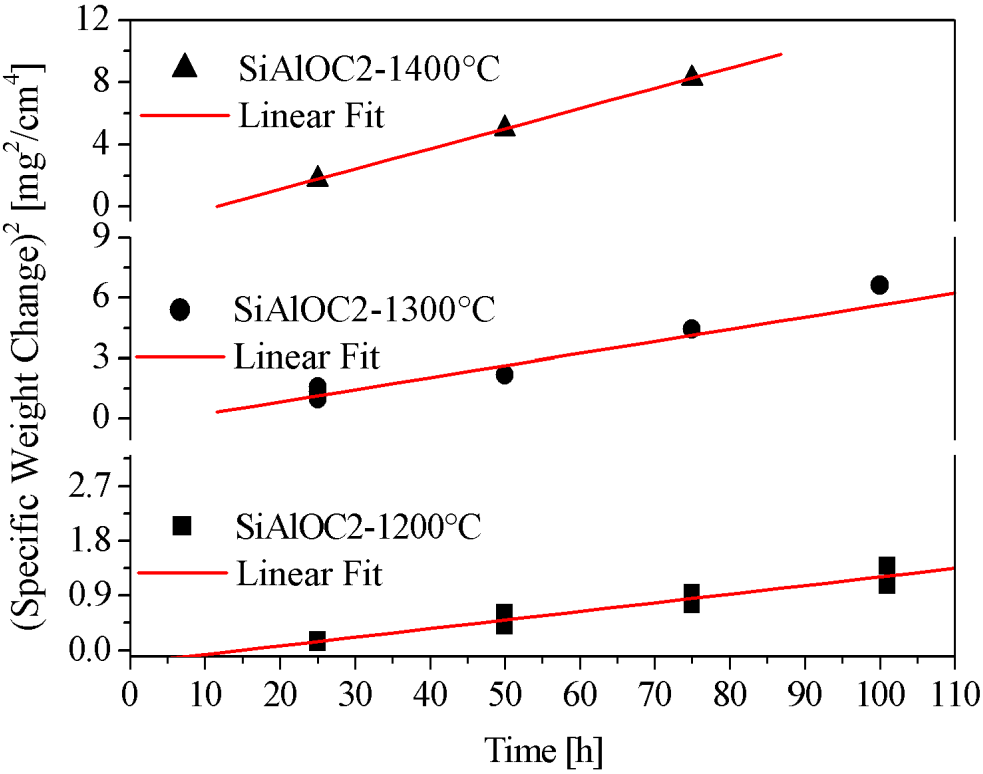
SiAlOC2-1400°C
Linear Fit
SiAlOC2-1300°C
Linear Fit
SiAlOC2-1200°C
Linear Fit
(Specific Weight Change)² [mg²/cm⁴]
Time [h]

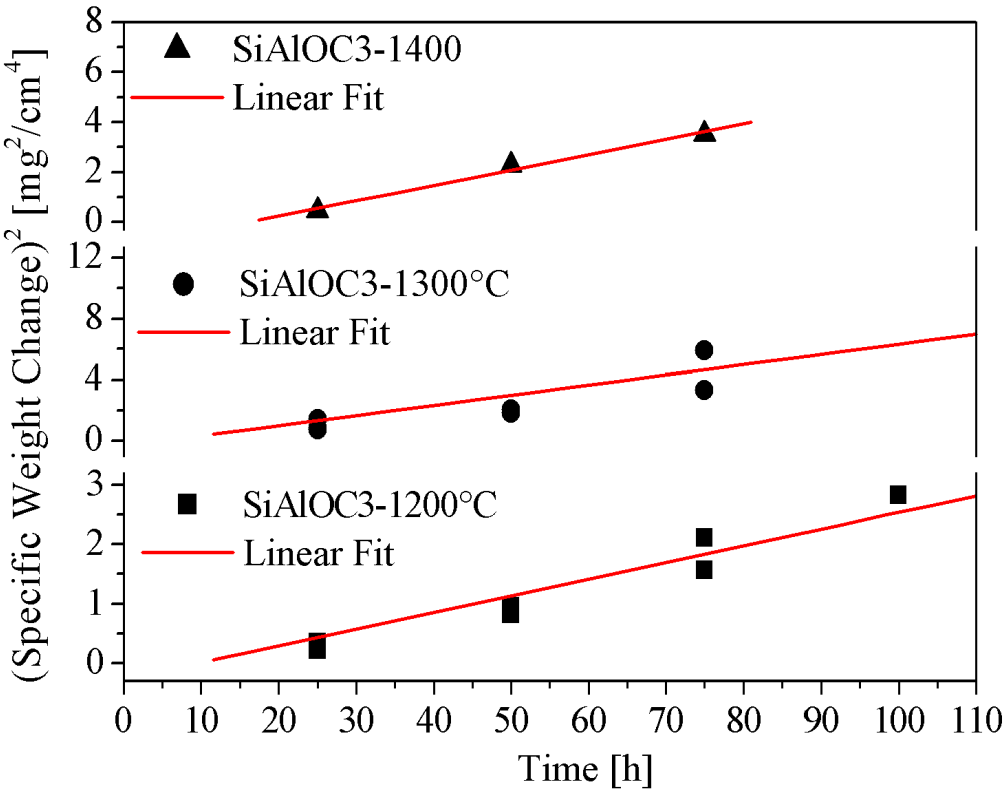

Figure 5.55: Thermo-gravimetric investigation of SiAlOC bulk ceramic in air at 1400°C: (a) weight gain versus time and (b) (weight gain)^2 versus time.

measuring the net weight gain after oxidation. For detailed quantification of oxidation kinetics several samples in cylindrical form were investigated at 1200, 1300, 1400°C in air and the results of (specific weight change)^2 versus time are shown in Fig. 5.55. The data clearly fits to a linear function, the bold lines in the figure represent the linear fit confirming the parabolic nature of oxidation. The SiC equivalence and free carbon content for all SiAlOC compositions are listed in Table: 5.3. In general, aluminum addition reduces the total carbon content as compared to SiOC ceramic. Also, increasing the aluminum content in SiAlOC ceramic reduces the amount of SiC equivalence and increases the amount of free carbon. The oxidation process is the net result of diffusion of oxidizing species inside or diffusion of decomposition product outside. If this is the case

Temp	**K_p(mg^2/cm^4h)**		
(°C)	*SiAlOC1*	*SiAlOC2*	*SiAlOC3*
1200	1.172 x 10^{-2}	1.418 x 10^{-2}	1.912 x 10^{-2}
1300	5.437 x 10^{-2}	5.981 x 10^{-2}	3.846 x 10^{-2}
1400	7.918 x 10^{-2}	9.530 x 10^{-2}	6.142 x 10^{-2}
E_{oxid} [kJ/mol]	198 ± 30	197 ± 25	119 ± 5

Table 5.12: Rate constants and oxidation activation energy for bulk SiAlOC bulk ceramics.

than at all temperatures namely from 1200−1400°C the oxidation is controlled according to Eqs. (3.42) and (3.43). As taken from Fig. 5.55 and Table: 5.12 at 1200°C, the oxidation weight gain increases with increasing aluminum content with highest parabolic rate of 1.912 x 10^{-2} [mg^2/cm^4h] for SiAlOC3 composition. The parabolic rate constant at higher temperature differ in magnitude with aluminum content and will be explained later.

Arrhenius behavior is observed for the oxidation rate constant K_p and oxidation temperature by the equation $K_p = K_0 \exp[-E_{(oxi)}/(RT)]$, where K_0 is a constant, E_{oxi} the activation energy, and R the ideal gas constant. The activation energy values given in Table: 5.12 were determined from the slope of the straight lines for K_p vs. $1/T$. The activation energy for the SiAlOC1 and SiAlOC2 composition show higher values in comparison to those reported for the oxidation of SiC at temperatures <1350°C. Jacobson reported this activation energy value in the range of 120 to 140 [kJ/mole] and is similar to that of molecular diffusion through amorphous SiO_2. Present finding supports possible mixed mechanism as a rate-controlling step for oxidation i.e inward molecular diffusion of oxidizing species and slow outward decomposition of decomposition species.

The change in K_p values with temperatures is seen hereafter in co-relation with the properties of oxide layer as well as core at oxidizing temperatures. For example, the creep investigation discussed in the earlier section proves that at 1200°C, the core material for all three composition has not reached the softening or glass transition. Thus the effect of glass softening on oxidation is not observed for all compositions at this temperature. The viscosity of the surface oxide layer and the core is highest for SiAlOC1 ceramic and is lowest for SiAlOC3 ceramic

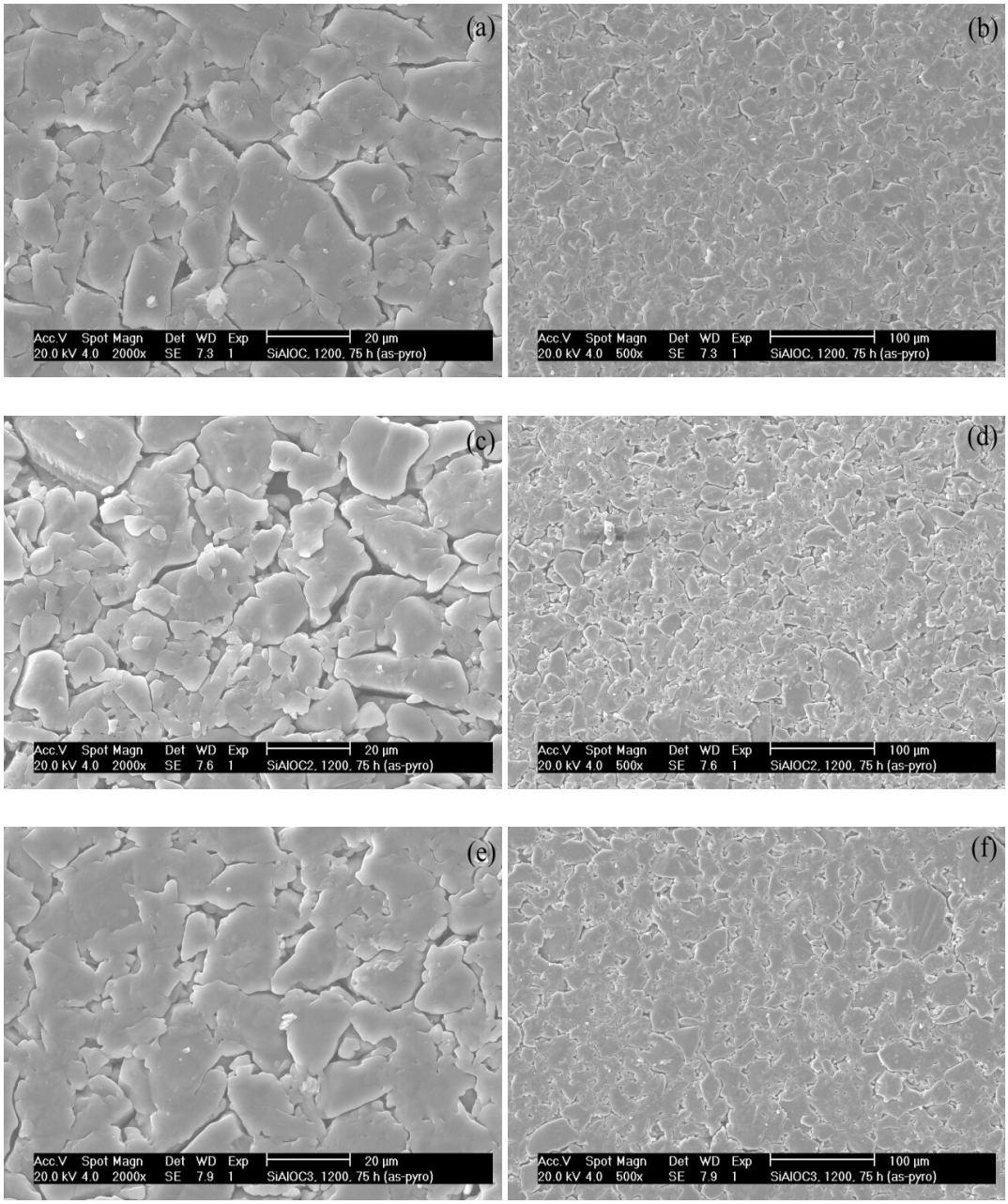

Figure 5.56: Surface morphology of oxidized SiAlOC bulk ceramics at 1200°C and 75 h holding time viewed at different magnifications: (a) SiAlOC1, 2000X; (b) SiAlOC1, 500X; (c) SiAlOC2, 2000X; (d) SiAlOC2, 500X; (e) SiAlOC3, 2000X; (f) SiAlOC3, 500X.

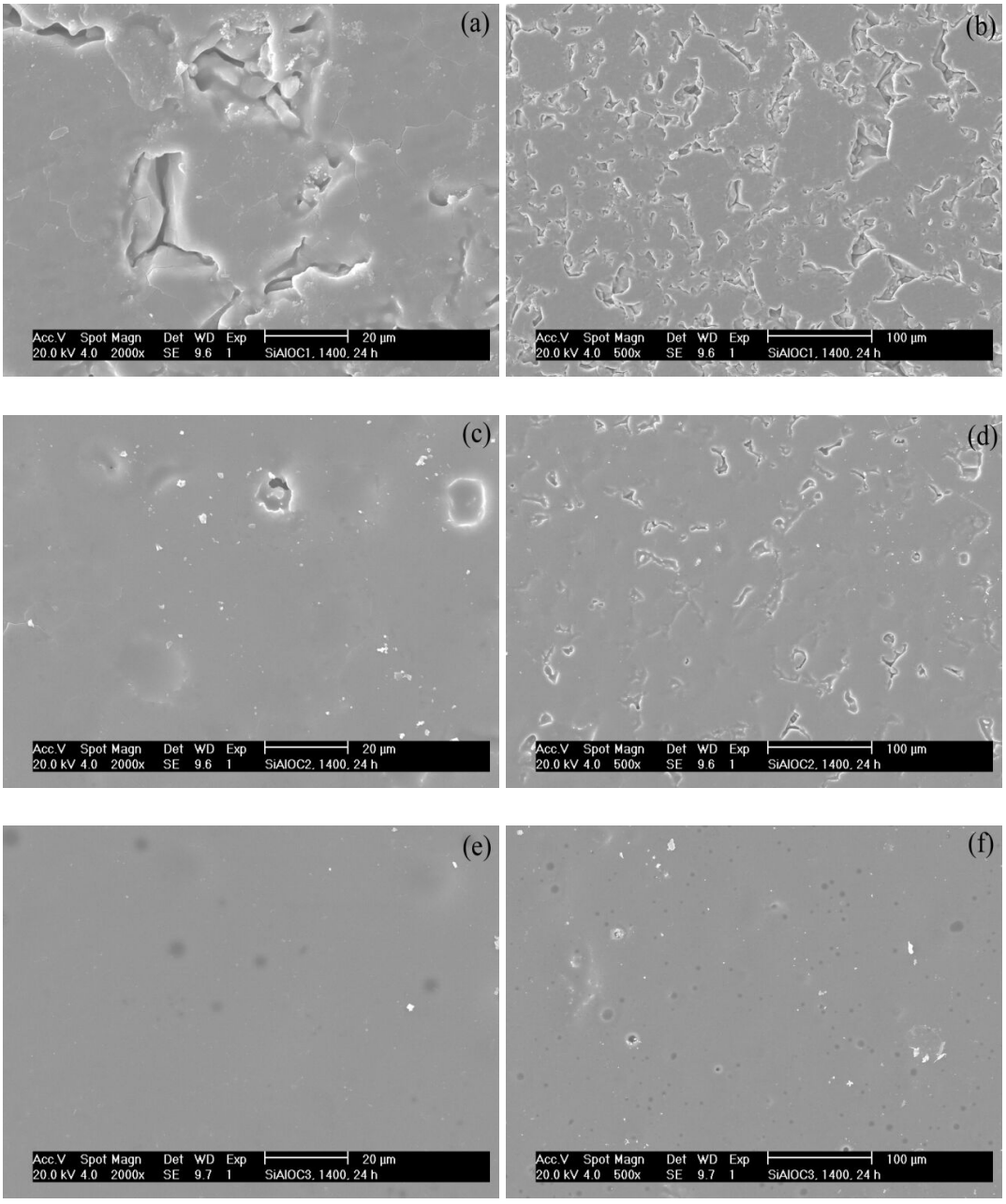

Figure 5.57: Surface morphology of oxidized SiAlOC bulks ceramics at 1400°C and 24 h holding time viewed at different magnifications: (a) SiAlOC1, 2000X; (b) SiAlOC1, 500X; (c) SiAlOC2, 2000X; (d) SiAlOC2, 500X; (e) SiAlOC3, 2000X; (f) SiAlOC3, 500X.

at all temperatures and the difference increases with temperature. This reduced viscosity has a positive as well as a negative effect on the oxide morphology. Positively lower viscosity possess high flowability for the glass which can fill the pores but negatively there is enhanced diffusion of the gaseous species. The oxide layer on aluminum modified samples exhibit a striking morphological change and is dependent on the temperature. Pores are still present on the surface of all compositions after oxidation for 75 h at 1200°C, and are shown in Fig. 5.56. But raising the temperature to 1400°C covers the surface pores producing smooth oxide surface and it is more prominent for SiAlOC3 ceramic even at low holding time like 25 h, as shown in Fig. 5.57. Thus the oxide layer morphology is more sensitive to temperature than to oxidizing holding time. At this temperature the oxide layer viscosity difference with composition is significant and also the core materials has reached or crossed the softening temperature. It is most likely that this lowered viscosity for high aluminum SiAlOC3 materials increases the transport mechanisms resulting in less hindered outgassing of decomposition species. The excess carbon for SiAlOC3 composition thus increases the weight loss at high temperature. Also the rate values or K_p is seen to be lower for SiAlOC3 composition after 1300°C in comparison to the values for low aluminum compositions at the same temperature.

Concluding the above discussion it is seen that the oxidation rate of SiOC ceramics is three to four order of magnitude less than SiAlOC ceramic (see Table: 5.11 and Table: 5.12. This result indicates that the oxidation resistance of SiOC ceramic is better than that of the SiAlOC ceramic. However the production of dense SiOC bulk forms is difficult due to cracking. Moreover, the SiOC ceramic cannot be effectively used for cyclic oxidation as during the first cycle (heating and cooling) the oxide layer produces cracks. Applications in form of thin coatings or intermediate layers, however should be possible.

The past discussion indicates that the viscosity of the solid material plays a key role in the transport phenomenon. If the material is reheated to its glass transition temperature regime may show a reduction in specific weight change and oxidation rate as compared to the pyrolyzed material. Hence, oxidation of the SiAlOC ceramics is further investigated with respect to the effect of pre-annealing of the bulks at high temperature.

5.12.2 Oxidation of Heat-Treated Bulk Si(Al)OC Ceramics

Structural relaxation and the glass transition of SiAlOC ceramics has been already discussed in the kinetic and compressive creep study. Accordingly, the SiAlOC2 and SiAlOC3 ceramics have already reached the glass transition if heated up to 1300°C while the SiAlOC1 ceramic has not. The temperature of 1300°C was selected for all bulk samples to investigate the effect of heat-treatment on the oxidation behavior.

The structurally relaxed and thermally modified bulk samples are polished and subsequently oxidized. The corresponding oxidation results are presented in Fig. 5.58 (a)−(c). Continuous weight gain is observed for all tested temperatures and holding time. The observations are again in contrast to SiOC ceramics. This is because even the SiC equivalence for both compositions is almost the same there is a significant reduction in the free carbon content for SiAlOC compositions. Hence, the weight loss by decomposition reaction is higher for SiOC than the weight gain and results in net weight loss after oxidation.

As can be taken from Fig. 5.58, the absolute weight gain for pre-treated samples at all oxidation temperatures decreases with the aluminum content. Here, the absolute net weight change values (with weight gain) are similar for SiAlOC1 and SiAlOC2 composition but the values are significantly reduced for SiAlOC3 composition for all investigated temperatures. This could easily make us conclude that SiAlOC3 has a superior oxidation resistance producing a passive oxide layer, which resists further oxygen diffusion. However, this is not the case and will be explained in the following section with help of SIMS and SEM. Nevertheless, our studies indicate that the thermal history of the sample plays a key role in the oxidation kinetics of investigated SiAlOC ceramics.

The rate constant for all tested temperatures are calculated from the slopes of Fig. 5.58 (a)−(c) and are plotted in Fig. 5.59. The oxidation activation energies are estimated from the parabolic rates for aluminum modified ceramics and the values are listed in Table: 5.13. The activation energy values seem sensitive to the impurity concentration.

Again the oxidation phenomenon can be explained with reference to the composition and the pre-treatment before oxidation. For example if we compare between as-pyrolyzed and pre-treated samples (Table: 5.12 and Table: 5.13),

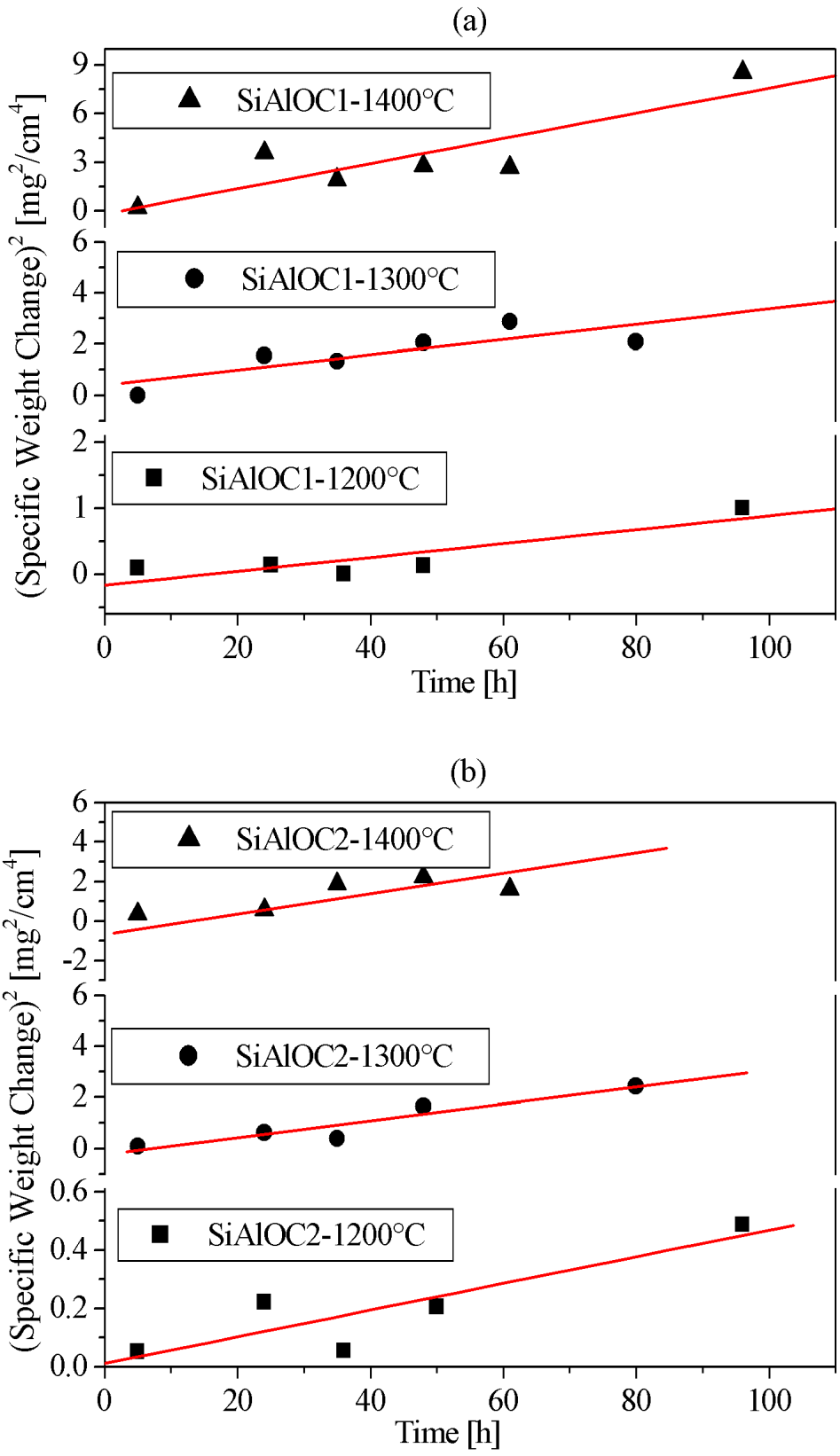
(a)
SiAlOC1-1400°C
SiAlOC1-1300°C
SiAlOC1-1200°C
(Specific Weight Change)^2 [mg^2/cm^4]
Time [h]
(b)
SiAlOC2-1400°C
SiAlOC2-1300°C
SiAlOC2-1200°C
(Specific Weight Change)^2 [mg^2/cm^4]
Time [h]

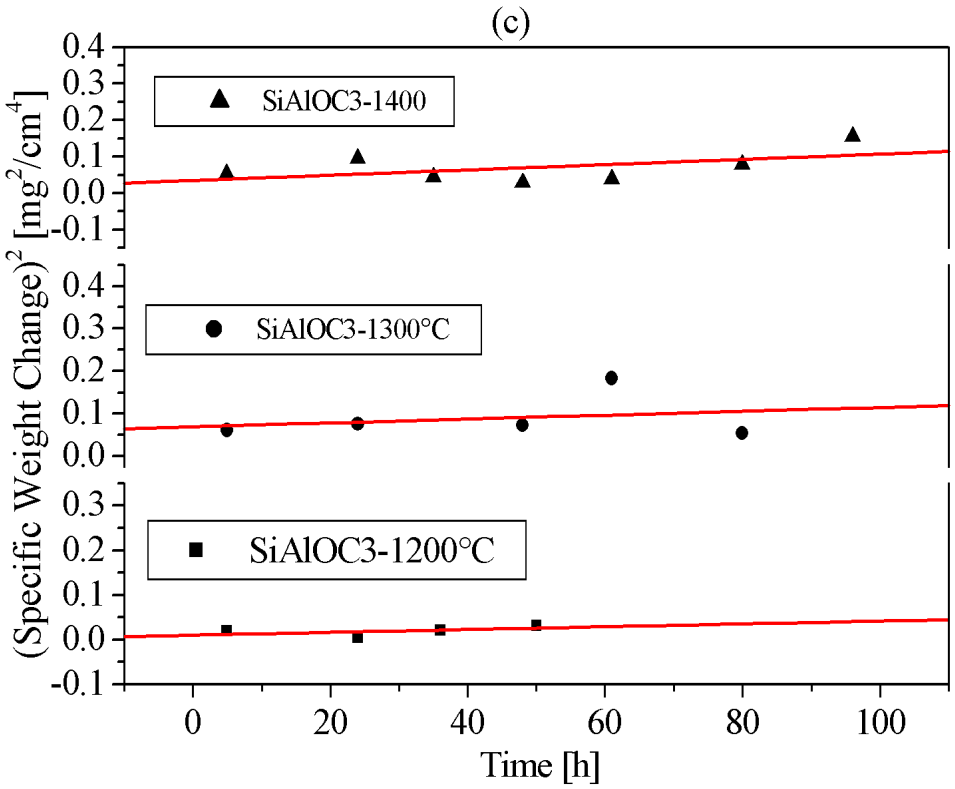

Figure 5.58: Oxidation behavior of heat-treated SiAlOC bulk ceramic in air at different temperatures: (a) SiAlOC1, (b) SiAlOC2 and (c) SiAlOC3 ceramic.

Temp	**K_p(mg^2/cm^{4}h)**		
(°C)	*SiAlOC1*	*SiAlOC2*	*SiAlOC3*
1200	1.053 x 10^{-2}	0.671 x 10^{-2}	3.138 x 10^{-4}
1300	2.979 x 10^{-2}	2.442 x 10^{-2}	4.570 x 10^{-4}
1400	7.766 x 10^{-2}	4.746 x 10^{-2}	9.443 x 10^{-4}
E_{oxid} [kJ/mol]	205 ± 2	201 ± 15	112 ± 12

Table 5.13: Rate constants and oxidation activation energy for heat-treated and polished bulk Si(Al)OC ceramics.

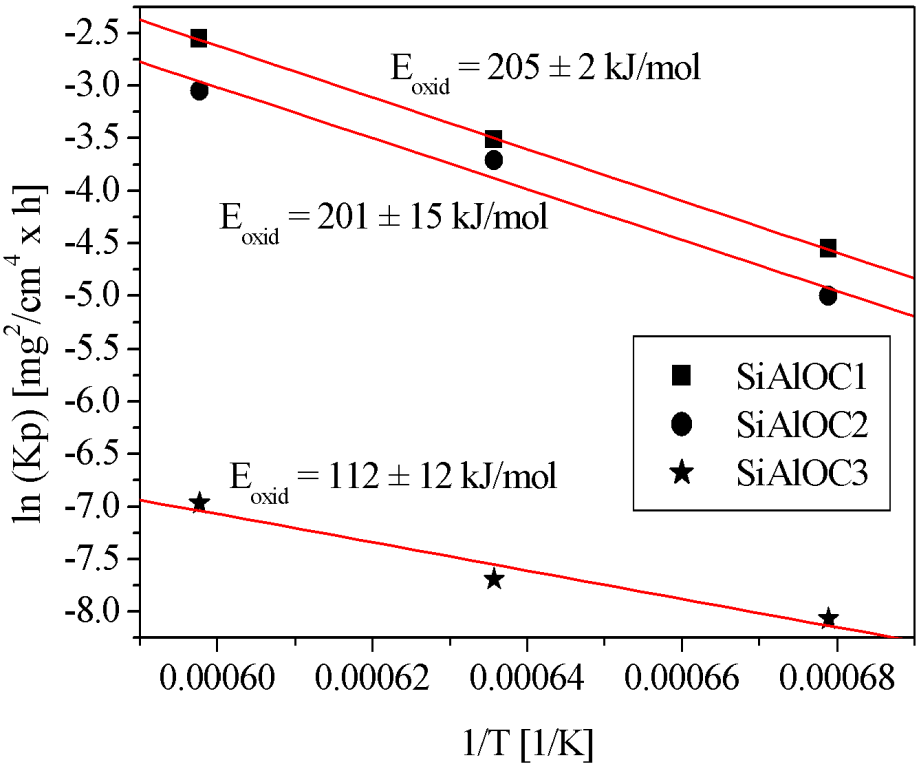

Figure 5.59: Arrhenius relation between parabolic rate constant and temperature for oxidation of densified SiAlOC bulk ceramic.

there is a striking change (reduction) in the oxidation parabolic rates at 1200°C for SiAlOC2 and SiAlOC3 whereas they remain unaltered for SiAlOC1. This finding is due to the fact that the compositions have already undergone glass transition during heat treatment and contain relatively high amount of free carbon (refer to Table: 5.3). Free carbon is oxidized easily by fast inward diffusion of oxygen and quickly removed as CO or CO_2. The differences observed in the oxidation behavior related to the aluminum concentration will be explained hereafter from compositional profiles using SIMS and can be seen in Fig. 5.60.

The oxide layer thickness is again estimated from the point where the oxygen level starts reducing from a constant higher value at the surface. At 1200°C the SiAlOC ceramic has an oxide layer thickness of around 0.2−0.3 µm. Similar to

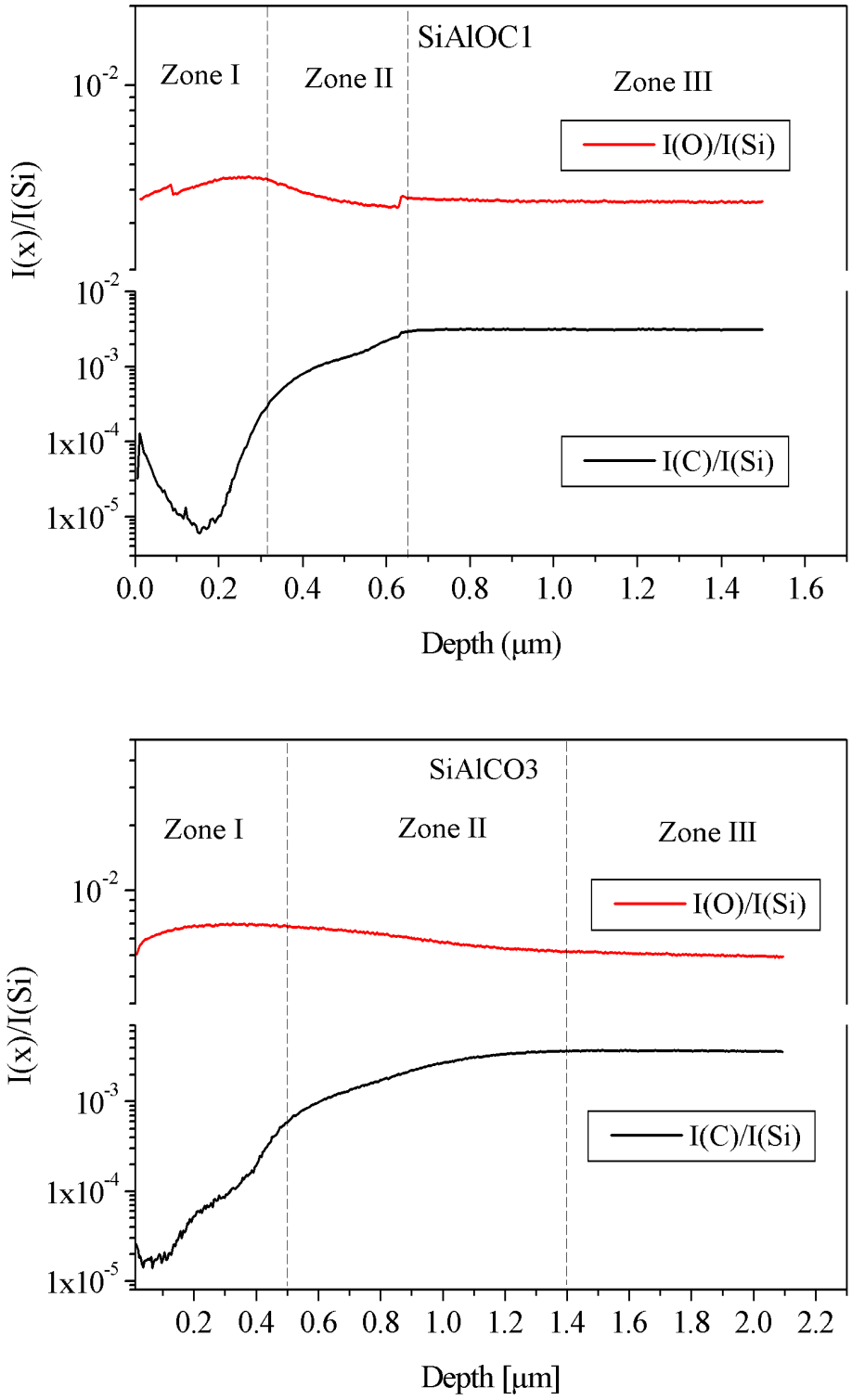

Figure 5.60: SIMS depth profile of SiAlOC1 (top) and SiAlOC3 (bottom) bulk ceramic after oxidation in air at 1200°C for 24h.

SIMS profile seen in the earlier section for SiOC ceramic, there is an upward carbon gradient in the oxide surface (Zone I in Fig. 5.60) for SiAlOC1 ceramic but not for SiAlOC3. This result indicates that the viscosity of the oxide layer for SiAlOC3 composition is extremely low, which suddenly removes the carbonaceous species.

Higher oxidation depths are observed for the samples oxidized at high temperature namely 1300°C and this effect is extreme in case of SiAlOC3 ceramic as can be seen in Fig. 5.61. For example, the depth of oxide layer for the SiAlOC1 and SiAlOC2 sample held at 1300°C for 24 h is approximately 0.4−0.5 μm (Zone I), which is slightly higher than that observed for these material at 1200°C. In contrast the oxide depth observed for SiAlOC3 at 1300°C for 24 h holding is around 1.0−1.1 μm, which is almost double than that seen at 1200°C. Additionally, unlike SiAlOC1, SiAlOC2 compositions no gradient in the carbon SIMS is detected in the case of SiAlOC3 ceramic. The carbon SIMS results for 1200°C and 1300°C are similar. It is assumed that there is no significant diffusion of aluminum in the oxide layer controlling the oxidation kinetic process. However the concentration of aluminum in the material as such changes the diffusion properties of the oxide by forming low viscosity alumino-silicate glass and increases the depth of oxide layer (or in general oxidized volume). The relatively low SiC equivalence with free carbon content and accompanied by low viscosity oxide layer may probably creates a balance between weight change reactions, which justifies the reduced oxidation rates for SiAlOC3 ceramic (as quantified in Table: 5.13).

A comparison between oxide surface morphology of the oxidized samples in as-pyrolyzed condition with that of the heat-treated samples shows considerable differences. Comparing Fig. 5.56 and Fig. 5.62 the surface morphology for SiAlOC1 ceramic after heat-treatment (densification) is much smoother and contains less open pores than that observed for the as-pyrolyzed sample. The surface of SiAlOC2 and SiAlOC3 ceramic is enveloped by a smooth oxide layer and the open porosity minimizes with the aluminum content. As explained earlier that the surface oxide morphology is more sensitive to temperature than time is exactly seen in the Fig. 5.63. Here, for SiAlOC2 and SiAlOC3 composition the surface pores are completely filled but are still present for SiAlOC1 ceramic. This supports that the oxide viscosity is lowered with aluminum and can flow in the pores easily. At low oxidation temperature i.e. 1200°C oxide

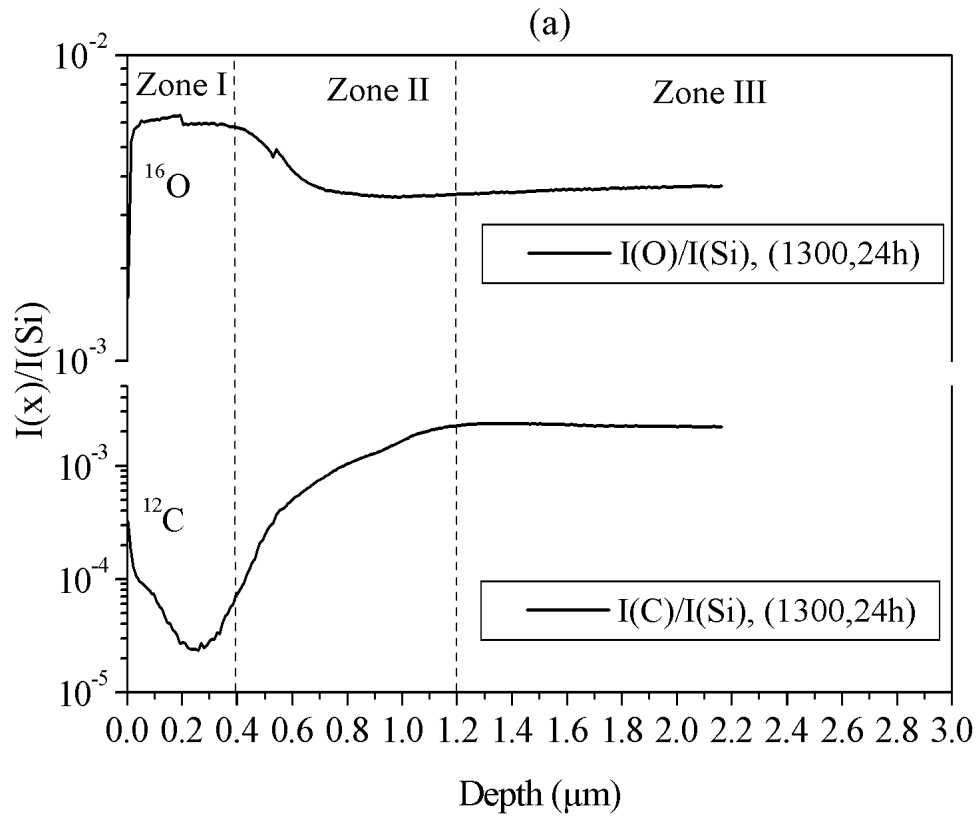
(a)
Zone I
Zone II
Zone III
^{16}O
^{12}C
I(O)/I(Si), (1300,24h)
I(C)/I(Si), (1300,24h)
I(x)/I(Si)
Depth (μm)

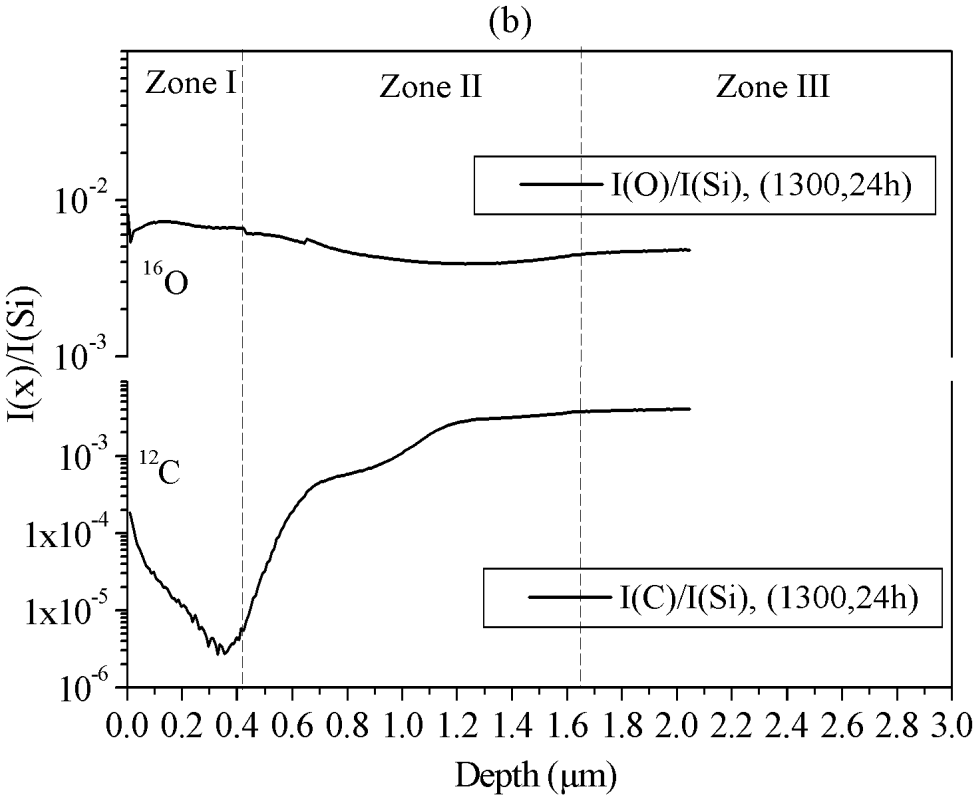
(b)
Zone I
Zone II
Zone III
^{16}O
^{12}C
I(O)/I(Si), (1300,24h)
I(C)/I(Si), (1300,24h)
I(x)/I(Si)
Depth (μm)

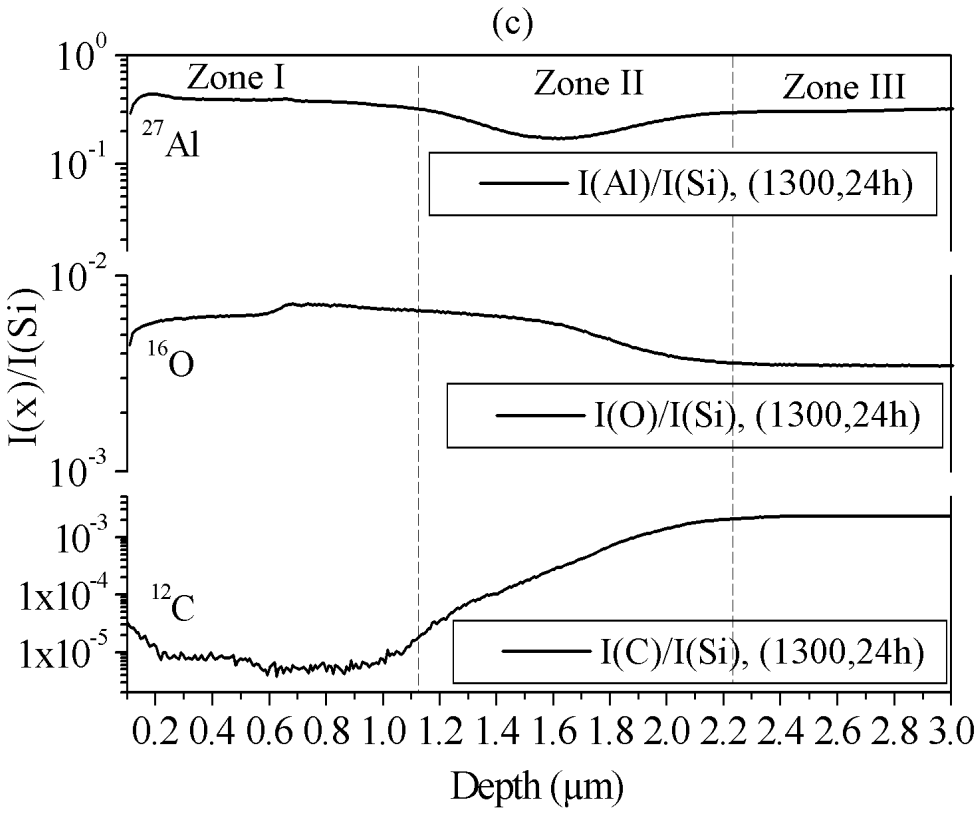

Figure 5.61: SIMS depth profile of bulk ceramic after oxidation in air at 1300°C for 24h (a) SiAlOC1, (b) SiAlOC2 and (c) SiAlOC3.

surfaces of all compositions indicate crack formation. Cracks are also present for SiAlOC1 ceramic at 1300°C but not present for the SiAlOC2 and SiAlOC3 samples. Cracking is observed to be originated at the pore vicinity and is believed to be initiated during the fast cooling of the sample after oxidation or because of the formation of cristobalite in the oxide layer. XRD analysis of all SiAlOC ceramics confirmed cristobalite as crystalline phase. The presence of cristobalite after etching of the sample is shown for SiAlOC3 ceramic in Fig. 5.64. This result indicates that cristobalite does not form in high volume fraction as for SiOC ceramic. The crystallites are small and acicular in morphology. Fig. 5.64 shows that, the crack first initiates at the fault i.e at a pore and then propagates in the surrounding region. Moreover, cracking is formed at the vicinity of crystallites due to the transformation volume change during cooling.

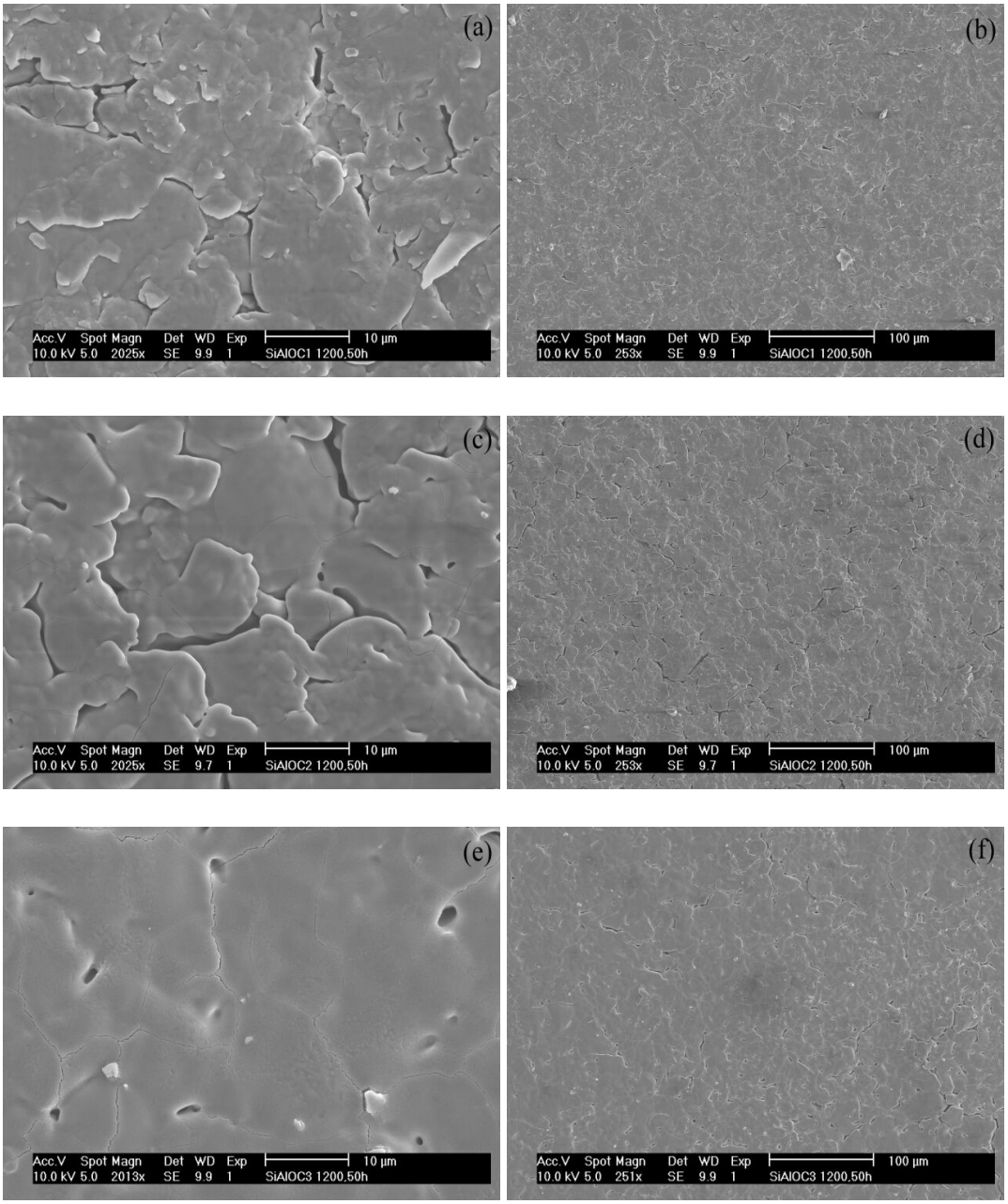

Figure 5.62: Surface morphology of oxidized (pre-densified) bulks of SiAlOC bulk ceramic at 1200°C and 50 h holding time viewed at different magnifications: (a) SiAlOC1, 2000X; (b) SiAlOC1, 250X; (c) SiAlOC2, 2000X; (d) SiAlOC2, 250X; (e) SiAlOC3, 2000X; (f) SiAlOC3, 100X.

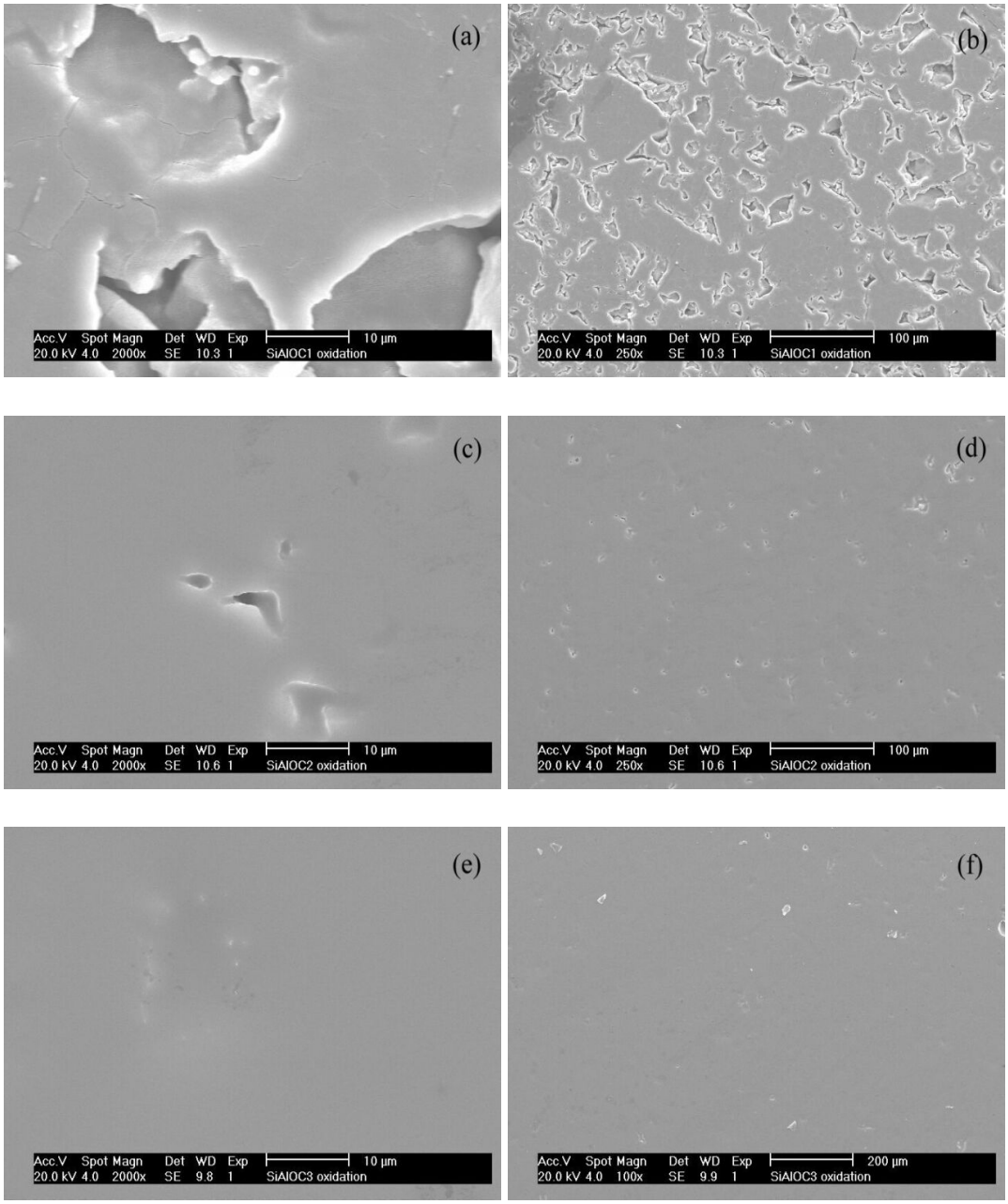

Figure 5.63: Surface morphology of oxidized (pre-densified) bulks of SiAlOC bulk ceramic at 1300°C and 50 h holding time viewed at different magnifications: (a) SiAlOC1, 2000X; (b) SiAlOC1, 250X; (c) SiAlOC2, 2000X; (d) SiAlOC2, 250X; (e) SiAlOC3, 2000X; (f) SiAlOC3, 100X.

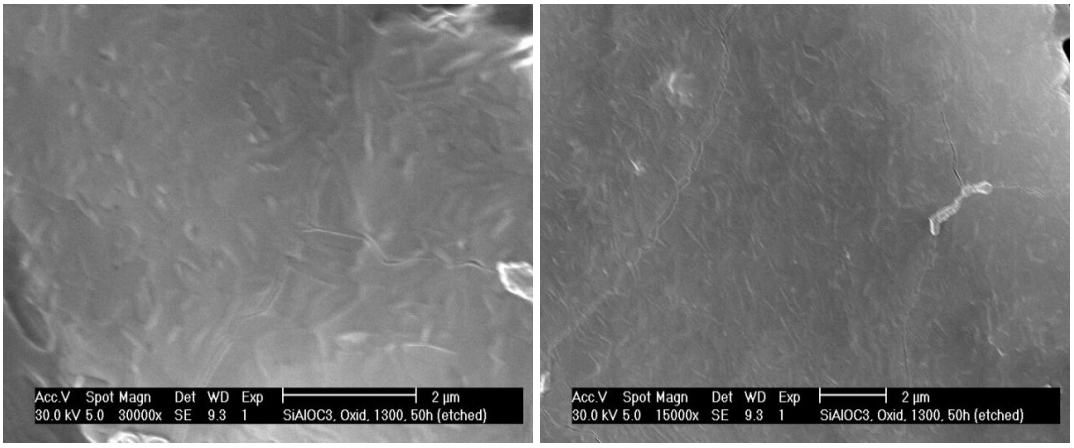

Figure 5.64: Surface morphology of oxidized (pre-densified) SiAlOC3 bulk ceramic at 1300°C and 50 h holding time after etching.

It will be interesting to see the surface morphology of SiAlOC3 ceramic at higher temperature, i.e., at 1400°C. This is because even at 1300°C the volume affected due to oxidation is very high. The oxide with higher aluminum content possesses extremely low viscosity which fills all the pores during oxidation and any oxidation product like CO or CO_2 must come out through this layer. Due to higher free carbon content it is believed that the amount of gas formation is enormous. This should either form blisters by retaining the gas in the subsurface or form bubbles. Blisters are formed if the glass phase resists the out gassing due to relative high viscosity at the tested temperature. No such formation of blisters or bubbles are observed up to 1300°C but at 1400°C they are visible for the SiAlOC3 sample. The surface morphology of SiAlOC3 ceramic oxidized at 1400°C for 100 h is shown in Fig. 5.65. Bubbles in large numbers and sizes are observed on the oxide surface also supporting extensive degassing during the oxidation process.

In the case of SiOC and SiAlOC3 ceramic with free carbon content the former does not show any bubbling while the latter does. This behavior is caused by the oxide viscosity, which is low for the aluminum modified ceramic. To conclude, it can be said that addition of aluminum always does not help to improve the oxidation resistance. Excess aluminum like in SiAlOC3 ceramic loses its oxidation capacity at higher temperature > 1300°C. Optimum oxidation resistance can be achieved by the SiAlOC2 composition and can be used as high as 1400°C, which

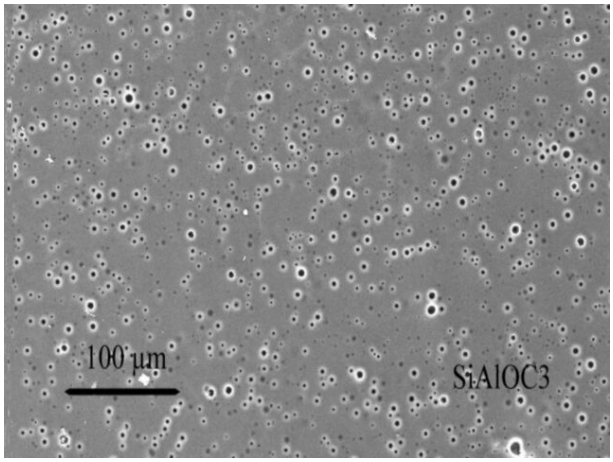

Figure 5.65: Surface morphology of (pre-densified) SiAlOC3 bulk ceramic after oxidation in air at 1400°C for 100 h

produces a thin oxide layer and even fills the surface pores and acts as barrier for further oxidation. Aluminum modification however reduces the volume of cristobalite which causes extensive cracks as seen for pure SiOC ceramics.

5.13 Applications

Although a large variety of silicon containing polymers with high ceramic yield have been developed, only low-dimensional products, such as fibers and thin films, have found application. To date, most preceramic polymers have been employed as precursors to ceramic fibers, coatings, matrices, and as binders for ceramic products. In line with these applications the investigation of micro-devices and CMC's derived from polysiloxanes will be briefly viewed in the following sections.

5.13.1 MEMS: General

The past decade has seen rapid growth of microelectromechanical systems (MEMS), an important area of technology, which as well expected to continue its development in the future. The basic advantage behind the concept of MEMS is that the efficiencies of high volume production and low unit cost achieved by the microelectronics industry over the past 50 years can be translated to devices in which mechanical and electrical components are integrated within a single chip

or equivalent structure. In addition to the potential economic benefit, unique capabilities can be achieved by such integration to realize devices at very small scales such as sensors, actuators, power producing devices, chemical reactors and biomedical devices.[151]

For these purposes, traditional MEMS are limited by their materials because silicon and polysilicon is not a structural material. It has a fracture toughness of ~ 0.7 MPa$\sqrt{\text{m}}$, a softening temperature of 600°C and a high degree of reactivity to oxygen and water. The same is true for metals and polymers used in fabrication techniques derived from LIGA (the acronym stems from the German expressions for the major process steps: Lithography, Galvanoformung (electroforming) and Abformung (molding).[151] Thus, the creation of many new, revolutionary MEMS systems requires that they be constructed from various materials, including ceramics.

Several attributes of ceramics are highly suitable for MEMS applications. The chemical inertness of ceramics make them useful in biological application. Ceramics resist corrosion at high temperatures, making them suitable for chemical engineering and micro-sensor application in severe environments. The same attributes are vital in overcoming problems of friction in micro-motorized systems. The low density and high-temperature mechanical properties of ceramics make them materials of choice for high-speed device such as nano-turbines. Because ceramics are flaw-size sensitive, their strength and reliability can be expected to increase in small-scale applications.

Although various methods like CVD or micro-machining have already been developed for fabrication of ceramic MEMS, this techniques can be time consuming, expensive, and technically challenging. Moreover, these processes are used for the development of SiC MEMS. In addition, the planar nature of CVD SiC makes it difficult to construct complex shaped structures. Therefore, the development of new materials and low-cost micro fabrication techniques for high temperature MEMS is of great interest to MEMS community.

Recently SiCN ceramic MEMS have been reported using low cost techniques like photo-polymerization and micro-forging. Photo polymerization is a low cost approach to fabricating polymer structures. By adding a photo-initiator to the liquid precursor, solidification can be accomplished by exposure to UV radiation rather than by heat addition. Thus by performing photolithography directly

on the precursor, solid polymer shapes may be obtained without the need of a mold.[152]

Green form of net shape can also be prepared by micro-forging liquid ceramic precursor into a mold that has been prepared by conventional methods.[153],[154] The precursor can be a chemical − for example, a metal organic − or it can be a slip. In the latter case, the micro-forging process can be considered as a micro version of the conventional slip-casting process. The present discussion, however, is limited to the fabrication of a new class of ceramics, namely silicon oxycarbide (Si-O-C).

5.13.1.1 SiOC Ceramic Micro-Component Feasibility Study

For this particular application, the silicon polymer should have the following requirements:

1. Sufficient wetting of the micro mold by polymer used to produce a component like the micro gear investigated in this study.

2. Solidification of the polymer, e.g., by chemical or thermal cross-linking after complete filling of the mold to retain the shape of the mold cavity.

3. Easy demolding of the green micro component.

A rheological investigation confirms the aforementioned requirements as shown by the visco-elastic behavior of the MK polymer with a cross-linking-agent, which is represented in Fig. 5.10 (refer to page 105). In the present study a steel mold with micro gear cavities was used. Silicone oil spray was applied as a lubricating agent for easy release of the green compact. The mold is inserted in a press cavity and the polymer powder (MK + 1%CLA) is added. The press cavity is heated at 10°C/min up to 150°C, held at this temperature for 15 min, and subsequently cooled to room temperature. Mechanically stable green compacts with micro gears are formed. Green compact thickness is controlled to 0.6−0.7 mm by optimizing the initial polymer mass feed. Bulk SiOC ceramic gears were obtained after pyrolysis of the green compact in argon atmosphere with 25°C/h up to 1100°C as can be seen in Fig. 5.66 (bottom). Higher magnification reveals crack-free and dense ceramic micro-gears.

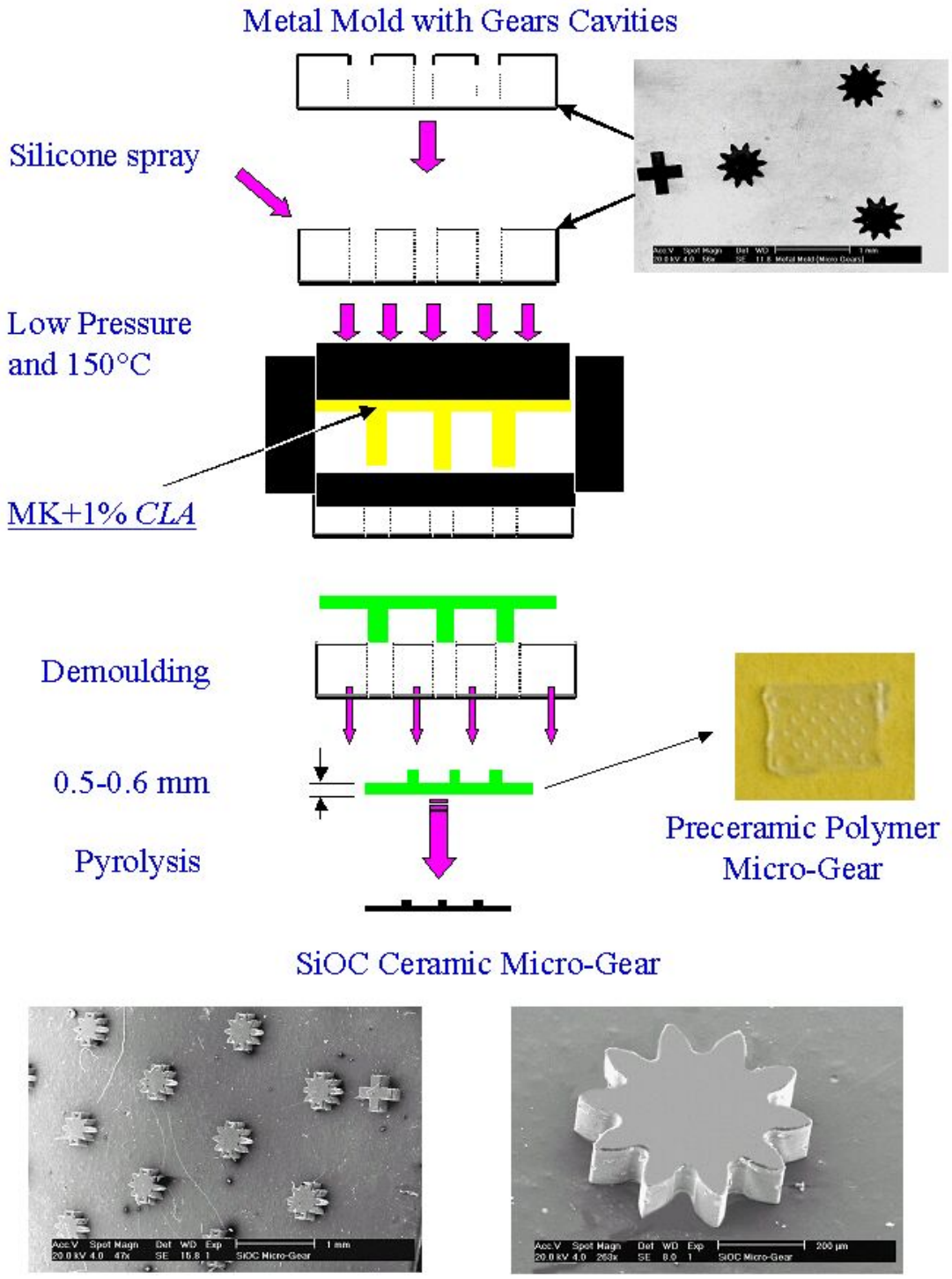

Figure 5.66: Schematic of SiOC ceramic micro-gear fabrication process by micro casting from commercial polysiloxane.

5.13.2 Ceramic Matrix Composites (CMC's)

The novel application of polymer derived ceramic lies in the easy processing of ceramic matrix composite (CMCs). Development of ceramics from MK polymer was divided into various parts and one part is to develop CMCs with various filler compounds and to form stable crack-free bulks. Accordingly, the preparation of titanium containing SiOC ceramics reported by F. Hönack is reviewed here.[116]

In this study, crack-free synthesis of Si-Ti-O-C ceramic in large bulk form was optimized by using Ti, TiH_2, TiC, TiB_2 as fillers and MK polymer as matrix material. In this system Ti and TiH_2 act as an active filler whereas TiC, TiB_2 is passive. This is because, during the thermal treatment gradual development of new phases as a function of temperature is observed. Among all these phases titanium carbide (TiC) and titanium silicide Ti_5Si_3 are most stable. At high temperature (> 1100°C), TiO_2 is reduced by carbothermal reduction process (with excess carbon from matrix) to titanium, which progressively transforms to TiC and Ti_5Si_3. This work reports on the formation of mixed carbide phase Ti_3SiC_2 from the mixtures containing titanium dihydrid.[116] All phase development is a function of particle size of the active fillers used and the temperature. One such microstructure of titanium containing CMCs is shown in Fig. 5.67. The microstructure clearly indicate the filler particles embedded in the SiOC matrix. Investigation of phases by XRD after pyrolysis at 1100°C reveals the formation of TiC, TiO_2, and Ti_5Si_3. TiB_2 is remaining as a passive filler. The effect of various fillers (in various amount) on the strength development is well mentioned in this work.

In other work (not reported) researchers used MK polymer along with different fillers like Al_2O_3, $MoSi_2$, SiC in various volume fraction to form CMCs with suitable electrical properties. The volume of fillers can control the electrical property of the CMC and make them electrically conductive or insulating. However, maintaining the requirement of present time, i.e., forming complex shape or fine structure topograph ceramic components with enormous strength is investigated in the present study. Here SiC is used as a passive filler as the transformed CMC may posses high strength and wear resistance. For complex topography an Euro coin is used which contains very detailed protrusion of parts of the bird eagle. The mold and coin is coated by silicon oil spray. MK poly-

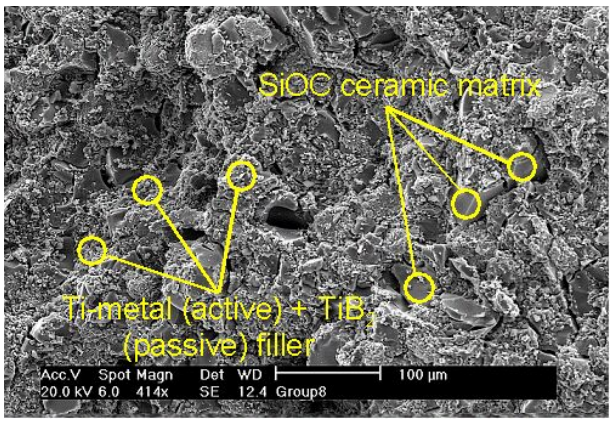

Figure 5.67: Microstructure of fractured Si-Ti-O-C CMC containing Ti (active filler), and TiC (passive filler) embedded in SiOC matrix after pyrolysis in argon at 1100°C.[116]

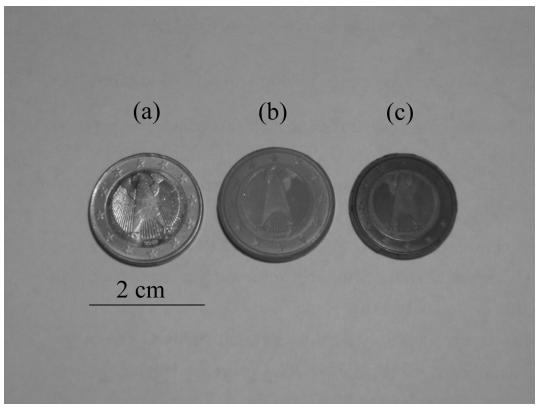

Figure 5.68: Mechanically stable ceramic matrix composite formation with complex structure: (a) euro coin as a mold (b) euro green form after warm pressing MK-polymer + 1 wt.%CLA mixture + 30 vol.% SiC filler and (c) euro coin with detailed surface topograph in ceramic state after pyrolysis in argon at 1100°C.

mer with 1 wt.% *CLA* and 30 vol.% SiC powder (UF15 from HCST, Germany, particle size 0.5 µm) mixture is prepared in ball mill. The mixture is filled in a warm press mold along with the Euro coin. Green body is formed after warm pressing of the mixture at 150°C and ejecting the solid mass after cooling. The green form is subsequently transformed to ceramic after pyrolysis at 1100°C in argon atmosphere. The green and ceramic form together with the Euro coin are pictured in Fig. 5.68. The topographic microstructural details of the ceramic Euro coin is shown in Fig. 5.69. This study confirms that crack-free green and

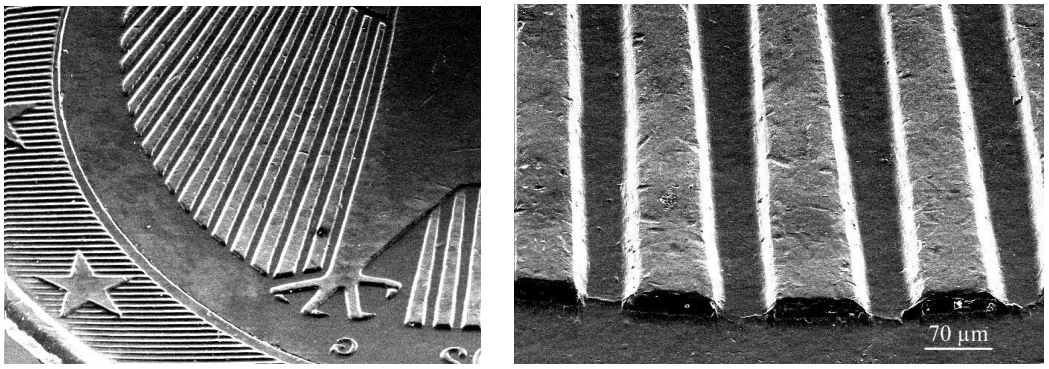

Figure 5.69: Formation of crack-free SiC filled SiOC ceramic matrix composite: retention of euro coin topographic details in pyrolyzed state.

ceramic CMC's with complex shapes can be produced using passive fillers. The processed SiC filled SiOC CMC is mechanically stable.

6 Conclusions

Preparation of novel ceramic materials through thermal decomposition of preceramic polymers in controlled atmosphere has been continuously investigated since the last two decades. In this regard, the oxide systems have potential interest in the high temperature application area for components working under harsh atmospheric conditions.

The present research is focused on the pyrolysis of unfilled commercial poly(methylsilsesquioxane) and its aluminum modification to form a novel ceramic system Si(Al)OC. Among all available commercial polysiloxanes, the investigated polymer is selected as it gives clean, easy processing advantage and properties versatile for use in injection molding. Cross-linking of this polymer is shown to occur thermally and the kinetics of this reaction is accelerated by using a *CLA*. Detailed rheological investigation allows optimizing the polymer and *CLA* mixture procedure as well as the *CLA* content. Further, thermal decomposition process of mixtures with and without *CLA* is discussed and the presence of *CLA* reveals significant rise in the ceramic yield. The weight loss is observed in three stages of the complete thermal cycle and is due to evaporation of oligomers and polycondensation products in low temperature region and due to methane and hydrogen at higher temperature. After polycondensation further transformation of polymeric mass to an inorganic product is discussed with help of radical reactions. The commercial polysiloxane *CLA* mixture can be processed forming transparent green bodies, which can further convert to an inorganic bulk without cracks.

As mentioned above one of the aim of this research is to produce SiAlOC ceramic and is fulfilled by a solution route related to the sol-gel technique. The commercial polysiloxane investigated here could be modified into polyaluminosiloxane via chemical reaction with aluminum alkoxide. The gelation process is found to be sensitive with the amount of alkoxide and solvent used. Gelation is shown

to take place at room temperature if minimum 9 wt.% aluminum alkoxide is used together with isopropanol as solvent. The ceramic yield is observed to be reduce with increasing alkoxide content. Also the ceramic composition after polymer-to-ceramic transformation process reveals a high total carbon content for SiOC. The amount of carbon decreases with increasing aluminium content. Increasing the aluminum also reduces the amount of SiC in the ceramic. It is shown that all Si(Al)OC compositions contain considerable amount of free carbon as quantified by chemical analysis. Solid state NMR studies confirmed the presence of Si−O and Si−C bonds in the SiAlOC ceramic. Aluminum is found to be present in all possible Al-O coordination sites i.e., Al(4), Al(5), and Al(6) with significant octahedral contribution. The distribution of the coordination sites in the pyrolyzed samples strongly depends on the aluminum content.

The formation of SiAlOC bulk ceramics without generation of cracks are possible. In contrast SiOC can only be produced as thin samples from unmodified polysiloxanes. The reason for cracking in the case of SiOC is related to the isotropic shrinkage during the polymer-to-ceramic transformation which is not found for SiAlOC ceramics. The SiAlOC ceramic is not as dense as the SiOC counterpart and possesses around 3-4% residual porosity.

At high temperature SiOC, ceramics are not stable and crystallize to form $\beta-$SiC at T >1300°C. Crystallization is accompanied by weight loss and cracking of the samples. In contrast, the SiAlOC ceramic remains amorphous or nanocrystalline even at 1500°C. It crystallizes to nano mullite and SiC between 1350 to 1600°C and is dependent on the amount of aluminum. Mullite formation temperature is lowest for high aluminum samples. Crystallization of intermediate alumina phase is not observed. The SiAlOC ceramics densify between 1200-1600°C. Densification occurs via transient viscous sintering along with low weight loss compared to SiOC ceramics. The SiAlOC ceramic does not decompose up to 1600°C. At higher temperature weight loss occurs due to decomposition of the network structure.

Bulk SiAlOC ceramics undergo two distinct processes with temperature when reheated after pyrolysis. These two processes are observed in different non-overlapping regions as found by kinetic studies. The first process is softening and structural relaxation and is reflected in continuous deformation of the samples. At high temperature the deformation is hindered by crystallization. The

resistance to deformation increases with the aluminum content. Thus crystallization of mullite, which is higher for high aluminum ceramic is discussed to resist densification. The deformation behavior changes with heating rate and shown to contain information about activation energy for softening and crystallization. The activation energy for softening is estimated by Moynihan theory and the crystallization activation energy is calculated by Kissinger and Moynihan theory. Accordingly, the activation energy for softening of 403−632 [kJ/mole] is calculated and is mentioned to be minimum for higher aluminum content. The average activation energy for crystallization thus estimated is about 503 [kJ/mole]. This low value along with the crystallization behavior indicates that the material behaves like a monophasic system rather than a diphasic or hybrid material.

The softening kinetics discussed above could not confirm the glass transition temperature for any SiAlOC ceramics as glass transition temperature depends on the heating rate. Another suitable method to identify glass transition temperature is the calculation of the shear viscosity. Shear viscosity data were derived from compression creep experiments. The total strain measured in axial and radial direction is converted to creep strain and sintering/cavitation strain. It is shown that, the deformation below the glass transition temperature region is mainly related to creep with small sintering part. The shear viscosities calculated from this study indicate that the glass transition temperature is highest (1300°C) for low aluminum ceramic and is lowest (1220°C) for highest aluminum samples. The shear viscosity for SiAlOC is two order of magnitude higher at all temperatures compared to silica glass. This is due to the presence of strong covalent Si−C bonds in the ceramic. Increasing the aluminum content reduces the viscosity values at all temperatures. The increased defect concentration allows easy flow for high aluminum glass composition. Accordingly, the activation energy for flow for high aluminum materials is 375 [kJ/mole]. The activation value for flow is compared to be similar to that calculated for softening of the matrix. This indicates that same molecular motions are involved in above two processes.

Oxidation of SiOC ceramics show weight loss at T > 1200°C and times. The weight loss indicates that free carbon content is contributing more compared to weight gain from Si−C bonds. Surface morphology of oxide layer shows heavy cracking and is formed during the cooling cycle by volume change due to cristo-

balite transformation. In contrast, SiAlOC ceramic always show weight gain at all oxidation temperatures and times. The oxidation behavior is proved to obey a parabolic law. Accordingly, the parabolic rate constant of 6.1 x 10^{-2} [mg^2/cm^4h] is calculated for low aluminum sample which is one order of magnitude higher than CVD-SiC ceramic. The parabolic rate constants reduce with aluminum content but it is very sensitive to the thermal history of the sample. Heat-treatment of the samples indicate that high aluminum samples, which undergo glass transition during heat-treatment, reduce the specific net weight to low values. Low aluminum ceramics show carbon gradient in the oxide layer away from the growth interface and is in agreement with the behavior of SiOC ceramic. The carbon gradient is not observed for high aluminum material because of low viscosity oxide layer.

The commercial polysiloxane investigated in this study has find its suitability in formation of micro-components, namely MEMS. Finally, the polymer can be ideally used for mass production of ceramic matrix composites with distinguished electrical, mechanical or high temperature properties.

7 Outlook

The main focus of this project is fulfilled by producing bulk Si(Al)OC ceramics and investigating the effect of aluminum modification on the properties like crystallization, bulk deformation at high temperature and oxidation resistance. Although this research has set a foundation for the manufacturing of Si(Al)OC ceramics utilizing polymer technology, future research is needed to built up this foundation. As such, the following suggestions for future research are given:

1. Si(Al)OC ceramics behave like black glass and can be used as a sintering additive. Thus, the effect of aluminum concentration on the mechanical properties of structural bulk material like SiC can be investigated.

2. More focus should be given on producing SiOC ceramic fibers from such low cost polysiloxanes and should be compared with the properties of Si-C-(O) Nicalon fibers.

3. The effect of aluminum modification on the mechanical properties like hardness, elastic modulus and electrical properties need to be investigated and compared with SiOC ceramic in as-pyrolyzed and heat-treated condition.

4. It has been investigated that substitution of oxygen by nitrogen improves the stability of the material. For example the oxidation resistance of Si-C-O-N is superior to that of Si-C-O.[96] Thus, the Si-Al-O-C system can be converted to Si-Al-O-C-N by pyrolyzing the gel system in ammonia or nitrogen.

5. The above mentioned Si-Al-O-C-N can be further characterized for the following:

    - High temperature stability and crystallization kinetics and phase development.

- High temperature compression creep.
- Oxidation kinetics of bulks.

Among all above mentioned suggestions the use of Si(Al)OC ceramic powder as a glass phase binder is currently under investigation. For this research, the SiOC ceramic powder from poly(methylsilsesquioxane) and the aluminum modified SiAlOC ceramic powder will be mixed with SiC and will be hot-pressed/sintered for bulk processing.

Bibliography

[1] K. Wynne and R. Rice. "Ceramics via Polymer Pyrolysis". *Annual Review Materials*, 14, pp. 297–334, 1984.

[2] R. Rice. "Ceramics from Polymer Pyrolysis, Opportunities and Needs - A Materials Perspective". *Ceramic Bulletin*, 62[8], pp. 889–892, 1983.

[3] G Pouskouleli. "Metalorganic Compounds as Preceramic Materials. I. Non-Oxide Ceramics". *Ceramic International*, 15, pp. 213, 1989.

[4] P. Chantrell and P. Popper. "Inorganic Polymers and Ceramics". *Special Ceramics 1964*, edited by P. Popper, New York: Academic, 1964, pp. 87–104, 1964.

[5] W. Verbeek and G. Winter. "Formkörper aus Siliciumcarbide und Verfahren zu ihrer Herstellung". *German Patent No. 2236078*, (Bayer AG), 21 March 1974.

[6] G. Winter, W. Verbeek and M. Mansmann. "Formkörper aus homogenen Mischungen von Siliciumcarbide und Siliciumnitrid und Verfahren zu ihrer Herstellung". *German Patent No. 2243527*, (Bayer AG), 18 April 1974.

[7] S. Yajima, J. Hayashi and M. Omori. "Continuous Silicon Carbide Fiber of High Tensile Strength". *Chemistry Letters*, 9, pp. 931–934, 1977.

[8] S. Yajima, Y. Hasegawa, K. Okamura and T. Matsuzawa. "Development of High-Tensile Strength Silicon Carbide Fiber Using an Organosilicon Polymer Precursor". *Nature*, 273, pp. 525–527, 1978.

[9] S. Yajima, J. Hayashi, M. Omori and K. Okamura. "Development of Silicon Carbide Fiber with High Tensile Strength". *Nature*, 261, pp. 683–685, 1976.

[10] R. Riedel, A. Kienzle, W. Dressler, L. Ruwisch, J. Bill and F. Aldinger. "A Siliconboron Carbonitride Ceramic Stable to 2000". *Nature*, 382, pp. 796–798, 1996.

[11] R. Riedel, H-J. Kleebe, V. Schönfelder and F. Aldinger. "A Covalent Micro/Nano-Composites Resistant to High Temperature Oxidation". *Nature*, 374, pp. 526–528, 1995.

[12] Y. Li, E. Kroke, R. Riedel, C. Fasel, C. Gervais and F. Babonneau. "Thermal Cross-Linking and Pyrolytic Conversion of Poly(ureamethylvinyl)silazanes to Silicon-Based Ceramics". *Applied Organometallic Chemistry*, 15, pp. 820–832, 2001.

[13] E. Kroke, Y. Li, C. Konetschny, E. Lecomte, C. Fasel and R. Riedel. "Silazane Derived Ceramics and Related Materials". *Mater. Sci. Eng.*, 26, pp. 97–199, 2000.

[14] P. Padmaja, G. Anilkumar and K. Warrier. "Formation of Mullite Phase in Diphasic Gels Consisting of TEOS and Boehmite With and Without Dehydroxylation". *J. of European Ceramic Soc.*, 18, pp. 1765–1769, 1998.

[15] D. Treadwell, D. Dabbs and I. Aksay. "Mullite ($3Al_2O_3-2SiO_2$) Synthesis with Aluminosiloxanes". *Chemistry of Materials*, 8, pp. 2056–2060, 1996.

[16] P. Greil and M. Seibold. "Modelling of Dimensional Changes During Polymer-Ceramic Conversions". *J.of Material Science*, 27, pp. 1053–1059, 1991.

[17] P. Greil. "Active- Filler - Controlled Pyrolysis of Preceramic Polymers". *J. of American Ceramic Soc.*, 78[4], pp. 835–848, 1995.

[18] D Carlsson, J. Cooney, S. Gauthier and D. Worsford. "Pyrolysis of Silicon-Backbone Polymers to Silicon Carbide". *J. of American Ceramic Soc.*, 73[2], pp. 237–241, 1990.

[19] J. Lipowitz, G. Legrow, T. Lim, and N. Langley. "Silicon Carbide Fibers From Methylpolysilane (MPS) Polymers". *Ceramic Eng. Sci. Proc.*, 9[7-8], pp. 943–948, 1988.

[20] C. Schilling Jr., J. Wesson, and T. Williams. "Polycarbosilane Precursors for Silicon Carbide". *American Ceramic Society Bulletin*, 62[8], pp. 912–915, 1983.

[21] N. Langley, G. LeGrow and J. Lipowitz. "Properties of Ceramic Fibers From Orgaosilicon Polymers". *in; Fiber Reinforced Ceramics Composities*, edited by K. Mazdiyasni, New Jersey: Noyes Publications, pp. 63, 1990.

[22] S. Yajima. "Special Heat Resistant Materials From Organometallic Polymers". *American Ceramic Society Bulletin*, 62[8], pp. 889–892, 1983.

[23] E. Fitzer and R. Gadow. "Fiber Reinforced Silicon". *American Ceramic Society Bulletin*, 65[2], pp. 326–335, 1986.

[24] W. Schmidt, V. Sukumar, W. Hurley Jr., R. Garcia, R. Doremus, L. Interrante and G. Rendlund. "Silicon Nitride Derived From Organometallic Polymer Precursor: Preparation and Characterization". *J. of American Ceramic Soc.*, 73[8], pp. 2412–2418, 1990.

[25] G. LeGrow, T. Lim, J. Lipowitz and R. Reaoch. "Ceramics From Hydridopolysilazanes". *American Ceramic Society Bulletin*, 66[2], pp. 363–367, 1987.

[26] D. Seyferth, G. Wiseman and C. Prud'Homme. "A liquid Silazane Precursor to Silicon Nitride". *J. of American Ceramic Soc.*, 66, pp. C–13–4, 1983.

[27] D. Seyferth, T. Wood, H. Tracy and J. Robinson. "Near−Stoichiometric Silicon Carbide from an Economical Polysilane Precursor". *J. of American Ceramic Soc.*, 75, pp. 1300–1302, 1992.

[28] B. Walker Jr., R. Rice, P. Becher, B. Bender and W. Coblenz. "Preparation and Properties of Monolithic and Composite Ceramics Produced by Polymer Pyrolysis". *American Ceramic Soc. Bulletin*, 62, pp. 916–923, 1983.

[29] S. Yu. "Net-Shape Formation of Bulk Composite Materials via the Porolysis of Poly(siloxanes) Filled with Chemically Active Titanium and Inactive Silicon Carbide Fillers". *PhD Thesis, State University of New Jersey*, 1996.

[30] S Yajima, T. Iwai, T. Yamamura, K Okamura, and Y. Hasegawa. "Synthesis of Polytitanocarbosilane and its conversion into Inorganic Compounds". *J.of Material Science*, 16, pp. 1349–1355, 1981.

[31] T. Ishikawa, T. Yamamura and K. Okamura. "Production of Polytitanocarbosilane and Its Conversion into Inporanic Materials". *J.of Material Science*, 27, pp. 6627, 1992.

[32] K. Schwarz, D. Rowcliffe, Y. Blum and R. Laine. "Thermal Conversion of Preceramic Polysilazanes to Si_3N_4: Characterization of Pyrolysis Products". *Mat. Res. Soc. Symp. Proc.*, 73, pp. 407, 1986.

[33] A. Lavedrine, D. Bahloul, P. Goursat, N. Yive, R. Corriu, D. Leclerq, H. Mutin and A. Vioux. "Pyrolysis of Polyvinylsilazane Precursor to Silicon Carbonitride". *J. of European Ceramic Soc.*, 8, pp. 221, 1991.

[34] M. Peuckert, T. Vaahs and M. Bruck. "Ceramics from Organometallic Polymers". *Adv. Materials*, 2, pp. 398, 1990.

[35] D. Seyferth, G. Wiseman, J. Schwark, Y. Yu and C. Poutasse. "Organosilicon Polymers as Precursors for Silicon-Containing Ceramics". *American Ceramic Soc. Symp. Ser.*, 360, pp. 143, 1987.

[36] D. Seyferth and H. Plenio. "Borosilazane Polymeric Precursors for Borosilicon Nitride". *J. of American Ceramic Soc.*, 73, pp. 2131–2133, 1990.

[37] H. Baldus, O. Wagenr and M. Jansen. "Synthesis of Advance Ceramics in the System Si-B-N and Si-B-N-C Employing Novel Precursor Compounds". *Mater. Res. Soc. Sym. Proc.*, 271, pp. 821, 1992.

[38] F. Hurwitz, P. Heimann, S. Farmer and D. Hembree. "Characterization of the Pyrolytic Conversion of Polysilsequioxanes to Silicon Oxycarbides". *J.of Material Science*, 28, pp. 6622, 1993.

[39] R. Ellis. "Method of Making Electrically Conducting Glass and Articles Made Thereform". *U.S Patent. 2,556,616*, June 1951.

[40] C. Smith and W. Crandall. "Method of Making Carbon Containing Glasses". *U.S Patent. 3,378,431*, 1968.

[41] R. Elmer and H. Meissner. "Increase of annealing point of 96% SiO_2 glass on incorporation of carbon". *J. of American Ceramic Soc.*, 59[5], pp. 206–209, 1976.

[42] J. Homeny, G. Nelson and S. Risbud. "Oxycarbide Glasses in the Mg-Al-Si-O-C System". *J. of American Ceramic Soc.*, 71[5], pp. 386 – 390, 1988.

[43] D. Coon. "Effect of silicon carbide additions on the crystallization behavior of a magnesia-lithium-alumina-silica system". *J. of American Ceramic Soc.*, 72[7], pp. 1270–1273, 1989.

[44] H. Zhang and C. Pantano. "Synthesis and Characterization of Silocon Oxycarbide Glasses". *J. of American Ceramic Soc.*, 73[4], pp. 958–963, 1990.

[45] V. Lavrenko, S. Jones and R. Pampuch. "Petrographic and X-ray Identification of Phases Formed by Oxidation of Silicon Carbide". *Ceramic International*, 2, pp. 75–76, 1981.

[46] A. Yurkov and B. Polyak. "Contact Phenomenon and Interactions in the system SiC-SiO_2-R_xO_y in Condensed Matter". *Adv. Ceramic Materials*, 31[10], pp. 2729–2733, 1996.

[47] J. Lipowitz, H. Freeman, R. Chen and E. Prack. "Composition and Structure of Ceramic Fibers Prepared from Polymer Precursors". *Adv. Ceramic Materials*, 2[2], pp. 121–128, 1987.

[48] J. Lipowitz. "Polymer Derived Ceramic Fibers". *Ceramic Bulletin*, 70[12], pp. 1888–1894, 1991.

[49] F. Chi. "Carbon-Containing Monolitic Glasses via the Sol-Gel Process". *Ceramic Eng. Sci. Proc.*, 4, pp. 704–717, 1983.

[50] F. Babonneau, G. Soraru, G. D'Andrea and S. L. Bois Dire. "Silicon Oxycarbide Glasses from Sol-Gel Precursors". *Mat. Res. Soc. Symp. Proc.*, 271, pp. 789–794, 1992.

[51] C. Pantano, A. Singh and H. Zhang. "Silicon Oxycarbide Glasses". *J. of Sol-Gel Science and Technology*, 14, pp. 7–25, 1999.

[52] F. Babonneau, L. Bois and J. Livage. "Silicon Oxycarbide via Sol-Gel Route: Characterization of the Pyrolysis Process". *Journal of Non-Crystalline Solids*, 147/148, pp. 947, 1992.

[53] G. D. Soraru. "Silicon Oxycarbide Glasses from Gels". *J. of Sol-Gel Science and Technology*, 2, pp. 843–848, 1994.

[54] V. Belot, R. Corriu, D. Leclercq, P. Mutin and A. Vioux. "Organosilicon Gels Containing Silicon-Silicon Bonds, Precursors to Novel Silicon Oxycarbide Glasses". *J. of Non-Crystalline Solids*, 144, pp. 287–297, 1992.

[55] V. Belot, R. Corriu, D. Leclercq, P. Mutin and A. Vioux. "Thermal Reaction Occuring During Pyrolysis of Cross-Linked Polysilazane Gels, Precursors to Silicon Oxycarbide Glasses". *J. of Non-Crystalline Solids*, 147/148, pp. 52–55, 1992.

[56] G. M. Renlund and S. Prochazka. "Silicon Oxycarbide Glasses: Part I. Preparation and Chemistry". *J. of Material Research*, 6[12], pp. 2716–2722, 1991.

[57] R. Wills, R. Markle and S. Mukherjee. "Siloxanes, Silanes , and Silazanes in the Preparation of Ceramics and Glasses". *Ceramic Bulletin*, 62[8], pp. 904–915, 1983.

[58] A. Wilson, G. Zank, K. Eguchi, W. Xing, B. Yates and J. Dahn. "Polysiloxane Pyrolysis". *Chemistry of Materials*, 9, pp. 1601–1606, 1997.

[59] E. Radovanovic, M. Gozzi, M. Gonçalves and I. Yoshida. "Silicon Oxycarbide Glasses from Silicone Networks". *J. of Non-Crystalline Solids*, 248, pp. 37–48, 1999.

[60] J. Brus, F. Kolář, V. Machovič and J. Svítilová. "Structure of Silicon Oxycarbide Glasses Derived From Poly(methlysiloxane) and Poly[methly(phenyl)siloxane] Precursor". *J. of Non-Crystalline Solids*, 289, pp. 62–74, 2001.

[61] P. Mutin. "Role of Redistribution Reaction in the Polymer Route to Silicon-Carbon-Oxygen Ceramics". *J. of American Ceramic Soc.*, 85[5], pp. 1185–1189, 2002.

[62] G Soraru, D'Andrea, G, R Campostrini, F Babonneau, and G. Mariotto. "Structural Characterization and High- Temperature Behavior of Silicon Oxycarbide Glasses Prepared from Sol-Gel Precursors Containing Si-H Bonds". *J. of American Ceramic Soc.*, 78[2], pp. 379–387, 1995.

[63] H. Kleebe, C. Turquat and G. Soraru. "Phase Seperation in an SiCO Studied by Transmission Electron Microscopy and Electron Energy Loss Spectroscopy". *J. of American Ceramic Soc.*, 84[5], pp. 1073–1080, 2001.

[64] K. Kaneko and K. Kakimoto. "HRTEM and ELNES analysis of Polycarbsilane-Derived Si-C-O Bulk Ceramics". *J. of Non-Crystalline Solids*, 270, pp. 181–190, 2000.

[65] G. Soraru, E. Dallapiccola and G. D'Andrea. "Mechanical Characterization of Sol-Gel Derived Silicon Oxycarbide Glasses". *J. of American Ceramic Soc.*, 79[8], pp. 2074–2080, 1996.

[66] G. M. Renlund and S. Prochazka. "Silicon Oxycarbide Glasses: Part II. Structure and Properties". *J. of Material Research*, 6[12], pp. 2723–2734, 1991.

[67] K Schwartz, and D. Roweliffe. "Modelling Density Contribution in Preceramic Polymer/Ceramic Powder Composites". *J. of American Ceramic Soc.*, 69[5], pp. C–106–108, 1986.

[68] T Erny, M Seibold, O Jarchow and P. Greil. "Microstructure Development of Oxycarbide Composites During Active-Filler-Controlled Polymer Pyrolysis". *J. of American Ceramic Soc.*, 76, pp. 207, 1993.

[69] G. Soraru, H. Kleebe, R. Ceccato and L. Pederiva and. "Development of mullite-SiC nanocomposites by pyrolysis of filled polymethylsiloxane gels". *J. of the European Ceramic Society*, 20, pp. 2509–2517, 2000.

[70] T. Michalet, M. Parlier, F. Beclin, R. Duclos and J. Crampon. "Elaboration of Low Shrinkage Mullite by Active Filler Controlled Pyrolysis of Siloxanes". *J. of European Ceramic Soc.*, 22, pp. 143–152, 2002.

[71] D Seyferth, N Brysob, D Workman, and C. Sobon. "Preceramic Polymers as Reagents in the Preparation of Ceramics". *J. of American Ceramic Soc.*, 74, pp. 2687, 1991.

[72] F. Babonneau and G. Soraru. "Synthesis and Characterization of Si-Zr-C-O Ceramics from Polymer Precursors". *J. of European Ceramic Soc.*, 8, pp. 29–34, 1991.

[73] F. Babonneau, G. Soraru, K. Thorne and J. Mackenzie. "Chemical Characterization of Si-Al-C-O Precursor and Its Pyrolysis". *J. of American Ceramic Soc.*, 74[7], pp. 1725–1728, 1991.

[74] G. Soraru, N. Dallabona, C. Gervais and F. Babonneau. "Organically Modified SiO_2 -B_2O_3 Gels Displaying a High Content of Borosiloxane (≡ B-O-Si ≡) Bonds". *Chemistry of Materials*, 11, pp. 910–919, 1999.

[75] G. Soraru, F. Babonneau, S. Maurina and J. Vicens. "Sol- Gel Synthesis of SiBOC Glasses". *Journal of Non-Crystalline Solids*, 224, pp. 173–183, 1998.

[76] G. Soraru, M. Mercadini, R. Maschio, F. Taulelle, and F. Babonneau. "Si-Al-O-N Fibers from Polymeric Precursor: Synthesis, Structural, and Mechanical Characterization". *J. of American Ceramic Soc.*, 76[10], pp. 2595 – 2600, 1993.

[77] A. Wootton, M. Rappensberger, M. Lewis, S. Kitchin, A. Howes and R. Dupree. "Structural Properties of Multi-Component Silicon- Oxycarbide Glasses Derived from Metal Alkoxide Precursors". *J. of Non-Crystalline Solids*, 204, pp. 217–227, 1996.

[78] H. Yinnon and D. Uhlmann. "Applications of Thermoanalytical Techniques to the Study of Crystallizaiton Kinetics in Glass-Forming Liquids, Part I:Theory". *J. of Non-Crystalline Solids*, 54, pp. 253–262, 1983.

[79] C. Moynihan, A. Easteal, J. Wilder and J. Tucker. "Dependence of the Glass Transition Temperature on Heating and Cooling Rate". *J. of Physical Chemistry*, 78, pp. 2673–2677, 1974.

[80] T. Rouxel, G. Soraru and J. Vicens. "Creep Viscosity and Stress Relaxation of Gel-Derived Silicon Oxycarbide Glasses". *J. of American Ceramic Soc.*, 84[5], pp. 1052–1058, 2001.

[81] J Costello and R. Tressler. "Oxidation Kinetics of Hot-Pressed Sintered α-SiC". *J. of American Ceramic Soc.*, 64[6], pp. 327–331, 1981.

[82] E. Deal and S. Grove. "General Relationship for the Thermal Oxidation of Silicon". *Journal of Applied Physics*, 36[12], pp. 3770–3778, 1965.

[83] K. Luthra. "Some New Perspectives on Oxidation of Silicon Carbide and Silicon Nitride". *J. of American Ceramic Soc.*, 74[5], pp. 1095– 1103, 1991.

[84] J. Costello and R. Tressler. "Oxidation of Silicon Carbide Crystals and Ceramics: I, In Dry Oxygen". *J. of American Ceramic Soc.*, 69[9], pp. 674–681, 1986.

[85] K. Motzfeld. "On the Rates of Oxidation of Silicon and Silicon Carbide in Oxygen and Correlateion with Permeability od Silica Glass". *Acta Chem. Scand.*, 18[7], pp. 1596–1606, 1964.

[86] Z. Zheng, R. Tressler and K. Spear. "Oxidation of Single-Crystal Silicon Carbide, Part I. Experimental Studies". *J. Electrochem. Soc.*, 137[3], pp. 854–858, 1990.

[87] Z. Zheng, R. Tressler and K. Spear. "Oxidation of Single-Crystal Silicon Carbide". *J. Electrochem. Soc.*, 137[9], pp. 2812–2816, 1990.

[88] K. Luthra and H. Park. "Oxidation of Silicon Carbide−Reinforced Oxide−Matrix Composites at 1375°C to 1575°C". *J. of American Ceramic Soc.*, 73[4], pp. 1014–1023, 1990.

[89] A. Heurer, L. Ogbuji and T. Mitchell. "The Microstructure of Oxide Scale on Oxidized Si and SiC Single Crystals". *J. of American Ceramic Soc.*, 63[5-6], pp. 354–355, 1980.

[90] S. Singhal and F. Lange. "Effect of Alumina Content on the Oxidation of Hot-Pressed Silicon Carbide". *J. of American Ceramic Soc.*, 58[9-10], pp. 433–435, 1975.

[91] J. Costello, R. Tressler and I. Tsong. "Boron Redistribution in Sintered α-SiC During Thermal Oxidation". *J. of American Ceramic Soc.*, 64[6], pp. 332–335, 1981.

[92] N. Jacobson. "Corrosion of Silicon Based Ceramics in Combustion Environments". *J. of American Ceramic Soc.*, 76[1], pp. 13–28, 1993.

[93] J. Fergus and W. Worrell. "Effect of Carbon and Boron on the High−Temperature Oxidation of Silicon Carbide". *J. of American Ceramic Soc.*, 78[7], pp. 1961–1964, 1995.

[94] H. Choi, J. Lee and Y. Kim. "Oxidation Behavior of Liquid-Phase Sintered Silicon Carbide with Aluminum Nitride and Rare-Earth Oxides (Re_2O_3), where Re = Y, Er, Yb)". *J. of American Ceramic Soc.*, 85[9], pp. 2281–2286, 2002.

[95] E. Bouillon, F. Langlais, R. Pailler, R. Naslain, F. Cruege, P. Huong, J. Sarthou, A. Deppuech, C. Laffon, P. Lagarde, M. Monthioux and A. Oberlin. "Conversion Mechanism of a Polycarbosilane Precursor into an SiC−Based Ceramic Material". *J.of Material Science*, 26, pp. 1333–1345, 1991.

[96] G. Chollon. "Oxidation Behavior of Ceramic Fibers from the Si−C−N−O System and Related Sub−System". *J. of European Ceramic Soc.*, 20, pp. 1959–1974, 2000.

[97] C. Ramberg, K. Spear, R. Tressler and Y. Chinone. "Oxidation Behavior of CVD and Single Crystal SiC". *Journal of Electrochem. Soc.*, **1100**, 142[11], pp. L214–L216, 1995.

[98] C. Ramberg, G. Crutiani and R. Tressler. "Passive Oxidation Kinetics of High Purity Silicon Carbide from 800°C to 1100°C". *J. of American Ceramic Soc.*, 79[11], pp. 2897–2911, 1996.

[99] C. Brewer, D. Bujalski and V. Parent. "Insights into the Oxidation Chemistry of SiOC Ceramics Derived from Silsesquioxanes". *J.of Sol-Gel Science and Technology*, [14], pp. 49–68, 1999.

[100] I. Hasegawa, T. Nakamura and M. Kajiwara. "Synthesis of Continuous Silicon Carbide−Titanium Carbide Hybrid Fibers Through Sol-Gel Processing". *Mater. Res. Bull.*, 31[7], pp. 869–875, 1996.

[101] T. Yamamura. "Development of New Continuous Si-Ti-C-O Fiber Using an Organometallic Polymer Precursor". *J.of Material Science*, 23, pp. 2589–2594, 1988.

[102] T. Ishikawa. "SiC Polycrystalline Fiber and its Fiber-Bonded Ceramic". *Ann. Chim. Sci. Mat.*, 25, pp. 517–522, 2000.

[103] K. Sato, T. Suzuki, O. Funayama and T. Isoda. "Preparation of Carbon Fiber Reinforced Composite by Impregnation with Perhydropolysilazane Followed by Pressureless Firing". *Ceram. Eng. Sci. Proc.*, 13[9-10], pp. 614–621, 1992.

[104] Allied Signal Inc. "Promotional Literature on Blackglass^{TM}".

[105] F. Hurwitz, J. Gyekenyesi and P. Conroy. "Polymer Derived Nicalon/Si-C-O Composites Processing and Mechanical Behavior". *Ceram. Eng. Sci. Proc.*, 10[7-8], pp. 750–763, 1989.

[106] J. Haggerty and Y. Chiang. "Reaction-Based Processing Methods for Ceramics and Composites". *Ceram. Eng. Sci. Proc.*, 11[7-8], pp. 757–781, 1990.

[107] F. Hurwitz, P. Heimann, , J. Gyekenyesi, J. Manovi and X. Bu. "Polymeric Routes to Silicon Carbide and Silicon Oxycarbide CMC". *Ceram. Eng. Sci. Proc.*, 12[7-8], pp. 1293–1303, 1991.

[108] P. Heimann, F. Hurwitz, D. Wheeler and J. Eldridge. "Preceramic Polymers for Use as Fiber Coatings". *Ceram. Eng. Sci. Proc.*, 16[4], pp. 417–423, 1995.

[109] K. Ueno, S. Kose and M. Kinoshita. "Toughness Enhancement by Polycarbosilane Coating on SiC Whiskers Incorporated in Si_3N_4 Matrix Composites". *J.of Material Science*, 28, pp. 5770–5774, 1993.

[110] J. Bill and D. Heimann. "Polymer-Derived Ceramic Coatings on C/C-SiC Composites". *J. of European Ceramic Soc.*, 16, pp. 1115–1120, 1996.

[111] R. Harshe. "Preparation of Si(B)CN Coating on Carbon-Carbon Composite Material By Dip-Coating and Polymer Pyrolysis.". *Master Project Thesis*, [Unpublished], 2000.

[112] B. Lawn and V. Howes. "Elastic Recovery at Hardness Indentations". *Journal of Material Science*, 16, pp. 2745–2752, 1981.

[113] G. Socrates. "Infrared characteristic group frequencies tables and charts". II Edition, J. Wiley & Sons, 1994.

[114] R. Beyreuther and R. Vogel. "Spinnability of Polymer Melts". *International Polymer Processing*, XI[2], pp. 154–156, 1996.

[115] T. Erny. "Herstellung, Aufbau und Eigenschaften polymer abgeleiteter Verbundkeramik des Ausgangssystems $MeSi_2$/Polysiloxane". Diss. Universität Erlangen Nürnberg, VDI Verlag, 1996.

[116] F. Hönack. "SiOC − Keramiken mit titanhaltigen Füllstoffen". Diss. Universität Darmstadt, WP Verlag, 2003.

[117] P. Lespade, A. Marchand, M. Couzi and F. Cruege. "Characterization of Carbonaceous Materials by Raman Microspectroscopy". *Carbon*, 23[[4-5]], pp. 375–385, 1984.

[118] D. Knight and W. White. "Characterization of Carbon Films by Raman Spectroscopy". *Journal of Material Research*, 4[[2]], pp. 385–393, 1989.

[119] A. Putnis. "Introduction to Mineral Sciences". *Cambridge University Press*, [ISBN 0 521 41922 0], pp. 86, 1992.

[120] J. Mcmanus, S. Ashbrook, K. Mackenzie and S. Wimperis. "^{27}Al Multiple-Quantum MAS and ^{27}Al(^{1}H) CPMAS NMR Study of Amorphous Aluminosilicates". *J. of Non-Crystalline Solids*, 282, pp. 278–290, 2001.

[121] S. Komarneni, R. Roy, C. Fyfe, G. Kennedy and H. Strobl. "Solid-State ^{27}Al and ^{29}Si Magic-Angle Spinning NMR of Aluminosilicate Gels". *J. of American Ceramic Soc.*, 69[3], pp. C–42–C–44, 1986.

[122] K. Kakimoto, F. Wakai, J. Bill and F. Aldinger. "Synthesis of Si-C-O Bulk Ceramics with Various Chemical Compositions from Polycarbosilane". *J. of American Ceramic Soc.*, 82[9], pp. 2337–2341, 1999.

[123] C. Turquat, H. Kleebe, G. Gregori, S. Walter and G. Soraru. "Transmission Electron Microscopy and EELS Study of Nonstoichiometric Silicon-Carbon-Oxygen Glasses". *J. of American Ceramic Soc.*, 84[10], pp. 2189–2196, 2001.

[124] J. Jean and T. Gupta. "Alumina as Divitrification Inhibitor during Sinteriang of Borosilicate Glass Powders". *J. of American Ceramic Soc.*, 76[8], pp. 2010–1016, 1993.

[125] Y. Imanaka, S. Aoki, N. Kamehara and K. Niwa. "Cristobalite Phase Formation in Glass/Ceramic Composites". *J. of American Ceramic Soc.*, 78[5], pp. 1265–1271, 1993.

[126] M. Sacks, N. Bozkurt and G. Scheiffele. "Fabrication of Mullite and Mullite-Matrix Composites by Transient Viscous Sintering of Composites Powders". *J. of American Ceramic Soc.*, 74[10], pp. 2428–2437, 1991.

[127] H. Morikawa, S. Miwa, M. Miyake, F. Marumo and S. Toshiyuki. "Structural Analysis of $SiO_2-Al_2O_3$ Glasses". *J. of American Ceramic Soc.*, 65[2], pp. 78–81, 1982.

[128] D. Cassidy, J. Woolfrey, J. Bartlett and B. Ben-Nissan. "The Effect of Precorsor Chemistry on the Crystallization and Densification of Sol−Gel

Derived Mullite Gels and Powders". *J. of Sol-Gel Science and Technology*, 10, pp. 19–30, 1997.

[129] D. Li and W. Thomson. "Mullite Formation Kinetics of a Single−Phase Gel". *J. of American Ceramic Soc.*, 73, pp. 964–969, 1990.

[130] T. Takei, Y. Kameshima, A. Yasumori and K. Okada. "Crystallization Kinetics of Mullite from Al_2O_3−SiO_2 Glasses under Non-Isothermal Conditions". *J. of European Ceramic Soc.*, 21, pp. 2487–2493, 2001.

[131] W. Wei and W. Halloran. "Transformaiton Kinetics of Diphasic Aluminosilicate Gels". *J. of American Ceramic Soc.*, 71, pp. 581–587, 1988.

[132] J. Huling and G. Messing. "Epitactic Nucleation of Spinel in Aluminosilicate Gels and its Effect on Mullite Crystallization". *J. of American Ceramic Soc.*, 74, pp. 2374–2381, 1991.

[133] D. Li and W. Thomson. "Mullite Formation from Non-stoichiometric Diphasic Precursors". *J. of American Ceramic Soc.*, 74, pp. 2383–2387, 1991.

[134] J. S. Lee and S. C. Yu. "Mullite Formation Kinetics of Coprecipitated Al_2O_3−SiO_2 Gels". *Mater. Res. Bull.*, 27, pp. 405–416, 1992.

[135] A. Gualtieri, M. Bellotto, G. Artioli and S. Clark. "Kinetic Study of the Kaolinite-Mullite Reaction Sequence. Part II: Mullite Formation". *Phys. Chem. Miner*, 22, pp. 215–222, 1995.

[136] A. Boccaccini, T. Khalil and M. Bruker. "Activation Energy for the Mullitization of a Diphasic Gel Obtained from Fumed Silica and Boehmite Sol". *Mater. Letter*, 38, pp. 116–120, 1999.

[137] T. Takei, Y. Kameshima, A. Yasumori and K. Okada. "Crystallization Kinetics of Mullite in Alumina - Silica Glass Fiber". *J. of American Ceramic Soc.*, 82, pp. 2876–2880, 1999.

[138] C. Brinker and G. Scherer. "Sol−Gel Science". *Academic Press, Inc.*, [ISBN 0-12-134970-5], pp. 557–562, 1990.

[139] T. Rouxel, G. Massouras and G Soraru. "High Temperature Behavior of a Gel-Derived SiOC Glass: Elasticity and Viscosity". *J. of Sol-Gel Science and Technology*, [14], pp. 87–94, 1999.

[140] M. Rahman, L. DeJonghe and R. Brook. "The Effect of Shear Stress on Sintering". *Lawrence Berkeley Laboratory*, University of California; Berkeley[Rept. No. 18706], Nov.1984.

[141] M. Rahman and L. DeJonghe. "Sintering Under Low Applied Stress:CdO". *Lawrence Berkeley Laboratory*, University of California; Berkeley[Rept. No. 18049], July,1984.

[142] K. Venkatachari and R. Raj. "Shear Deformation and Densification of Powder Compacts". *J. of American Ceramic Soc.*, 69[6], pp. 499–506, 1986.

[143] R. Raj. "Separation of Cavitational−Strain and Creep−Strain during Deformation". *Communication of the American Ceramic Society*, C−46, 1982.

[144] R. Doremus. "Viscosity of Silica". *Journal of Applied Physics*, 92[[12]], pp. 7619–7629, 2002.

[145] G. Urbain, Y. Bottinga and P. Richet. "Viscosity of Liquid Silica, Silicates and Alumino−Silicates". *Geochimica et Cosmochimica Acta*, 46, pp. 1061–1072, 1982.

[146] J. Gilman. "Flow via Dislocation in Ideal Glasses". *J. of Applied Physics*, 44[[2]], pp. 675–679, 1973.

[147] O. Narayanaswamy and. "A Model of Structural Relaxation in Glass". *J. of American Ceramic Soc.*, 54, pp. 491–98, 1971.

[148] C. Moynihan, S. Lee, M. Tatsumisagoo and T. Ninami. "Estimation of Activation Energies for Structural Relaxation and Viscous Flow from DTA and DSC Experiments". *Thermochim. Acta*, 280/281, pp. 153–62, 1996.

[149] H. Lopez and W. Phoomiphakdephan. "High Temperature Oxidation of Nitride Bonded SiC-Ceramic". *Materials Letters*, [36], pp. 65–69, 1998.

[150] D. Mieskowski, T. Mitchell and A. Heuer. "Bubble Formation in Oxide Scales of SiC". *J. of American Ceramic Soc.*, 67[1], pp. C17–C18, 1984.

[151] S. Spearing. "Materials Issues in Microelectromechanical Systems (MEMS)". *Acta Mater.*, 48, pp. 179–196, 2000.

[152] L. Liew, R. Luo, Y Liu, W. Zhang, L. An, V. Bright, M. Dunn, J. Daily and Rishi Raj. "Fabrication of Multi-Layered SiCN Ceramic MEMS Using Photo-Polymerization of Precursor".

[153] L. Liew, R. Luo, Y Liu, W. Zhang, L. An, V. Bright, M. Dunn, J. Daily and Rishi Raj. "Fabrication of SiCN MEMS Structures Using Microforged Molds".

[154] L. Liew, W. Zhang, L. An, S. Shah, R. Luo, Y. Liu, T. Cross, M. Dunn, V. Bright, J. Daily and Rishi Raj. "Ceramic MEMS". *American Ceramic Society Bulletin*, [80], pp. 25–30, 2000.

8 Vita, Conferences/Publications and Awards

Educational Background

Master of Technology (M.Tech) (1998-2000): Master's In Metallurgical Engineering (Materials Technology) from Indian Institute of Technology (IIT), Madras, India.
CGPA for Master's: 9.69/10 (First in Materials Technology)

Bachelor (B.E) (1990-1995): Metallurgical Engineering with first class and Distinction (76%) from College of Engineering Pune, India.

Awards and Achievements

- Stood first in Master's course at Indian Institute of Technology (IIT), Madras and received a Gold Medal for best academic record.
- Recipient of Deutscher Akademischer Austauschdienst (DAAD) scholarship for research in Germany at TU-Darmstadt as part of an exchange program between IIT Madras, India and German institutes.
- Rank holder in Bachelor of Engineering (Pune University) program for Metallurgical Engineering.
- Best Poster Award (2^{nd} Place) at CONCIM 2003 "Conference on non-crystalline inorganic materials synthesis structure modelling", University of Bonn, Germany.

Publication

"Amorphous Si(Al)OC Ceramic from Polysiloxanes: Bulk Ceramic Processing, Crystallization Behavior and Applications", *Journal of European Ceramic Soc.*, 24, [12], 3465-3470, 2004.

International Conferences

- 26^{th} Annual Cocoa Beach Conference and Exposition on Advance Ceramics and Composites, Held in Feb 2002, Cocoa Beach, Florida, USA.
  Presentation Title: Synthesis and Characterization of Novel Si-(Al)-C-O Bulk Ceramics with Various Chemical Compositions.

- Annual Meeting and Exposition of the American Ceramic Society, Saint Louis, USA, Held in April 2002.
  Presentation Title: Processing and Oxidation Behavior of Polysiloxane-Derived Si(M)CO (M = Al, Mo, $MoSi_2$) Ceramics.

- Advanced Research Workshop: Engineering Ceramics 2003, Held in May 2003, at Smolenice Castle, Slovakia. **Presentation Title:** Si(Al)CO Amorphous Bulk Ceramics from Commercial Polysiloxanes by Polymer Pyrolysis: Oxidation, Crystallization Behavior and Applications.

- CONCIM 2003: **Poster Presentation:** "Conference on non-crystalline inorganic materials synthesis structure modelling", University of Bonn, Germany.